DIRECT CLUTCH SYSTEM FOR SINGLE CYLINDER MULTI-PURPOSE DIESEL ENGINE IN AGRICULTURAL TRANSPORT

SUPHAKRIT KOOCHAROENPRASIT

A THESIS SUBMITTED IN PARTIAL FULFILLMENT

OF THE REQUIREMENT FOR THE DEGREE OF

MASTER OF ENGINEERING IN AUTOMOTIVE ENGINEERING

(INTERNATIONAL PROGRAM)

INTERNATIONAL COLLEGE

KING MONGKUT'S INSTITUTE OF TECHNOLOGY LADKRABANG

2014

KMITL-2014-IC-M-004-007

Thesis title	Direct Clutch System for Single Cylinder Multi-Purpose Diesel Engine in Agricultural Transport
Student	Mr. Suphakrit Koocharoenprasit
Student ID	52600905
Degree	Master of Engineering in Automotive Engineering (International Program)
Year	2013
Thesis advisors	Assoc. Prof. Dr. Jaruwat Charoensuk Dr. Chi-na Benyajati Prof. Dr. Ichiro Hagiwara

ABSTRACT

In this work, a transmission improvement of agricultural truck or E-TAND was investigated with an objective to replace a conventional belt transmission by a direct clutch system. The design and selection processes for the direct clutch prototype with specific concerned topics and constraints of the main parts i.e. a clutch contact surface, a clutch housing, a shaft adapter, and a clutch set, were explained. The computer aided design (CAD) modeler was used to prepare computational models of components for part alignments, dimensional checking, as well as for relevant computational analyses. In case of the simulation work, each part was analyzed using finite element analysis (FEA) according to various specific design issues such as stress analysis and fatigue analysis from an engine vibration load or stress analysis when a transmission system lock up occurred. As a result, safety factors of 3.95, 8.45, and 5.15 were calculated for the proposed clutch housing, clutch contact surface, and shaft adapter, respectively. Furthermore, in order to obtain the optimum design of the clutch housing, the response surface method (RSM) was performed with objectives of weight reduction and sufficient structural strength. The optimization led to a final clutching housing model of spoke-and-strip configuration with a weight reduction of 15.41Kg from the original design of the housing. After all designs were finalized, prototypes of relevant parts were constructed and assembled for performance test experiments on a specifically developed test rig frame. The belt transmission system

and the direct clutch transmission system were tested for performance and efficiency comparisons by means of corresponding slips and torques of each system. The results showed that the maximum improvement of performance of approximately 20% could be expected from using the direct clutch system under full load conditions.

ACKNOWLEDGEMENTS

The study was a scholarship in Automotive Engineering program under Thailand Advanced Institute of Science and Technology and Tokyo Institute of Technology (TAIST-Tokyo Tech) which is a collaboration of National Science and Technology Development Agency (NSTDA), Thailand, Tokyo Institute of Technology (Tokyo Tech), Japan, and King Mongkut's Institute of Technology Ladkrabang (KMITL), Thailand. This study has been conducted during the year 2009-2014 as a part of a research project in the Automotive Laboratory, National Metal and Materials Technology Center (MTEC), Thailand.

I would like to express my special gratefulness thanks to Dr. Chi-na Benyajati, my major thesis advisor and head of Automotive Laboratory, for his support, technical guidance, and encouragement all the time during the research work.

I would like to direct my gratitude to my advisors, Associate Professor Dr. Jaruwat Charoensuk, department of Mechanical Engineering, KMITL

I would like to sincerely thanks, Professor Dr. Ichiro Hagiwara, Department of Mechanical Sciences and Engineering, Tokyo Institute of Technology, Japan, for kind advice and suggestions.

I am very grateful to Dr. Sittikorn Lapapong, Mr. Jenwit Soparat, Mr. Prasit Wattanawongsakun, Mr. Wuttipong Sritham and all members in Automotive Laboratory for their help and technical guidance in data acquisition and experimental measurement during field research. I would like to extend my appreciation to Mr. Dittapoom Shinabuth, Mr. Saharat Chanthanumataporn and Mr. Mahassajun Suwancharoen, TAIST-Tokyo Tech students, for their information, help, and time for discussions. Finally, I would like to give this success to my family who always stand by me, encourage me, and have infinite faith in my research work.

Suphakrit Koocharoenprasit

May 2014

CONTENTS

Page

ABSTRACT I

ACKNOWLEDGEMENTS III

TABLE OF CONTENTS IV

LIST OF TABLES VIII

LIST OF FIGURES VIIII

CHAPTER 1 INTRODUCTION 1

1.1 Background and Problems 1

1.2 Objectives 2

1.3 Scopes 2

1.4 Result Expectation 3

1.5 Research Methodology 3

1.6 Thesis Outlines 3

1.7 Thesis Layout 5

CHAPTER 2 LITERATURE REVIEW & OVERVIEW 6

2.1 Background of Agricultural Truck or E-TAND in Thailand 6

2.2 Belt Transmission system 7

2.2.1 Belt Characteristics and Belt Losses 7

2.2.2 Belt Experiment 10

2.3 Clutch Transmission System 12

2.4 Model Analysis and Optimization 14

2.4.1 Finite Element Analysis (FEA) 14

2.4.2 Fatigue Analysis 18

2.4.3 Structural Optimization 21

2.4.4 Previous Studies on Design, Analysis, and Structural 22

CHAPTER 3 DIRECT CLUTCH SYSTEM DESIGN CONCEPT AND SPECIFIC CONCERN 26

CONTENTS (CONT.)

Page

3.1 Conventional Model of an E-TAND or Agricultural Truck in Thailand 26

3.2 Modeling Concept and Designing Consideration 28

3.2.1 Clutch Set 29

3.2.2 Clutch Contact Surface 30

3.2.3 Clutch Housing 32

3.2.4 Gear Shaft Adapter 34

CHAPTER 4 METHODOLOGY 36

4.1 Vibration Load Profiles Measurement of One Cylinder Diesel Engine 36

4.1.1 Experimental Setup 36

4.1.2 Data Post Processing for Clutch Housing Analysis 38

4.2 Clutch Housing 40

4.2.1 Clutch Housing Structural And Fatigue Analysis 40

4.2.1.1 Mesh Model Preparation 40

4.2.1.2 Material 42

4.2.1.3 Boundary Conditions for Clutch Housing Structural and Fatigue Analysis 42

4.2.2 Clutch Housing Optimization 43

4.3 Clutch Contact Surface and Bolt Attached Analysis 45

4.3.1 Mesh Preparation 46

4.3.2 Boundary Conditions for Clutch Contact Surface and Bolt Analysis 47

4.4 Shaft Adapter Analysis 49

4.4.1 Mesh Preparation 50

4.4.2 Boundary Conditions for Shaft Adapter Analysis 50

4.5 Transmission Performance Comparison Experiment 51

4.5.1 Experimental Setup 51

4.5.1.1 Test Rig Frame Design 52

CONTENTS (CONT.)

Page

4.5.1.2 Belt Length Calculation and Selection for Experiment Test...54

4.5.2 Performance Test Procedures and Test Conditions...60

4.5.3 Data Processing...61

4.6 Strain Measurement on a Clutch Housing Prototype...62

CHAPTER 5 EXPERIMENTS, COMPUTATIONAL AND OPTIMIZIATION RESULTS...64

5.1 Vibration Load Profile Measurement of One Cylinder Diesel Engine...64

5.1.2 Data Post Processing and Preparing for Clutch Housing Analysis...65

5.2 Clutch Housing Analysis Results...67

5.2.1 Analytical Results: Clutch Housing Structural and Fatigue Analysis 67

5.2.2 Clutch Housing Optimization...68

5.3 Clutch Contact Surface And Bolts Attached Stress Analysis Results...80

5.3.1 Analytical Results: Clutch Contact Surface Stress Analysis...80

5.3.2 Analytical Results: Clutch Contact Surface Bolts Attached Stress Analysis...81

5.4 Shaft Adapter Analysis Results...84

5.5 Performance Comparing Experiment Test Results...85

5.5.1 Belt Transmission System...85

5.5.2 Direct Clutch Transmission System...98

5.6 Clutch Housing Strain Measurement Experimental Results...101

CHAPTER 6 DISSCUSION...103

6.1 Vibration Load Measurement...103

6.2 Clutch Housing Analysis and Optimization...103

6.2.1 Clutch Housing Fatigue Analysis...104

6.3 Clutch Contact Surface and Bolts Attached Stress Analysis...106

6.3.1 Clutch Contact Surface Stress Analysis...106

6.3.2 Bolt Attached Stress Analysis...106

6.4 Shaft Adapter Stress Analysis...107

6.5 Direct Clutch System Components Prototype...107

CONTENTS (CONT.)

Page

6.6 The Transmission Performance Test 109

6.6.1 Belt Transmission System 109

6.6.2 Direct Clutch Transmission System 113

6.6.3 Direct Clutch and Belt Transmission System Performance Comparison 114

6.7 Direct Clutch and Belt Transmission System General Comparison 118

6.8 The Finite Element Model Validation by Actual Strain measurement 118

CHAPTER 7 CONCLUSIONS AND SUGGESTIONS 120

7.1 Conclusions 120

7.1.1 Parts Analysis and Optimization 120

7.1.2 Transmission System Test 121

7.1.3 Strain Validation Experiment of Clutch Housing 122

7.2 Suggestions for Further Research 122

7.2.1 Clutch Housing System Prototype Design, Analysis, and Optimization 122

7.2.2 Experimental test 123

REFERENCES 124

APPENDIX A : LABVIEW BLOCK DIAGRAM 127

APPENDIX B : TRANSDUCER AND SENSOR SPECIFICATION 130

APPENDIX C : DATA ACQUISITION SPECIFICATION 135

APPENDIX D : PROCEEDING 141

BIOGRAPHY 174

LIST OF TABLES

Table		Page
3.1	Engine spec (KUBOTA RT140)	27
4.1	Mechanical properties of Structural steel from ANSYS ® software	41
4.2	Load conditions details of performance tests	62
5.1	Calculated maximum forces in each load case	66
5.2	DOE- 3^2 design table results	68
5.3	Design of experiment results for spokes variations	74
5.4	DOE- 3^2 design table results	77
6.1	Model comparison table	104
6.2	Improvement of power output while using direct clutch instead of belt transmission	118

LIST OF FIGURES

Figure		Page
1.1	Research methodology flow chart	5
2.1	An agricultural truck or E-TAND	7
2.2	Example of V-Belt	7
2.3	Belt losses categories chart	8
2.4	Belt drive showing the four flexing points: A, B, C and D	8
2.5	Slip curve characteristic	9
2.6	Shows the efficiency curve of V-Belt	10
2.7	Schematic of the experimental setup and instrument	11
2.8	Angular rotations measurement principle	12
2.9	Clutch system components: (a) Flywheel, (b) Clutch set: including clutch cover, clutch disc, and bearing, (c) Clutch pump lower, and (d) Clutch fork	13
2.10	Clutch system mechanism lay out	13
2.11	Example of clutch characteristic curve and force diagrams	14
2.12	Example of element types	15
2.13	Mesh element types	15
2.14	Skewness theory based on equilateral volume for triangular and normalized equiangular for quad	16
2.15	Shape of different aspect ratio for Quad and Triangle elements	16
2.16	Simple spring element	17
2.17	S-N curve of no endurance limit and endurance limit	19
2.18	Cycling loading conditions : (a) symmetrical about zero stress (Fully reversed loading), (b) asymmetrical about zero stress (Tension –Tension with applied stress), and (c) Random stress fluctuations or Spectrum loading	20
2.19	Comparison of mean stress equation	20
2.20	Example of a response surface for maximum von-Mises stress of Clutch fork parameter optimization by N. Kaya et al	22

LIST OF FIGURES (CONT.)

Figure		Page
2.21	Finite element model and result of the stress analysis of joint yoke and drive shaft	23
2.22	Variable amplitude load-times histories by SAE	24
2.23	I-Type cross sections and design variables	25
3.1	CAD model displaying basic structure of conventional E-TAND	27
3.2	Conventional transmission arrangement of E-TAND	27
3.3	One-cylinder diesel engine clutch transmission layout	28
3.4	Power transfer on clutch transmission driveline	28
3.5	Commercial TOYOTA Hilux EXEDY clutch set	29
3.6	Flywheel comparison (Left) one cylinder diesel engine flywheel (Right) conventional engine flywheel (Clutch disc contact surface : Green area)	31
3.7	Clutch contact surface design constraints: flywheel geomentries (all dimensions in mm)	31
3.8	Clutch contact surface prototype CAD model (all dimensions in mm)	32
3.9	Clutch housing design constraints (a) Design space area (b) Clutch fork mounting pivot distance	33
3.10	Clutch housing prototype CAD model (all dimensions in mm)	33
3.11	Clutch housing CAD model with a pivot mounting	34
3.12	Difference in spline size and type between gearbox and clutch disc	34
3.13	Gear shaft adapter CAD model (all dimension are in mm)	35
4.1	An experimental set up for vibration load measurement: (a) single axis accelerometers, (b) dynamometer load controller, (c) DAQ equipment, (d) dynamometer chassis with test engine, and (e) front panel for DAQ devices interface.	37
4.2	(a) accelerometer attach locations (b) accelerometers attachment configuration near engine base	38
4.3	Engine load distribution	39
4.4	EUDC standard: Driving cycle for 1 day, [23]	39
4.5	CAD models of clutch housing parts for computational analysis	40
4.6	Finite element model of clutch housing	41
4.7	S-N Curve of a structural steel from ANSYS Engineering data	42

LIST OF FIGURES (CONT.)

Figure		Page
4.8	Boundary conditions for clutch housing analysis	43
4.9	Design variable of clutch housing optimization, thickness (DV1), slope angle (DV2)	44
4.10	3 factor levels and 2 parameters, 3^2 factorial design or 9 design points	44
4.11	Middle portion of clutch housing (a) Initial design (b) Only spokes design (c) Spokes and stripes design	45
4.12	CAD models of clutch contact surface and bolts for computational analysis	46
4.13	Finite element model of clutch contact surface stress analysis	47
4.14	Finite element model of clutch contact surface bolts analysis	47
4.15	Shown clamp load applied on a clutch contact surface region	48
4.16	Boundary conditions and finite element model for bolt analysis	49
4.17	CAD model of Shaft adapter part for computational analysis	49
4.18	Finite element model of shaft adapter	50
4.19	Boundary conditions applied on the shaft adapter model	51
4.20	Frame base setups for belt and direct clutch system test	53
4.21	An experimental set up for transmission performance test: (a) Miki coupling, (b) Kistler torque transducer, (c) V-belt tension tester (d) DAQ equipment (e) Autonic rotary encoder, (f) Spotlight loading unit and (g) Overall experimental configuration of transmission performance test	53
4.22	Suggested service factors for v-belt drives [24]	55
4.23	Belt cross section selection chart	56
4.24	B Section belt length information [25]	57
4.25	Belt transmission experiment layout(Top: CAD layout, Bottom: Actual layout)	59
4.26	Direct clutch transmission experiment layout (Top: CAD layout, Bottom: Actual layout)	60
4.27	(left) Data acquisition tool NI-9235, (right) uniaxial TML strain gages	63
4.28	Three strain-measurement locations on a clutch housing set	63
4.29	Details of strain gages attachment on Clutch housing set	63
5.1	Engine vibration profiles measured at various loads.	64
5.2	Comparison between filtered (black) and non-filtered (grey) vibration data.	65

LIST OF FIGURES (CONT.)

Figure		Page
5.3	Combined loading history for fatigue analysis	66
5.4	Von-Mises stress distribution result in clutch housing with component thickness of 13 mm and 65 degree of slope angle	67
5.5	Maximum von-Mises stress response surface for clutch housing design parameters (DV1, DV2).	69
5.6	Volume response surface for clutch housing design parameters (DV1, DV2).	70
5.7	Sensitivity charts of parameters of first optimum model	70
5.8	Von-Mises stress distribution result in first optimum prototype clutch housing, component thickness of 8.7 mm and 67 degree of slope angle.	72
5.9	A side view of the initially optimized clutch housing prototype design with resulting stress distribution.	73
5.10	Clutch housing model with 6 spokes configuration (all dimensions are in mm.)	73
5.11	A relationship between amount of spokes and maximum von-Mises stresses	74
5.12	Calculated von-Mises stress distribution results for different number of spokes (4 to 11 spokes) on the revised clutch housing model.	75
5.13	Calculated Von-Mises stress distribution in 9 spokes clutch housing with double-sized spoke.	76
5.14	Clutch housing model with strip structure and relevant design parameters (Strip width and Strip gap)	77
5.15	Response surface of maximum von-Mises stress for clutch housing design parameters of strip gap and strip width	78
5.16	Sensitivity charts of strip gap and strip width parameters	79
5.17	Von-Mises stress distribution in optimum spokes-and-strips clutch housing	80
5.18	Calculated von-Mises stress distribution in clutch contact surface	81
5.19	Calculated von-Mises stress distribution on the clutch contact surface with attached bolts	82
5.20	Von-Mises stress distribution and maximum point on the clutch contact surface attached bolt (a) normal stress along x axis (b) normal stress along y axis (c) normal stress along z axis or axial stress (d) illustration of applied load	83
5.21	Von-Mises stress distribution on the shaft adapter with the maximum point	84

LIST OF FIGURES (CONT.)

Figure Page

5.22 Shear stress distributions on the shaft adapter with the maximum point 85

5.23 Experimental results of 1.7 Kg belt tension, Load L1: resulting RPM and Torque on both pulleys, Slip percentage, and Torque difference 87

5.24 Experimental results of 1.7 Kg belt tension, Load L2: resulting RPM and Torque on both pulleys, Slip percentage, and Torque difference 88

5.25 Experimental results of 1.7 Kg belt tension, Load L3: resulting RPM and Torque on both pulleys, slip percentage, and Torque difference 89

5.26 Experimental results of 1.7 Kg belt tension, Load L4: resulting RPM and Torque on both pulleys, Slip percentage, and Torque difference 90

5.27 Experimental results of 2.3 Kg belt tension, Load L1: resulting RPM and Torque on both pulleys, Slip percentage, and Torque difference 91

5.28 Experimental results of 2.3 Kg belt tension, Load L2: resulting RPM and Torque on both pulleys, Slip percentage, and Torque difference 92

5.29 Experimental results of 2.3 Kg belt tension, Load L3: resulting RPM and Torque on both pulleys, Slip percentage, and Torque difference 93

5.30 Experimental results of 2.3 Kg belt tension, Load L4: resulting RPM and Torque on both pulleys, Slip percentage, and Torque difference 94

5.31 Experimental results of 3 Kg belt tension, Load L1: resulting RPM and Torque on both pulleys, Slip percentage, and Torque difference 95

5.32 Experimental results of 3 Kg belt tension, Load L2: resulting RPM and Torque on both pulleys, Slip percentage, and Torque difference 96

5.33 Experimental results of 3 Kg belt tension, Load L3: resulting RPM and Torque on both pulleys, Slip percentage, and Torque difference 97

5.34 Experimental results of 3 Kg belt tension, Load L4: resulting RPM and Torque on both pulleys, Slip percentage, and Torque difference 98

5.35 Direct clutch system experimental results: RPM on both sides of the clutch transmission under L1 load conditions 99

LIST OF FIGURES (CONT.)

Figure Page

5.36 Direct clutch system experimental results: RPM on both sides of the clutch transmission under L2 load conditions 99

5.37 Direct clutch system experimental results: RPM on both sides of the clutch transmission under L3 load conditions 99

5.38 Direct clutch system experimental results: RPM on both sides of the clutch transmission under L4 load conditions 100

5.39 Direct clutch system: Measured Torque B under each engine load conditions 100

5.40 Direct clutch system: Measured Slip under different load conditions 101

5.41 Stress responses measurement during a full engine load on three different locations of the direct clutch housing, with corresponding RPM and torque outputs monitoring 102

6.1 Fatigue failure location of Clutch housing with 7 mm. of thickness 105

6.2 Correlation between fatigue life and maximum von-Mises stress 105

6.3 Hexagon head bolts and screws physical properties [27] 106

6.4 Maximum von-Misses stress and maximum shear stress locations on the shaft adapter model 107

6.5 Constructed Prototype parts for the direct clutch system prototype 108

6.6 Selected commercial parts for the direct clutch prototype:
(top) 3L toyota hilux clutch fork, (bottom) Toyota Hilux EXEDY Clutch set 108

6.7 Assembled Direct clutch system prototype for one-cylinder diesel engine 108

6.8 Belt transmission system averaged slip percentage comparison : (Top) 1.7Kg of belt tension case, (Middle) 2.3 Kg of belt tension case,
(Bottom) 3Kg of belt tension case 110

6.9 Belt transmission system averaged Torque B comparison : (Top) 1.7Kg of belt tension case (Middle) 2.3 Kg of belt tension case,
(Bottom) 3Kg of belt tension case 111

6.10 Belt transmission system efficiency comparison: (a) Efficiency in L1 case
(b) Efficiency in L2 case (c)) Efficiency in L3 case (d) Efficiency in L4 case 112

6.11 Direct clutch system: averaged slip percentage under each load conditions 113

6.12 Direct clutch system: averaged torque in each load conditions 114

LIST OF FIGURES (CONT.)

Figure Page

6.13 Direct clutch and belt transmission system comparison between a slip percentage (left) and a torque (right) 115

6.14 Slip percentage comparisons 116

6.15 Torque output comparisons 116

6.16 Power output comparisons between Belt transmission and direct clutch system 117

6.17 Comparison of measured results and calculated results with percentage deviation in each location 119

CHAPTER 1

INTRODUCTION

1.1 Background and Problems

In Thailand, agricultural product is one of main products for both domestic and export industries. As a result, agricultural machines and tools also become an important part. Agricultural trucks are the once of machines that are widely used in many rural parts of Thailand. The most basic and the most famous type is E-TAND. E-TAND is very famous because of its relatively low manufacturing and maintenance cost. E-TAND is also known as a multipurpose vehicle, due to its employment in many applications such as loading crops or farm produce, people transportation, etc. For E-TAND manufacturing, many parts of E-TAND such as suspension, transmission system, and steering system are built from second-hand parts because of a lower cost. However, the problems commonly associated with this kind of vehicle are low quality, no relevant standard, a need to modify and relative low safety. Nowadays, agricultural trucks or E-TAND use one cylinder diesel engine as a prime mover. Normally, a one-cylinder diesel engine is designed for use in many purposes, so that the choice of power transfer has to be simple or universal. As an engine of agricultural truck, the power will be transferred from pulley to gearbox by belts. In this case, V-belt type is selected. However this type of transmission is accompanied by a considerable amount of loss. Such loss is related to a lower operating efficiency of agricultural truck. In order to develop an agricultural truck or E-TAND with higher efficiency and, safety, a concept of direct clutch transmission has been proposed and studied in this work.

1.2 Objectives

In this work, the primary aim was to development of a new transmission system for an agricultural truck or E-TAND by using a direct clutch system instead of a conventional belt system to improve the efficiency of an E-TAND. In order to achieve this aim, following objectives were to be carried out:

1.2.1 Study the CAD/CAE program for design and analysis a direct clutch prototype components.

1.2.2 Study the optimization techniques and method.

1.2.3 Investigate belt transmission performance, characteristics, and install configuration for one cylinder diesel engine

1.2.4 Study the clutch components and engineering/designing/manufacturing limitation.

1.2.5 Compare the efficiency between belt and direct clutch system.

1.3 Scopes

The scope of the current study is could be divided into 4 main parts, study, design, analysis, and laboratory & flied test.

1.3.1 Study the V-belt performance and install configuration.

1.3.2 Design a direct clutch system parts under constrains and specific concerns of each part by using CAD.

1.3.3 Analyze and optimize prototype model of each component by using CAE and optimize methods.

1.3.4 Manufacture and test direct clutch system prototype

1.3.5 Compare the efficiency between belt and direct clutch system

1.4 Result Expectation

1.4.1 Learning the commercial CAD/CAE software

1.4.2 Gaining knowledge in a design optimization of engineering parts and components

1.4.3 Gaining knowledge in a transmission efficiency and transmission performance monitoring

1.5 Research Methodology

1.5.1 Consider a constrain of clutch system design from the conventional transmission system

1.5.2 Design parts and create relevant CAD models according to considered constraints.

1.5.3 Perform static and fatigue analysis of the proposed parts

1.5.4 Execute design optimization on prototype model

1.5.5 Construct a direct clutch system prototype

1.5.6 Set up an experiment of belt transmission and direct clutch system on a dual transmission test rig in order to measure transmission efficiencies under different driving conditions.

1.5.7 Compare the transmission experimental results.

1.6 Thesis Outlines

The thesis is divided into 7 Chapters, the contents of which are summarized as followed:

Chapter 1 : Introduction

This chapter introduces the general background of an, the problem and improvement of the agricultural truck or E-TAND, the objectives, the scopes, the result expectations, the research methodology, and thesis layout.

Chapter 2 : Background Theory and Literature Review

In this chapter, the belt transmission system, clutch transmission system, the basic equations related to finite element analysis of structural problems, fatigue analysis, and structural optimization are provided. With these background theories, several applications from the published literature are also reviewed.

Chapter 3 : Direct clutch system design concept and specific concern

This chapter presents the design concept of direct clutch system to replace of belt transmission. The specific concern points and special requirements or constraints are explained

Chapter 4 : Methodology

This chapter explains the process of finite element analysis and optimization. The computational processes are comprised of the mesh preparation, boundary conditions, optimization parameters, and the calculation solution. In addition, the experiment set up of vibration measurement and transmission performance test, procedures, and design of experiment were explained too.

Chapter 5 : Experiment, computational and optimization results

This chapter shows the model strength results of the prototype part of direct clutch system and all optimal design parameters given by the optimization. Moreover, the vibration load measurement and transmission performance are determined.

Chapter 6 : Discussions

The obtained results from the previous chapter are discussed in this chapter. The discussions consisted of the finite element model analysis results, the comparison of model improvement of clutch housing by optimization, the comparison of transmission performance.

Chapter 7 : Conclusions and Suggestions

This chapter illustrates a summary of the present study and provides suggestions for further research.

1.7 Thesis Layout

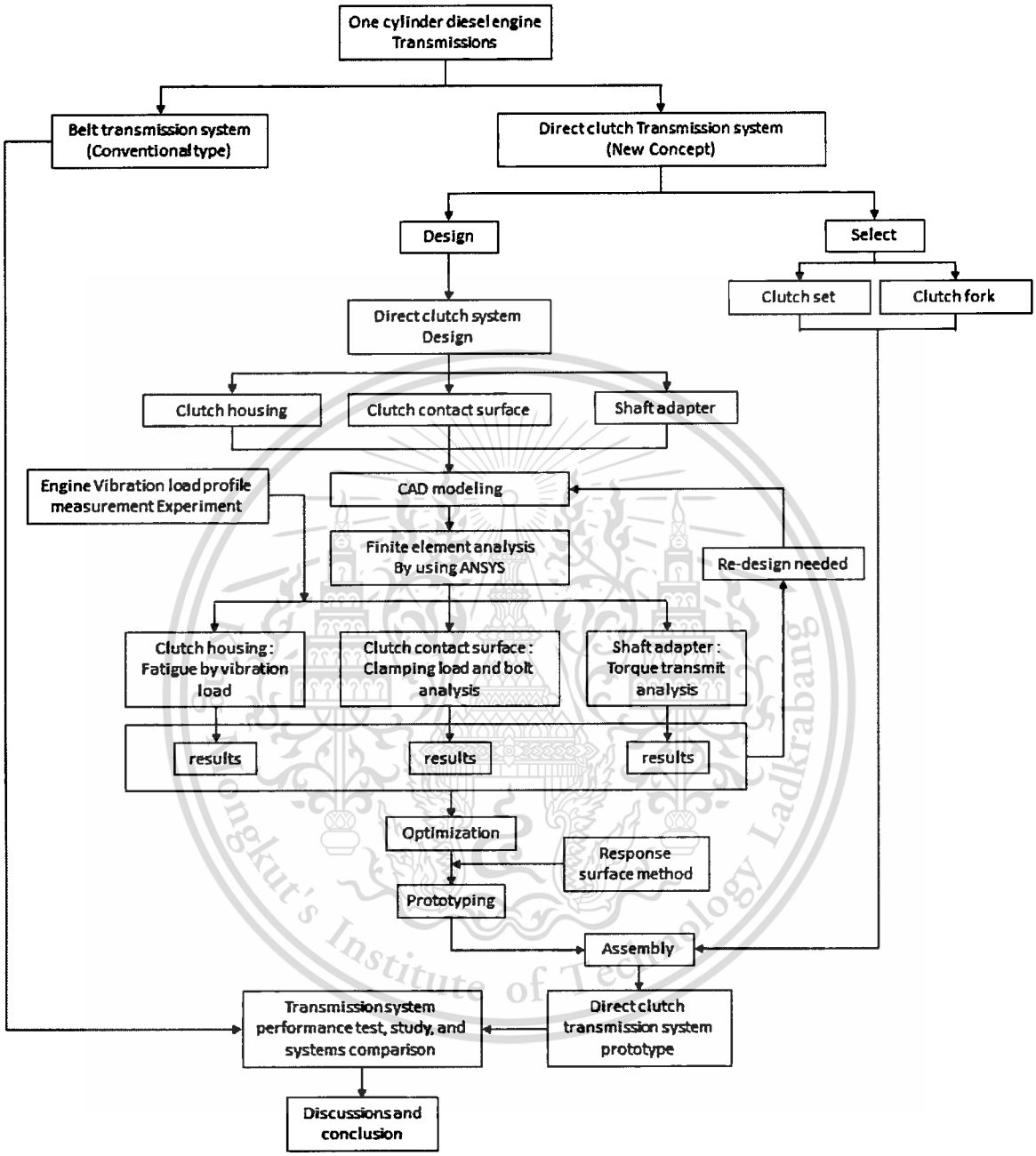

Figure 1.1 Research methodology flow chart

CHAPTER 2

LITERATURE REVIEW & OVERVIEW

2.1 Background of Agricultural Truck or E-TAND in Thailand

An example of agricultural truck widely used in several rural parts of Thailand is illustrated in Figure 2.1. For manufacturing process, E-TAND is generally assembled by local mechanics using second-hand parts that are available in a market. A main limitation of such approach is the varied conditions and specifications of these second-hand parts. Problem usually arises when certain parts are not available, leading to part modifying as a way to solve such a problem, hence difficulties in obtaining good quality control and proper engineering design. For a drivetrain, it could be seen from Figure 2.1 that one-cylinder diesel engines are commonly used as a prime mover. In addition, the commercial one cylinder diesel engines have been designed for used as a universal power source i.e. connecting to electric generator, water pump, etc. Therefore, the transmission of this engine has to be universal that the power is transferred from the engine to other mechanical load via belt configurations. In the light of E-TAND is used a ladder frame for a chassis, the engine is located on the top front of the E-TAND chassis. In contrast, the transmission housing set is located on lower level of chassis; in that case belts are installed in vertically to connect the transmission set and the engine. Then, a driveshaft with joint yokes is used to connect a rear axle to transmission set for a drive system. From this reason, the system is always causes a problem of match of transmission parts.

Figure 2.1 An agricultural truck or E-TAND

2.2 Belt Transmission System

Belt transmission system was introduced many decades ago. Belt transmission system is widely used in many industrials and applications. The main application of this system is used to drive coupled pulleys. Over 30 percent of motor transmissions used the belt drive system. The advantages of the belt drive are flexibility in the system alignment, adjustable speed ratio by variation of pulley diameters, and low maintenance.

V-belt type is the most common belt transmission type because it is a cheapest. The transmission efficiency is significantly reduced by material worn out of belt after a certain period of usage.

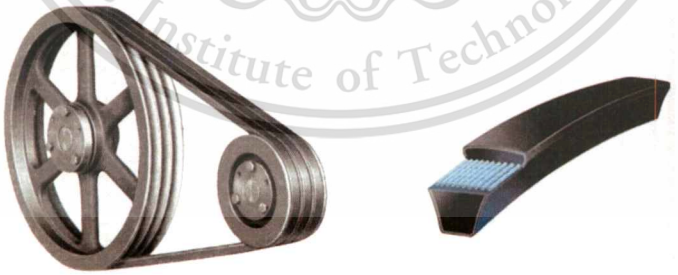

Figure 2.2 Example of V-Belt

2.2.1 Belt characteristics and Losses

Efficiency of belt transmission could be calculated by using mechanical power in driven and drive side as shown in following equations [1] :

$$Efficiency = \frac{Mechanical\ power\ to\ the\ driven\ device}{Mechanical\ power\ form\ the\ motor} \quad (2.1)$$

or

$$Efficiency = \frac{torque\ out \times r.p.m.out}{torque\ in \times r.p.m.in} \quad (2.2)$$

The efficiency drop is due to mechanical losses occurred by belts. The losses of belt could be separated to 2 main types: speed loss and torque loss. Speed loss consists of slip loss and creep loss, while hysteresis loss, windage loss, and frictional loss are considered as torque loss as illustrated in chart below.

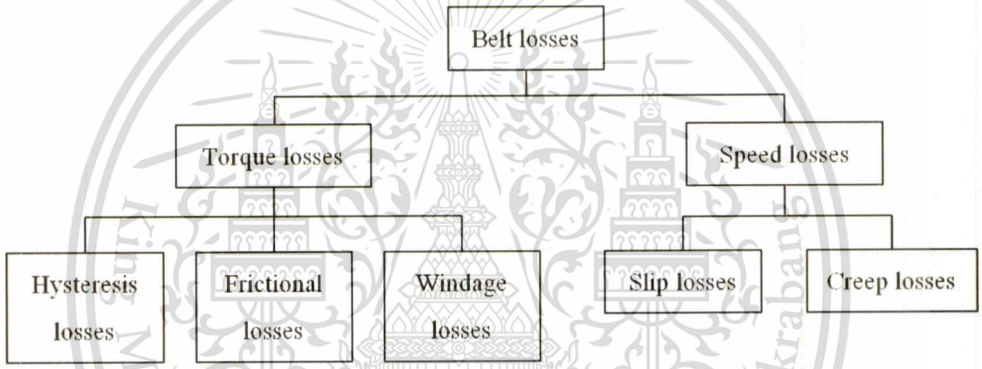

Figure 2.3 Belt losses categories chart

According to the belt losses chart above, hysteresis losses occurred by bending and unbending of belt around the pulleys at 4 points per cycle as shown in Figure 2.4. These losses are depending on the parameters of belt thickness, pulley diameter, and belt material.

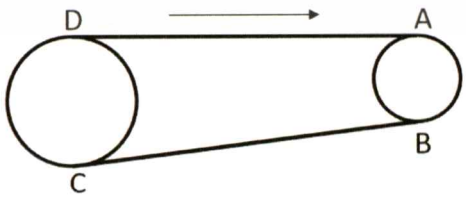

Figure 2.4 Belt drive showing the four flexing points: A, B, C and D [2]

-Frictional losses are losses in contact regions between the side walls of a belt and inside walls of a pulley. These losses occurred while the belt enters and leaves the pulley and use a grip to transmit the power. Therefore, larger frictional losses occurred on the groove pulley type than those of flat or synchronous belt type. Moreover, windage losses are losses occurred while belts moving through the surrounding air. This type of loss increases related to belt speed and roughness of belt surface. For speed losses, slip losses occur when a belt tension is less than a required value to provide enough static friction between belt and pulley. In addition, a belt will be stretched after certain amount of usage leading to a reduction in belt tension. Finally, the belt will slip on the surface of pulley. Moreover, the slips were separated into two main types i.e. micro slip and macro slip as shown on Figure 2.5.

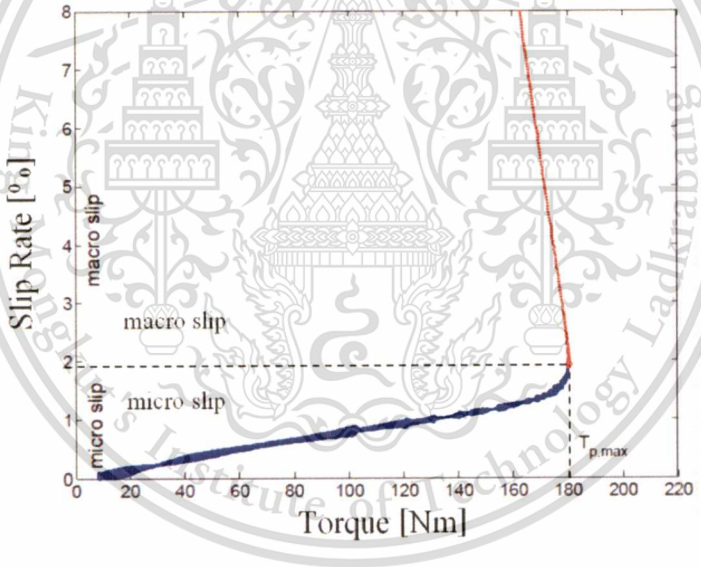

Figure 2.5 Slip curve characteristic [3]

On the other hand, creep losses due to belt are pulled by driver pulley and another end is leaving a driven pulley. In driver pulley side, the belt is pulled and increased in belt tension. Another side the belt is leaving the driven pulley with slower speed. Therefore, belt is effectively elongated.

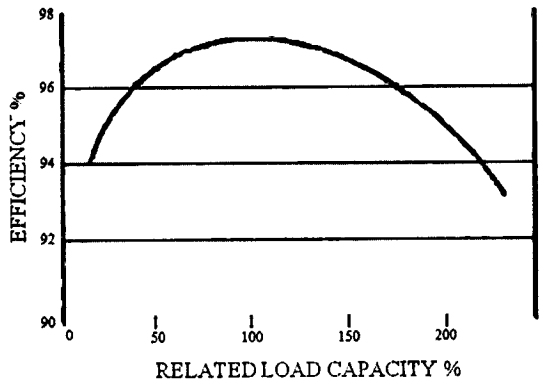

Figure 2.6 Typical efficiency curve of V-Belt [4]

In general, the v-belt transmission reaches the highest efficiency while the system operate under the 100% related load capacity. On the other hand, the efficiency drops when the belt is operated above or below 100% related load capacity as shown on Figure 2.6.

Rated load cause torque losses (hysteresis, friction, and windage). On the otherwise, the efficiency drops in an overload condition is caused by a slip type. In addition, majority of the belt losses are converted to heat. Therefore a high-loss belt will run warmer than a more efficient one.

2.2.2 Belt Experiment

There are many research work which investigated on a belt transmission performance. T. F. CHEND. et al. studied on a transmission efficiency of a rubber V-belt CVT [5]. An experiment of CVT efficiency measurement was done. In detail of experiment, two torque transducers and two rotary encoders were used to measure the input and output torques and speed of the system as shown on Figure 2.7. The results were discussed on power-loss mechanisms from torque loss and speed loss. It was concluded that external loads applied effect to a result of the variation of speed loss, torque loss and efficiency.

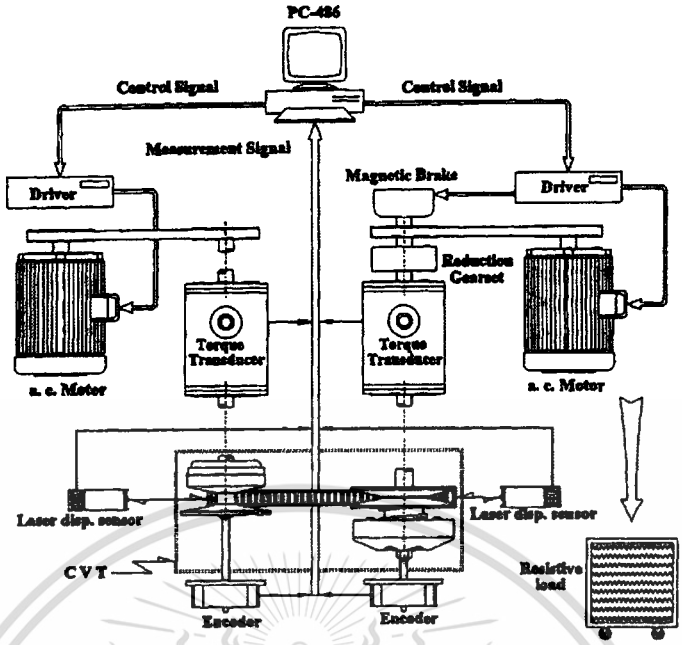

Figure 2.7 Schematic of the experimental setup and instrument for CVT belt efficiency measurement [5]

B.Bosen et al. [6] analyzed the slip in a continuously variable transmission (CVT). The test was setup using two torque sensors installed between a pulley and motor with encoder attached in each drive and brake of motor sides. The special hydraulic unit was setup with a CVT pulley to apply pressure for a clamp force. The slip was analyzed by a ratio of angular speed of secondary axle and primary axle minus by one. It was concluded that the transmission efficiency is depended on applied pressure, input speed and CVT ratio. Moreover, it was reported that the efficiency was clearly higher in medium than in overdrive or low ratio. In medium ratio no slip occurs between the blocks and the bands, on the other hand overdrive or low ratio the bands slip over the blocks.

H. Yamaguchi, et al. [7] presented the measurement and estimation technologies for experimental analysis of metal V-Belt type CVT. A CVT metal V-belt system was tested in a macro slip and a micro slip. The slip was determined by comparing a primary pulley revolution speed and secondary pulley revolution speed. Moreover, the slip velocities of primary and secondary section were investigated by calculating from a difference between belt velocity and pulley velocity.

L. Manin et al [8]. Carried out the experiment by using main apparatuses of rotary encoder (Normally, frequency operation above 2000 pulses/rev), torque sensor, belt tension sensor and data

logger with time synchronize to determine slip in serpentine belt transmission system. The definition of determining slip was each optical encoder delivers a signal of the rotation or change of angular position. Between two rising edges of this signal, there was a counter recorded the number of pulses given by a high frequency clock .The signal output is shown in Figure 2.8 and the slip cloud be determined by calculating from different signal timing.

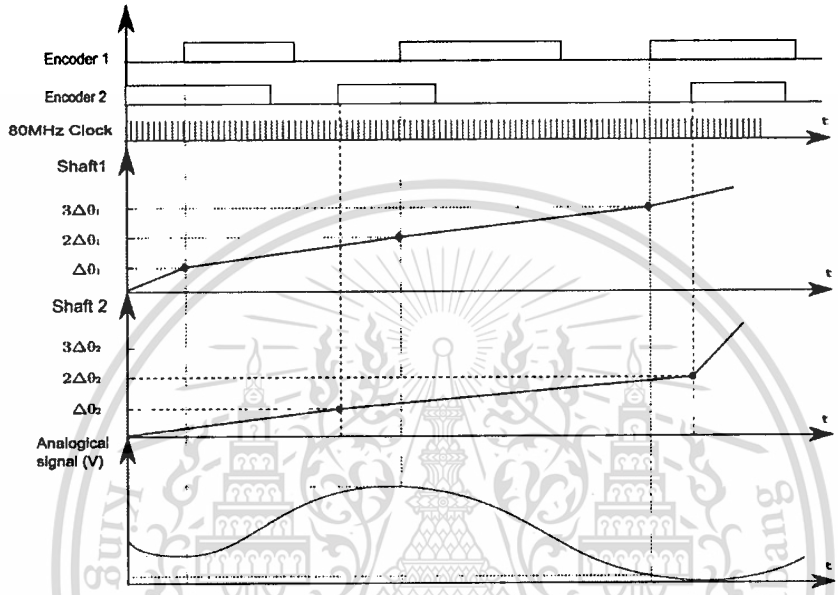

Figure 2.8 Angular rotations measurement of serpentine belt transmission [8]

2.3 Clutch Transmission System

Clutch is an equipment to control a power transmitted from the engine. Clutches are designed to engage and disengage the transmission system and the engine flywheel. The main roles of clutch system are to control a power when an engine runs at standstill or during gear box change.

Generally, the clutch transmission system consists of six main components i.e. fly wheel, clutch disc, clutch cover, clutch fork, clutch hydraulic pump, and clutch housing as shown in Figure 2.9. According to clutch mechanism shown in Figure 2.10, all parts have to work together to control the engagement of a clutch disc to a flywheel surface. When a clutch fork is actuated by a clutch pump, it would press onto a clutch cover spring diaphragm to lift a pressure plate of clutch cover out of the clutch disc surface to allow power disengagement in the system. For engagement configuration,

a clutch fork is released from a spring diaphragm to allow the pressure plate being pressed back to a clutch disc with the maximum force and transmitting the power from the engine to the drive train. In addition, inside clutch disc there is a cushion disc which is used for avoiding unpleasant shock loads, jerks and excessive drivetrain wear [9].

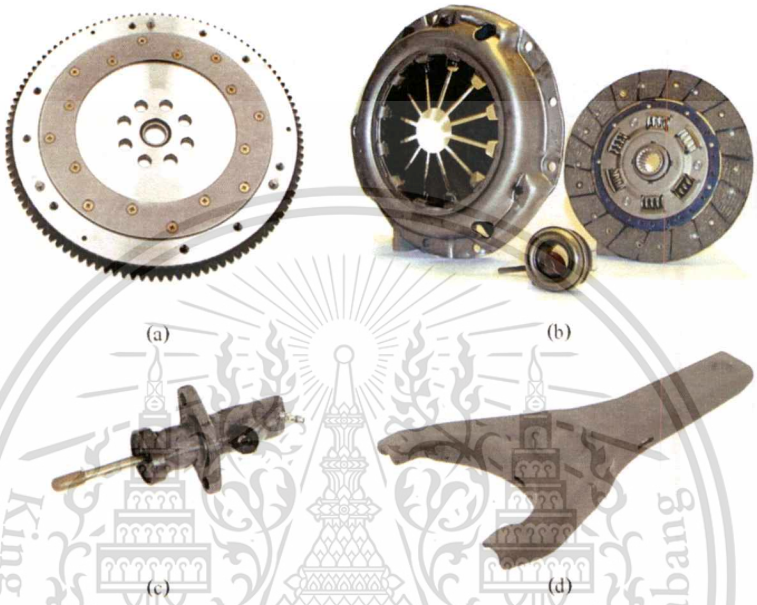

Figure 2.9 Clutch system components: (a) Flywheel, (b) Clutch set: including clutch cover, clutch disc, and bearing, (c) Clutch pump lower, and (d) Clutch fork

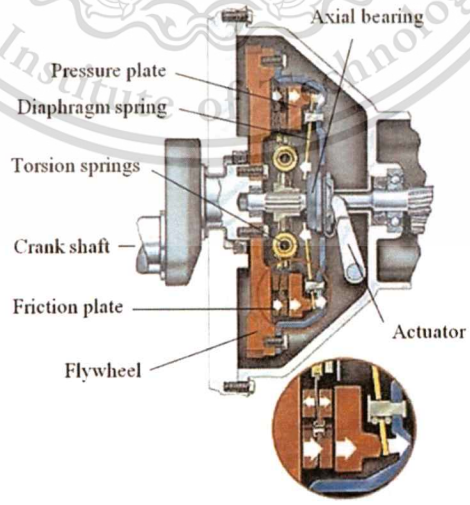

Figure 2.10 Clutch system mechanism lay out [22]

In detail of a specification of clutch system parts, a diaphragm spring and a clutch disc friction coefficient and size is important. Diaphragm spring is a component that generates clamp force to press a pressure plate firmly to a clutch disc and a flywheel. Then the clutch characteristic curves and force general clutch is introduced by Figure 2.11 for more understand in clutch mechanism. In Figure 2.11, the curve is show a clutch characteristic of clamp load force generated while the pressure plate lift or release bearing travel in new and worn clutch disc. In case of clamp load force, clamp load is started to generate while release bearing travel below 2.8 mm and much generate more clamp load when release bearing travel decreased. At the same time, if the release bearing travel more than 2.8mm the clamp load force is voided and the clutch pressure plate is started to lift. Normally, the pressure plate generate clamp load about 5800-6000 N during the operating point.

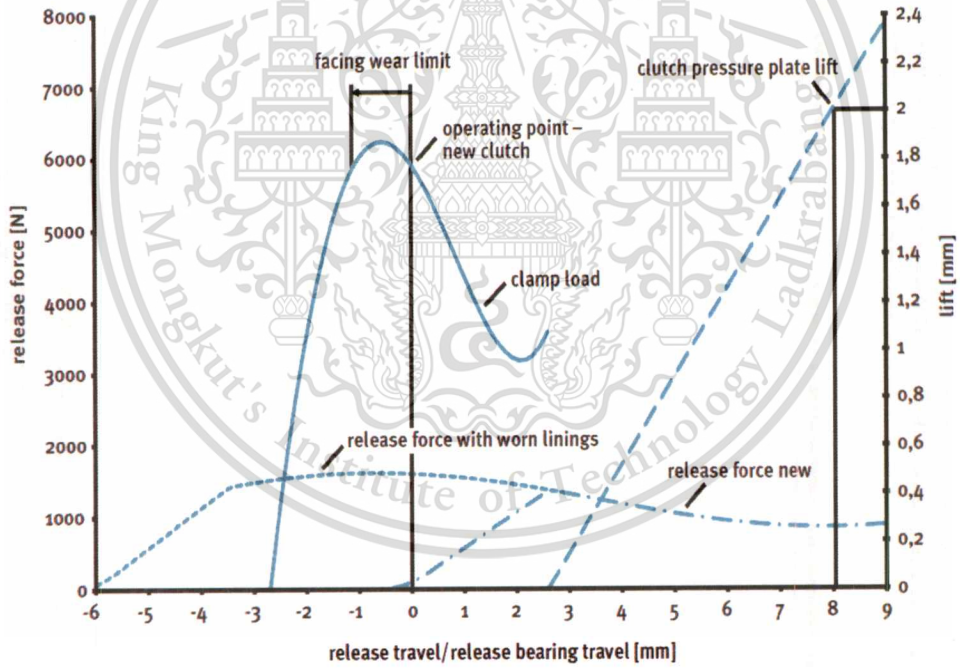

Figure 2.11 Example of clutch characteristic curve and force diagrams [22]

2.4 Model analysis and optimization

2.4.1 Finite element analysis (FEA)

Finite element analysis is used to approximate various problems encountered in mechanical parts such as stress analysis, fluid flow, heat transfer, etc. . In this work, all of analysis cases were related to the structural analysis problem.

The finite element analysis could be divided into three main steps in order to complete a computational estimation i.e. computational modeling, mesh generation, and solution.

Firstly, computational model representing the actual geometry of subject of interest are constructed by using CAD software. The computational models are then prepared for analysis by dividing the model into discrete regions or elements. Each element is connected by nodes. The elements could be divided into 2 dimension and 3 dimension element types depending on an appropriate problem cases as shown in Figure 2.12.

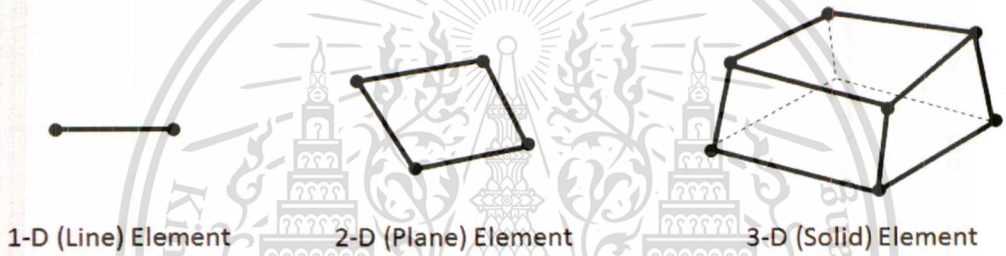

Figure 2.12 Example of element types [10]

Mesh generation is the one of important step in finite element analysis. In case of 3D meshing, element type and a shape quality directly affect to the computational results. Mesh element types are separated in to 4 common element types of Tetrahedron, Pyramid, Prism, and Hexahedron as shown in Figure 2.13.

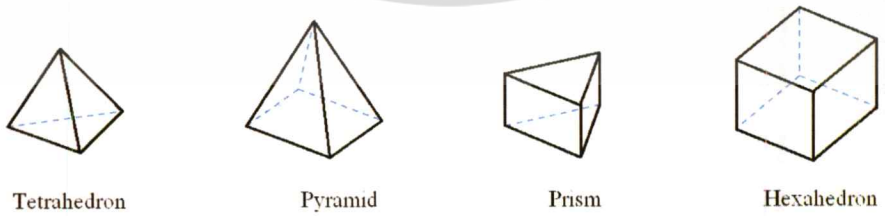

Figure 2.13 Mesh element types [10]

The mesh quality has to be checked by skewness and aspect ratio. For skewness , 0 value is represent the best condition while 1 is the worst with the highest acceptable skewness value of 0.85.

The skewness can be calculated by using equation 2.3 and equation 2.4 for an equilateral volume for triangular and quad as an illustration in Figure 2.14.

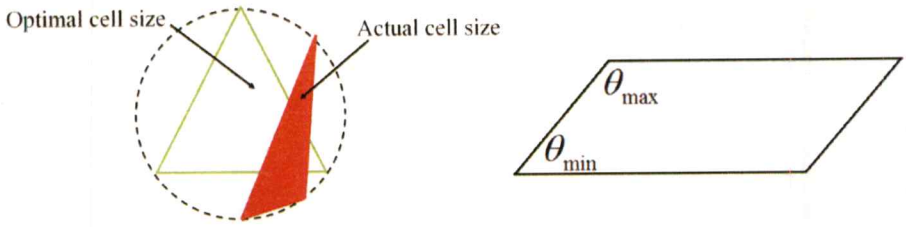

Figure 2.14 Skewness theory based on equilateral volume for triangular and normalized equiangular for quad [10]

Where equilateral volume skewness can be determined by

$$\boldsymbol{skewness} = \frac{\boldsymbol{optimal\ cell\ size - cell\ size}}{\boldsymbol{optimal\ cell\ size}} \tag{2.3}$$

And, normalized equiangular skewness can be determined by

$$\boldsymbol{max} = \left[\frac{\boldsymbol{\theta_{max} - \theta_e}}{\boldsymbol{180 - \theta_e}}, \frac{\boldsymbol{\theta_e - \theta_{min}}}{\boldsymbol{\theta_e}}\right] \tag{2.4}$$

Where $\boldsymbol{\theta_{max}}$ is the largest angle in face or cell

$\boldsymbol{\theta_{min}}$ is the smallest angle in face or cell

$\boldsymbol{\theta_e}$ is an angle for equiangular face or cell by 60 for triangle and 90 for square

The aspect ratio is defined as a ratio of the longest edge length to shortest edge length in a mesh element. The ideal aspect ratio is equal to 1 and increased with increasing of edge length different. The figure is shown on Figure 2.15.

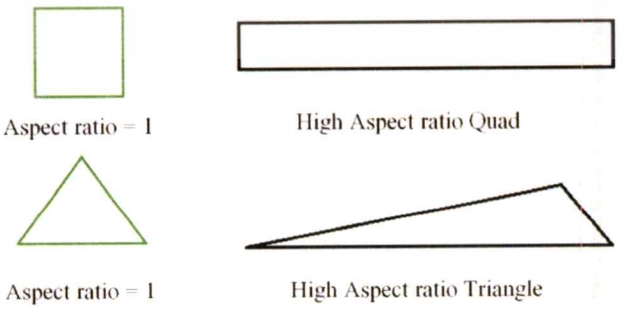

Figure 2.15 Shape of different aspect ratio for Quad and Triangle elements [10]

After the material properties and boundary conditions are applied to the work model, the formula of finite element is used to solve the displacement and the strain of each node and element until the whole model is calculated.

The basic equation of the finite element analysis is described briefly through following equations with a simple spring element [10].

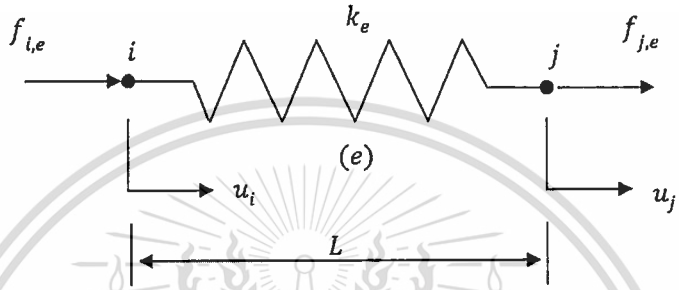

Figure 2.16 Simple spring element

According to the simple spring element, the finite element equation start from the Hooke's law by

$$\sigma = E\varepsilon \tag{2.5}$$

Where σ is a stress and ε is a strain, there are equal force per area and displacement per overall length, respectively.

Firstly, considered on node i by applied force to node i and fixed node j. The equation can be written as

$$\frac{f_{i,e}}{A} = E\left(\frac{u_i - u_j}{L}\right) \tag{2.6}$$

Where A is a constant cross-sectional area

L is a length

E is an elastic modulus

On the other wise, when node i is fixed. The equation can be written as

$$\frac{f_{j,e}}{A} = E\left(\frac{u_j - u_i}{L}\right) \quad (2.7)$$

According to basic spring equation

$$F = Ku \quad (2.8)$$

The spring stiffness can be written as

$$k = \frac{AE}{L} \quad (2.9)$$

Then, the equation (2.8) and (2.9) can be rewritten as

$$f_{i,e} = k_e(u_i - u_j) = k_e u_i - k_e u_j \quad (2.10)$$

$$f_{j,e} = k_e(u_j - u_i) = k_e u_j - k_e u_i \quad (2.11)$$

Write (2.10) and (2.11) equations in to the matrix form

$$\begin{Bmatrix} f_{i,e} \\ f_{j,e} \end{Bmatrix} = \begin{bmatrix} k_e & -k_e \\ -k_e & k_e \end{bmatrix} \begin{Bmatrix} u_i \\ u_j \end{Bmatrix}$$

Then, $\{F\} = [K]\{u\}$ (2.12)

Where [k] is the element stiffness matrix

{u} is the vector of nodal displacement

{F} is of nodal forces

2.4.2 Fatigue analysis

The fatigue failures [12,13,14] normally occur in a mechanical and structural component suffering from cycle stresses while cycle load is applied. Theoretically, the fatigue failure occurr when the component is applied by a cyclic force with an amplitude lower than the ultimate strength. When, the applied force generated a stress level more than fatigue strength of material at N cycles following a S-N curve, the fatigue failure occurs following this step, first crack initiation occurs at

stress concentration point and then crack propagation is started related to load cycle. On the other hand, if generated stress level below the endurance limit of the material, the structure is regarded to have an infinite life. Therefore, S-N curve data in material property is necessary and used to explain a material endurance. The S-N curves are separated into two types of material; endurance limit material and no endurance limit material. Examples of S-N curve of both materials are shown on Figure 2.17.

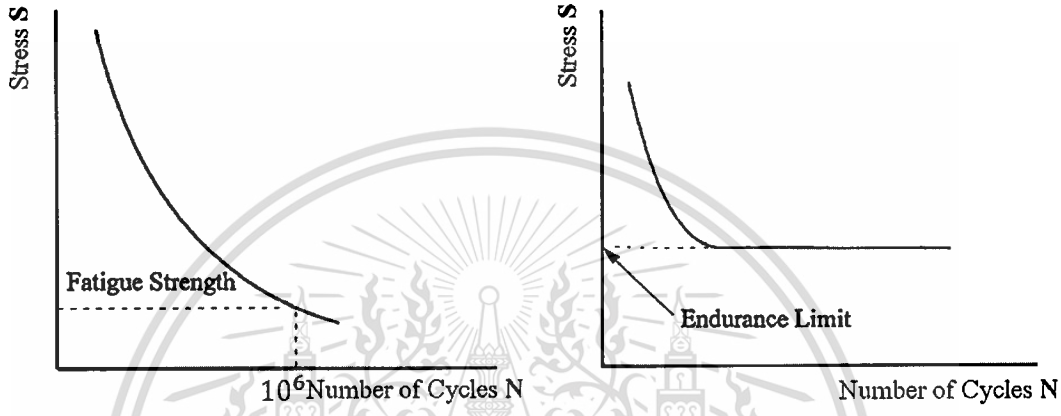

Figure 2.17 S-N curve of no endurance limit and endurance limit

For applied load, a load history data is needed to control a load cycle and generate a stress result. The generated stress results are divided into symmetrical about zero stress, asymmetrical about zero stress, and random stress fluctuations as shown in Figure 2.18. To determine a failure of material Goodman, Gerber, Soderberg, or Morrow method cloud be used to predict a fatigue life. The equation of each method is descripted below.

Goodman (England, 1899) : $$\frac{S_a}{S_e} + \frac{S_m}{S_u} = 1 \quad (2.13)$$

Gerber (Germany, 1874) : $$\frac{S_a}{S_e} + \left(\frac{S_m}{S_u}\right)^2 = 1 \quad (2.14)$$

Soderberg (USA, 1930) : $$\frac{S_a}{S_e} + \frac{S_m}{S_y} = 1 \quad (2.15)$$

Morrow (USA, 1960s) : $$\frac{S_a}{S_e} + \frac{S_m}{\sigma_f} = 1 \quad (2.16)$$

Where S_a is the stress amplitude (σ_a) : $$\sigma_a = \frac{\sigma_{max} - \sigma_{min}}{2} \quad (2.17)$$

S_m is the mean stress (σ_m) : $$\sigma_m = \frac{\sigma_{max} + \sigma_{min}}{2} \quad (2.18)$$

And, S_e is the ratio of the endurance strength, S_u is the ultimate strength, σ_f is the true fracture stress.

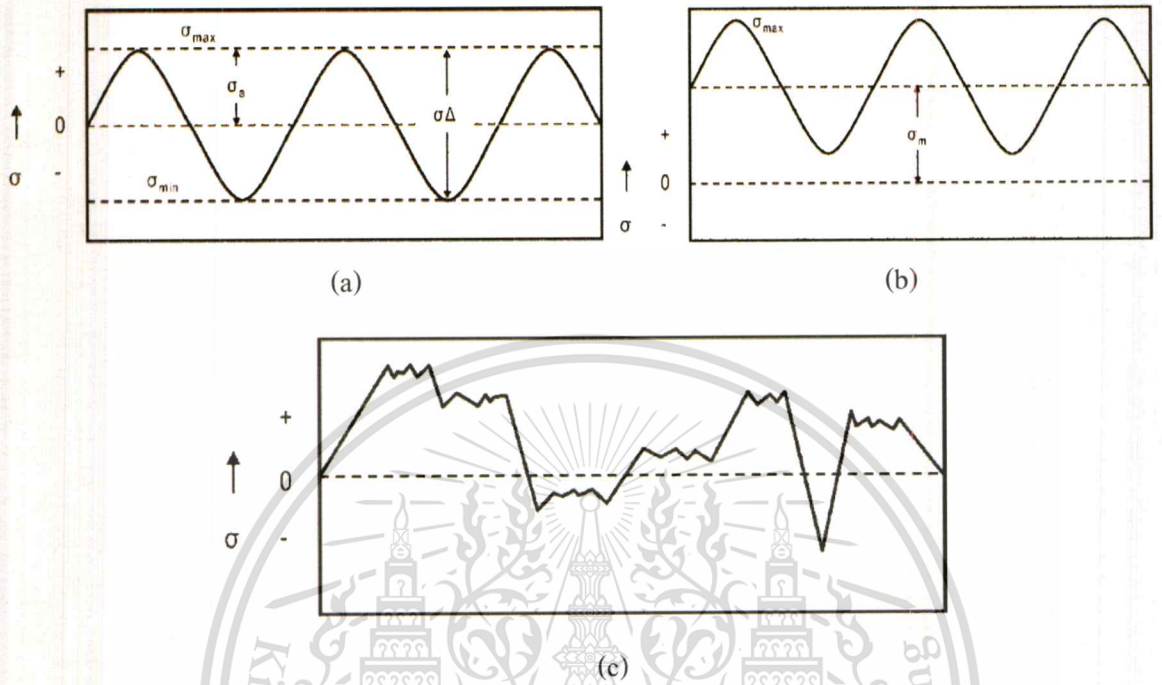

Figure 2.18 Cycling loading conditions : (a) symmetrical about zero stress (Fully reversed loading), (b) asymmetrical about zero stress (Tension –Tension with applied stress), and (c) Random stress fluctuations or Spectrum loading [15].

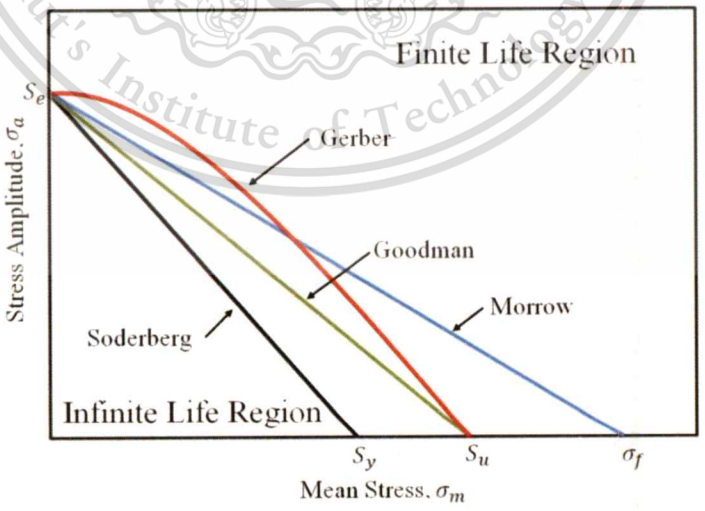

Figure 2.19 Comparison of mean stress equation [10]

2.4.3 Structural Optimization

Optimization is a mathematical technic to predict an optimum point of assigned parameters to archive a specific goal following given constraints. The optimization by a response surface method is one of optimization technics. The procedure starts from a set of design of experiment (DOE) by using the face central composite designs (CCD). The Face –centered CCD becomes a three level design or 3^n factorial design. As a result of DOE, the value is used to construct an equation of relation [16],[17].

In details of equation of relation constructed, the general equation of 2nd order polynomial was expressed as:

$$y = \beta_0 + \beta_1 x_1 + \beta_2 x_2 + \beta_3 x_3^2 + \beta_4 x_4^2 + \beta_5 x_5 \qquad (2.19)$$

Where y is simulated result of maximum von-Mises stress or Volume

x_1 is a 1st parameter variable

x_2 is a 2nd parameter variable

x_3 is a x_1^2

x_4 is a x_2^2

x_5 is a $x_1 x_2$

The coefficient of the 2nd polynomial equation (β) could be obtained from following equation:

$$\beta = (X^T X)^{-1} X^T Y \qquad (2.20)$$

Where

$$Y = \begin{Bmatrix} y_1 \\ y_2 \\ \dots \\ y_n \end{Bmatrix}, \quad X = \begin{bmatrix} 1 & x_{11} & x_{21} & \dots & x_{51} \\ 1 & x_{12} & x_{22} & \dots & x_{52} \\ \dots & \dots & \dots & \dots & \dots \\ 1 & x_{1n} & x_{2n} & \dots & x_{5n} \end{bmatrix}, \quad \beta = \begin{Bmatrix} \beta_0 \\ \beta_1 \\ \beta_2 \\ \beta_3 \\ \beta_4 \\ \beta_5 \end{Bmatrix}$$

Finally, the resulting equations are used to plot a response surface and find an optimum point on response surface on an example Figure 2.20.

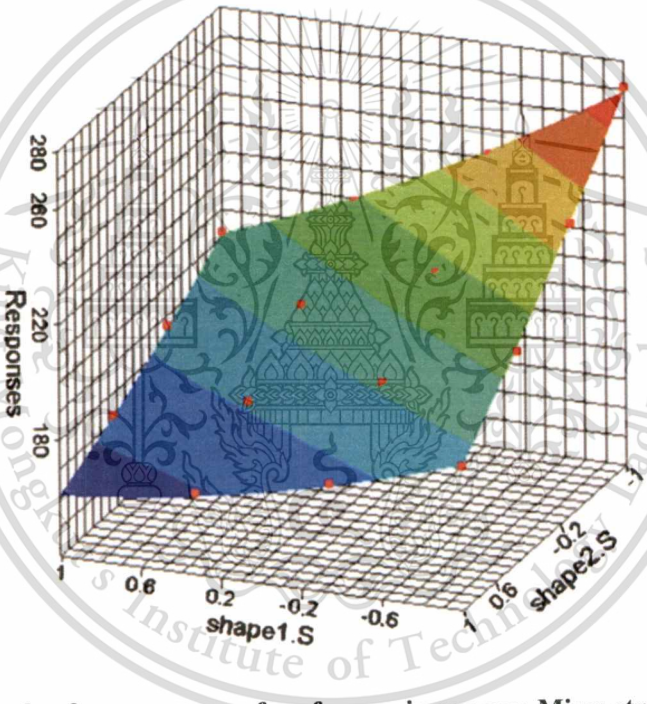

Figure 2.20 Example of a response surface for maximum von-Mises stress of Clutch fork parameter optimization by N. Kaya et al [18].

2.4.4 Previous studies on design, analysis, and structural optimization

In recent years, there have been many studies involving the finite element method to predict failures or analyze resulting stresses. In automotive industry, this method has been used to analyze many automotive parts such as joint yoke and a drive shaft, lower suspension arm, rear axle housing, clutch fork, and etc.

H. Bayrakceken et al.[19] investigated a failure analysis in a universal joint yoke and a drive shaft. In details of study, the failure in joint yoke and drive shaft were investigated by crack failure. First, the material of the joint yoke and driveshaft were investigated for use in the analysis. The AISI 5046H and AISI 94B30H was assigned to be material properties of joint yoke and drive shaft, respectively. The stress analysis was used to determine the stress distribution at the failed section and possible design improvement of each part was investigated. Finally, it was concluded that crack initiation was most likely at a location corresponding to the highest stress point as shown on Figure 2.21.

Figure 2.21 Finite element model and result of the stress analysis of joint yoke and drive shaft [19]

Fatigue life prediction of lower suspension arm was analyzed and investigated by M. M. Rahman et al. [20]. This research was based on fatigue life analysis with some material optimization. After lower suspension arm CAD was modeled. The FE model was prepared for an analysis by using tetrahedral mesh element type. For a loading history, a variable amplitude loading history profile from SAE loading history profile as shown in Figure 2.22 was considered. In this analysis, the fatigue life of part was concerned. Moreover, the materials were set to be a variable by 2014-T6, 2024-T6, 3004-H36, 5456-H116, 6061-T6, 6062-T6, and 7075-T6 to study a possible improvement of fatigue life.

Topaç et al. carried out a fatigue failure prediction of rear axle housing prototype by using finite element analysis [21]. In this case, the rear axle housing was used under high loading capacity. To validate the prototype before mass production, the rear axle housing was tested on the test rig by applied loading from hydraulic actuator. It was found that some of rear axle housings displayed below standard service lifes, therefore the finite element analysis was used to investigate a problem. In this analysis, ANSYS Workbench V11.0 finite element software was used. The load history of cyclic tensile stress was used. It was predicted by the simulation that the crack causing fracture would be initiated at the stress concentrated area of the housing.

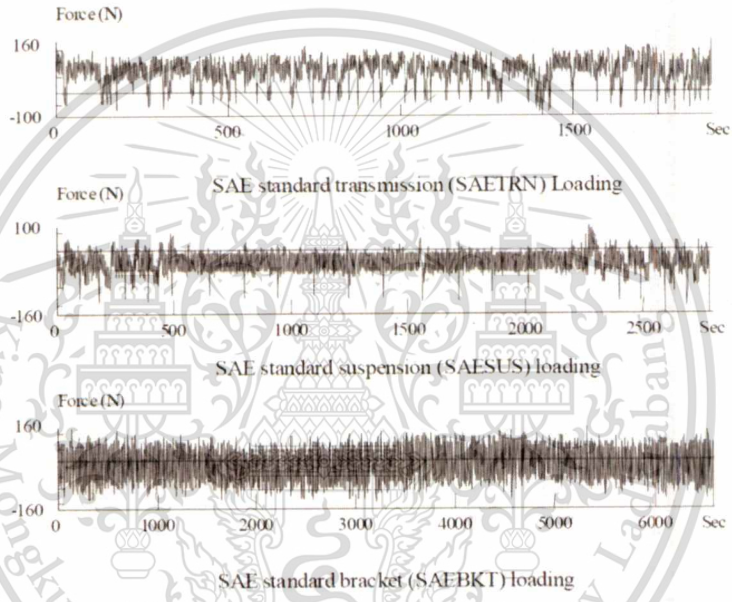

Figure 2.22 Variable amplitude load-times histories by SAE [20]

It could be seen that many work in literature employed a similar kind of sequence or methodology to carry out the research on failure and fatigue study of parts. The common methodology was comprised of modeling a CAD model, performing stress and fatigue life analysis (the boundary conditions and loads needed), and validating results by comparison with experimental results. In some cases, after the finite element was used to analyze a stress, the optimization was carried out to optimize a structure. For example, N. Kaya et al. [18] carried out a stress and fatigue analysis on a clutch fork in order to design a new clutch fork by using topology and response surface optimization method. For a stress and fatigue analysis, a 600N force load was measured in laboratory

and was assigned for a boundary condition to determine a strength of clutch fork by considering maximum von-Mises stress. Furthermore, stress life approach fatigue crack imitation analysis for high cycle fatigue was done to determine a fatigue life of original clutch fork. After that, the new clutch fork was designed by using a topology optimization to create new clutch fork pattern model. In order to get the optimum new clutch fork model, sizes of new clutch fork was set as design variables and optimized by using response surface optimization method to archive a goal of strength and less weight. In details of shape of new clutch fork, the researcher assigned I- type cross section for a new clutch fork with design variables of a beam thickness (dv1, dv2) as shown in figure 2.23.

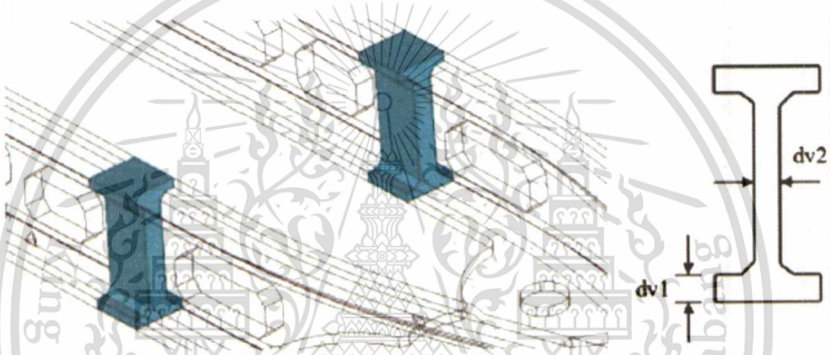

Figure 2.23 I-Type cross sections and design variables [18]

CHAPTER 3

DIRECT CLUTCH SYSTEM DESIGN CONCEPT AND SPECIFIC CONCERN

3.1 Conventional model of an E-TAND or agricultural truck in Thailand

Normally, E-TAND is assembled by local mechanics, often with limited engineering skills and consists of parts from the second hand market especially those in transmission system such as gear box, rear axle, etc. A typical structural layout of E-TAND is shown in Figure 3.1. E-TAND chassis is used C channel steels assembly into flat ladder shape chassis by welding. Leaf springs with shock absorbers are used in front and rear of E-TAND suspension. A drum brake is selected for E-TAND as used in general truck. For transmission system, a one-cylinder diesel engine is selected to be a prime mover of this type of vehicle. The engine is assembled on to a sub frame that mounted in front of chassis. In addition, this engine has a dry weight of 116 kg that generate maximum horsepower of 14 HP at 2400RPM with a maximum torque of 5 kg-m at 1600 RPM as mention on Table 3.1. In detail of power transmission, a V-belt is used to deliver the power from the engine to the gearbox as shown in Figure 3.2 with two pulleys are attached on an engine flywheel side and a clutch system side. In the clutch side driveline, a shaft is connected directly to a clutch and after that a gearbox. In order to change a transmission ratio, a clutch has been actuated to regulate a power to allow gear shifting. According to the characteristics of the V-belt transmission, this system is normally accompanied by noticeable loss in transmission efficiency. Thus, the concept of direct clutch system has been introduced for this type of vehicle in this study.

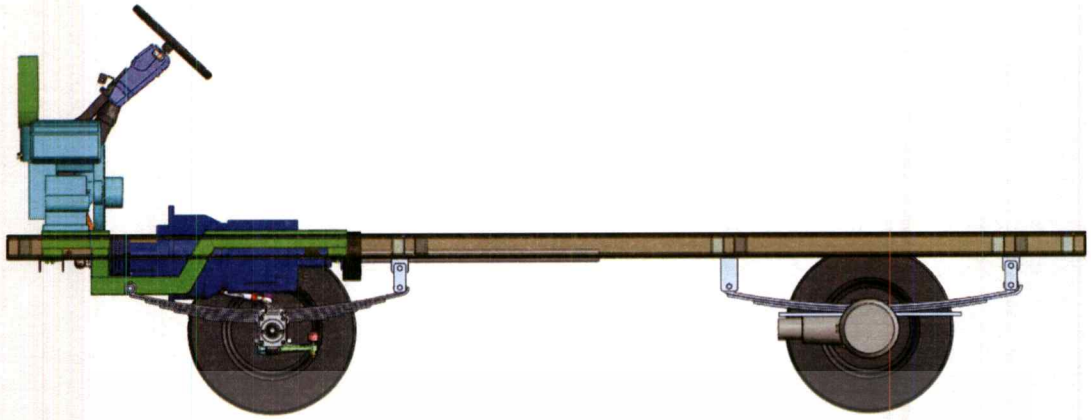

Figure 3.1 CAD model displaying basic structure of conventional E-TAND

Figure 3.2 Conventional transmission arrangement of E-TAND

Table 3.1 Engine Specification (KUBOTA RT140)

Description	Technical data
Number of cylinders	1
Displacement	709 cc.
Maximum output	14/2400 HP/rpm
Continuous rated output	12.5/2400 HP/rpm
Maximum torque	5.0/1600 kg-m/rpm
Dry weight	116 kg

3.2 Modeling concept and design considerations

In this section, specific concern for design and selection of each part are described. The design part will be explained following the sequence as shown on chart diagram in Figure 3.4.

The concept of direct clutch system is removing a belt system out from a power transmission sequence. For a design space, the engine and the gearbox are fix constraints. A space between two constraints is the direct clutch system design space. The direct clutch system consisted of a clutch contact surface, clutch housing, clutch set and clutch fork. These lists of components have to be design follow constraints and specific concerns.

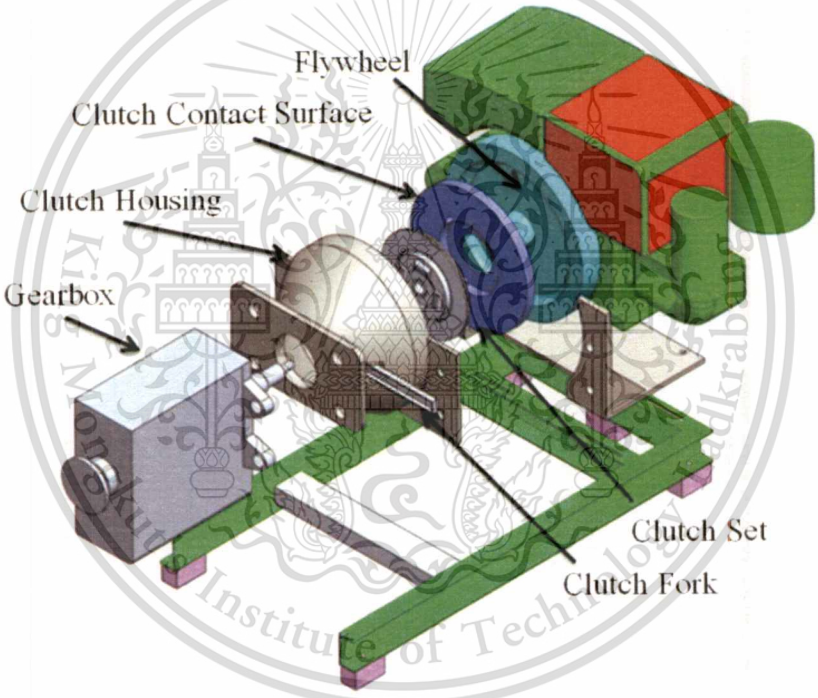

Figure 3.3 One-cylinder diesel engine clutch transmission layout

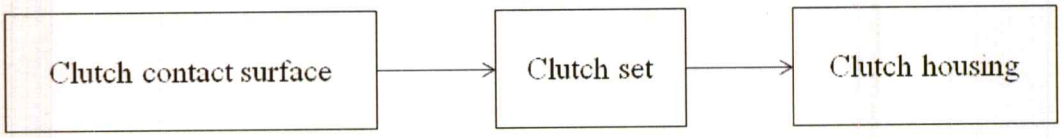

Figure 3.4 Power transfer chart on clutch transmission driveline

3.2.1 Clutch set

Clutch set consists of clutch disc and clutch cover. In this work, a clutch set was selected from the commercial product available in the market to match with type of the engine i.e. 14HP with maximum torque of 5 kg-m. The TOYOTA Hilux EXEDY single organic clutch disc set (Figure 3.5) was selected due to torque capacity, size, and availability in local markets. The most important part was matching the dimension with the clutch contact surface. Generally, TOYOTA Hilux EXEDY clutch set is used to transmit the power in light truck with an engine torque of approximately 162 Nm. In addition, the inner and outer diameters of friction pad are 153.8mm and 235mm respectively. Rated friction coefficient of organic facing type friction pad is about 0.27-0.32. To confirm the clutch set torque capacity, the transmittable torque was calculated by using equation (3.1) [Luk].

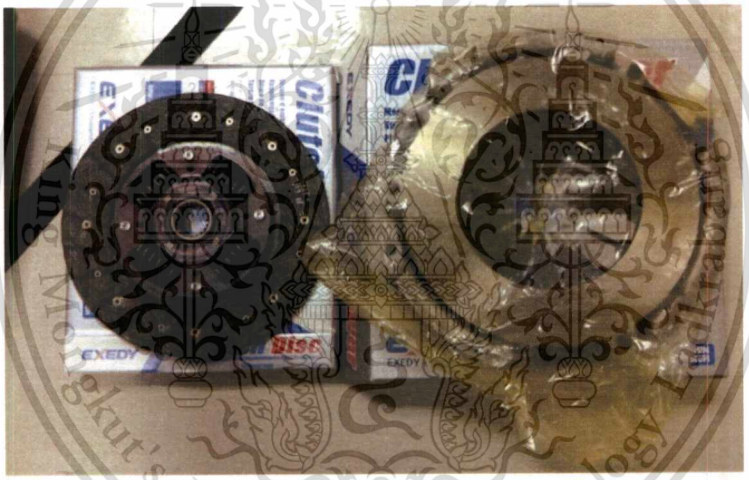

Figure 3.5 Commercial TOYOTA Hilux EXEDY clutch set

The Transmittable torque equation [22]:

$$T = r_m \cdot n \cdot \mu \cdot F \tag{3.1}$$

Where

T is Transmittable torque (Nm)

$r_m = \frac{d_m}{2} = \frac{1}{2}\left(\frac{d_i + d_o}{2}\right)$ is Mean friction radius (m)

d_m is Mean friction diameter (m)

d_i is inner diameter (m), d_0 is outer diameter (m)

n is Number of clutch facing (single disc = 2)

μ is Friction coefficient

F is Clamp load (N) (clamp load ≈ 3500N)

Result

$$T = \frac{1}{2}\left(\frac{0.1538+0.235}{2}\right) \cdot 2 \cdot 0.27 \cdot 3500$$

$$T = 183.70 \text{ Nm}$$

From calculation results, the selected clutch set could provide the transmittable torque of approximately 183.70Nm which was higher than maximum torque generated by engine of 49.05 Nm. So, this clutch set could be used in this system.

3.2.2 Clutch contact surface

Clutch contact surface is used to transfer the power from the engine to the clutch system. Generally, a conventional car flywheel would have a portion of surface already assigned for a clutch disc contact. On the other hand, a flywheel of one-cylinder diesel engine has no such surface feature. Therefore, an additional clutch contact surface had to be integrated into the system. The design conditions of clutch contact surface were installation space, and minimum weight. The size of clutch contact surface was restricted by a dimension of clutch set, pilot bearing, and mounting location on original flywheel as shown on Figure 3.6. For ease of use, it was decided that the new clutch contact surface was to be installed onto the engine flywheel by means of bolts through the existing pulley mounting locations.

Figure 3.6 Flywheel comparison (Left) one cylinder diesel engine flywheel (Right) conventional engine flywheel (Clutch disc contact surface : Green area)

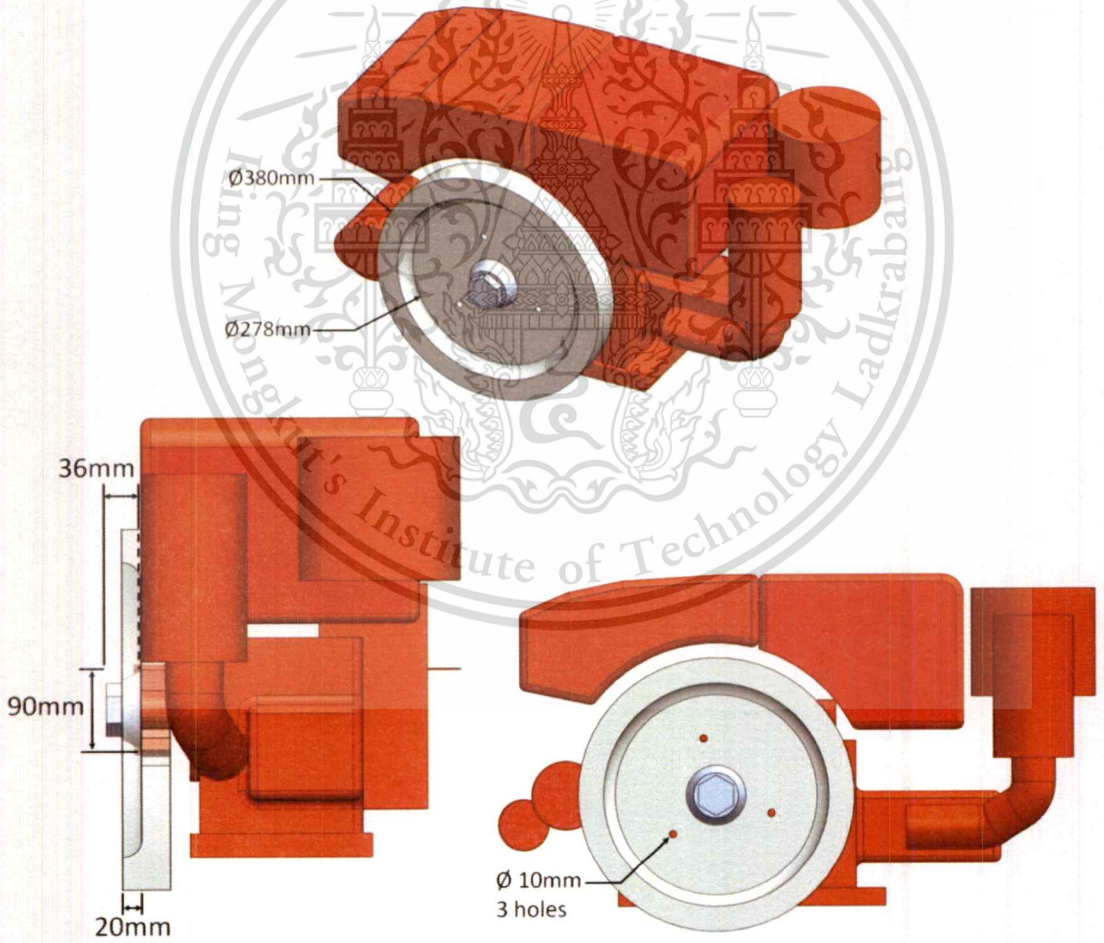

Figure 3.7 Clutch contact surface design constraints: flywheel geomentries (all dimensions in mm)

From the original flywheel dimension shown in Figure 3.7, there were 7 concerning points for clutch contact surface design. There are consisted of height and diameter of flywheel locker nut, inside and outside diameter of flywheel rib, height of flywheel rib, pilot bearing housing, clutch set and mounting location. According to all constrained mentioned, a clutch contact surface should has a roughly dimension of 320 mm. of out diameter with a space on locker nut of 90 mm. and 40 mm of depth on the back. In the front, a 160 mm of diameter with 5 mm of depth are required for space of a clutch disc hub located. Lastly, 6 drill holes are needed for fly wheel and clutch cover mounting by 3 each.

After clutch contact surface was designed following concern topics. The final model, ready for computational analysis, was obtained as shown in Figure 3.8.

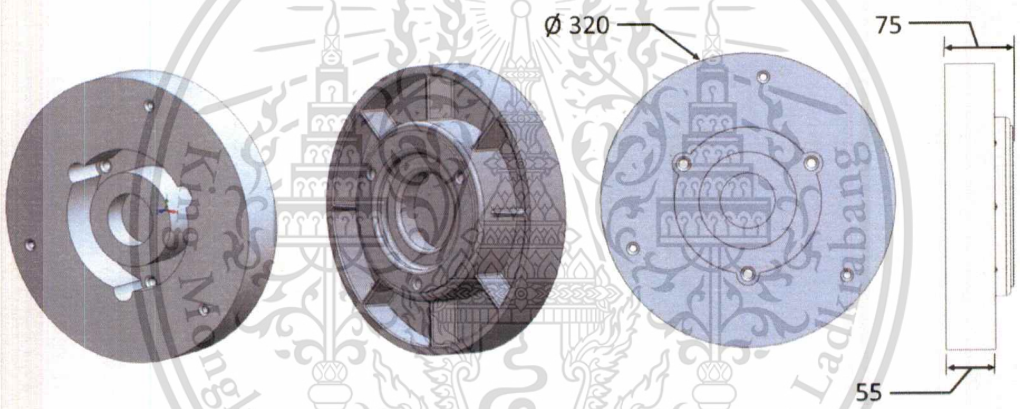

Figure 3.8 Clutch contact surface prototype CAD model (all dimensions in mm)

3.2.3 Clutch housing

Clutch housing was a part that would be located between engine and gearbox while covering all components of the direct clutch system. The overall design was constrained by an access point of clutch fork with pivot mounting, and dimensions of clutch system and flange of gearbox. The design space and working space constrain are illustrated in Figure 3.9.

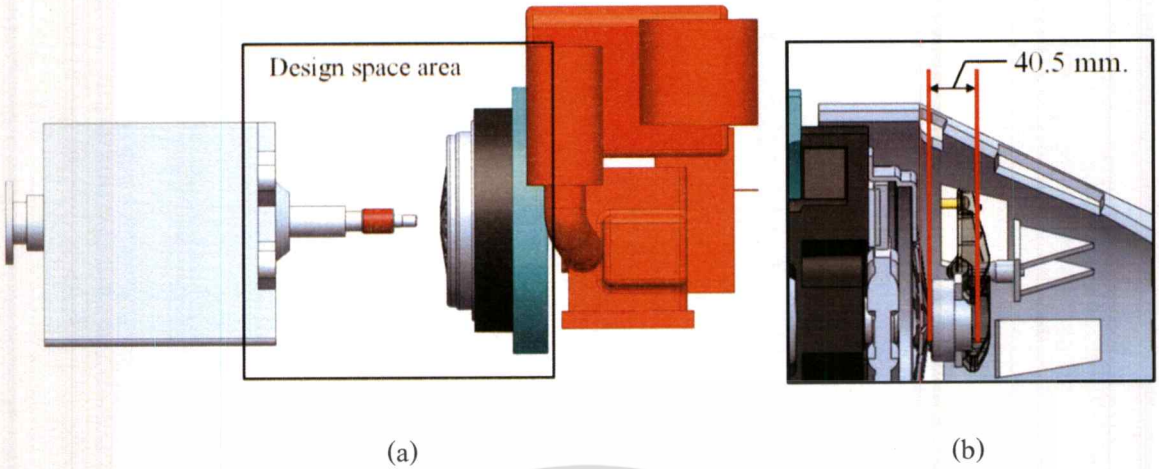

Figure 3.9 Clutch housing design constraints (a) Design space area (b) Clutch fork mounting pivot distance

In addition, this clutch housing was designed for using with one cylinder diesel engine which is commonly known to generate very high amplitude of vibration during operations. Therefore, a misalignment problem was to be expected. In theory, the engine and the clutch housing should vibrate together to avoid a problem of misalignment when the engine was operated. In order to solve this problem, a mounting part was introduced to connect the engine with the clutch housing on the same platform. The mounting part was designed to be a support plate under the engine base while on another side was the flange for bolting onto the clutch housing. The initial clutch housing model is shown in Figure 3.10. This clutch housing set consisted of 2 parts i.e. housing part and mounting part.

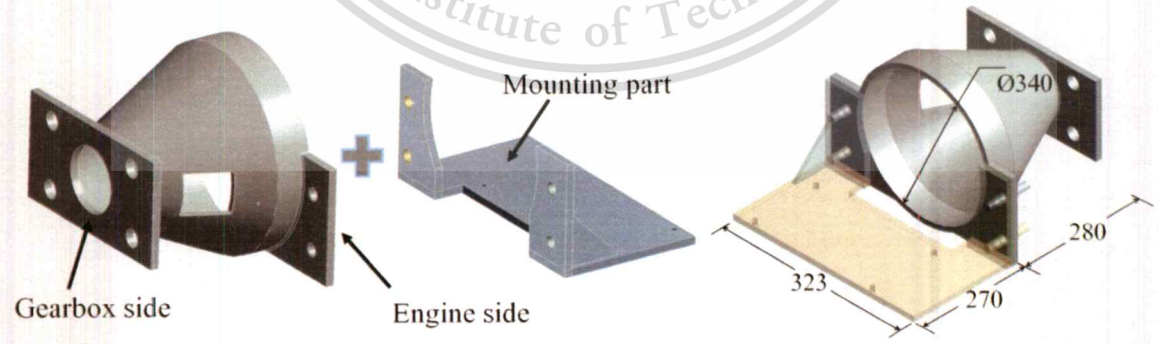

Figure 3.10 Clutch housing prototype CAD model (all dimensions in mm)

According to the engine vibration and clutch housing model, the assumption of failure or structural weak point caused by engine vibration was mainly considered on the middle portion of the clutch housing. In this case, modeled clutch housings were analyzed by using finite element software. Furthermore, to achieve weight efficiency for design of the clutch housing, the physical design aspect of the clutch housing would be investigated under an optimization process. All these analytical details will be reported in the next chapter.

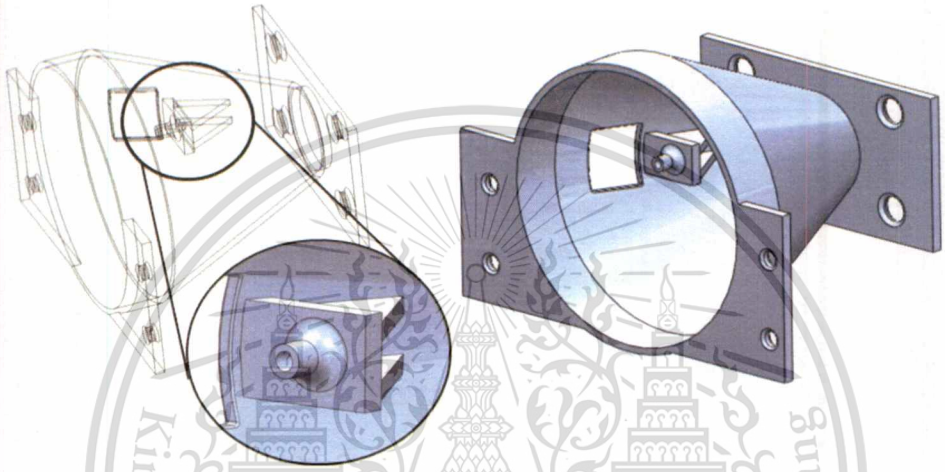

Figure 3.11 Clutch housing CAD model with a pivot mounting.

3.2.4 Gear shaft adapter

In this study, the selected gearbox was a big truck gear box while, as reported in the previous section, the selected clutch set was from a small-size truck. As a result, the gear box shaft spline and the clutch disc spline hub were not matching for assembly as shown on Figure 3.12.

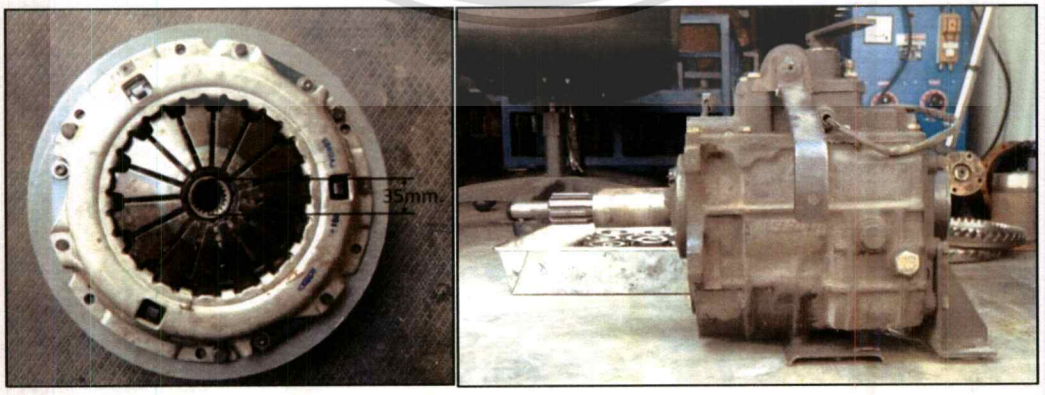

Figure 3.12 Difference in spline size and type between gearbox and clutch disc

To solve this problem, an additional shaft adapter was designed to act as a connecting part. Sizes of gearbox shaft, clutch dish hub, and length of clutch housing were considering points. The appearance of design gear shaft adapter was a small piece of shaft with a two different sets of spline and diameter on each side as shown in Figure 3.13. This part was located on the middle section between the gearbox and the clutch disc. From mechanical point of view, the proposed shaft adapter had to be analyzed under the condition of a twisted load presumably from the torque transmitted from the engine to the gear box. The analytical work is reported in the next chapter.

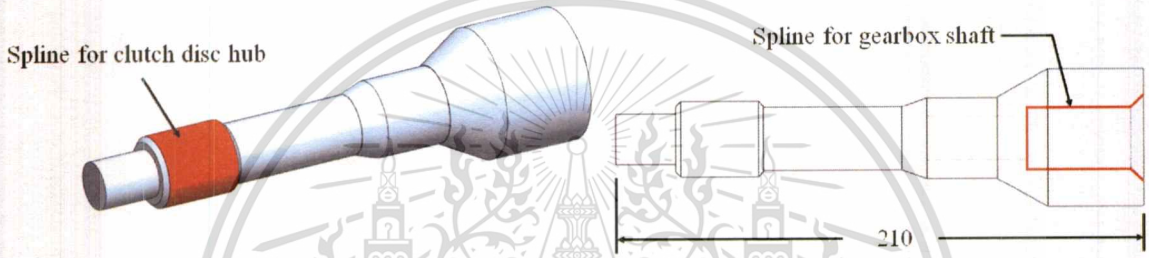

Figure 3.13 Gear shaft adapter CAD model (all dimension are in mm)

In this section, general constraints and specific concerns of direct clutch system for system design were presented. Firstly the clutch set was selected by calculating through the transmittable torque equation to compare with an engine power. After that, the appropriate clutch set dimensions were used as a design constraint for a clutch housing and a clutch contact surface design. Then, the clutch housing including mounting plate and the clutch contact surface were parallel designed following constraints of dimension and mounting space of the clutch set, the engine, and the engine flywheel. Moreover, the clutch housing was confronted with an engine vibration load, while the clutch contact surface faced with clamp load from the clutch set. In detail of clutch contact surface was mounted by bolts, stress generated on each bolts had to be take care. Lastly, a gear shaft adapter was designed with a torsion load design was concerned.

CHAPTER 4

METHODOLOGY

4.1 Vibration load profiles measurement of one cylinder diesel engine

In present work, vibrational load profiles were measured at various engine load conditions. The test was carried out on a dynamometer test configuration. The RT140 KUBOTA engine, which was commonly used in E-TAND, was selected to study and investigate.

4.1.1 Experimental setup

The apparatuses of vibration experiment (Figure 4.1) were comprised of

- 14HP,Direct injection engine (KUBOTA RT140)
- Data acquisition tools :NIcDAQ-9172 and NI 9234
- Accelerometers; Brüel&Kjær Type 4507 B002
- Dynamometer with Dynamo controller
- NI Sound and Vibration Assistant software

In this experiment, the test engine was operated at 3 different load cases which were idle load (1120 rpm), partial load (60% of throttle, 1800 rpm), and full load (100% of throttle, 2200 rpm). The accelerometers were connected with NI DAQ set and were attached at front and rear end of engine wood base plate as shown in Figure 4.2. The test results were recorded by using NI Sound and Vibration Assistant software with a sampling rate of 1000Hz. The experiments were repeated for 3 times at each location for all load cases to confirm a repeatability of the results.

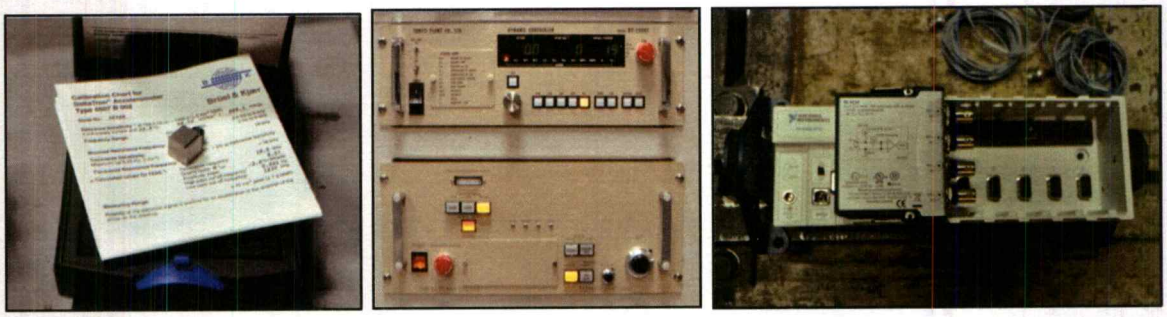

(a) (b) (c)

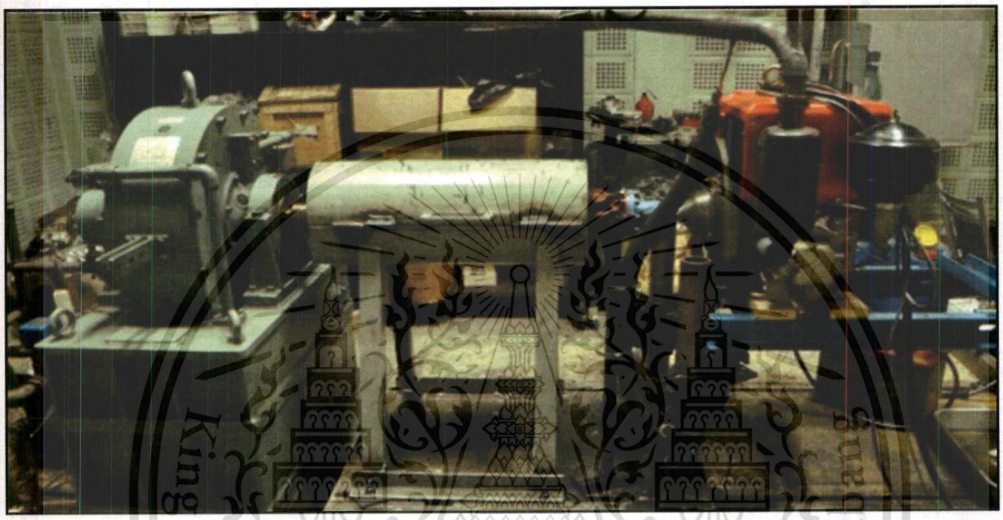

(d)

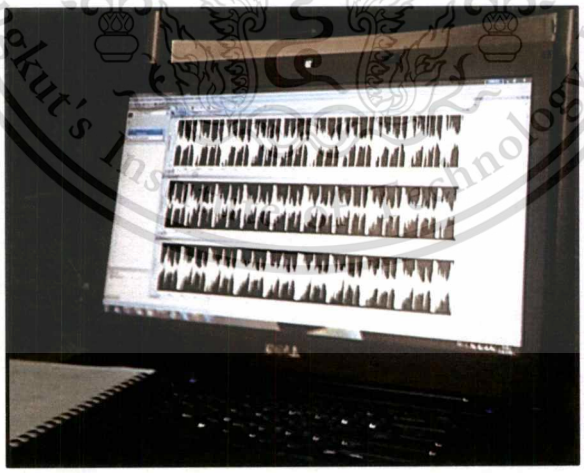

(e)

Figure 4.1 An experimental set up for vibration load measurement: (a) single axis accelerometers, (b) dynamometer load controller, (c) DAQ equipment, (d) dynamometer chassis with test engine, and (e) front panel for DAQ devices interface.

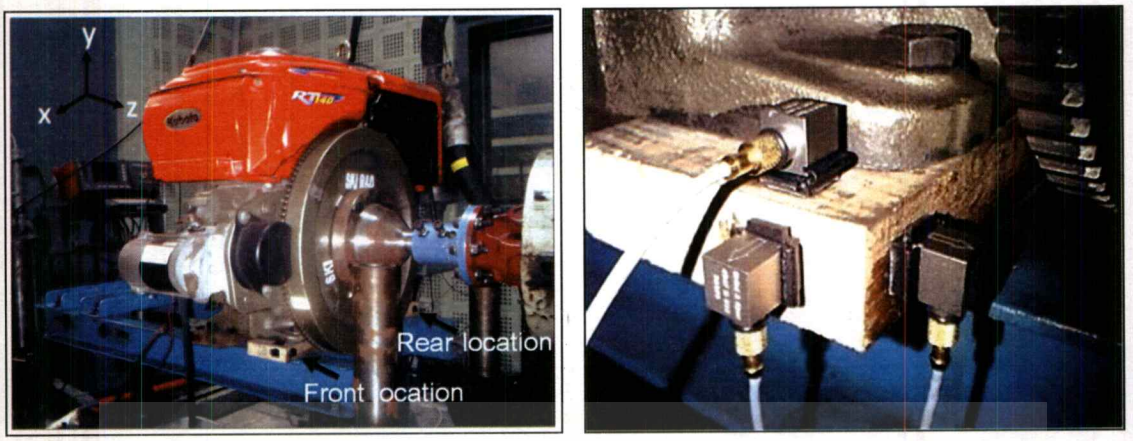

(a) (b)

Figure 4.2 (a) accelerometer attach locations (b) accelerometers attachment configuration near engine base.

4.1.2 Data post processing for clutch housing analysis

In order to use the obtained experiment data in a simulation analysis of the clutch housing, the raw data were passed through a low pass filter to collect corresponding data in a frequency range below 60Hz while at a maximum load engine operates at 2200 RPM or 36.67Hz. In this step, the MATLAB software "FILTFILT" function was used to filter a data.

For the structural and optimization analysis, an input parameter had to be applied as a force. Therefore, the measured acceleration values were converted into corresponding forces by multiplying with an engine effective mass in front and rear portions. Assuming that center of gravity (C.G) of engine was located at center of a flywheel, effective mass of engine at front and rear support locations were calculated by basic Newton's law as shown in equations (4.1), (4.2) to be 73.51 kg and 38.49kg. The engine load distribution is shown in Figure 4.3.

$$\sum \circlearrowleft + M_{rear} = 0 \quad 112 \times 212 = W_{front} \times 323 \tag{4.1}$$

$$W_{front} = 73.51\ kg$$

$$\sum + \uparrow F = 0 \quad 112 - 73.51 - W_{rear} = 0 \tag{4.2}$$

$$W_{rear} = 38.49\ kg$$

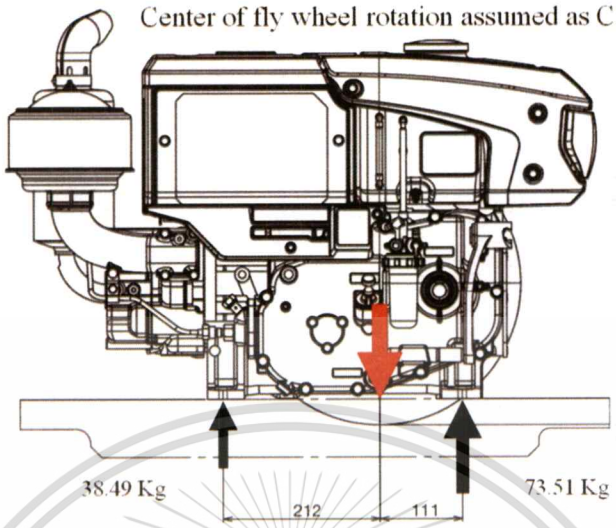

Figure 4.3 Engine load distribution

Furthermore, for fatigue failure mode simulation, a load history was required. As results, vibration profiles from each experiment cases were combined together with reference to TIS (Thai Industrial Standard) 2155-2546 driving cycle which was an equivalent of EUDC (Extra Urban Cycle Test) shown in Figure 4.4. The assumption of a relationship between a driving cycle and an engine load were defined such that while the vehicle was accelerated, the engine ran with full load. On the other hand, the engine ran at partial load and no load, when vehicle ran on cruise speed and decelerated respectively.

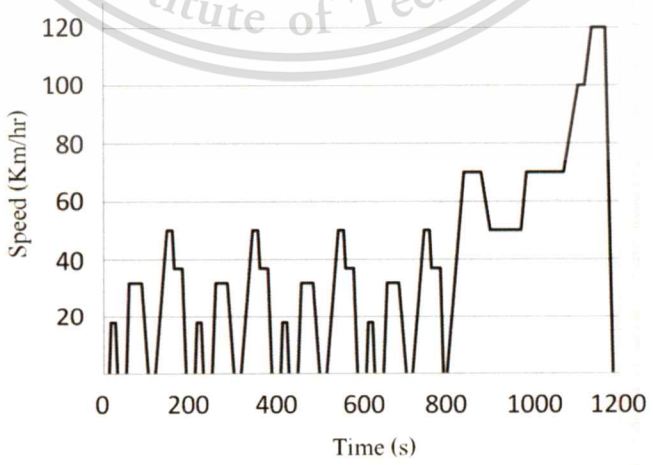

Figure 4.4 EUDC standard: Driving cycle for 1 day, [23]

4.2 Clutch housing

The computational analyses consisted of structural stress and fatigue life analysis by converting measured vibration profile from engine experiments into corresponding forces as explained in previous section. Moreover, an optimization technique was used to find an optimum design of a clutch housing suitable for one cylinder diesel engine application.

4.2.1 Clutch housing structural and fatigue analysis

In order to determine the stress generated and analyze a fatigue failure of the clutch housing under the vibrational loads from the engine, the finite element analysis was applied on to the CAD models. The main clutch housing components that were necessary for computational analysis were combined of total 3 parts as shown in Figure 4.5. Furthermore, as initial parameters of simulation, the mounting plate and the clutch housing were assigned a thickness of 13mm with a clutch housing slope angle of 65 degrees.

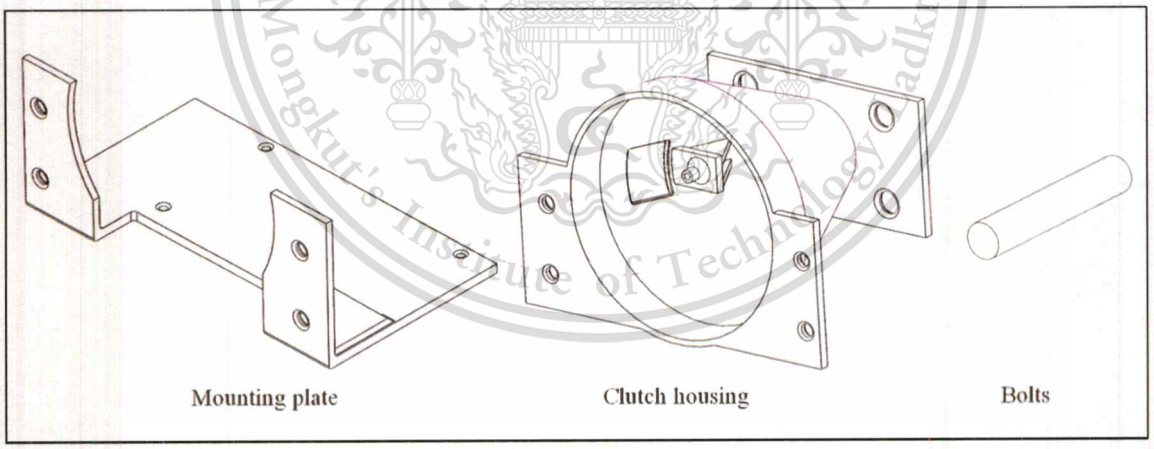

Figure 4.5 CAD models of clutch housing parts for computational analysis

4.2.1.1 Mesh model preparation

A mesh model of assembled clutch housing was prepared using ANSYS® software. Two types of mesh element were used, i.e. hexahedron for bolts and mounting part, and tetrahedron for

clutch housing with a global element size of 6mm, 4mm, and 5mm respectively. In addition, each part was contained with elements which had skewness value lower than 0.75. The clutch housing FE model is illustrated in Figure 4.6.

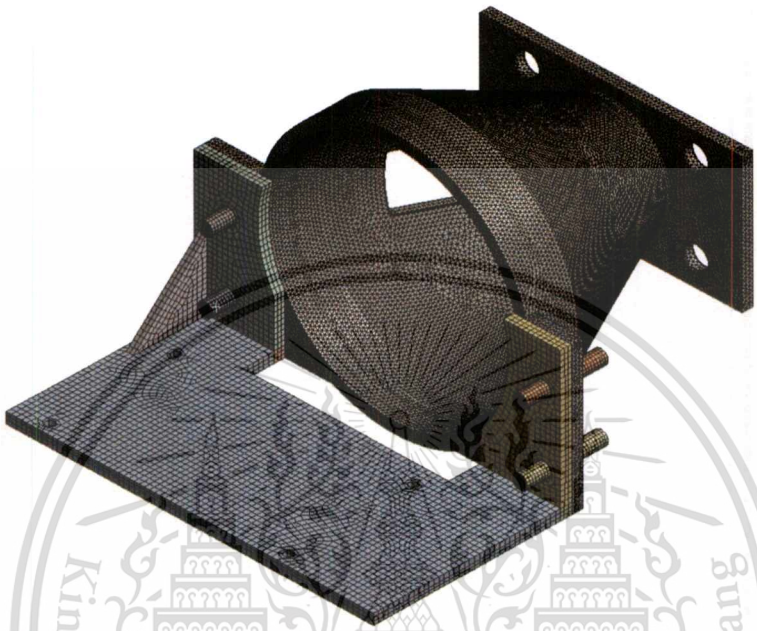

Figure 4.6 Finite element model of clutch housing

Table. 4.1 Mechanical properties of Structural steel from ANSYS ® software

Properties	**Value**
Density: ρ (kg/m^3)	7850
Young's modulus: E (GPa)	200
Poisson's ratio: v	0.3
Yield strength: σ_y (MPa)	250

4.2.1.2 Material

For a computational analysis, a structural steel was chosen as material for all parts. Corresponding mechanical properties were taken from engineering data in ANSYS® software. Table 4.1, including S-N curve for fatigue analysis is shown in Figure 4.7.

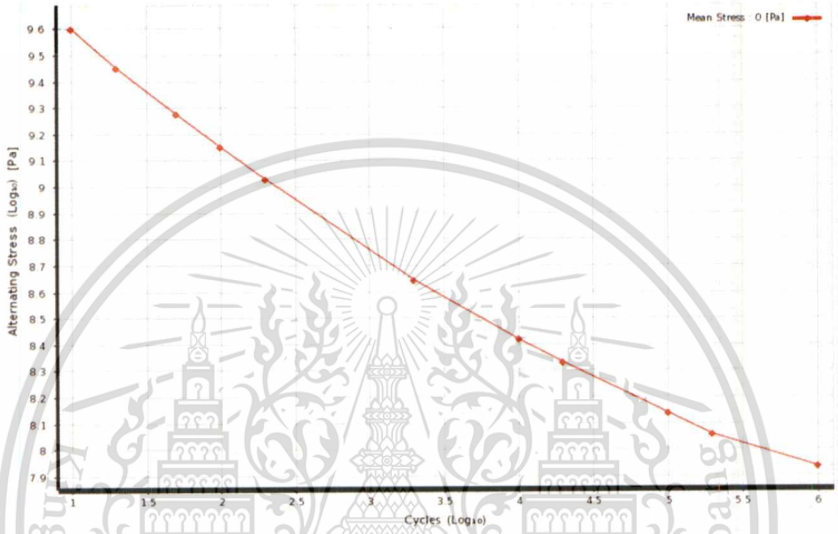

Figure 4.7 S-N Curve of a structural steel from ANSYS Engineering data

4.2.1.3 Boundary Conditions for Clutch housing Structural and Fatigue analysis

Boundary conditions applied in this study are graphically shown in Figure 4.8. The clutch housing was considered under a stress when subjected to engine vibrations. The loads collected from the experiment were applied as a force loading. Amplitude of force loading was referred to a maximum force in full load conditions as mentioned in chapter 4.1. In addition, the input force loading was applied on both front and rear holes at the engine base plate of mounting part to simulate a clutch housing twisted situation similar to a real system operation.

An amplitude force was used in a static structural analysis while combined force amplitudes were applied as a load history for fatigue analysis. On the other hand, a fixed support was applied on the inner holes surface flange of clutch housing at the gearbox side. Moreover, the mean stress Goodman criterion was used in this work. In addition, a safety of factor of 3 was considered.

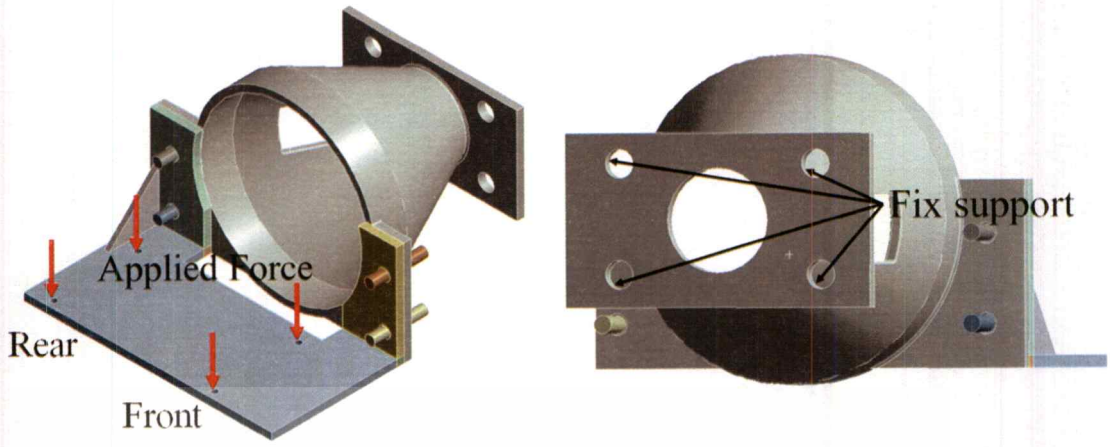

Figure 4.8 Boundary conditions for clutch housing analysis

4.2.2 Clutch housing optimization

In order to find the optimum design for the clutch housing, and making sure that the possible lightest weight clutch housing is take care of for merit. Therefore, the optimization was carried out by using response surface method with full 2^{nd} order polynomial algorithm.

The optimization processes were combined by a use of ANSYS® Design Exploration Response Surface with the full 2nd order polynomial algorithm and MATLAB software to calculate and find the optimum clutch housing prototype model. The goals of this optimization were to reach a safety factor target of 3 or maximum von-Mises stress equal to 83.33MPa with structural steel as a material, to minimize volume or weight of clutch housing, and to have no failure in fatigue mode.

The optimization step started with a design of experiment (DOE). The design of experiment (DOE) used 3 factor levels and 2 parameters (3^n factorial design) i.e. 3^2 or 9 design points. Each parameter was divided into 3 ranges of value i.e. maximum, middle, and minimum for each factor design point. After 9 design points were completed, the equation of parameters relation were constructed by using 2^{nd} order polynomial technique from the DOE table results as mentioned in section 2.4.3. Finally, a response surface was plotted and the optimum point was found on that response surface.

In the first part of optimization process which was a size optimization, design of experiment (DOE) were based on 2 variable parameters including thickness of clutch housing (DV1) and slope angle of clutch housing (DV2) with varied value of 7-13mm and 64-67 degree, respectively as shown in Figure 4.9.

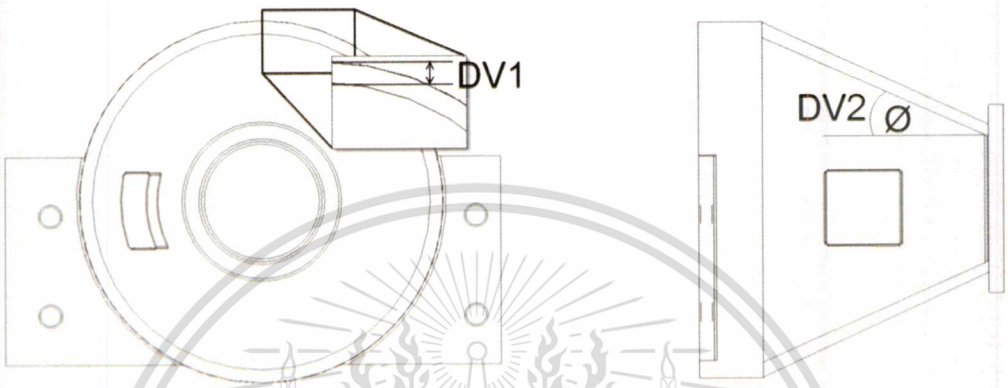

Figure 4.9 Design variable of clutch housing optimization, thickness (DV1), slope angle (DV2)

A relationship between maximum von-Mises stress and component geometries was studied during the optimization process by varying the clutch housing thickness from 7mm to 13mm and the slope angle of clutch housing from 64 degree to 67 degree. Each parameter was divided into 3 points and ordered into 9 design points of design of experiment as shown in Figure 4.10.

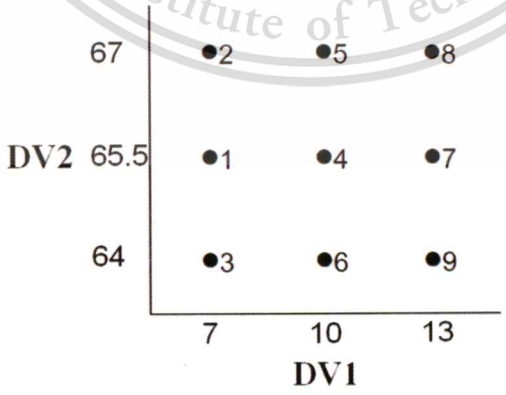

Figure 4.10 3 factor levels and 2 parameters, 3^2 factorial design or 9 design points

After the size optimization had been done, the shape optimization was carried out to reduce a weight of system. In this process, a middle portion of the clutch housing was changed into a spokes and stripes model as shown in Figure 4.11. The amount of spokes and stripe and also position and size were varied to find an optimum design of clutch housing.

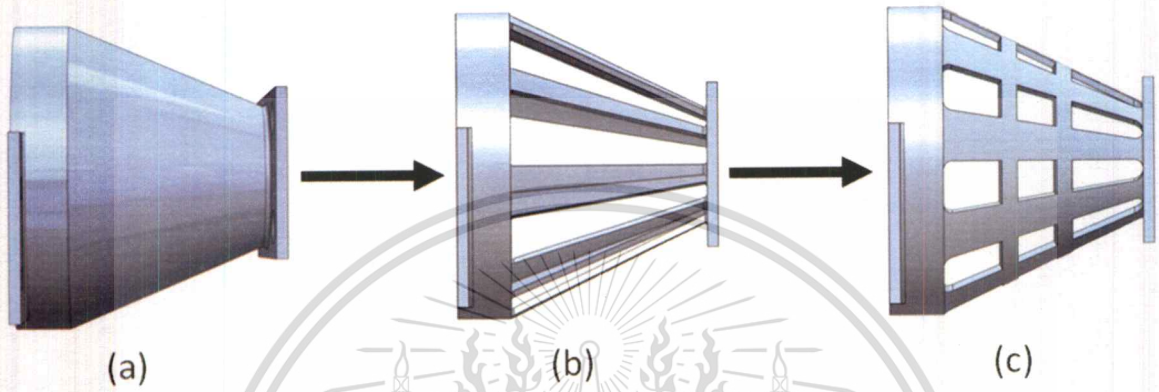

Figure 4.11 Middle portion of clutch housing (a) Initial design (b) Only spokes design (c) Spokes and stripes design

In details of shape optimizations, the amount of spokes model was studied to see a sensitivity of parameter and appropriate amount of spokes by varying amount of spokes from 4 to 11 spokes. Moreover, the stripes were added into the model to improve the clutch housing strength.

4.3 Clutch contact surface and bolts attached analysis

As explained in the previous chapter, the clutch contact surface was clamped by a clutch disc to transmit power from the flywheel to a gearbox shaft. In this section, the clutch contact surface and attached bolts were analyzed to investigate stresses occurred on bolts when a torque was applied from an engine to a flywheel. The analysis was carried out under a critical condition where the clutch contact surface did not move relative to a flywheel rotation i.e. mechanical lockup situation. As a result, boundary conditions of this analysis were such that degrees of freedom (DOF) of the clutch contact surface and the flywheel was fixed apart from a rotation around the center of flywheel clockwise direction. Then, a moment load was applied at the flywheel. For material properties, all the

parts in this model were assigned with properties of structural steel from ANSYS® software as mentioned in Table. 4.1.

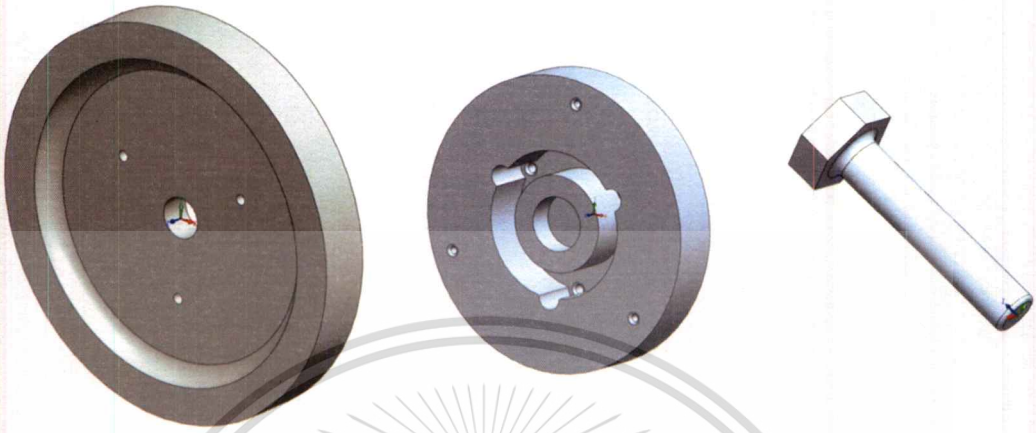

Figure 4.12 CAD models of clutch contact surface and bolts for computational analysis

4.3.1 Mesh preparation

Mesh model of clutch contact for contact surface stress analysis and bolts analysis were prepared by using ANSYS® software. First, hexahedron mesh elements were used for clutch contact surface FE model for stress analysis. Second, the hexahedron 5mm. mesh elements were used in the clutch contact surface bolts analysis. Since the analysis was concerned with stresses generated in bolts on a flywheel, mesh elements was refined to 2mm in the bolts and 0.5 mm at contact region. The FE models of the clutch contact surface stress analysis and clutch contact surface bolts analysis are illustrated in Figure 4.13 and Figure 4.14, respectively.

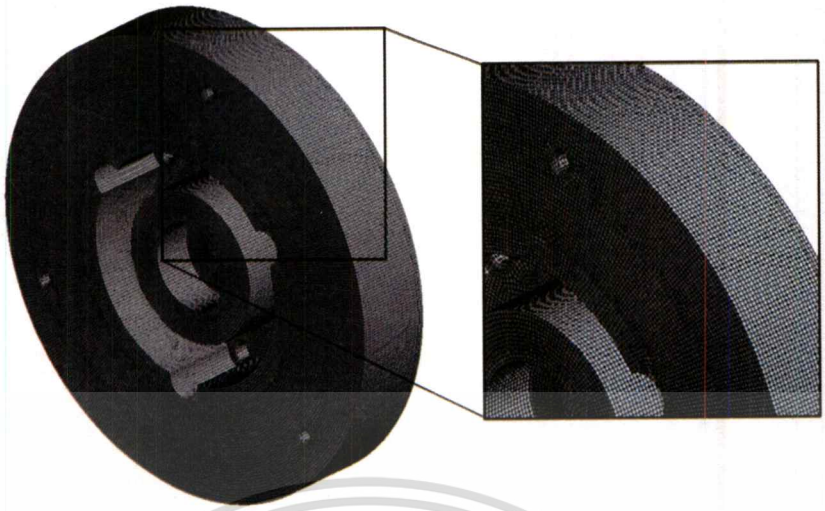

Figure 4.13 Finite element model of clutch contact surface stress analysis

Figure 4.14 Finite element model of clutch contact surface bolts analysis

4.3.2 Boundary conditions for clutch contact surface and bolt analysis

The clamp load of the clutch cover is about 3500-6000 N as referenced by LuK Clucth force diagram [22]. Therefore, 6000N was selected to represent a severe-condition case for a simulation as shown in Figure 4.15. The target Safety of Factor of 4.4 was used as suggested in the Assessment of Power Beam Flywheel Technology by J.M. Starbuck et al.[26] .

The analysis was a simulation of a stress occurred on bolts when a torque was applied from an engine to a flywheel. The analysis was carried out under a critical condition where clutch contact surface did not move relative to a flywheel rotation. As a result, boundary conditions of this analysis were such that degrees of freedom (DOF) of the clutch contact surface and the flywheel was fixed apart from a rotation around y-axis. Then, a moment load of maximum 5 $Kg \cdot m$ of torque from the RT 140 engine specification, the value was applied to flywheel to generate a shear force on mounting bolts. The boundary conditions are graphically shown in Figure 4.16.

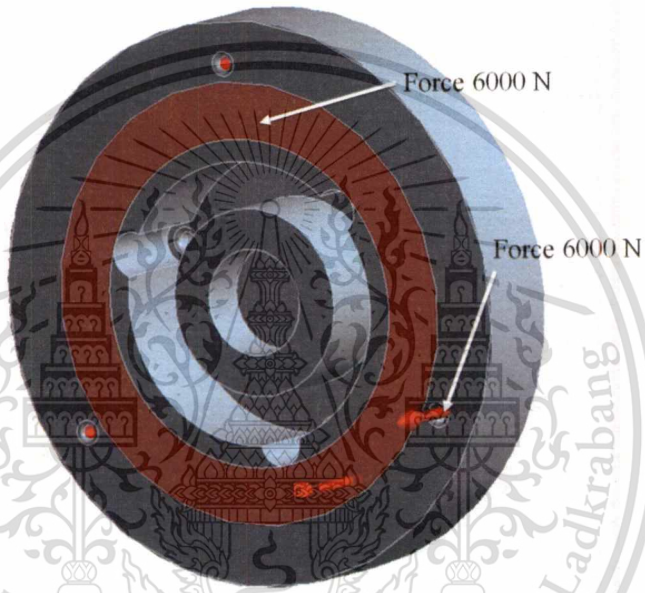

Figure 4.15 Shown clamp load applied on a clutch contact surface region

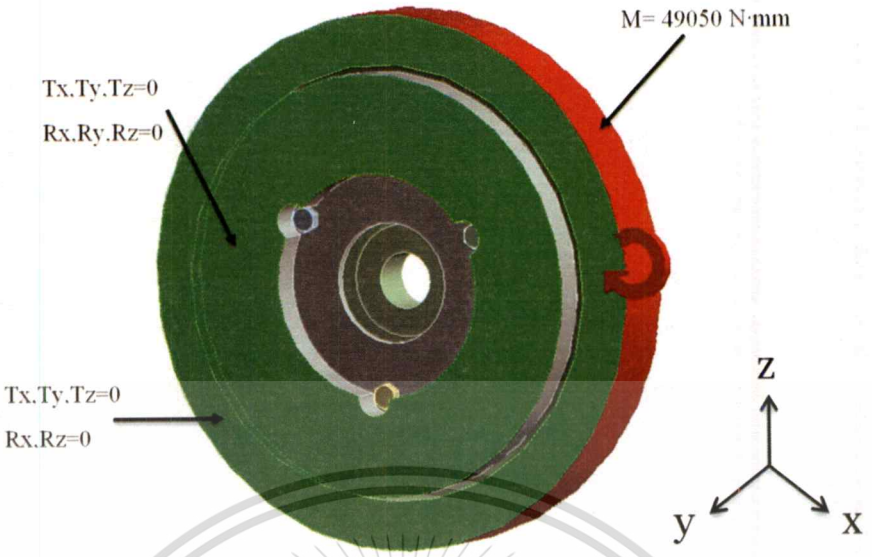

Figure 4.16 Boundary conditions and finite element model for bolt analysis

4.4 Shaft adapter analysis

The Shaft adapter component was prepared for an analysis as a CAD model as shown in Figure 4.17

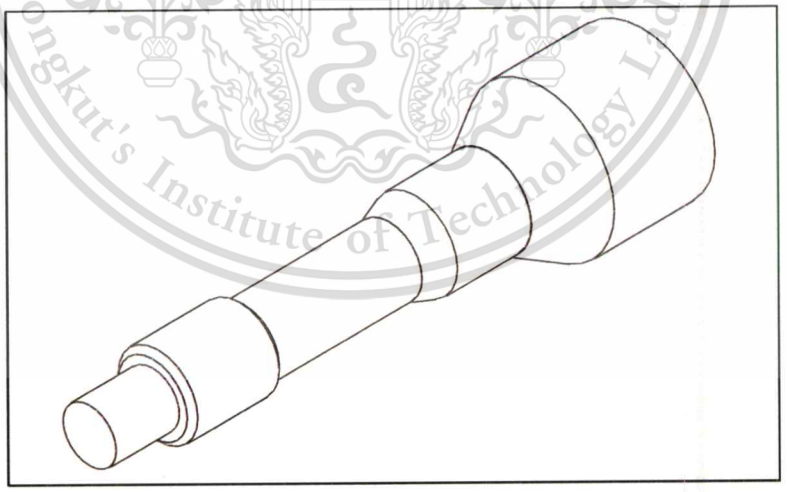

Figure 4.17 CAD model of Shaft adapter part for computational analysis

4.4.1 Mesh preparation

Mesh model of shaft adapter was prepared using ANSYS® software. Tetrahedron element mesh type was used for shaft adapter with a global element size of 1 mm. In addition, each part was contained with elements which had skewness value lower than 0.75. The FE model of the clutch housing is illustrated in Figure 4.18.

Similar to the previous parts considered, the shaft adapter model used properties of structural steel from ANSYS® software listed in Table 4.1.

Figure 4.18 Finite element model of shaft adapter

4.4.2 Boundary Conditions for Shaft Adapter Analysis

As mentioned in previous chapter, the shaft adapter was located between clutch disc and gearbox. It was used to transmit a power from the clutch disc to the gearbox shaft. Therefore, the extreme operating case for such component was when the maximum torque generated from the engine was transmitted through the shaft adapter and the gearbox side was no moving condition.

In this simulation, the shaft adapter was assigned to a rotational load of 5 $Kg \cdot m$ (49500 $N \cdot mm$) on a clutch disc spline side, because of the power from the engine directly transfer to a clutch disc. On the other hand, a fixed support was used on inner surface of gearbox hub side as shown in Figure 4.19 . The target safety of factor about 3 was set as a goal in this analysis.

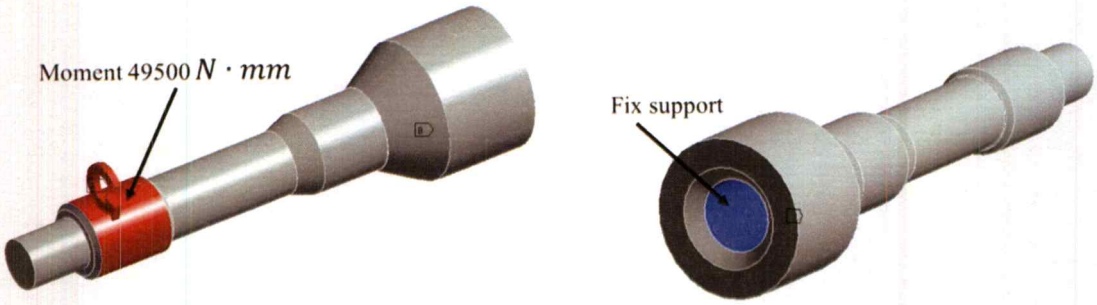

Figure 4.19 Boundary conditions applied on the shaft adapter model

4.5 Transmission performance comparison experiment

In this project, the direct clutch system was designed to replace a conventional belt transmission system in an agricultural truck (E-TAND). An experiment on transmission performance was separated into two main sections i.e. belt transmission and direct clutch transmission. Both systems were tested by following agricultural truck using conditions and set up configurations. In addition, the effect of setup configurations of belt transmission on transmission performance was studied.

The belt transmission performance was tested under the assumption of slip loss occurring while engine was in operation. This slip loss was measured by using a lagging in revolution rates on both driving and driven pulleys. To measure revolutions rate of pulleys, rotary encoders were used to determine revolutions per minute of each pulley. Furthermore, torque transducers were used to determine a torque transmitted on each shaft. The direct clutch transmission system was tested under the same criterion.

4.5.1 Experimental setup

For experimental setup, various apparatuses were required for the whole test system. These apparatuses , also displayed in Figure 4.21 were consisted of:

- One cylinder diesel engine KUBOTA RT140
- 2 KISTLER 4502R200RA Torque transducers with rotary encoder
- Autonic E40S6-3600-6-L-5 rotary encoder
- Kojima Dynamometer
- Spotlight electric loading unit
- Data acquisition tools :NIcDAQ-9172, NI 9205, and NI 9401
- Good Year Industrial V-Belt tension tester
- Drive line set
    - Flywheel shaft adapter
    - Drive shafts for drive and driven pulley
    - Dynamometer shaft adapter
    - Shaft adapter for direct clutch system clutch disc spline
- 4 MIKI MM-28K flexible Coupling shaft
- 4 grooves 128 mm. V Type pulley
- 3 Good Year belts
- Direct clutch system for one cylinder diesel engine
- Test Rig frame
- Uni-axial strain gauges

4.5.1.1 Test rig frame design

A test rig was designed under a concept of allowing tests on both transmission systems to be conducted. The test rig was separated into two frame bases as shown in Figure 4.20. There were a main frame base and a multi-transmission frame base. The mainframe base was for an engine mounting while the multi-transmission mounting frame base was used to accommodate both belt transmission and direct clutch system. These two frame bases were constructed by using 75 × 40 mm. c-channel steels and only use bolts as means of fastening.

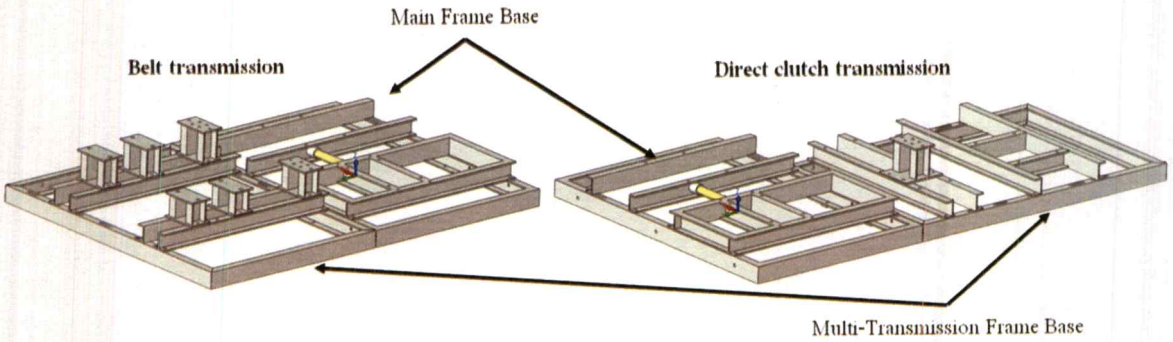

Figure 4.20 Frame base setups for belt and direct clutch system test

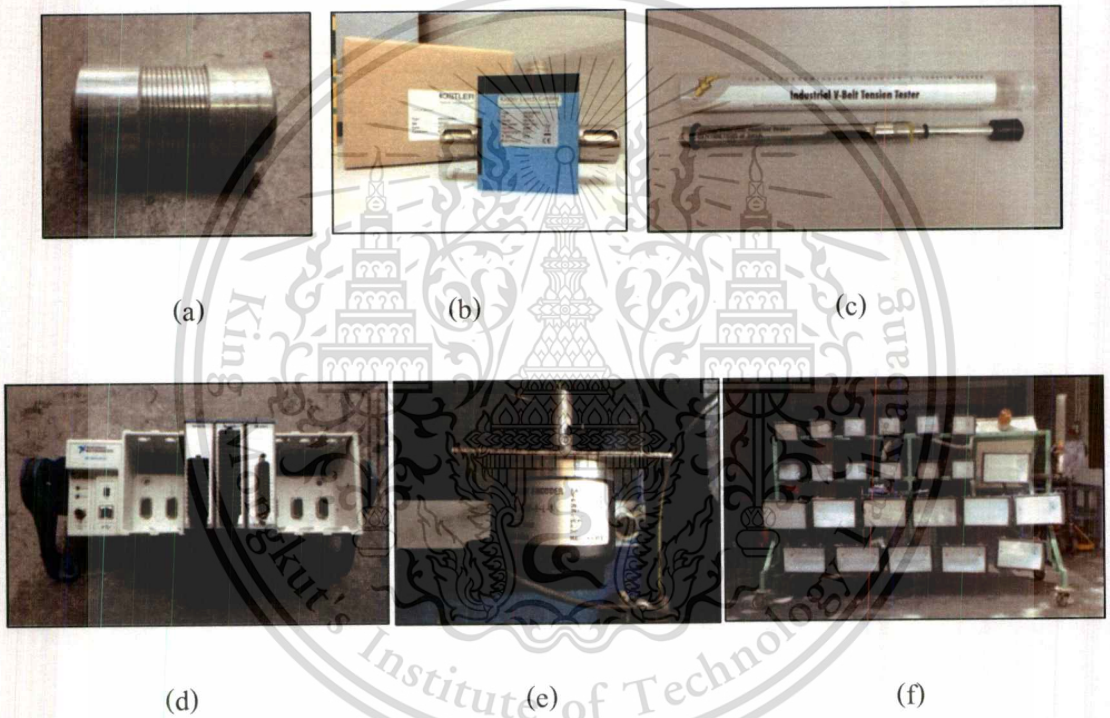

Figure 4.21 An experimental set up for transmission performance test: (a) Miki coupling, (b) Kistler torque transducer, (c) V-belt tension tester (d) DAQ equipment (e) Autonic rotary encoder, (f) Spotlight loading unit and (g) Overall experimental configuration of transmission performance test

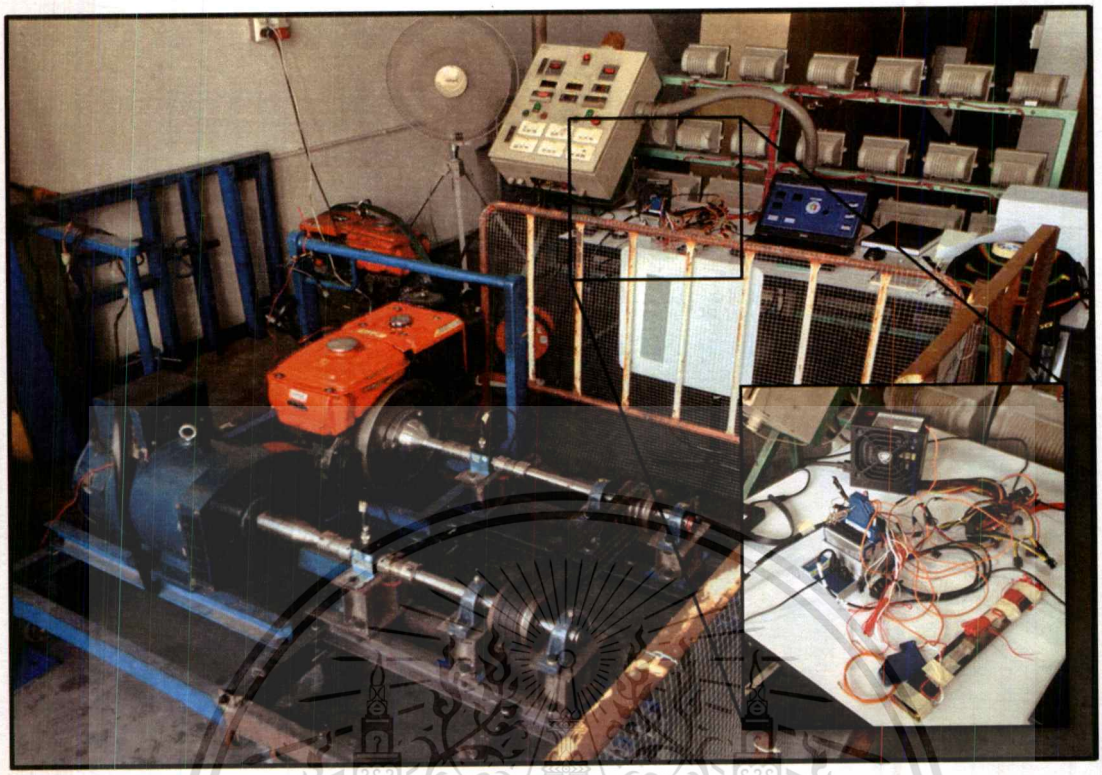

(g)

Figure 4.21 (cont.) An experimental set up for transmission performance test: (a) Miki coupling, (b) Kistler torque transducer, (c) V-belt tension tester (d) DAQ equipment (e) Autonic rotary encoder, (f) Spotlight loading unit , and (g) Overall experimental configuration of transmission performance test

4.5.1.2 Belt length calculation and selection for experiment test

The calculation was carried out to determine an appropriate length of belt for 560mm shaft distance and a 128 mm diameter of pulley with rated 14 horsepower. First, a design horsepower was calculated by referencing a service factor from Figure 4.22.

$$\text{Design horse power} = \text{Rated horse power} \times \text{Service factor} = 14 \times 1.4 \quad (4.3)$$

$$= 19.6 \text{ HP}$$

TYPE OF DRIVEN MACHINES	TYPE OF DRIVING UNITS					
	AC Motors: Normal Torque, Squirrel Cage, Synchronous and Split Phase. DC Motors: Shunt Wound, Multiple Cylinder Internal Combustion Engines.			AC Motors: High Torque, High Split, Repulsion-Induction, Single Phase Series Wound and Compound Wound, Single Cylinder Internal Combustion Engines. Line Shafts. Clutches		
	Intermittent Service (3-5 Hours Daily or Seasonal)	Normal Service (8-10 Hours Daily	Continuous Service (16-24 Hours Daily)	Intermittent Service (3-5 Hours Daily or Seasonal)	Normal Service (8-10 Hours Daily)	Continuous Service (16-24 Hours Daily)
Agitators for Liquids Blowers and Exhausters Centrifugal Pumps and Compressors Fans up to 10 HP Light Duty Conveyors	1.0	1.1	1.2	1.1	1.2	1.3
Belt Conveyor for Sand, Grain, etc. Dough Mixers Fans Over 10 HP Generators Line Shafts Laundry Machinery Machine Tools Punches-Presses-Shears Printing Machinery Positive Displacement Rotary Pumps Revolving and Vibrating Screens	1.1	1.2	1.3	1.2	1.3	1.4
Brick Machinery Bucket Elevators Exciters Piston Compressors Conveyors (Drag-Pan-Screw) Hammer Mills Paper Mill Beaters Piston Pumps Positive Displacement Blowers Pulverizers Saw Mill and Woodworking Machinery Textile Machinery	1.2	1.3	1.4	1.4	1.5	1.6
Crushers (Gyratory-Jaw-Roll) Mills (Ball-Rod-Tube) Hoists Rubber Calenders-Extruders-Mills	1.3	1.4	1.5	1.5	1.6	1.8

Figure 4.22 Suggested service factors for v-belt drives [24]

After that, 19.6 design horsepower with 2400 rpm condition were used as a selecting condition for a belt cross section type from the diagram shown in Figure 4.23. In this case, the designed system required a B-section V-Belt.

For speed ratio of system

$$\frac{RPM\ of\ faster\ shaft}{RPM\ of\ slower\ shaft} = \frac{2400}{2400} = 1 \qquad (4.4)$$

Speed ratio of 1 was used because the system had to be compared with a characteristic and efficiency of direct clutch system.

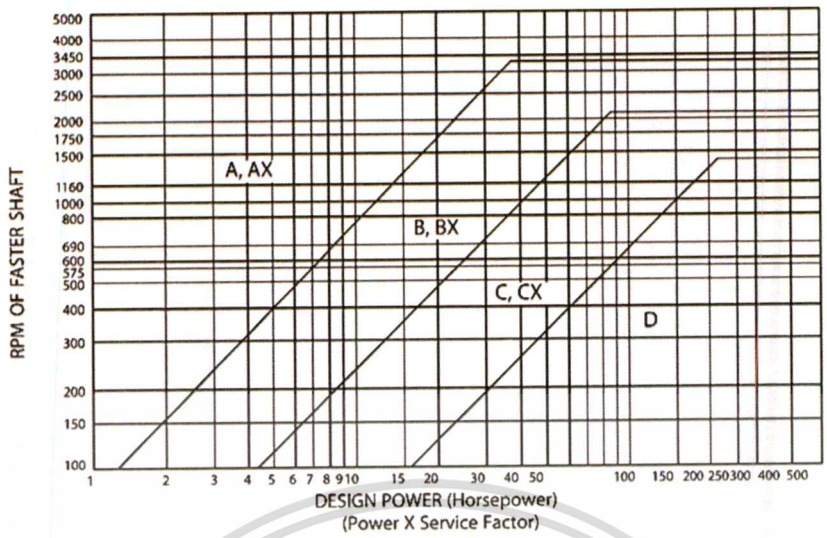

Figure 4.23 Belt cross section selection chart [24]

A Pulley diameter of 128mm was used in small and large pulleys. In order to determine the V-belt length, the following equation Eq. 4.5 was used

$$\text{Belt length} = 2C + \left[3.14\left(\frac{D+d}{2}\right)\right] + \left[\frac{(D-d)^2}{4C}\right] \quad (4.5)$$

Where D = Pitch circle of Large diameter pulley

d = Pitch circle of Large diameter pulley

C = Center distance between pulley

D = 128 mm., d = 128 mm., and C = 560 mm.

Then, $$\text{Belt Pitch length} = 2(560) + \left[3.14\left(\frac{128+128}{2}\right)\right] + \left[\frac{(128-128)^2}{4(560)}\right] \quad (4.6)$$

$$= 1521.92 \text{ mm.}$$

According to belt pitch length is greater than an inside length. By B- Belt section has difference about 46 mm.

Then, Inside length = Pulley diameter belt length – length difference (4.7)

= 1521.92 – 46 = 1475.92 mm.

Compare this value with B section Belt type Goodyear standard on Figure 4.22

B SECTION

Part Number	Approx. Outside Length (in)	Part Number	Approx. Outside Length (in)	Part Number	Approx. Outside Length (in)	Part Number	Approx. Outside Length (in)	Part Number	Approx. Outside Length (in)
B22 (5L250)	25	B46 (5L490)	49	B70 (5L730)	73	B94 (5L970)	97	B144	147
B23 (5L260)	26	B47 (5L500)	50	B71 (5L740)	74	B95 (5L980)	98	B148	151
B24 (5L270)	27	B48 (5L510)	51	B72 (5L750)	75	B96 (5L990)	99	B150	153
B25 (5L280)	28	B49 (5L520)	52	B73 (5L760)	76	B97 (5L1000)	100	B154	157
B26 (5L290)	29	B50 (5L530)	53	B74 (5L770)	77	B98 (5L1010)	101	B158	161
B27 (5L300)	30	B51 (5L540)	54	B75 (5L780)	78	B99 (5L1020)	102	B162	165
B28 (5L310)	31	B52 (5L550)	55	B76 (5L790)	79	B100	103	B173	176
B29 (5L320)	32	B53 (5L560)	56	B77 (5L800)	80	B101	104	B180	183
B30 (5L330)	33	B54 (5L570)	57	B78 (5L810)	81	B103	106	B190	193
B31 (5L340)	34	B55 (5L580)	58	B79 (5L820)	82	B104	107	B195	198
B32 (5L350)	35	B56 (5L590)	59	B80 (5L830)	83	B105	108	B205	208
B33 (5L360)	36	B57 (5L600)	60	B81 (5L840)	84	B108	111	B210	213
B34 (5L370)	37	B58 (5L610)	61	B82 (5L850)	85	B111	114	B225	227
B35 (5L380)	38	B59 (5L620)	62	B83 (5L860)	86	B112	115	B240	242
B36 (5L390)	39	B60 (5L630)	63	B84 (5L870)	87	B115	118	B255	257
B37 (5L400)	40	B61 (5L640)	64	B85 (5L880)	88	B116	119	B270	272
B38 (5L410)	41	B62 (5L650)	65	B86 (5L890)	89	B118	121	B285	287
B39 (5L420)	42	B63 (5L660)	66	B87 (5L900)	90	B120	123	B300	302
B40 (5L430)	43	B64 (5L670)	67	B88 (5L910)	91	B124	127	B315	317
B41 (5L440)	44	B65 (5L680)	68	B89 (5L920)	92	B126	129	B330	332
B42 (5L450)	45	B66 (5L690)	69	B90 (5L930)	93	B128	131	B360	362
B43 (5L460)	46	B67 (5L700)	70	B91 (5L940)	94	B133	136	B394	396
B44 (5L470)	47	B68 (5L710)	71	B92 (5L950)	95	B136	139		
B45 (5L480)	48	B69 (5L720)	72	B93 (5L960)	96	B140	143		

GOODYEAR
ENGINEERED PRODUCTS

Figure 4.24 B Section belt length information [25]

Then, B58 Belt type was selected with a 5.15 Rated horsepower per belt according to general standard.

Thus, Number of belts = $\frac{Design\ horsepower}{Horsepower\ per\ belt} = \frac{14}{5.15}$ (4.8)

= 2.7 Then, use 3 belts

Finally, 3 of B-section V-belts type were used in this experiment.

In conclusion, all of the apparatuses were setup into 2 different layouts for both systems configurations on the test rig. In case of the belt transmission performance test rig assembly, the RT140 Engine flywheel was attached to flywheel shaft adapter and test rig frame base by bolts. The Flywheel shaft adapter was then connected to the KISTLER torque transducer via a flexible coupling shaft to allow misalignment with a maximum tolerance of 2mm. The same was also applied on another side of the torque transducer shaft that was connected to the main driveshaft. Finally, the main driveshaft was inserted to bearing housings and pulley. As a result, this section was called a Drive section. For a Driven section, the main drive shaft was inserted to bearing housings, pulley, and connected to torque transducer in the same manner as those in the Drive section apart from the last 2 components; Dynamo and Dynamo Shaft Adapter. In addition, the drive and driven section were connected together by belts and tensioners were assembled on both driveline bases to adjust belts tension. The layout of the belt transmission test rig is shown in Figure 4.25.

In case of the direct clutch system test rig, the direct clutch system was assembled with the RT140 engine and connected to clutch disc shaft adapter, flexible coupling shaft, torque transducer, and dynamo in a series driveline configuration. Moreover, a special Autonic rotary encoder was attached to the manual starter crake shaft on the back of the engine to determine an engine rpm as shown in Figure 4.26. The overall direct clutch transmission experiment layout was shown in Figure 4.26. After all system installations were completed , the LabVIEW software with a data acquisition protocol were used to make an interface between a laptop computer and all sensors for logging the relevant data while system was being tested.

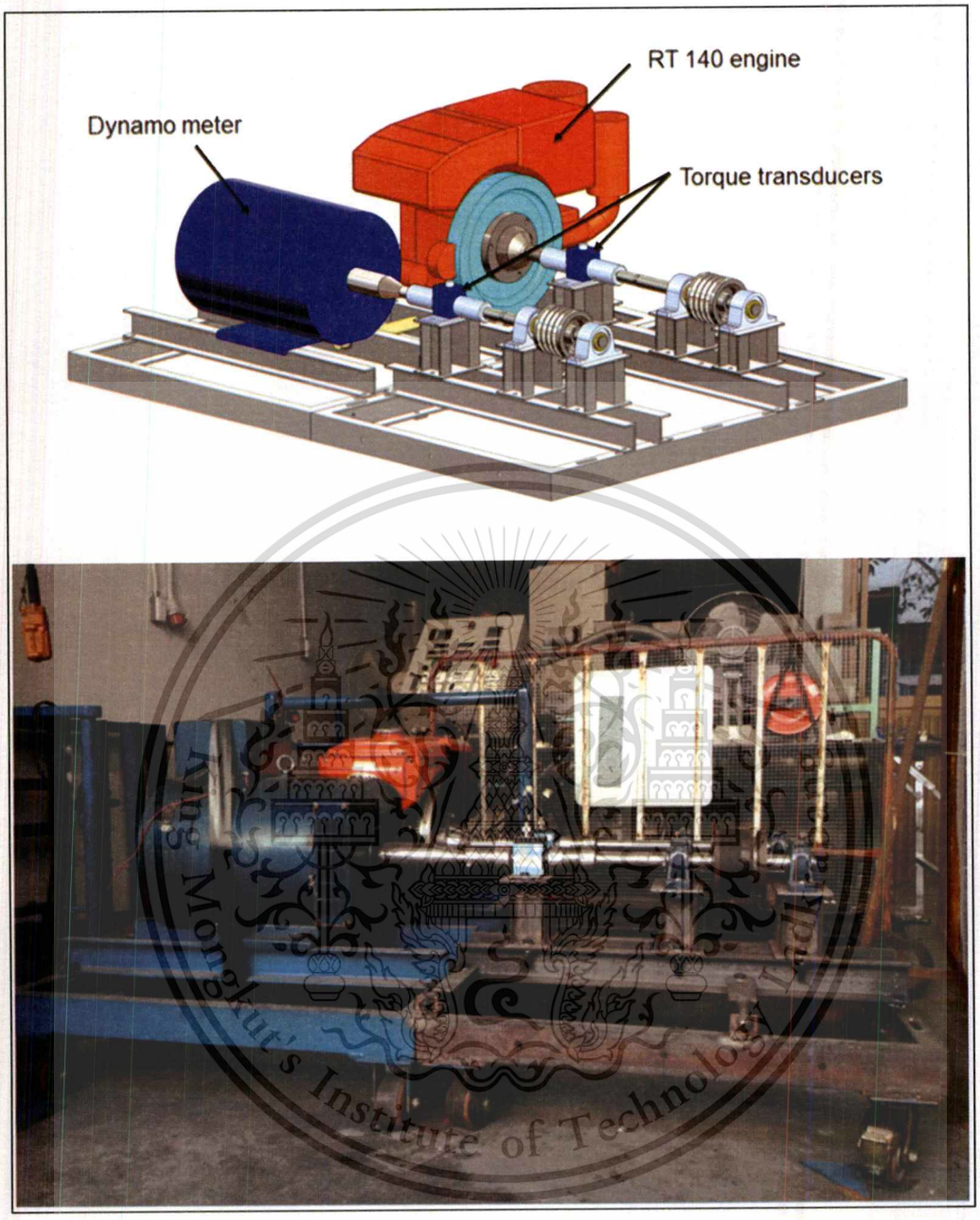

Figure 4.25 Belt transmission experiment layout

(Top: CAD layout, Bottom: Actual layout)

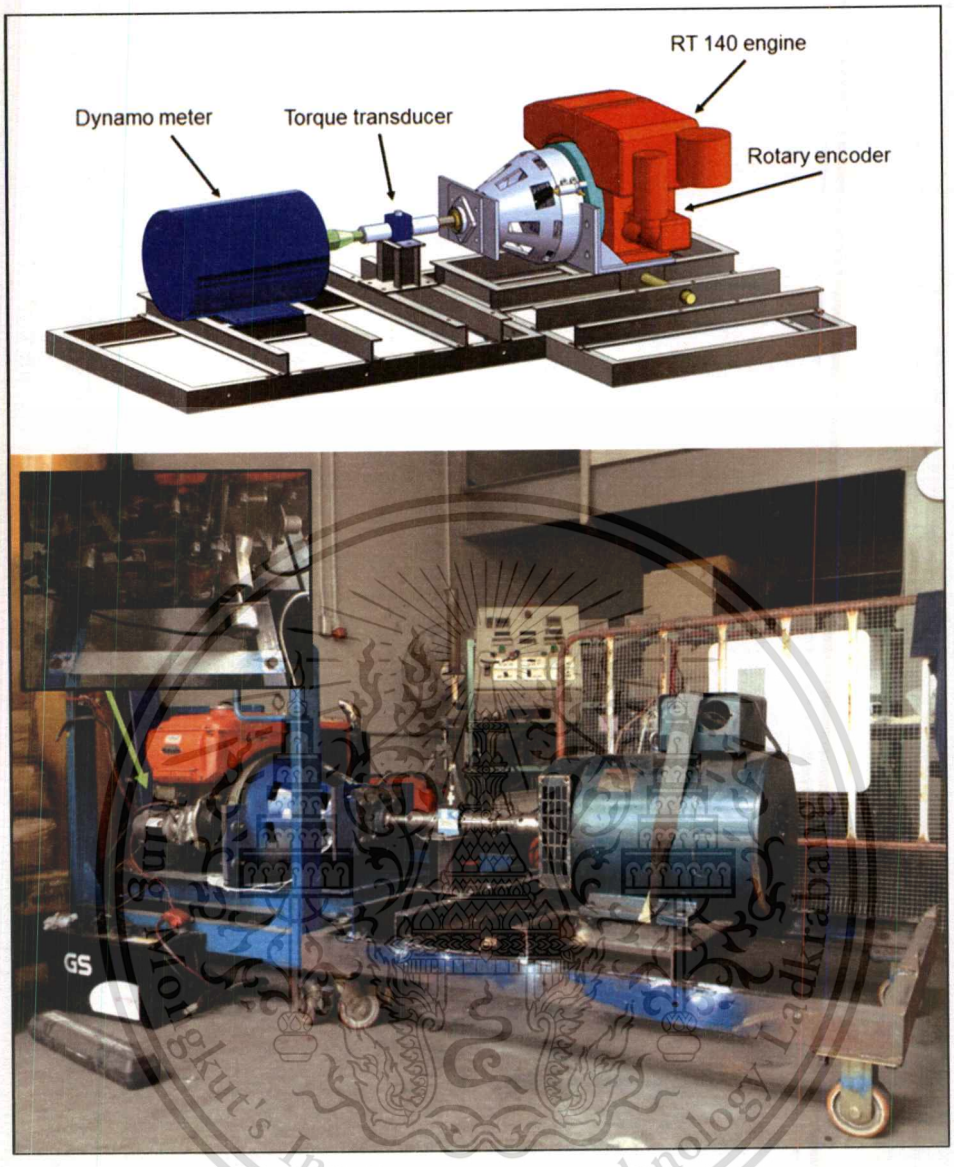

Figure 4.26 Direct clutch transmission experiment layout

(Top: CAD layout, Bottom: Actual layout)

4.5.2 Performance test procedures and test conditions

In the performance test experiment, the torque transducer with a rotary-encoder feature and another rotary encoder were used to determine a torque transmitted and revolution speeds of drive and driven system. This experiment was intended to simulate daily driving conditions of an agricultural truck (E-TAND. The engine was controlled to operate at 4 different load conditions by using a

spotlight electric loading unit, which could be separated into loading modules of L1, L2, L3, and L4 as explained on Table 4.2. For each load case, the engine was accelerated to the maximum revolution per minute (rpm) to determine efficiency loss, slip loss, and maximum torque capacity of each system under the condition of rapid acceleration and heavy carry load. In addition, the belt tensions were varied within a range of 2.4 Kg $\pm$ 0.48 Kg (Recommended tension by Goodyear is 2.3 Kg) and were measured by an industrial V-Belt tension tester. While drive and driven ratio was set as 1 for matching with the direct clutch system. The results were recorded by using NI with Lab View software. The experiments were repeated for 3 times for all load cases to confirm a repeatability of the results. As for direct clutch transmission tests, all procedures were similar to a belt transmission test in load condition and test procedure.

Table 4.2 Load conditions details of performance tests

Load Conditions	Spotlight light electric loading
L1	No Load
L2	2 x 1500 W light bulb
L3	3 x 1500 W light bulb
L4	3 x 1500 W, 6 x 1000 W, 2 x 500 W, and 6 x 300 W light bulb

4.5.3 Data processing

In order to convert analog voltage signals into torque results, the output analog voltages was multiplied by the scale factor of 40. According to torque transducer specifications, a torque transducer has a measure range by $\pm 200\ N \cdot m$ of maximum torque with analog volts output $\pm 0 - 5$ volts.

In case of revolutions speed determination, the derivative was applied on the signal. The revolution per minute was calculated by using a differential of rotations at time $T_{(0)}$ and $T_{(t)}$ divided by sampling time interval of a logging system as mention in equation (4.9)

$$N = \frac{dr}{dt} \tag{4.9}$$

Where dr is an differential of rotary encoder increment (rounds)

dt is an differential of data sampling interval (time)

Then N is revolutions per unit of time

In details of the efficiency and slip calculation, two general equations were used to calculate as expressed in equation 4.10 and 4.11:

$$\text{Efficiency \%} = \frac{torque\ out \times r.p.m.out}{torque\ in \times r.p.m.in} \times 100 \tag{4.10}$$

$$\text{Slip \%} = \frac{N(t)-N(0)}{N(0)} \times 100 \tag{4.11}$$

Where N(0) = revolution per minute of drive set

N(t) = revolution per minute of driven

4.6 Strain measurement on a clutch housing prototype

In order to validate the strain occurred on the clutch housing prototype model obtained from a simulation, strain gages were used to measure strains in a real prototype.

In case of experimental setup, the configuration of a direct clutch system performance test featured an extra module of Data acquisition tool NI-9235 Quarter- Bridge Analog Input with TML uniaxial strain gauges as shown in Figure 4.27. Strain gages were prepared and attached to the model at several concerned locations. There were three considered points of clutch housing set; the locations located at the base of mounting plate and the side and top of clutch housing spokes as shown in Figure 4.28. In each location, two of strain gages were used to measure a normal strain in two axes as illustrated in Figure 4.29. The resulting strains were investigated during the engine operation at a full

load condition. Then, the measured strains were converted to stresses using Hooke's law and were used in a validation of the simulation results.

Figure 4.27 (left) Data acquisition tool NI-9235, (right) uniaxial TML strain gages

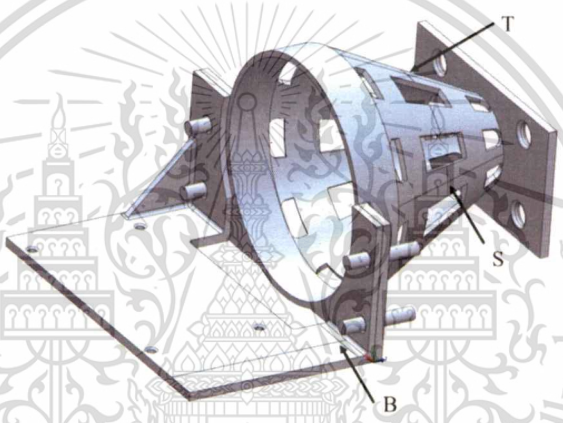

Figure 4.28 Three strain-measurement locations on a clutch housing set

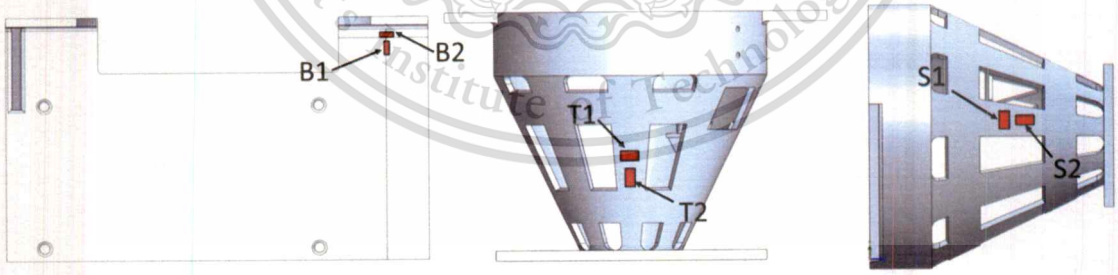

Figure 4.29 Details of strain gages attachment on Clutch housing set

CHAPTER 5

EXPERIMENTS, COMPUTATIONAL AND OPTIMIZATION RESULTS

5.1 Vibration load profile measurement of one cylinder diesel engine

The results were separated into three main cases (idle, partial, and full loads) with two measurement sensor locations for each case. The results are shown in Figure 5.1. Generally, all measured responses displayed a sinusoidal pattern for all load cases. Highest vibration amplitudes were observed during full load conditions in x and y axis directions.

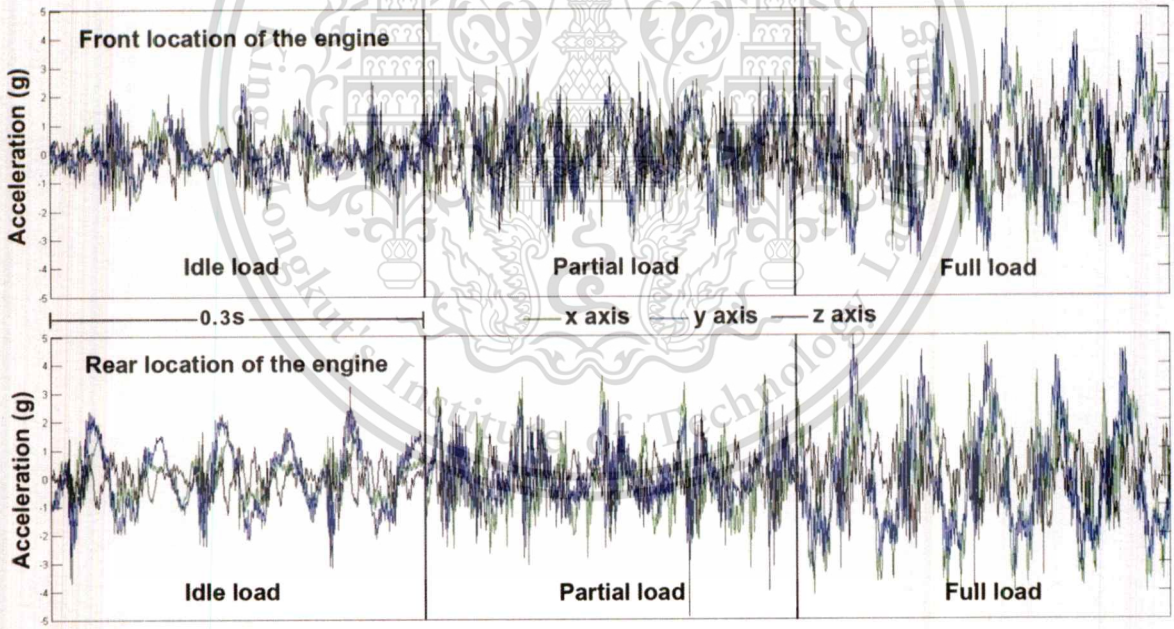

Figure 5.1 Engine vibration profiles measured at various loads.

5.1.2 Data post-processing and preparing for clutch housing analysis

After the raw data were collected, the important data were filtered by low-pass filter following the filter methodology as mentioned before. A graphical comparison between raw data and filtered data is shown in Figure. 5.2.

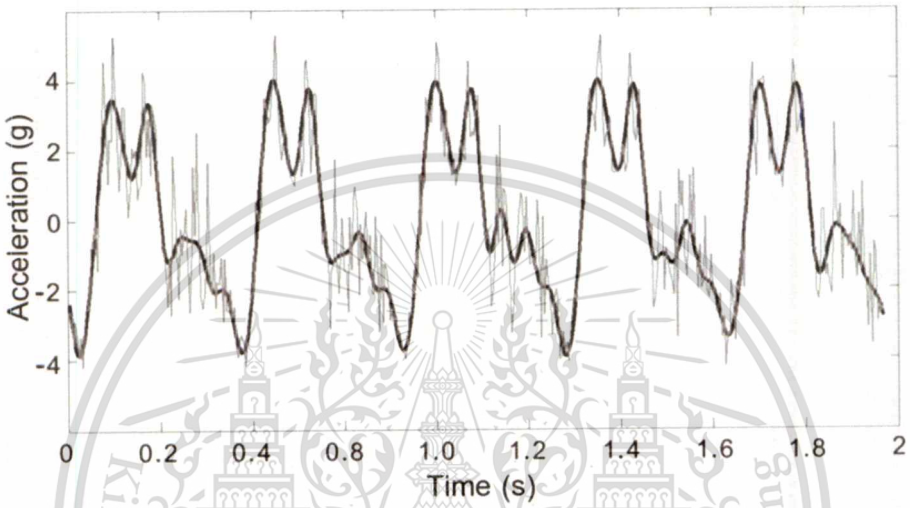

Figure 5.2 Comparison between filtered (black) and non-filtered (grey) vibration data.

To convert an acceleration data to force, the filtered data was multiply by effective mass of engine to obtain a maximum force on front and rear base of the engine in each load case. The calculated maximum forces in each load case, which were used in simulation, could be summarized in Table 5.1. It could be seen that the maximum force under full load condition was higher than those under partial and no load conditions by approximately a factor of 1.89 and 2.84 respectively.

Table 5.1 Calculated maximum forces in each load case

Cases	Maximum Force (N)		
	X	Y	Z
Front no load	1232	1564	792
Front partial load	1590	1640	1348
Front full load	2872	3048	2620
Rear no load	852	634	360
Rear partial load	1224	916	712
Rear full load	2346	1686	1446

In case of fatigue analysis, the maximum force in each load case was combined into an Extra Urban Driving Cycle (EUDC) under the relation of accelerated, cruise speed, and decelerated as mentioned on Chapter 4.1.2. As a result, the loading history which was used in this experiment could be seen in Figure 5.3.

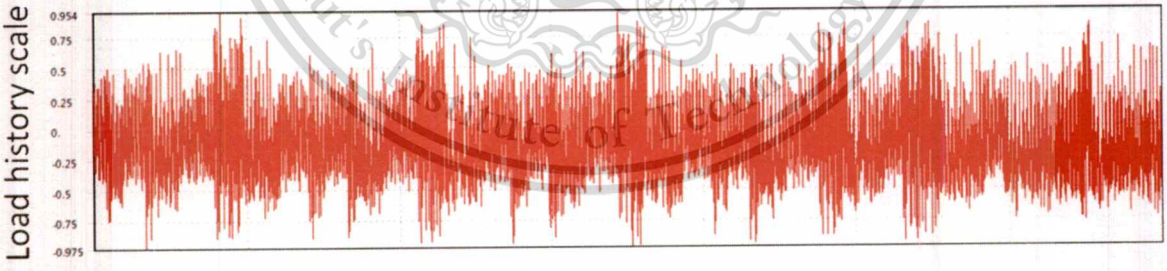

Figure 5.3 Combined loading history for fatigue analysis

5.2 Clutch housing analysis results

5.2.1 Analytical results: Clutch housing structural and fatigue analysis

Initially, the analysis was carried out with a 13 mm thickness and 65 degree of slope angle on the clutch housing model. The resulting stress distribution is shown in Figure 5.4. Maximum von-Mises stress was 65.807 MPa which gave a safety factor of 3.799 with non-failure of fatigue mode. Moreover, the volume of this design was $6500.30 \times 10^{3} mm^{3}$ and 51.03Kg of weight. Since the safety factor was higher than a target value of 3, i.e. indicating overdesign, the method of optimization was applied to find an appropriate thickness and slope angle of clutch housing to achieve the design goals.

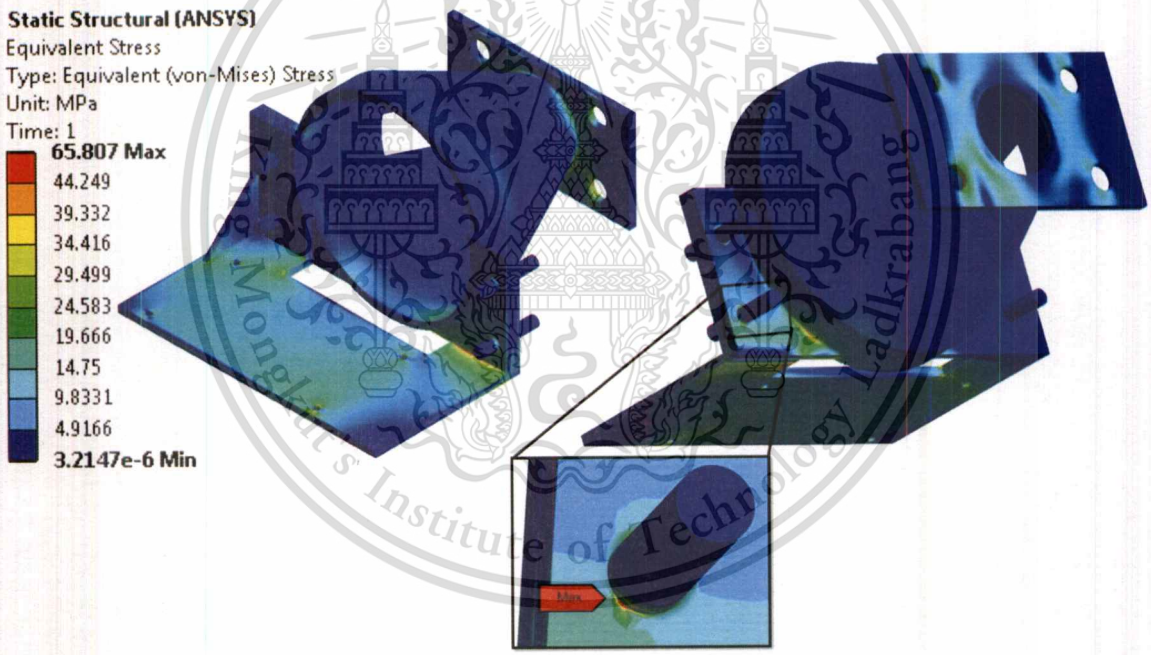

Figure 5.4 Von-Mises stress distribution result in clutch housing with component thickness of 13 mm and 65 degree of slope angle

5.2.2 Clutch housing optimization

For the first set of design of experiment, the effects of thickness (DV1) and slope angle (DV2) related to maximum von-Mises stress, volume, and minimum life of clutch housing are shown in Table 5.2.

Table 5.2 DOE- 3^2 design table results

Run #	DV1 (mm)	DV2 (degree°)	Maximum von-Mises Stress (MPa)	Volume ($x10^3 mm^3$)	Minimum Life (Days)
1	7	65.5	116.45	5063.19	188.22
2	7	67	112.02	5099.74	260.05
3	7	64	123.40	5025.50	121.64
4	10	65.5	81.05	5784.78	27563
5	10	67	63.61	5836.92	27563
6	10	64	85.06	5731.12	27563
7	13	65.5	63.93	6523.23	27563
8	13	67	58.54	6590.96	27563
9	13	64	69.82	6453.60	27563

Based on the DOE results in Table 5.2 , the relationship between DV1, DV2, and maximum von-Mises stress as well as volume was constructed to form a response surface by using 2nd order polynomial algorithm as mentioned on Chapter 2.4.3 following Equation 2.19 and Equation 2.20.

Where $x_1 = DV1, x_2 = DV2$

And $$Y = \begin{Bmatrix} y_1 \\ y_2 \\ \vdots \\ y_9 \end{Bmatrix}, X = \begin{bmatrix} 1 & x_{11} & x_{21} & x_{31} & x_{41} & x_{51} \\ 1 & x_{12} & x_{22} & x_{32} & x_{42} & x_{52} \\ 1 & \vdots & \vdots & \vdots & \vdots & \vdots \\ 1 & x_{19} & x_{29} & x_{39} & x_{49} & x_{59} \end{bmatrix}, \beta = \begin{Bmatrix} \beta_0 \\ \beta_1 \\ \beta_2 \\ \beta_3 \\ \beta_4 \\ \beta_5 \end{Bmatrix}$$

The equations of relationship are shown in Eqs. (1) and (2) where x is DV1 and y is DV2.

$$\text{Max. von-Mises stress (MPa)} = -2660.323 - 40.6072x + 96.0588y + 1.5688x^2 - 0.7712y^2 + 0.0056xy \quad (5.1)$$

$$\text{Volume (x10}^3\text{mm}^3\text{)} = 1431.32 - 7.3375x + 61.6688y + 0.9426x^2 - 0.47134y^2 + 3.541xy \quad (5.2)$$

These 2 equations were used to plot the response surface and show the sensitivity of each parameter as show on Figure 5.5, Figure 5.6, and Figure 5.7.

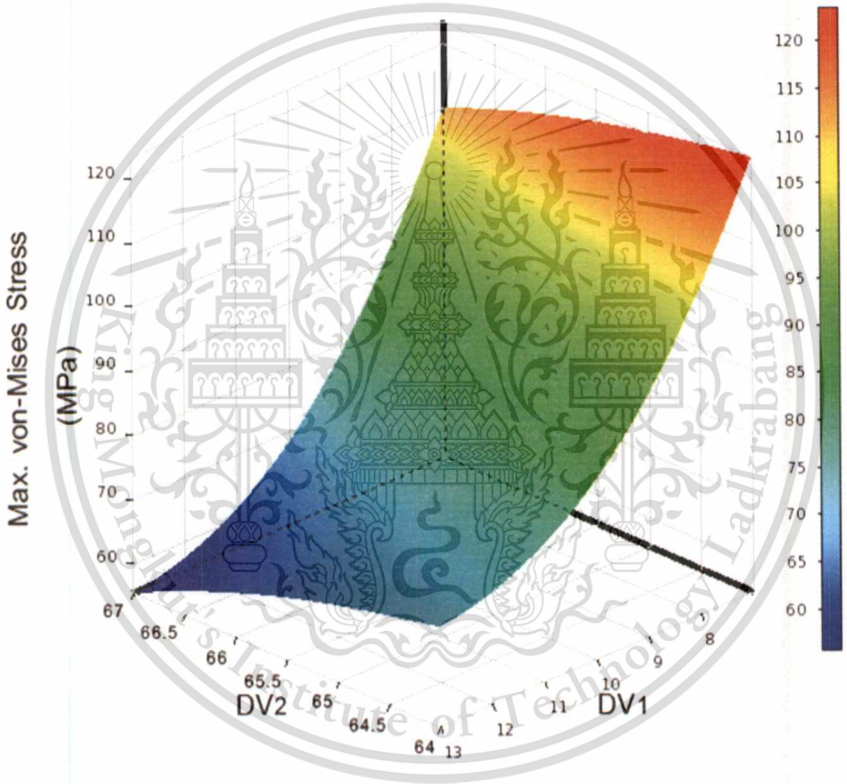

Figure 5.5 Maximum von-Mises stress response surface for clutch housing design parameters (DV1, DV2).

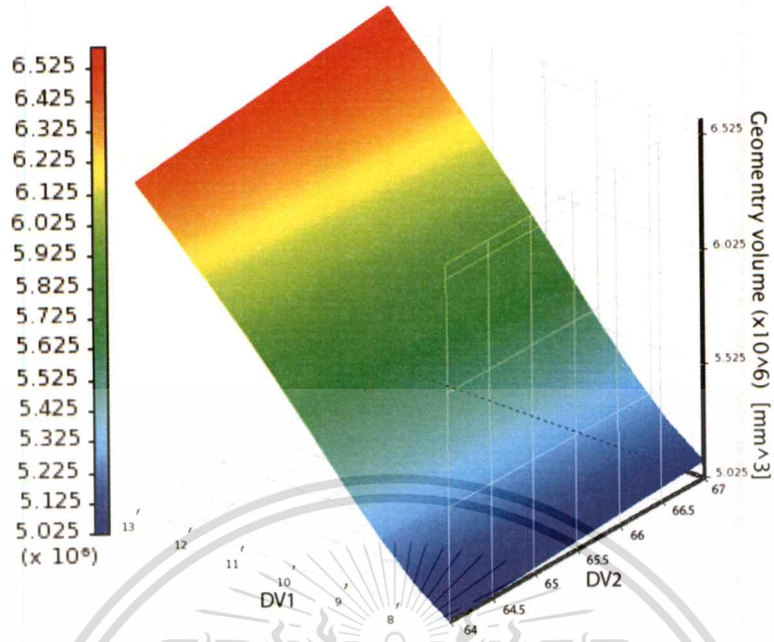

Figure 5.6 Volume response surface for clutch housing design parameters (DV1, DV2).

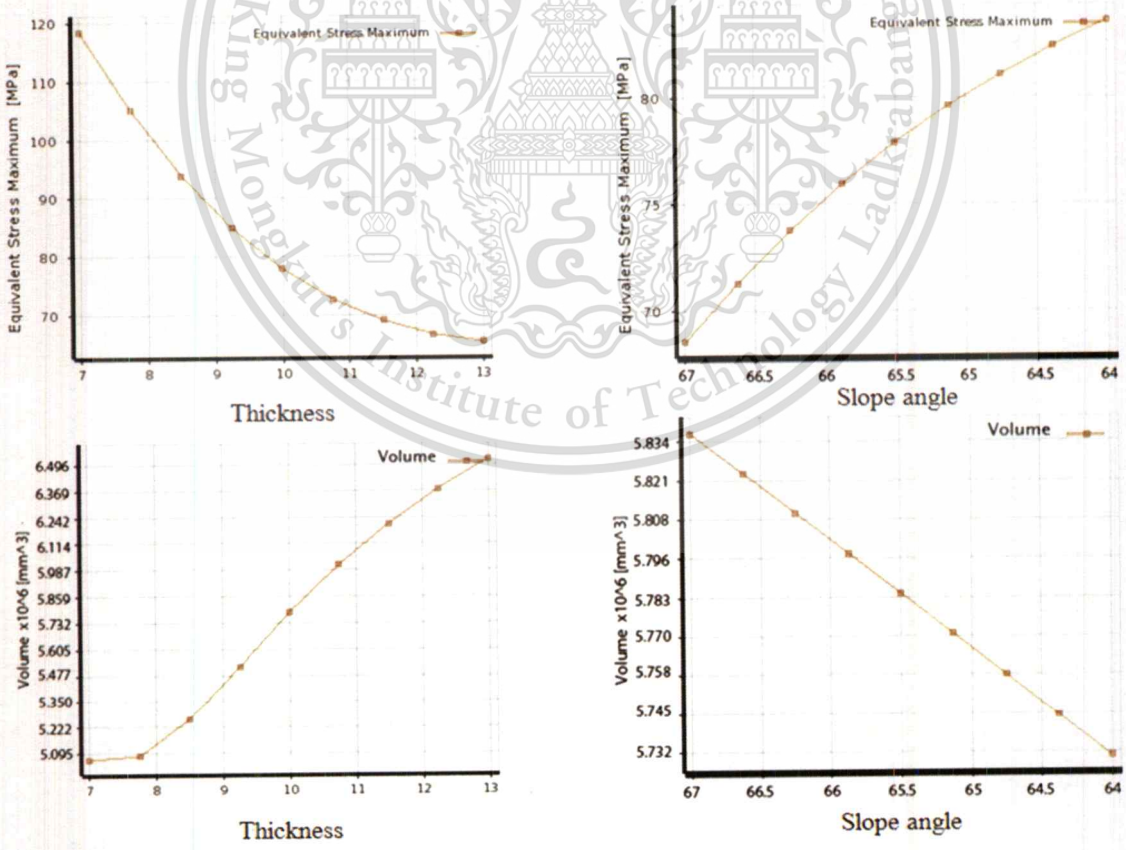

Figure 5.7 Sensitivity charts of parameters of first optimum model

According to the response surfaces and sensitivity chart, a sensitivity of the clutch housing slope angle was relatively low since incresing of slope angle resulting in a slight decrease in a maximum von-Mises stress. In contrast the variation of clutch housing thickness showed very high sensitivity such that maximum von-Mises stress significantly increased while the thickness was decreased. In addition, increasing of both parameters would result in an increase of the total volume of the model.

In this optimization, one of the goals was to minimise volume while a safety factor had to be higher than 3 or a maximum von-Mises stress of 83.33 MPa. Hence, 83.33 MPa was used as max. von-Mises stress in Equation (5.1), to calculate possible x and y. Moreover, every possible combinations of x and y results were substituted into Equation (5.2) to determine the minimum volume. From this calculation, the optimum point result was 8.7 mm of thickness and 67 degree of clutch housing slope angle.

In addition, this optimum point was used in an analysis to validate the results. Maximum von-Mises stress was 84.74 MPa with a corresponding safety factor of 2.95 and structural volume of 5515.43 x10^{3}mm.^{3} or 40.37Kg of weight, while fatigue life was also achieved as show in Figure 5.8.

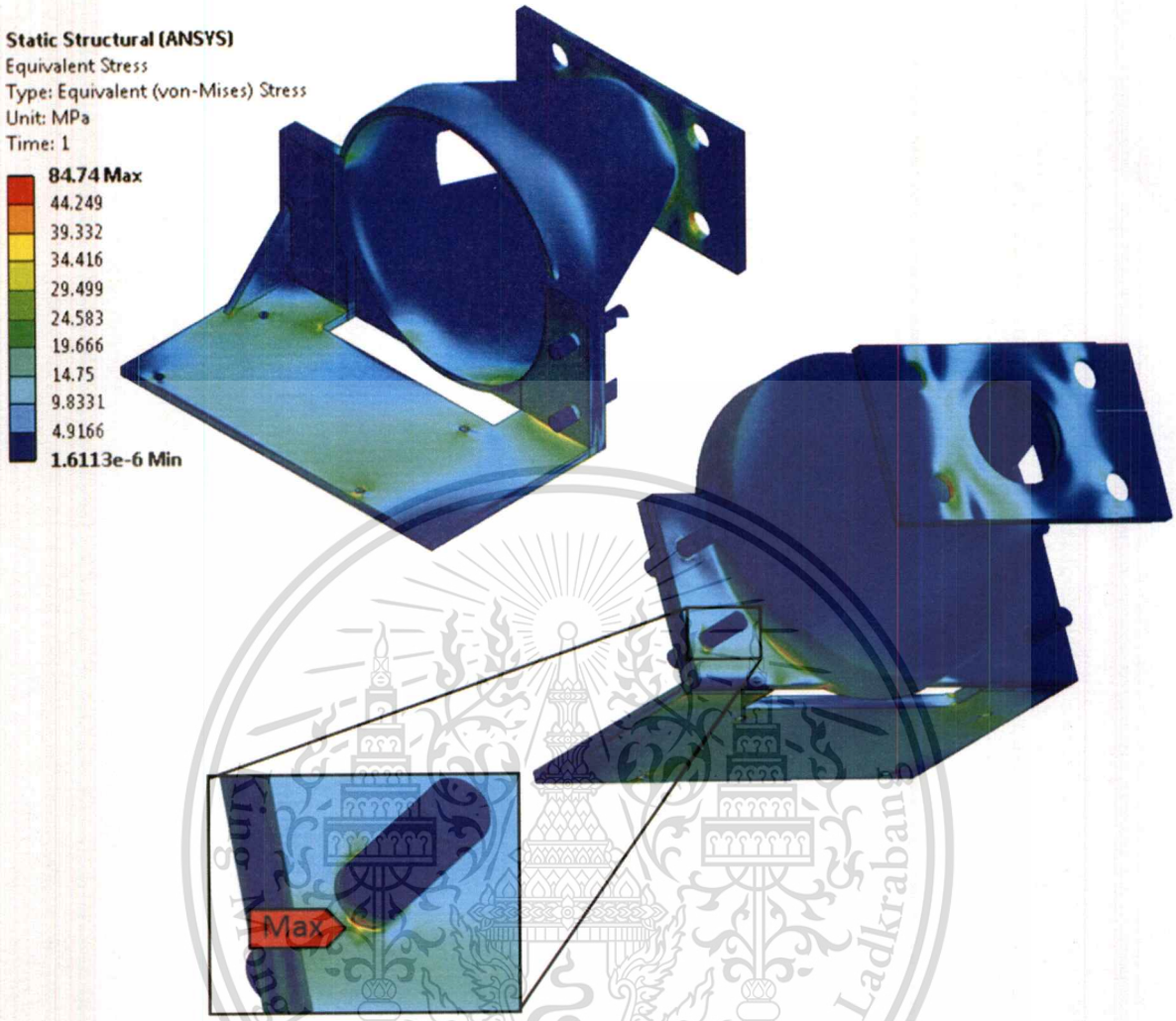

Figure 5.8 Von-Mises stress distribution result in first optimum prototype clutch housing, component thickness of 8.7 mm and 67 degree of slope angle.

The percentage error of the response surface calculation results compared to simulation results in maximum von-Mises stress, safety factor, and volume was 1.67%, 1.69%, and 0.06% respectively which were in acceptable ranges. Therefore, 8.7 mm. of thickness and 67 degree of slope angle were the optimum point of this first clutch housing prototype.

Furthermore, according to the stress distribution results, the middle portion of optimum clutch housing was subjected to a relatively low level of stress as shown in Figure 5.9. Therefore, it was

believed that this area could be redesigned to manage a better stress distribution under the goal of weight reduction.

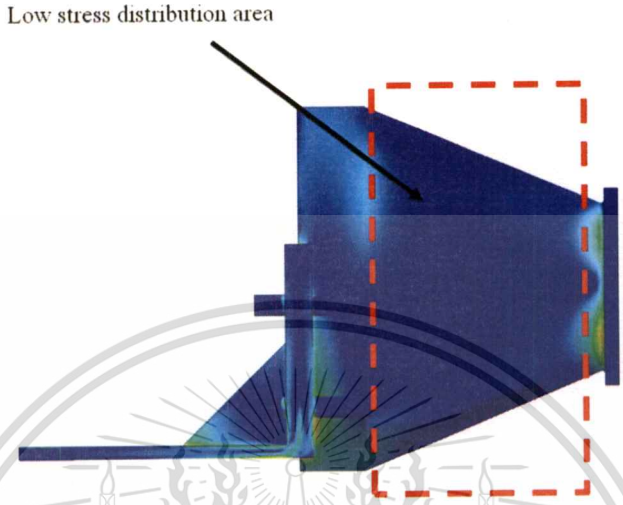

Figure 5.9 A side view of the initially optimized clutch housing prototype design with resulting stress distribution.

As a result, this particular section of clutch housing was redesigned into a spoke configuration, as shown in Figure 5.10. Consequently, the new purpose was to investigate the effect of amount of spokes on maximum von-Mises stress by varying the amount of spokes from 4 -11.

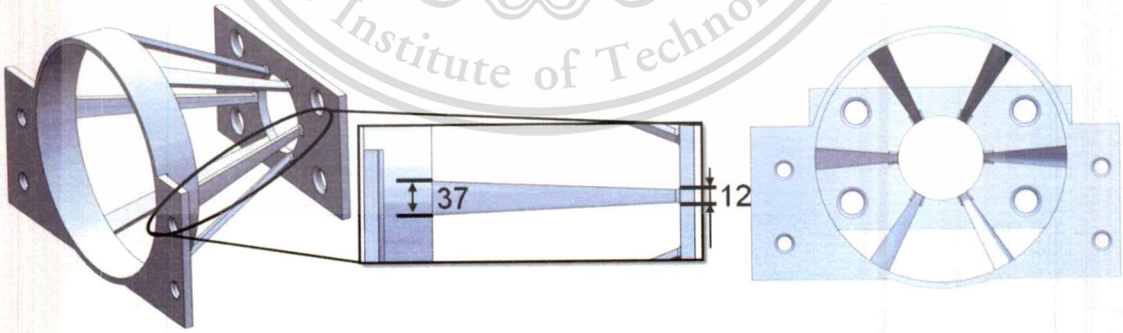

Figure 5.10 Clutch housing model with 6 spokes configuration (all dimensions are in mm.)

Each varied spokes model was analyzed using the similar conditions as in the previous model prototype. The results of an analysis are shown in Table 5.3 and Figure 5.12. Furthermore, the results

were used to determine a relationship between amount of spokes and maximum von-Mises stress slope as displayed in Figure 5.11.

Table 5.3 Design of experiment results for spokes variations

Amount of spokes	Max. von-Mises stress (MPa)	Stress reduction (MPa)	Stress reduction percentage (%)
4	670.04	-	-
5	595.17	74.87	11.17
6	507.94	87.23	14.65
7	455.49	52.45	10.33
8	407.09	48.4	10.62
9	370.01	37.08	9.11
10	339.73	30.28	8.18
11	314.23	25.5	7.51

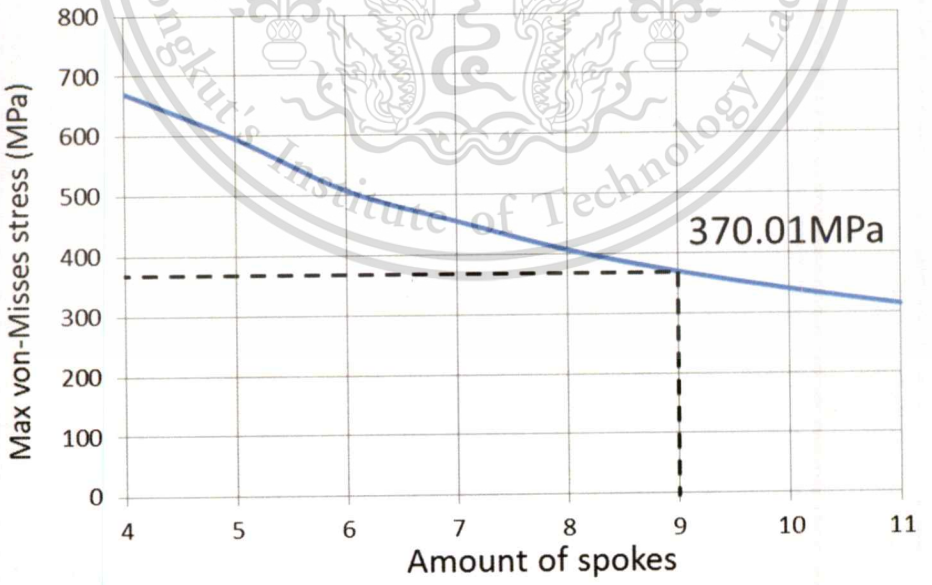

Figure 5.11 A relationship between amount of spokes and maximum von-Mises stresses

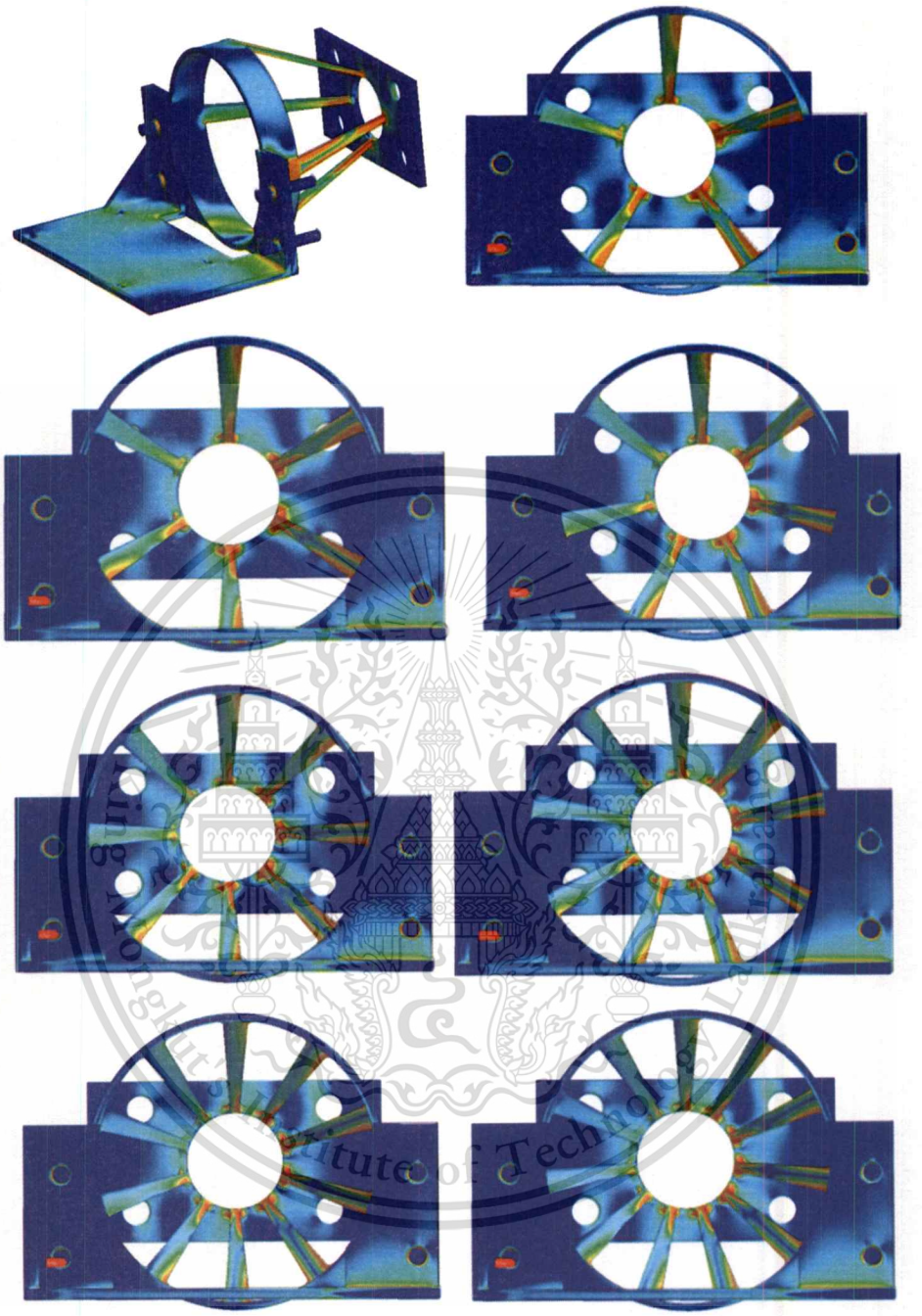

Figure 5.12 Calculated von-Mises stress distribution results for different number of spokes (4 to 11 spokes) on the revised clutch housing model

From results of number of spokes and maximum von-Mises stress, the resulting stresses decreased with increasing amount of spokes. However, overall maximum von-Mises stresses in all cases considered were still rather high. Therefore, the 9 spokes clutch housing model was selected for further improvement by assigning spoke width to be double of the initial value. In addition, a 10 spokes clutch housing was not selected under the reason that not being suitable for double width spoke process due to weight and stress reduction percentage.

In this step, the 9 spokes clutch housing was selected as an optimum amount of spoke configurations. However, this clutch housing model with double-sized spokes still generated a maximum von-Mises stress of 139.35 MPa which was higher than the required 83.33 MPa (Figure 5.13). Therefore, a cross structure was added to increase the overall stiffness of a model.

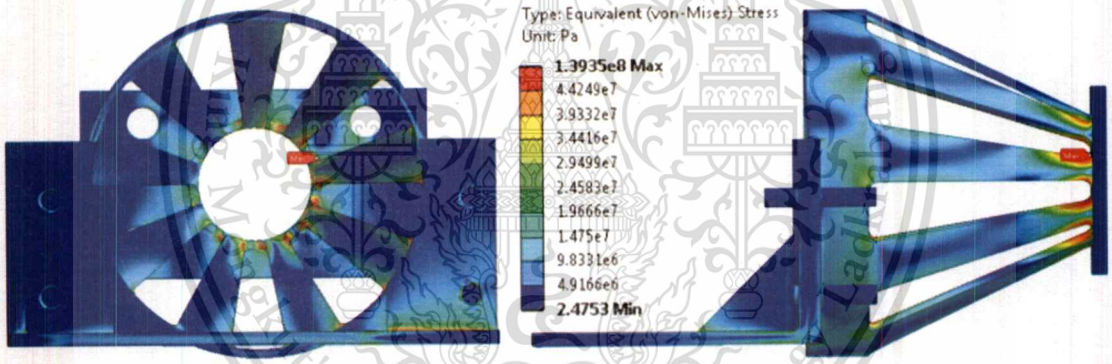

Figure 5.13 Calculated Von-Mises stress distribution in 9 spokes clutch housing with double-sized spoke.

For an addition of cross structure configuration, strips structures were added into the middle section of a 9 spokes (double-sized) clutch housing model as shown in Figure 5.14. Furthermore, the size and gap between each adjacent strip were varied. Each parameter sensitivity was investigated by varying the distant between each strip and the width of a strip from 50-100 mm. and 20-50 mm. respectively.

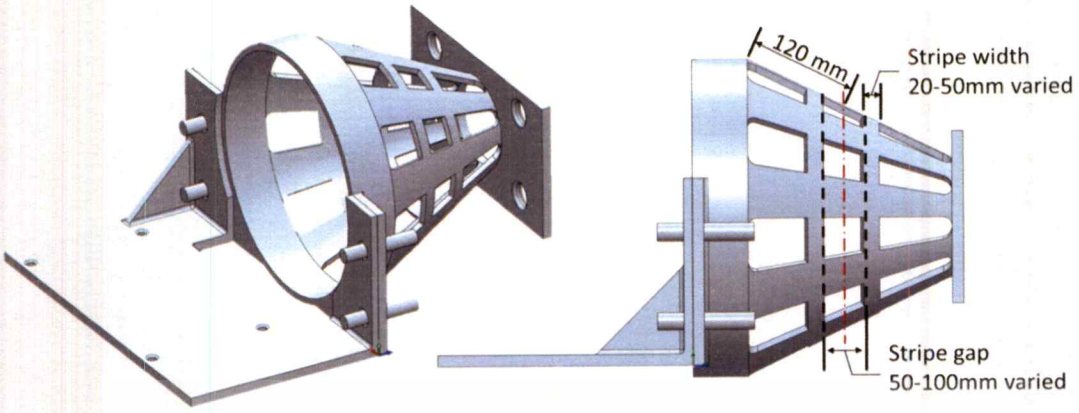

Figure 5.14 Clutch housing model with strip structure and relevant design parameters (Strip width and Strip gap)

After all design points were analyzed, the results were used to construct the equation describing a relationship between parameters of interest and maximum resulting von-Mises stress and a corresponding response surface (Figure 5.15) to predict the optimum point. The results of each design point are show in Table 5.4.

Table 5.4 DOE- 3^2 design table results

Design points	Strip width (mm)	Strip gap (mm)	Max. von-Mises stress (MPa)	Volume ($\times 10^3 mm^3$)	Weight (Kg)
1	20	50	106.88	4816.815	37.812
2	35	50	100.04	4907.621	38.522
3	50	50	93.86	4997.58	39.231
4	20	75	103.52	4816.815	37.812
5	35	75	95.19	4907.261	38.522
6	50	75	88.164	4997.58	39.231
7	20	100	98.44	4816.815	37.812
8	35	100	89.32	4907.261	38.522
9	50	100	80.28	4997.58	39.231

According to the DOE result, the equation of relation could then derived

Max. von-Mises stress (MPa) $= 110.98 - 0.2666x_1 + 0.3208x_2 + 0.0009x_1^2 - 0.0062x_2^2 - 0.008x_1x_2$ (5.3)

Volume (mm^3) $= 1000(4696 + 6x_1)$ (5.4)

Where x_1 = Strip width (mm)

x_2 = Strip gap (mm)

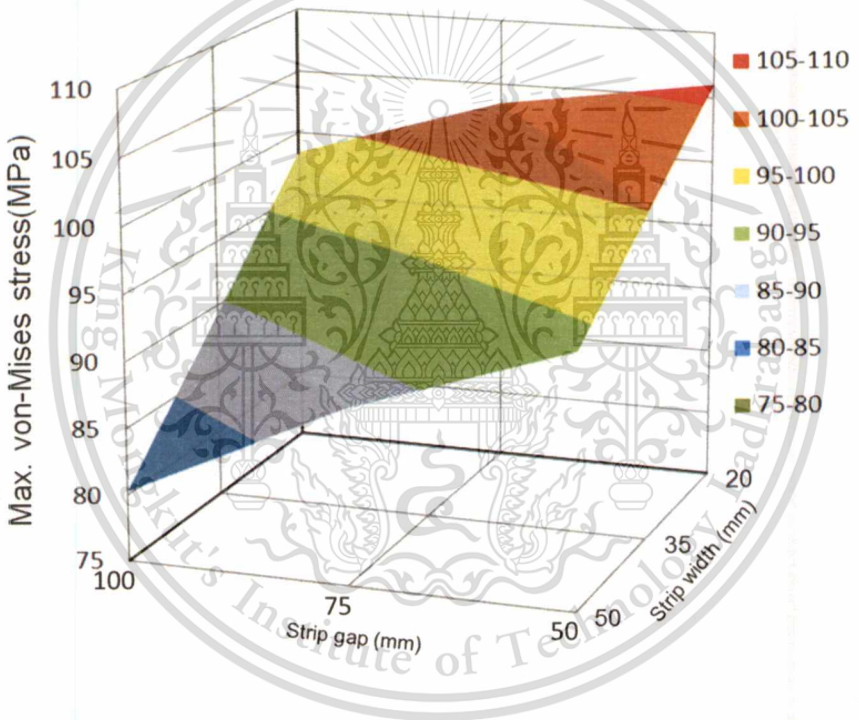

Figure 5.15 Response surface of maximum von-Mises stress for clutch housing design parameters of strip gap and strip width

According to the response surfaces and sensitivity chart, incresing of strip width and strip gap resulted in a decrease of a maximum von-Mises stress. Significantly, an increase of strip witdth parameter led to an incresing of weight whlie the strip gap had no effect. From the obtained response surface and sensitivity chart in Figure 5.15 and Figure 5.16, the optimum point was found at 47.2 mm strip width and 96.2 mm strip gap with a resulting maximum von-Mises stress of 83.27 MPa and satisfied fatigue life condition. Additionally, this proposed model would have a volume of $4899.26x10^{3}mm^{3}$ or 35.86Kg of weight. The corresponding stress distribution results are shown in Figure 5.17.

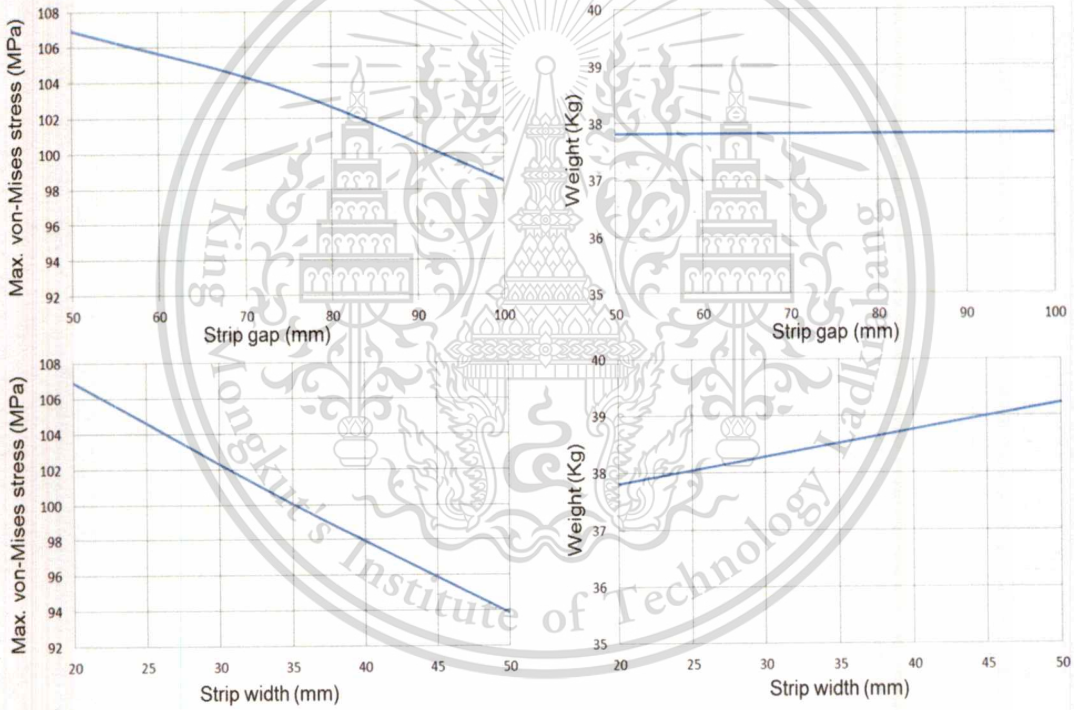

Figure 5.16 Sensitivity charts of strip gap and strip width parameters

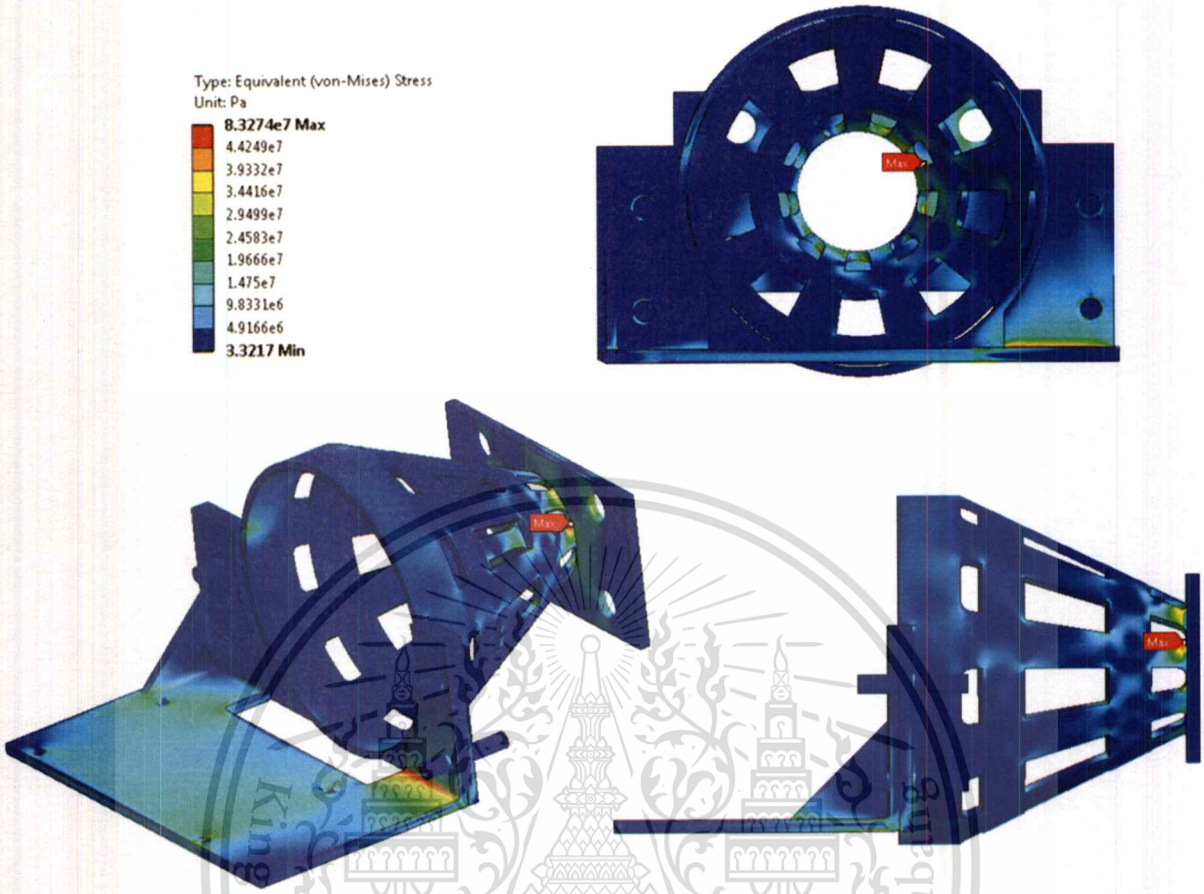

Figure 5.17 Von-Mises stress distribution in optimum spokes-and-strips clutch housing

5.3 Clutch contact surface and bolts attached stress analysis results

5.3.1 Analytical results: Clutch contact surface stress analysis

In case of the clutch contact surface stress analysis, the maximum von-Mises stress of 31.062 MPa was observed on the corner of back rib near a hole of clutch cover mounting as show in Figure. 5.18. In addition, majority part of the clutch disc contact surface area showed a small stress distribution von-Mises stress with an avearage value of 10 MPa. According to a minimum Safety of Factor requirement of 4.4, this design was archived with resulting Safety of Factor of 8.45.

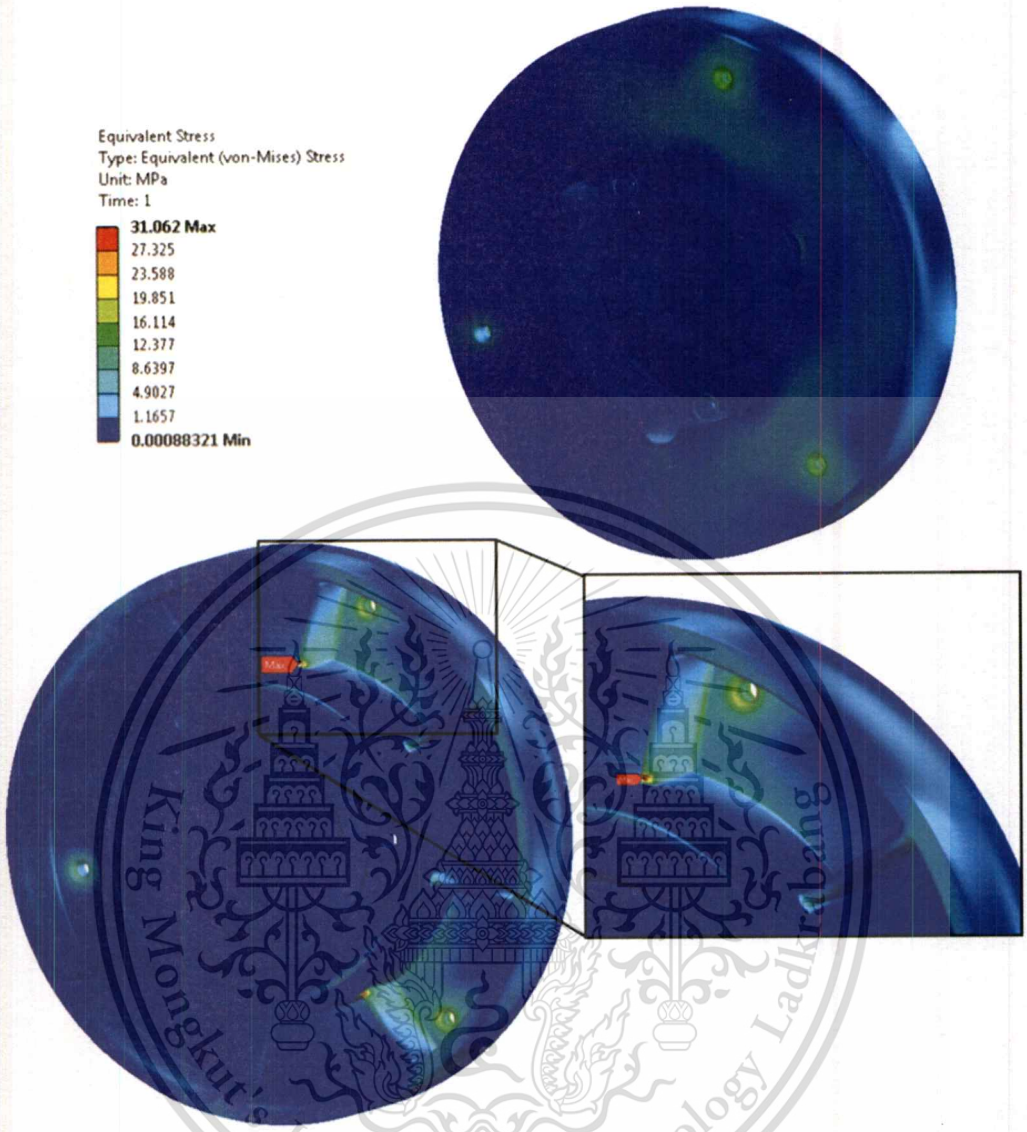

Figure 5.18 Calculated von-Mises stress distribution in clutch contact surface

5.3.2 Analytical results: Clutch contact surface bolts attached stress analysis

The analyzed results of the bolts attached with the loading moment were analyzed, the maximum Von-Mises stress was calculated to be 36.095 MPa on the bolt and on the flywheel at the clutch contact surface connection area as shown in Figure 5.19. In case of axial stress or normal stress of the critical bolt in x, y, z axis, the maximum values were 4.674 MPa, 27.269 MPa, and 4.067 MPa, respectivly. The graphical of stress distribution on the models are shown on Figure 5.20.

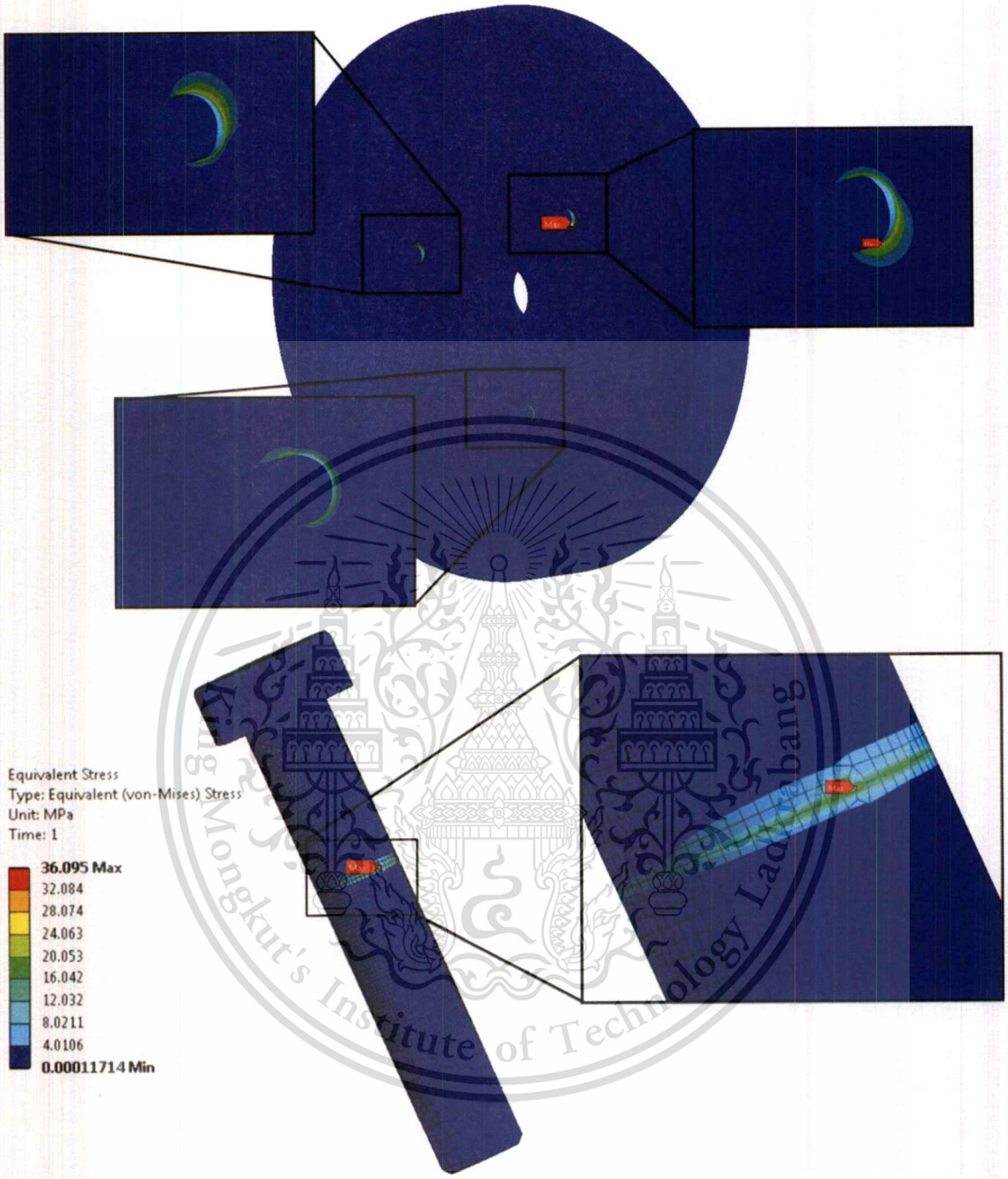

Figure 5.19 Calculated von-Mises stress distribution on the clutch contact surface with attached bolts

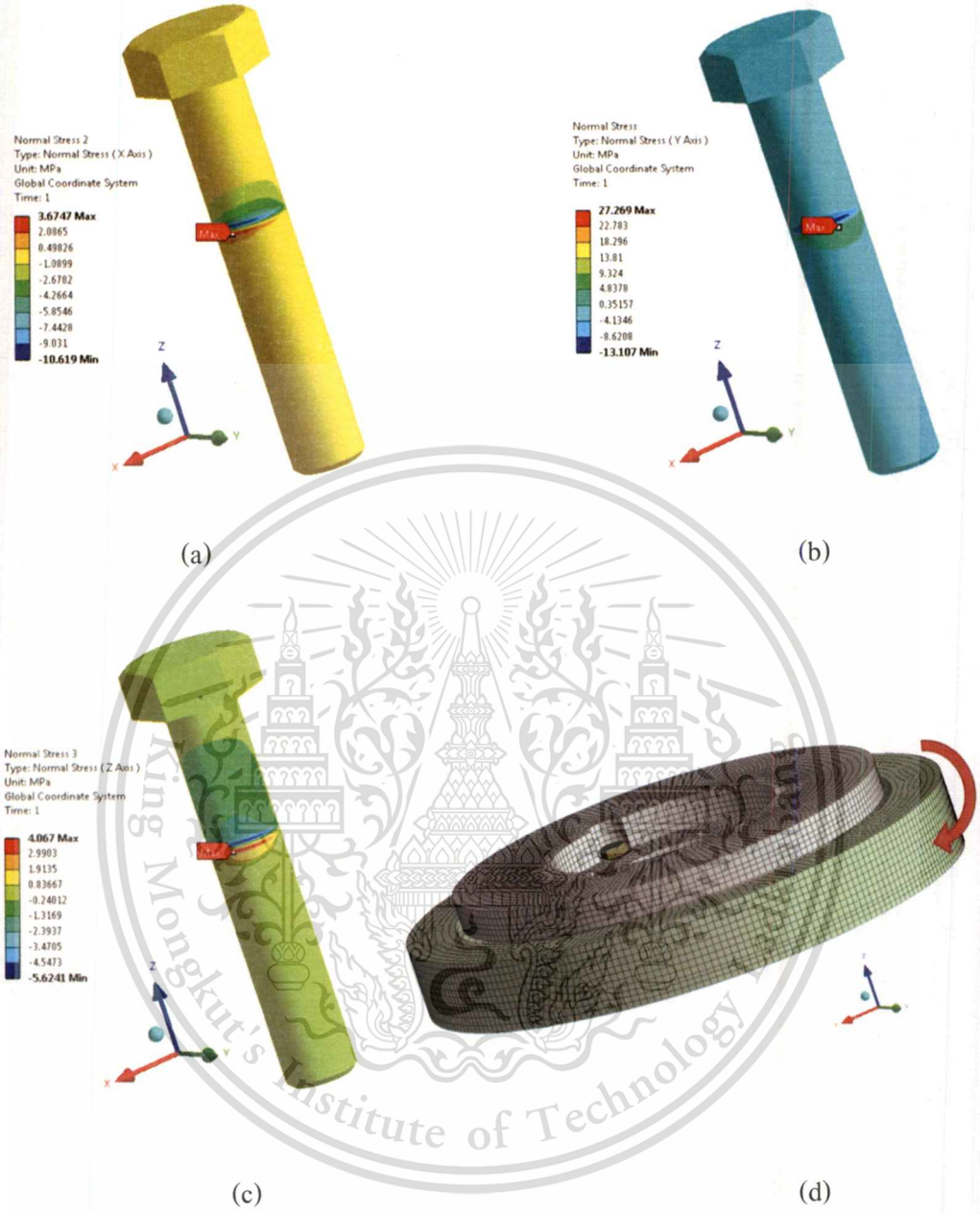

Figure 5.20 Von-Mises stress distribution and maximum point on the clutch contact surface attached bolt (a) normal stress along x axis (b) normal stress along y axis (c) normal stress along z axis or axial stress (d) illustration of applied load

5.4 Shaft adapter analysis results

The computational results on the shaft adapter prototype model indicated a maximum von-Mises stress of 48.548 MPa on the fillet of spline and shaft connection area as shown in Figure 5.21. In case of the middle section and inner area of the shaft, the von-Mises stress distribution was about 16-30 MPa from inside to outside of shaft cross section. In addition, a shear stress was calculated with a maximum stress result of 17.138 MPa as shown in Figure 5.22.

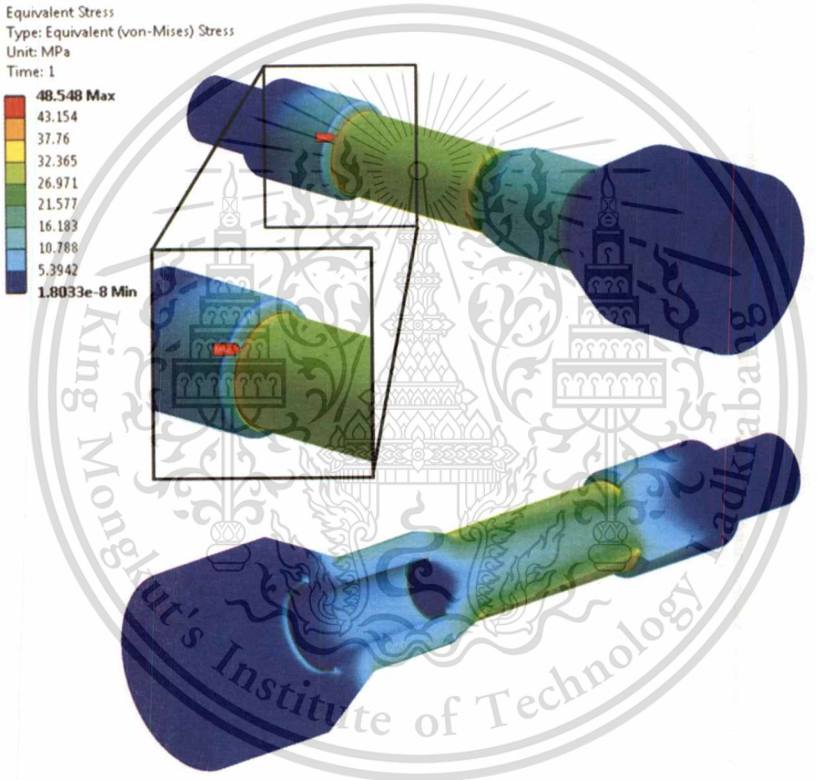

Figure 5.21 Von-Mises stress distribution on the shaft adapter with the maximum point

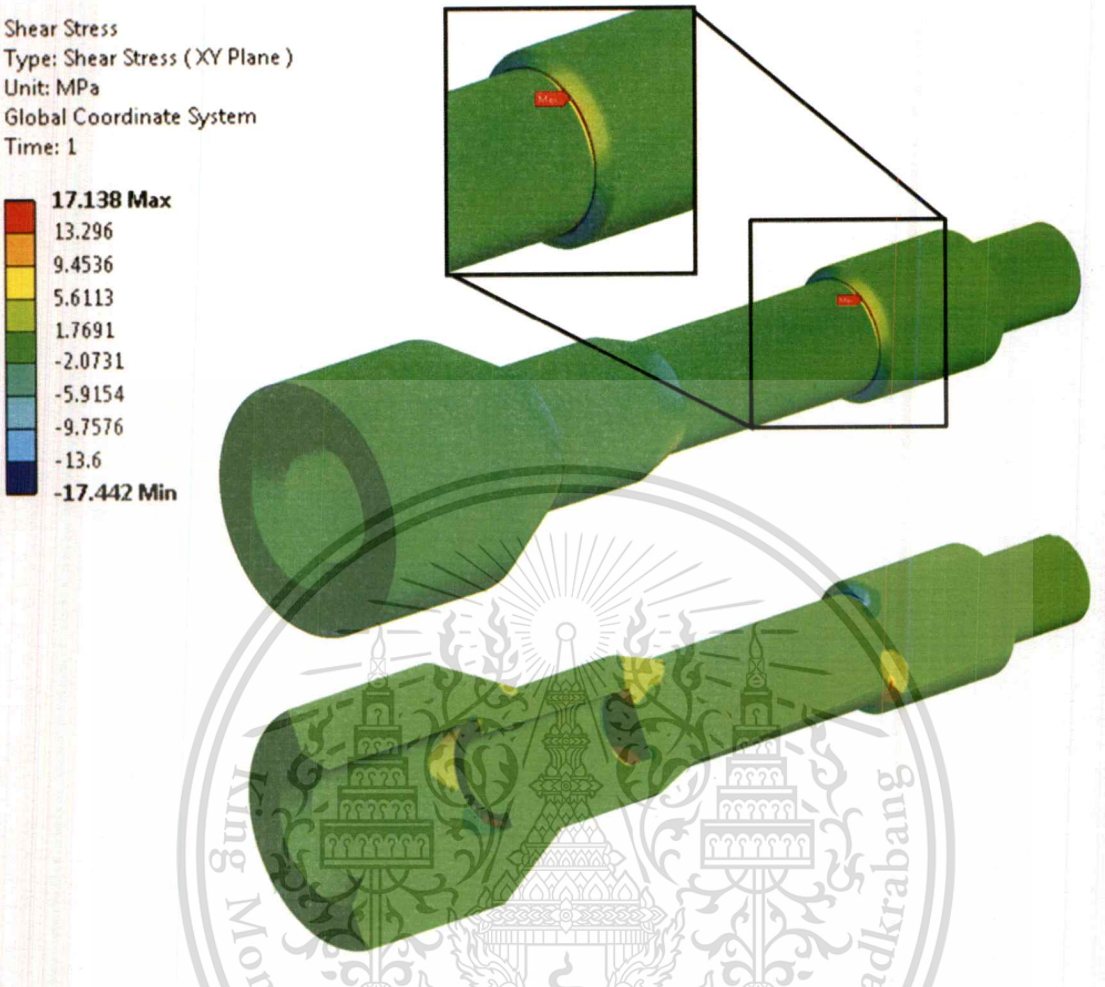

Figure 5.22 Shear stress distributions on the shaft adapter with the maximum point

5.5 Performance comparing experiment test results

5.5.1 Belt transmission system

The belt transmission experiments were carried out on the belt transmission test rig explained in the previous chapter. The tension of the belt was varied between 1.7, 2.3, and 3 Kg. Each of the belt tension values was then tested under different engine loads of L1, L2, L3, and L4 explained in the previous chapter. In this section, the revolution and torque results of drive shaft and driven shaft were denoted with A and B respectively such as RPM A, Torque B, etc. For each set of test, the results

were comprised of RPM A, RPM B, Torque A, Torque B, Slip percentage, and Torque difference. In addition, three sets of results were displayed together to visually show the repeatability of the results.

The results of belt transmission experiments under 1.7 kg belt tension are shown in Figure 5.23 to Figure 5.26. The maximum revolution speed of drive shaft (RPM A) could be observed as 2,510 rpm, 2,300 rpm, 1,700 rpm, and 980 rpm. Similar amount of speed was observed on another shaft (RPM B). From the experimental data, the torque on drive shaft (Torque A) at load L1-L4 was measured to be 13.5 Nm, 26 Nm, 33 Nm, and 37.5 Nm, respectively. On the other hand, the measured maximum Torque B was found to be 5.9 Nm, 19 Nm, 27.5 Nm, and 33 Nm, respectively. As a result, the torque difference between A and B was shown to be approximately 5-6 Nm. Moreover, the slip of the system was calculated and plotted. In this case, the slip of a transmission was investigated to be within the range of 0%-1.8%, 0.2%-1.8%, 0%-2%, and 0.5%-2.7% under the load condition L1-L4 respectively.

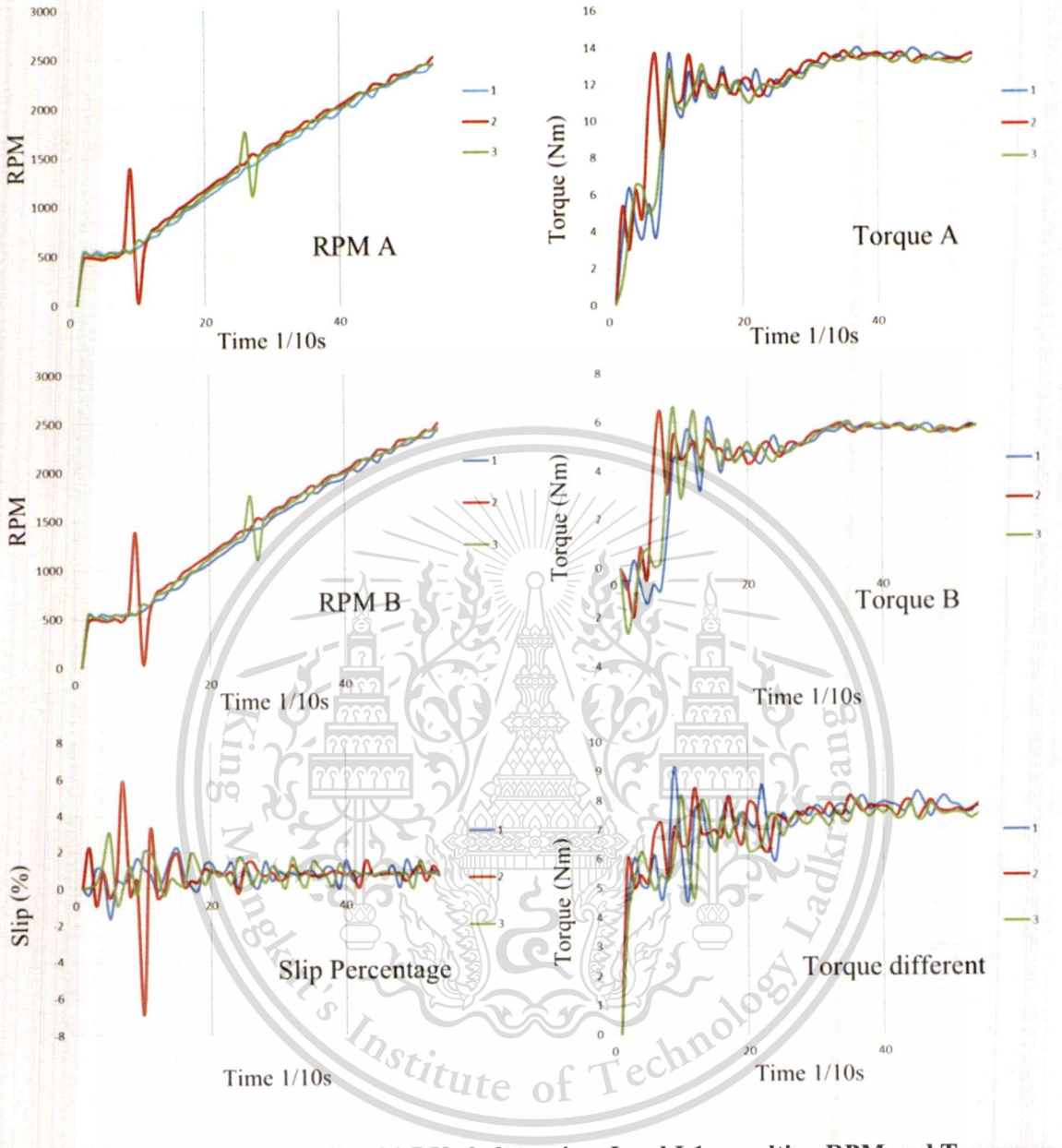

Figure 5.23 Experimental results of 1.7 Kg belt tension, Load L1: resulting RPM and Torque on both pulleys, Slip percentage, and Torque difference.

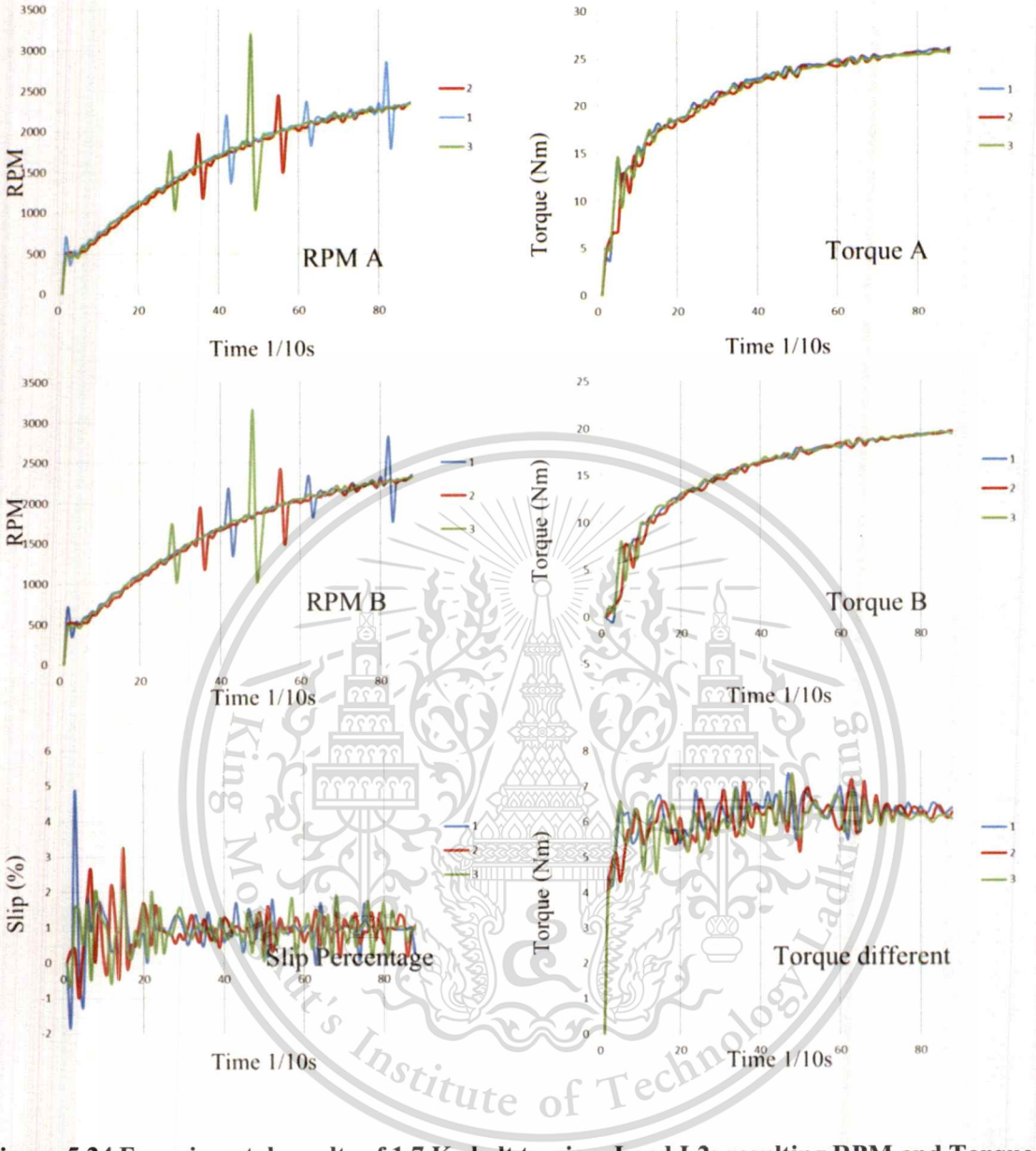

Figure 5.24 Experimental results of 1.7 Kg belt tension, Load L2: resulting RPM and Torque on both pulleys, Slip percentage, and Torque difference.

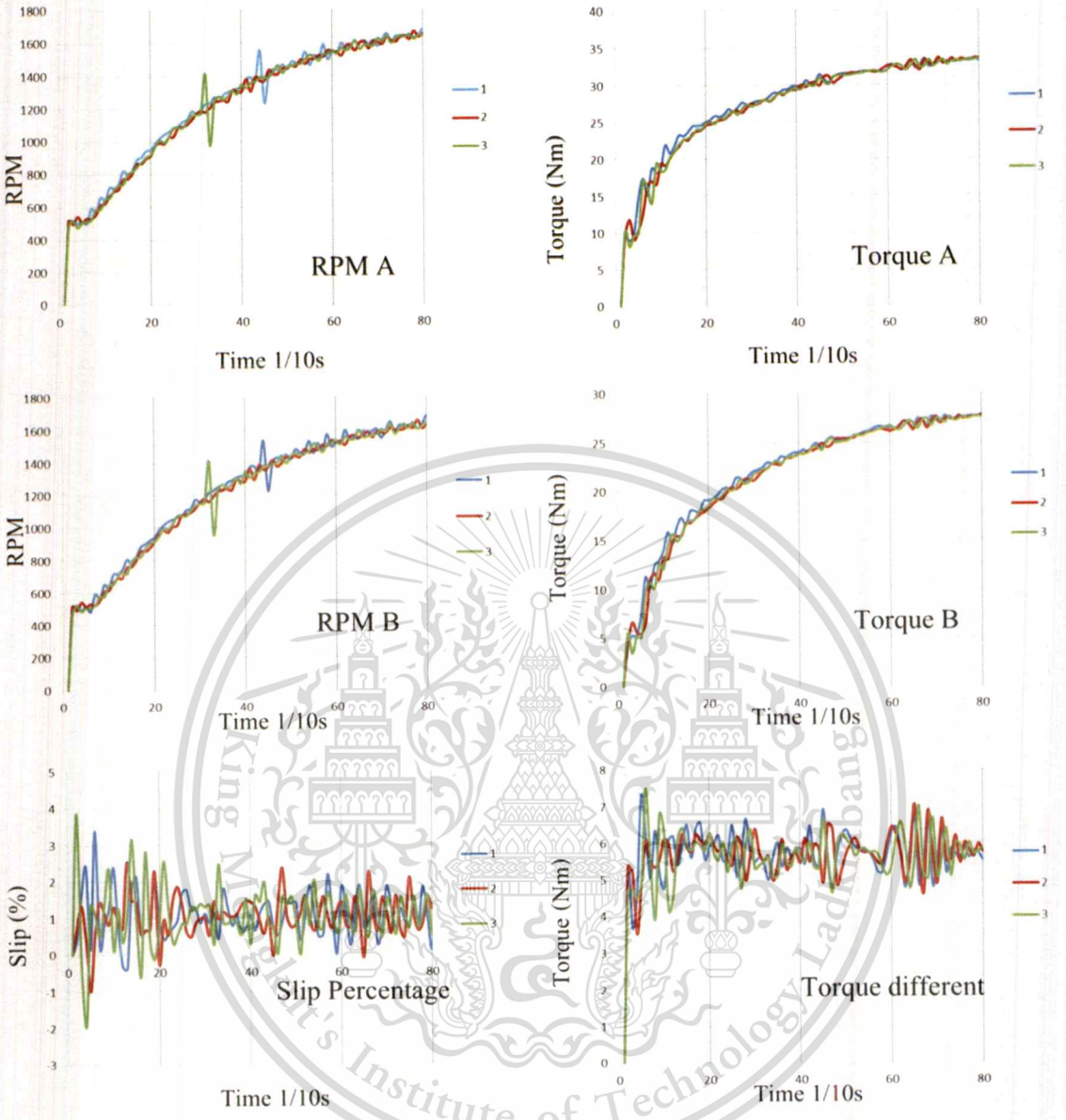

Figure 5.25 Experimental results of 1.7 Kg belt tension, Load L3: resulting RPM and Torque on both pulleys, slip percentage, and Torque difference.

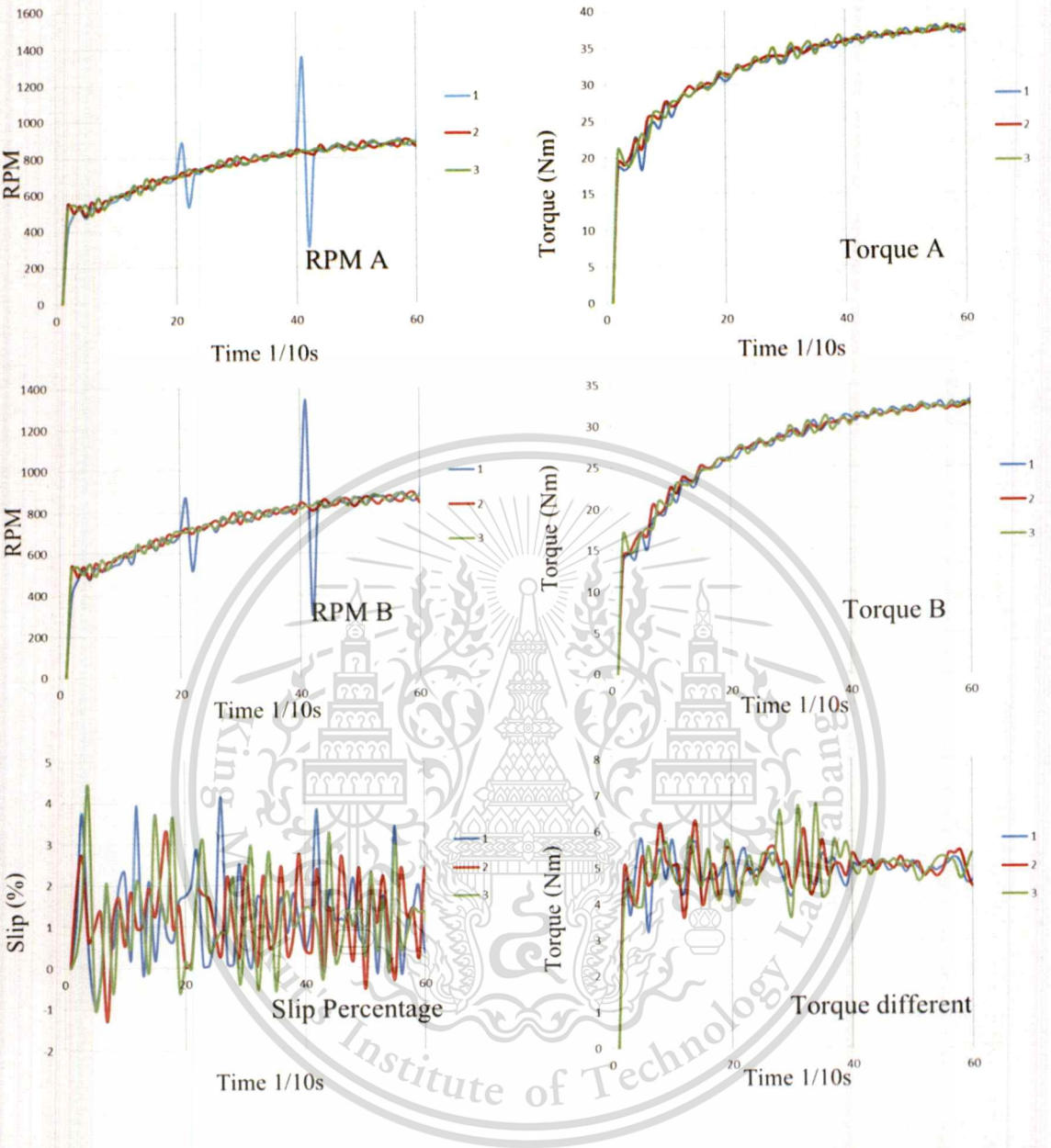

Figure 5.26 Experimental results of 1.7 Kg belt tension, Load L4: resulting RPM and Torque on both pulleys, Slip percentage, and Torque difference.

In case of 2.3 Kg belt tension experiments, the results data are shown from Figure 5.27 to Figure 5.30. The maximum of RPM A and RPM B were about 2500 rpm, 2400 rpm, 1680 rpm, and 920 rpm in respective to L1, L2, L3, and L4 load conditions. In experimental results data, a measured maximum Torque A at load L1-L4 was found to be 13 Nm, 26 Nm, 34.5 Nm, and 39 Nm. Furthermore, a maximum Torque B was found to be 6 Nm, 20 Nm, 29 Nm, and 34 Nm, respectively

with a torque difference about 5-6 Nm. In addition, the slip of a transmission was investigated as 0.2%-1%, 0.1%-1.75%, 0.2%-1.8%, and 0%-2% corresponding to increasing load.

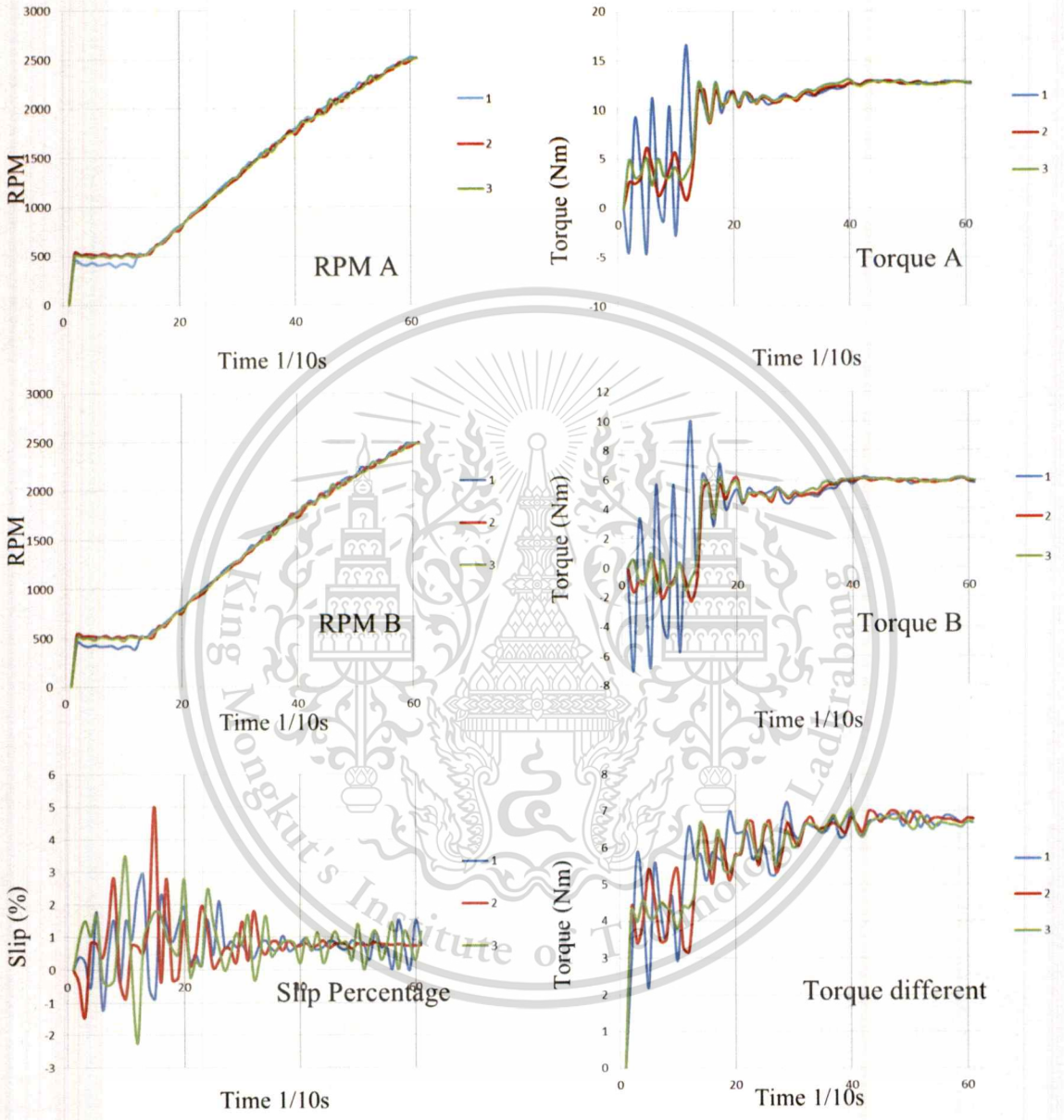

Figure 5.27 Experimental results of 2.3 Kg belt tension, Load L1: resulting RPM and Torque on both pulleys, Slip percentage, and Torque difference.

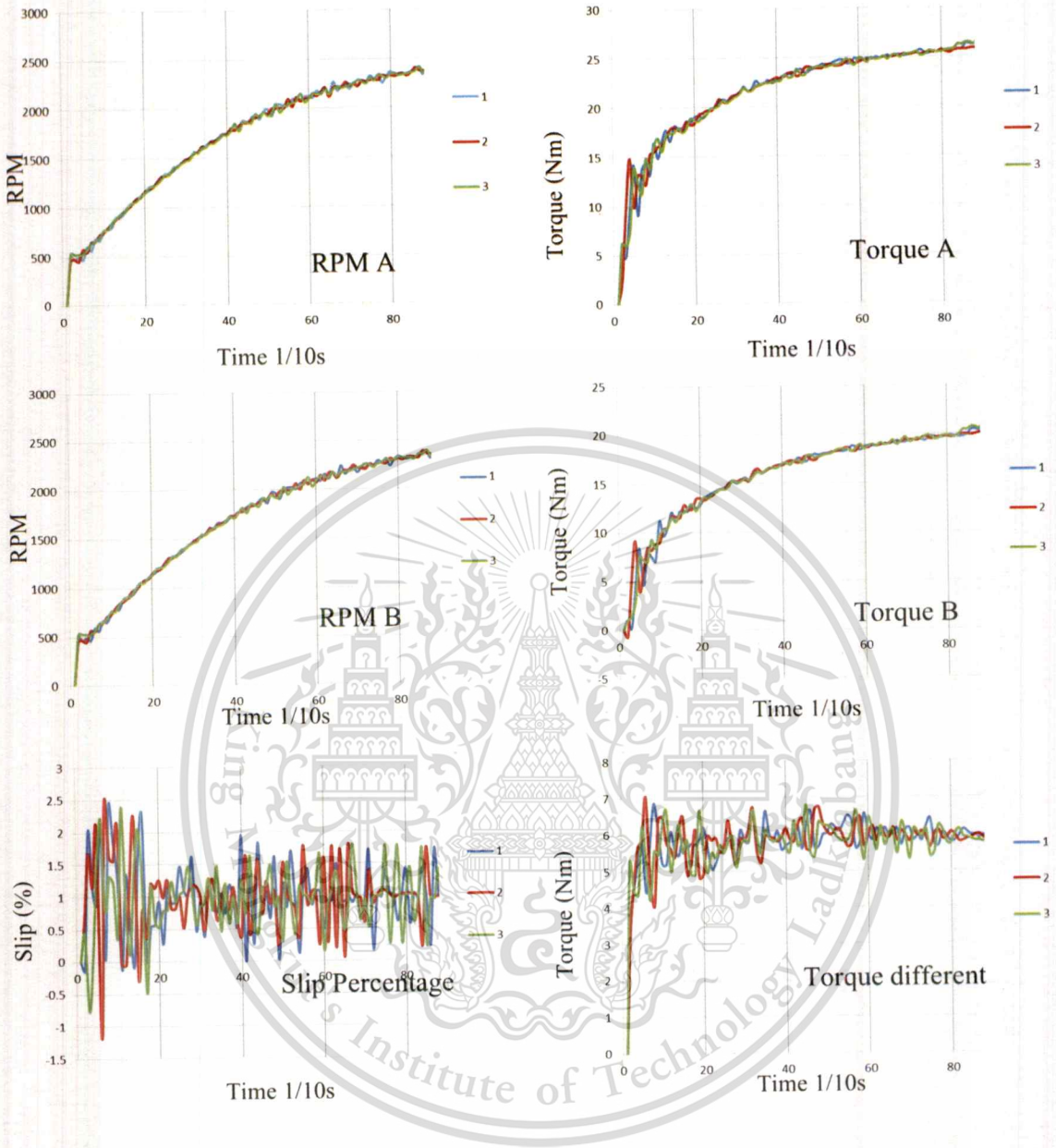

Figure 5.28 Experimental results of 2.3 Kg belt tension, Load L2: resulting RPM and Torque on both pulleys, Slip percentage, and Torque difference.

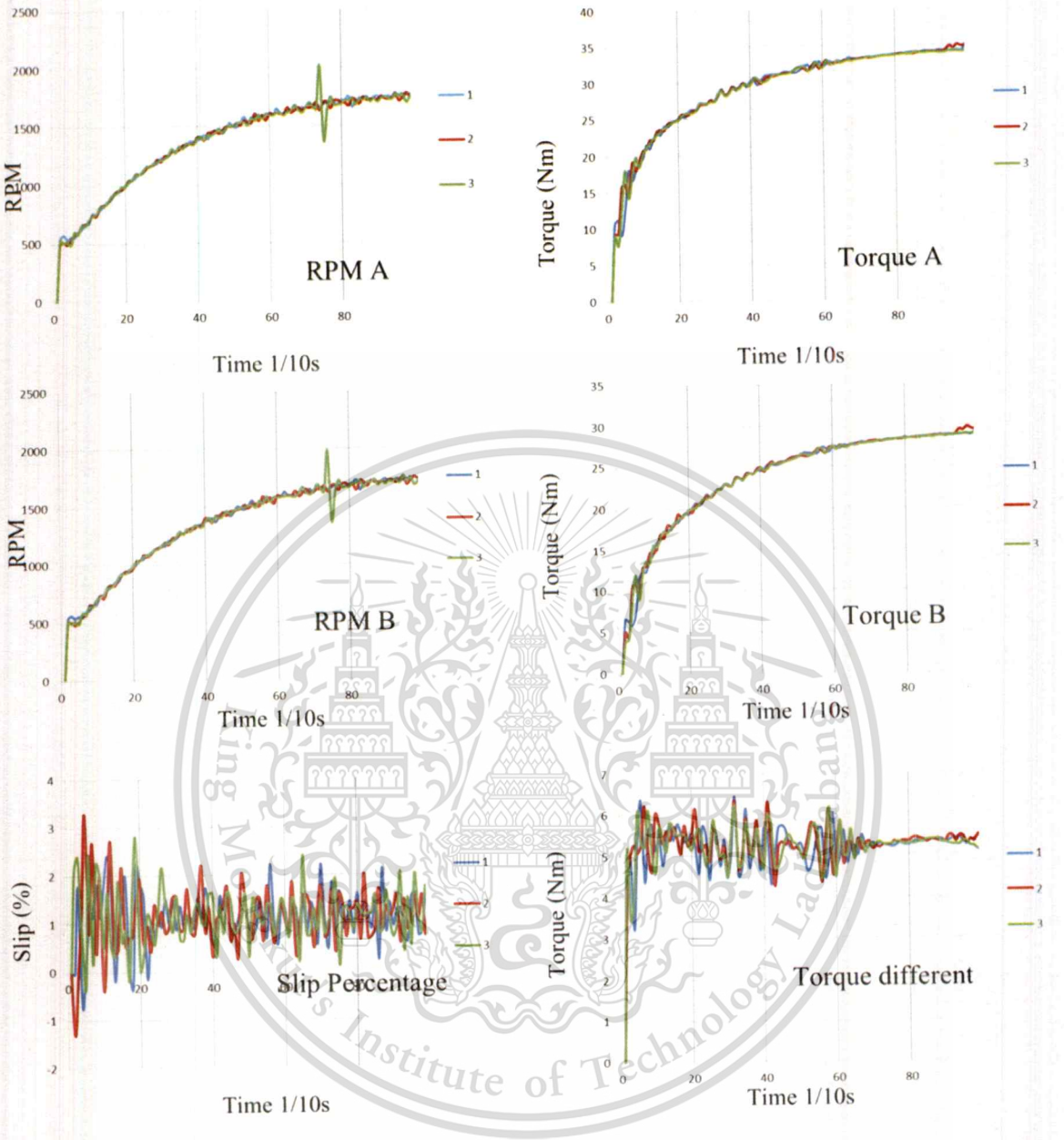

Figure 5.29 Experimental results of 2.3 Kg belt tension, Load L3: resulting RPM and Torque on both pulleys, Slip percentage, and Torque difference.

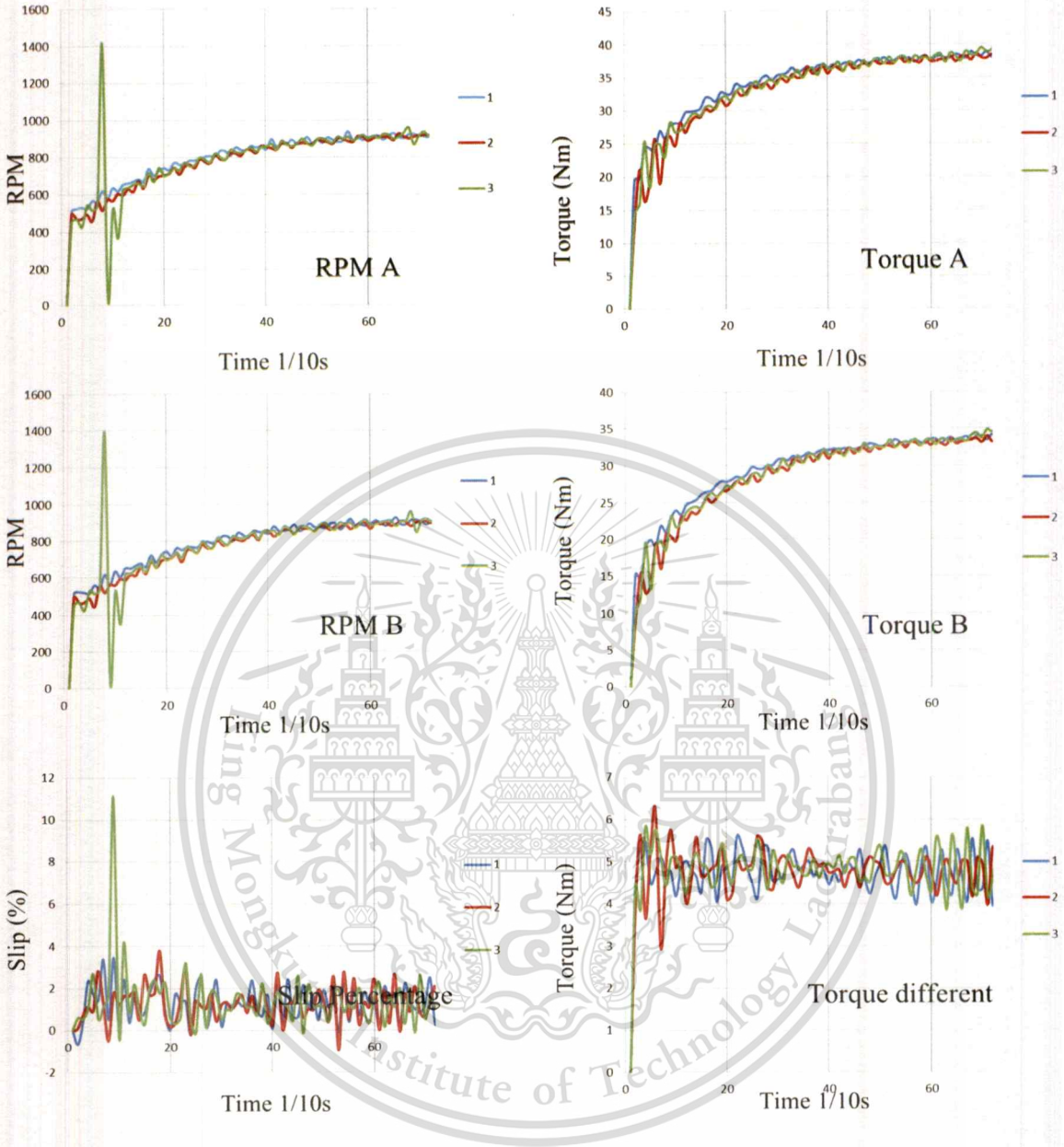

Figure 5.30 Experimental results of 2.3 Kg belt tension, Load L4: resulting RPM and Torque on both pulleys, Slip percentage, and Torque difference.

Results from 3 Kg belt tension tests are shown in Figure 5.31 to 5.32. It was found that the RPM A and RPM B reached maximum values of about 2500 rpm, 2400 rpm, 1470 rpm, and 980 rpm when the load was increased. Furthermore, a maximum Torque A was 12.4 Nm, 26 Nm, 34 Nm, and 39Nm. In view of Torque B the value was reduced to 6 Nm, 21.5 Nm, 30 Nm, and 35 Nm. Then, the

torque different could be determined as 5-6 Nm. Moreover, the system slip was about 0.98%, 0.6%-1.6%, 0.3%-2.2%, and 0.5%-2.2%.

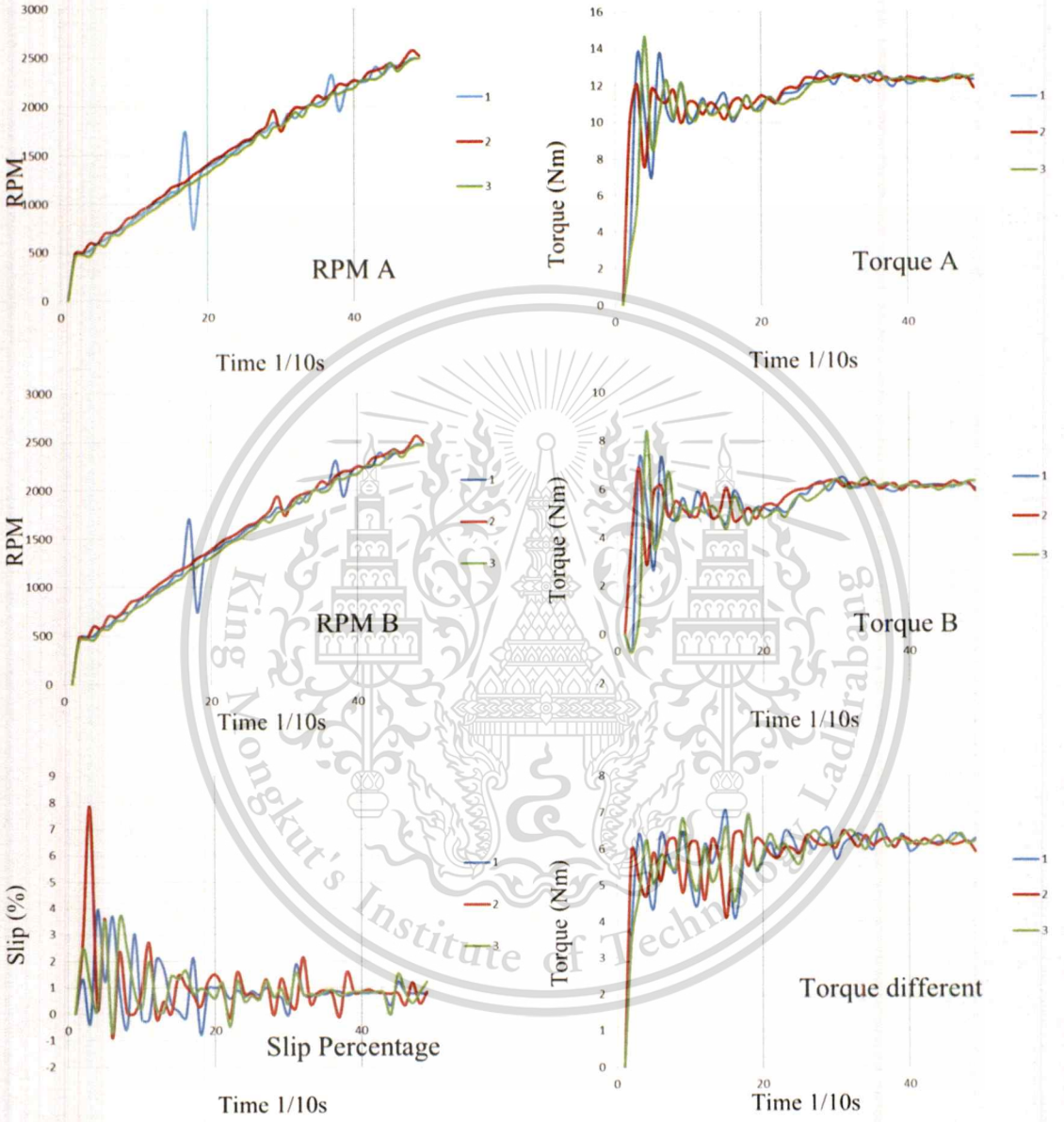

Figure 5.31 Experimental results of 3 Kg belt tension, Load L1: resulting RPM and Torque on both pulleys, Slip percentage, and Torque difference.

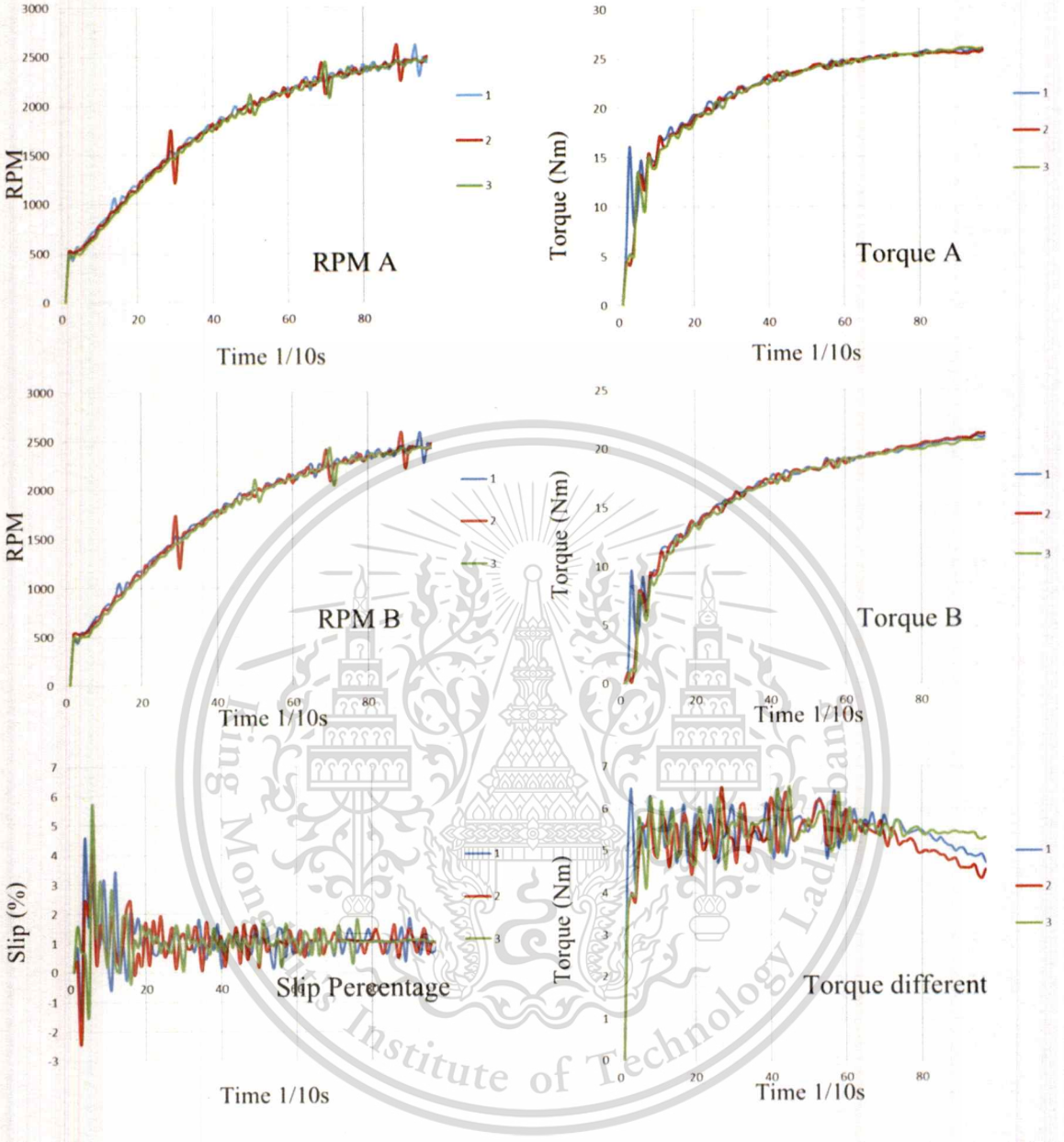

Figure 5.32 Experimental results of 3 Kg belt tension, Load L2: resulting RPM and Torque on both pulleys, Slip percentage, and Torque difference.

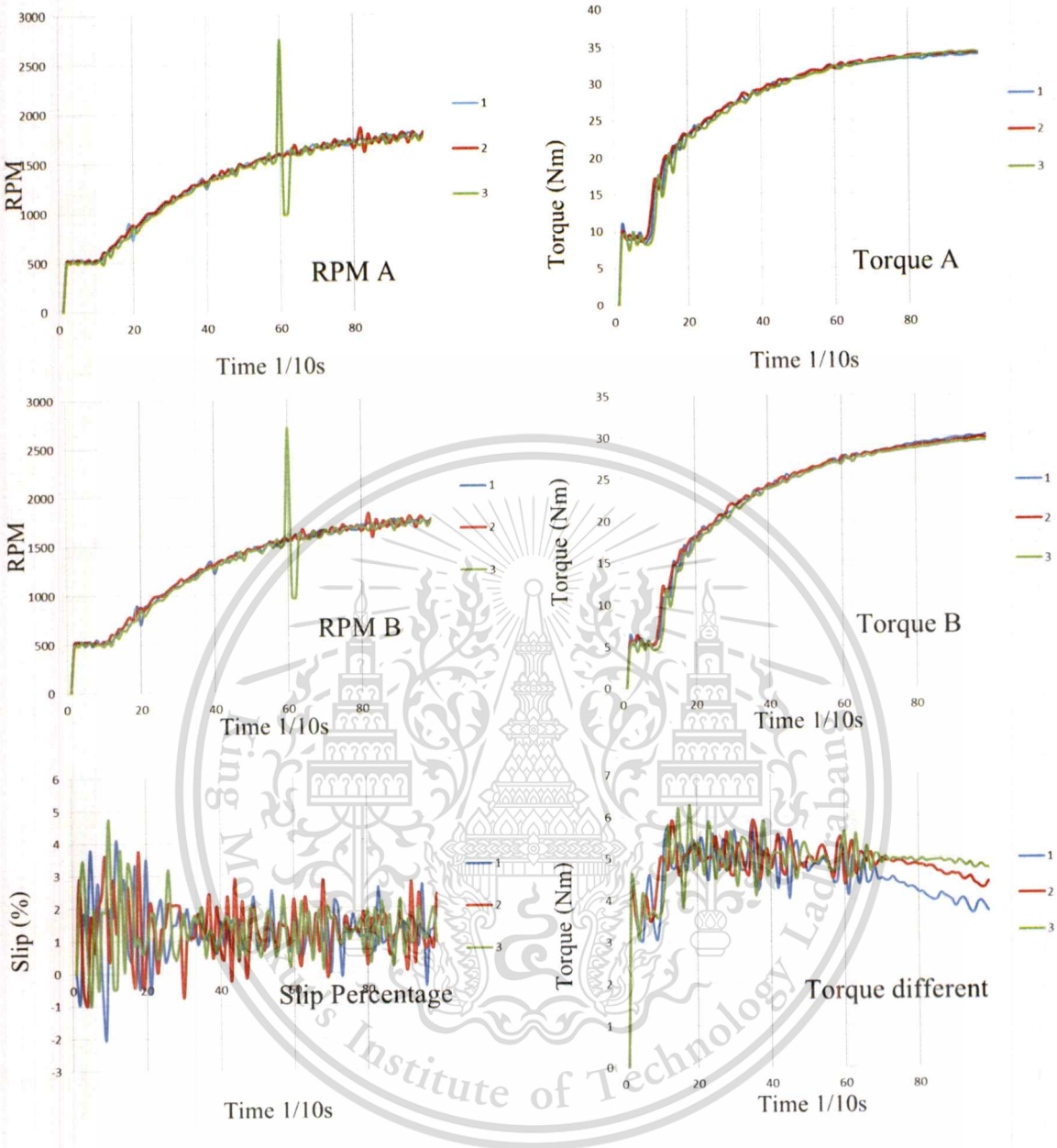

Figure 5.33 Experimental results of 3 Kg belt tension, Load L3: resulting RPM and Torque on both pulleys, Slip percentage, and Torque difference.

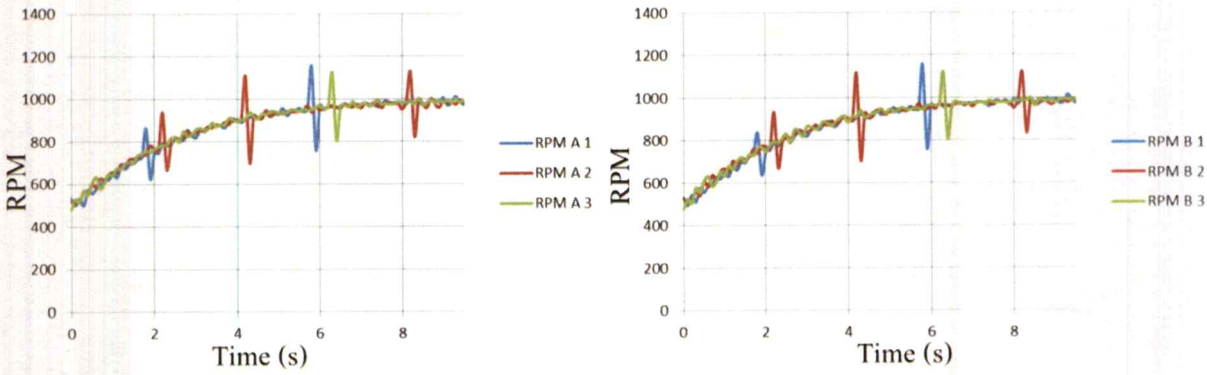

Figure 5.38 Direct clutch system experimental results: RPM on both sides of the clutch transmission under L4 load conditions

Figure 5.39 displays Torque B results from each load test conditions of direct clutch system while engine was fully accelerated. It could be seen that the transmitted Torque B was 5 Nm, 22.5 Nm, 31 Nm, and 38 Nm under load condition L1 to L4 respectively.

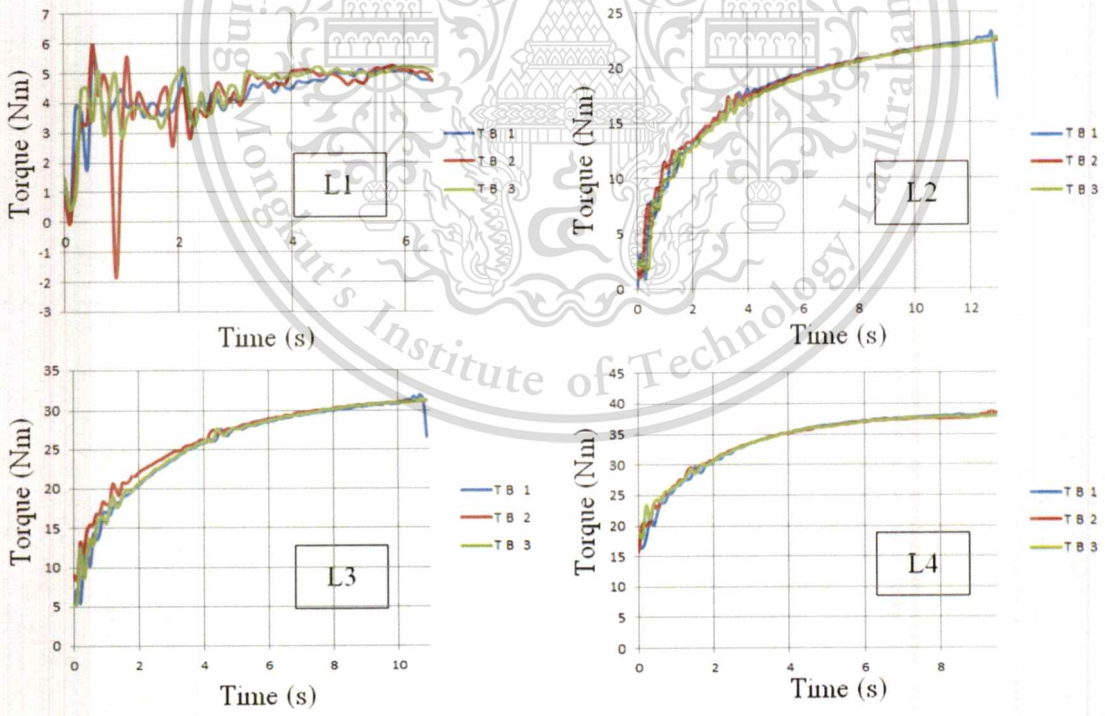

Figure 5.39 Direct clutch system: Measured Torque B under each engine load conditions

Furthermore, slip percentage results from each load test conditions of direct clutch system while engine was fully accelerated are shown in figure 5.40. Slip percentage was measured to be ±0.8%, ±0.5%, ±0.8%, and ±1% under increasing engine load conditions.

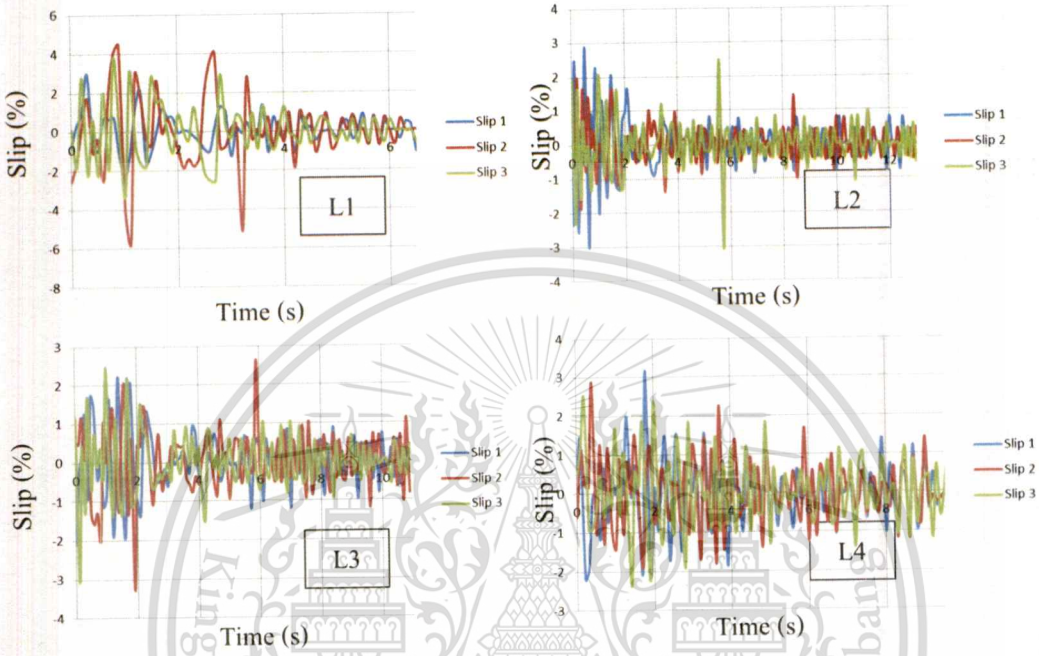

Figure 5.40 Direct clutch system: Measured Slip under different load conditions

5.6 Clutch housing strain measurement experimental results

In this section, the measured strains from the experiments were converted to a stress using Hook's law. The positive and negative values of level stress indicated a tensile and compressive stress respectively. The stress measurement results on three locations with six different strain gages data were logged only during the full load operation of the engine. From Figure 5.41, it could be seen that the maximum magnitude of stress at location B1, B2, S1, S2, T1, and T2 was -3.22, 1.00, 0.27, 0.23, 0.47, and 0.46 MPa respectively. In contrast, the computed stresses at these considered locations were 38.49, 9.79, -0.50, 2.66, 0.13, and 0.86 MPa. However, the most significant responses were observed at the measurement points located on location B that generated a maximum compressive stress of 3MPa and 1MPa of tensile stress which was also the same location as noticed with computational

results. For this reason, the possible reasons for difference between simulation and experiment results will be discussed in Chapter 6.

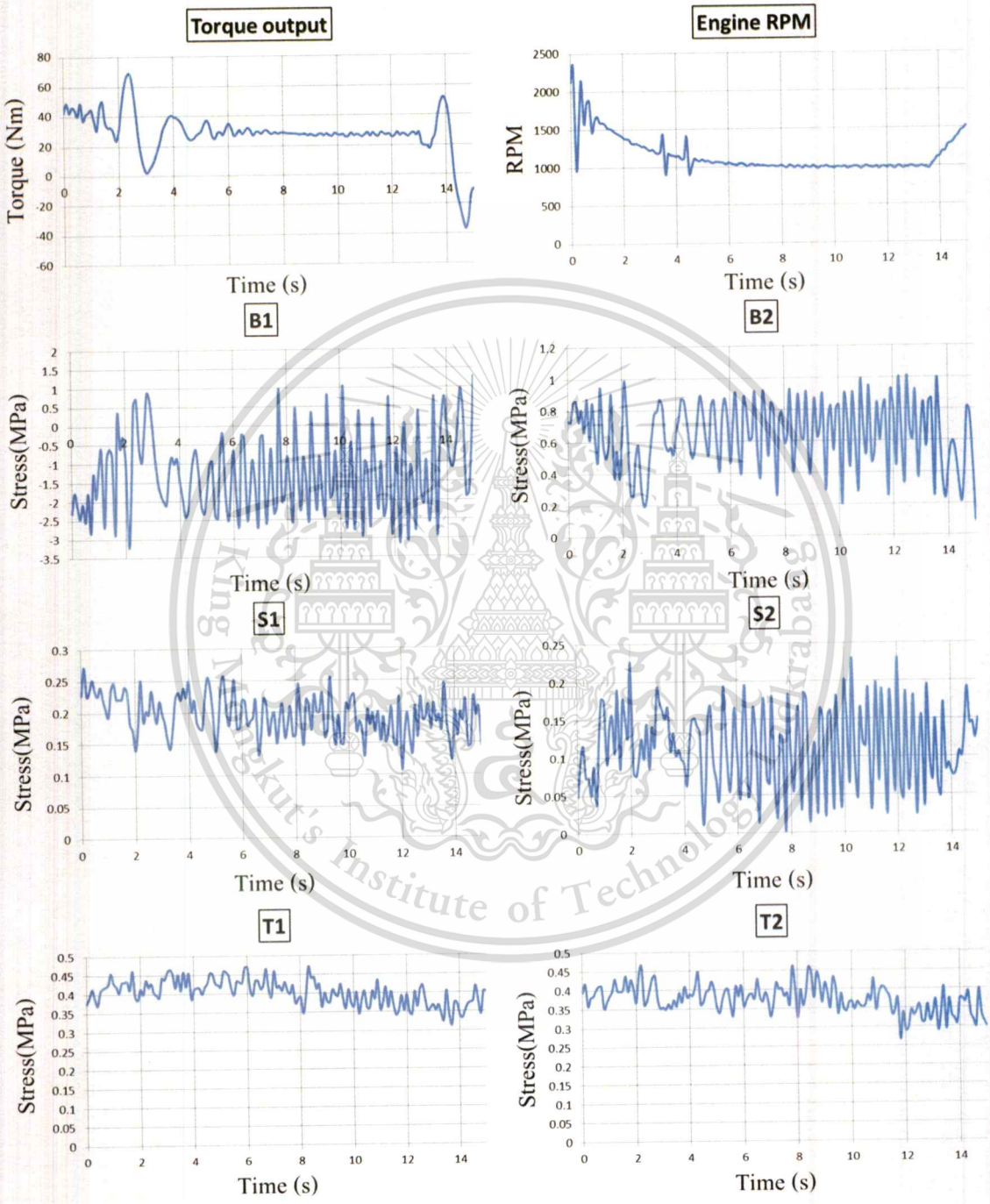

Figure 5.41 Stress responses measurement during a full engine load on three different locations of the direct clutch housing, with corresponding RPM and torque outputs monitoring

CHAPTER 6

DISCUSSIONS

6.1 Vibration load measurement

In vibration loading measurement, an engine vibration loading was measured and was later applied as input parameters (loads) in a finite element analysis. The experimental results showed that a vibration loading amplitude of one cylinder diesel engine could increase from 0.002g to 4.22g with an increasing engine load. The dominant vibration amplitude occurred on a plane corresponding to a piston cylinder movement. Also, in order to employ the measured data effectively, a low pass filtering was needed.

6.2 Clutch housing analysis and optimization

In the first design, the clutch housing was designed to be a conical-shaped sloped housing model. According to the first response surface results (Figure. 5.5), a sensitivity of the clutch housing slope angle was relatively low since incresing of a slope angle only resulting in a slight decrease in correspondingmaximum von-Mises stresses. In contrast, a variation of clutch housing thickness showed a very high sensitivity such that maximum von-Mises stress significantly increased when the thickness was decreased. In addition, increasing of both parameters would result in an increase of the total volume of the model. Finally, the weight of the optimum model was 40.37 Kg.

After the first analysis, it was observed that the middle section of clutch housing model was containing a low stress distribution. Therefore, the middle section was redesigned into a spoke model. For analyses of spoke design sensitivities ,the maximum von-Mises stress was greatly decreased with an increasing number of spokes. However, the maximum von-Mises stress was still over the required value of 83.33 MPa. The double-sized spokes were assigned to further decrease the resulting maximum von-Mises stress. The optimum number of double-sized spokes number was 9, which resulted in 139.35 MPa of maximum von-Mises stress, or 265.55% decrease from 370.01 MPa with smaller spokes. The reason for choosing 9-spokes model was that it was the highest number of spoke which could be fitted in the available space after doubling a spoke width.

For the strips-added model, the response surface optimization technics was again used to find the optimum location and size of strips. As a result, the maximum von-Mises stress was decreased with an increasing strip gap and strip width while the former was a much more sensitive parameter. Lastly, the optimum spokes strips model was found via the response surface at 47.2 mm strip width and 48.1 mm strip gap under the corresponding maximum von-Mises stress of 83.27 MPa with a satisfactory fatigue performance and the overall weight of 35.86 Kg.

In addition, all models were compared to present the difference between each model. For the weight effective purpose, the spokes-and-strips clutch housing model was the best such that the weight was reduced from 51.27 Kg of the first design clutch housing model to 35.86 Kg. In other words, the overall weight of the housing model was decreased by 29.72%. While the first optimum model could only result in a weight reduction of just 20.88%. Details of each clutch housing model were compared and shown in Table 6.1.

Table 6.1 Model comparison table

Model Types	Volume (mm^3)	Weight (Kg)	Weight reduction (%)	
			First optimum model	First design model
First design model	6500.30×10^3	51.27	-	-
First optimum model	5515.43×10^3	40.37	-	20.88
Spokes with strips optimum model	4899.26×10^3	35.86	11.17	29.72

6.2.1 Clutch housing fatigue analysis

According to the clutch housing analysis, there was no failure in fatigue mode. To study further about the fatigue aspect of the model, the thickness of clutch housing was reduced to 7 mm to generate a fatigue failure situation. Analytical results of fatigue failure locations are illustared in Figure 6.1. After the relation of a fatigue life and a maximum von-Mises stress had been investigated it was concluded that fatigue failure would occur when the safety of factor was lower than 3 as shown in Figure 6.2.

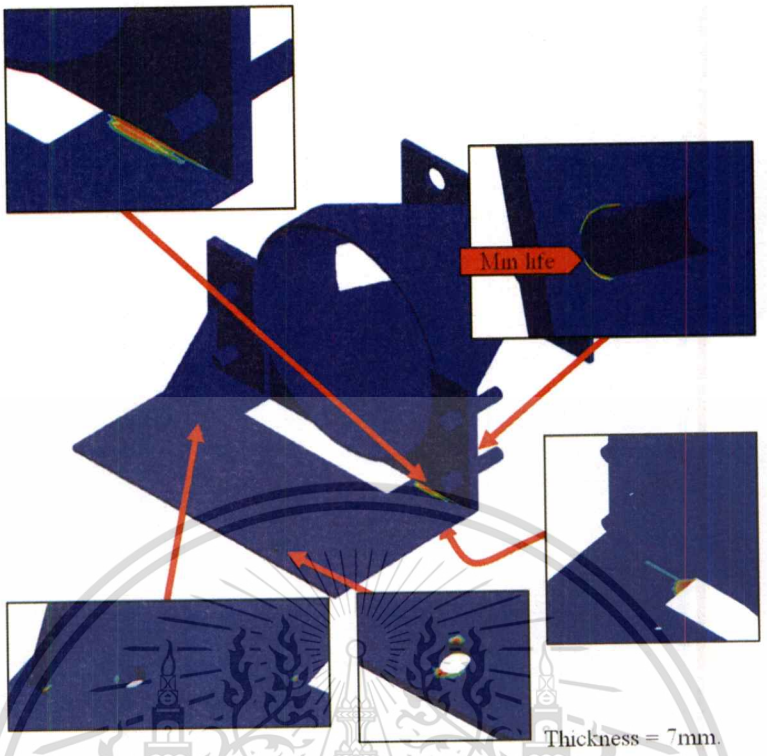

Figure 6.1 Fatigue failure location of Clutch housing with 7 mm. of thickness

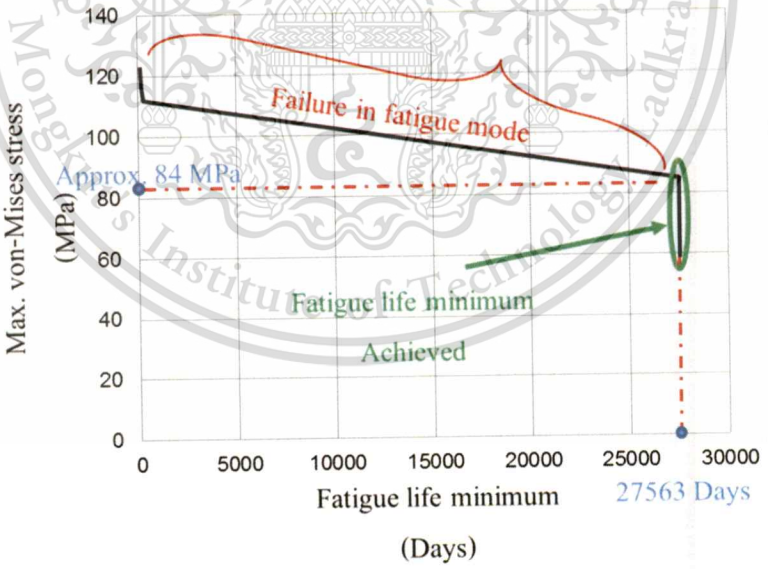

Figure 6.2 Correlation between fatigue life and maximum von-Mises stress

6.3 Clutch contact surface and bolts attached stress analysis

6.3.1 Clutch contact surface stress analysis

From a result of clutch contact surface analysis, the maximum von-Misses stress of about 31.062 MPa was generated on the back rib location near a clutch cover mounting area. Then, the majority of high-level stress was distributed on the clutch disc contact area and ribs on the back of model. The safety of factor of this model was 8.45, which was about double that of the requirement of 4.4 as suggested by J.M. Starbuck et al. [26]. This indicated that this model was still overdesign.

6.3.2 Bolt attached stress analysis

In this analysis, three bolts were analyzed in a static fashion under a load from the engine in case of an extremely condition i.e. transmission lock up. From a result of maximum von-Misses stress shown in the previous chapter, the peak stress was located on the contact portion between the clutch contact surface and the original flywheel on the bolt with a value of 36.095 MPa. In order to determine suitable classes of M10 bolt to ensure that the selected bolt was strong enough, 36.095 MPa (N/mm^2) was used to compare with shear strengths and yield strengths in a bolt standard chart as shown in Figure 6.3. In this study, M10 class 8.8 was selected for use in this prototype with 640 MPa of yield strength and 480 MPa of shear strength.

Hexagon Head Bolts/Screws

RITZ

Metric Series - Physical Properties - Tightening Torques

Physical Properties:

PROPERTY CLASS			8.8				10.9	
Diameter			≤ M16		> M16		all diameters	
Unit			N/mm²	Kgf/mm²	N/mm2	Kgf/mm²	N/mm²	Kgf/mm²
Tensile Strength, Min.			800	81.5	830	84.6	1040	106.0
Yield Strength, 0.2% offset Min.			640	65.2	660	67.3	940	95.8
Proof Load Stress			580	59.1	600	61.2	830	84.6
Shear Strength, Min.			480	48.9	498	50.8	624	63.6
Hardness	Brinell	HB	219-285		242-319		295-362	
	Rockwell	HRC	20-30		23-34		31-39	
Elogation % on GL = 5.65A. A=Cross Sectional Area			12% Min.				9% Min.	

Figure 6.3 Hexagon head bolts and screws physical properties [27]

6.4 Shaft adapter stress analysis

The static analysis was used to determine the strength of the shaft adapter prototype model under torsional loadings from an engine. A 5 Kg·m of moment load was applied to a clutch disc spline side of the shaft adapter model. Computational results of 48.548 MPa of maximum von- Mises stress and 17.138 MPa of maximum shear stress on the same portion but opposite side were obtained as shown in Figure 6.4. This shaft adapter achieved the stress analysis design goal by exhibiting a safety factor of 5.15 with a 2.5 mm of diameter shaft.

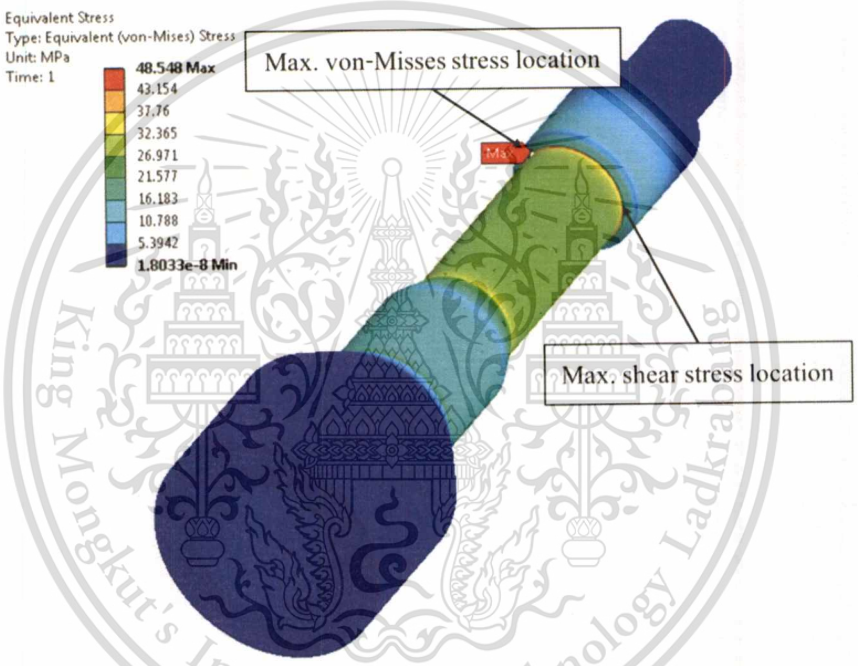

Figure 6.4 Maximum von-Misses stress and maximum shear stress locations on the shaft adapter model

6.5 Direct clutch system components prototype

The constructed and selected components of the direct clutch system prototype are shown below in Figure 6.5 and Figure 6.6. In case of the constructed parts, the simple manufacturing processes, such as turning, milling, drilling, and welding, were employed to fabricate the prototypes. However, for the clutch housing, a roll process was needed for rolling sheet metal strips to form the

body structure of a housing part. All the components were then assembled into the direct clutch system as illustrated in Figure 6.7.

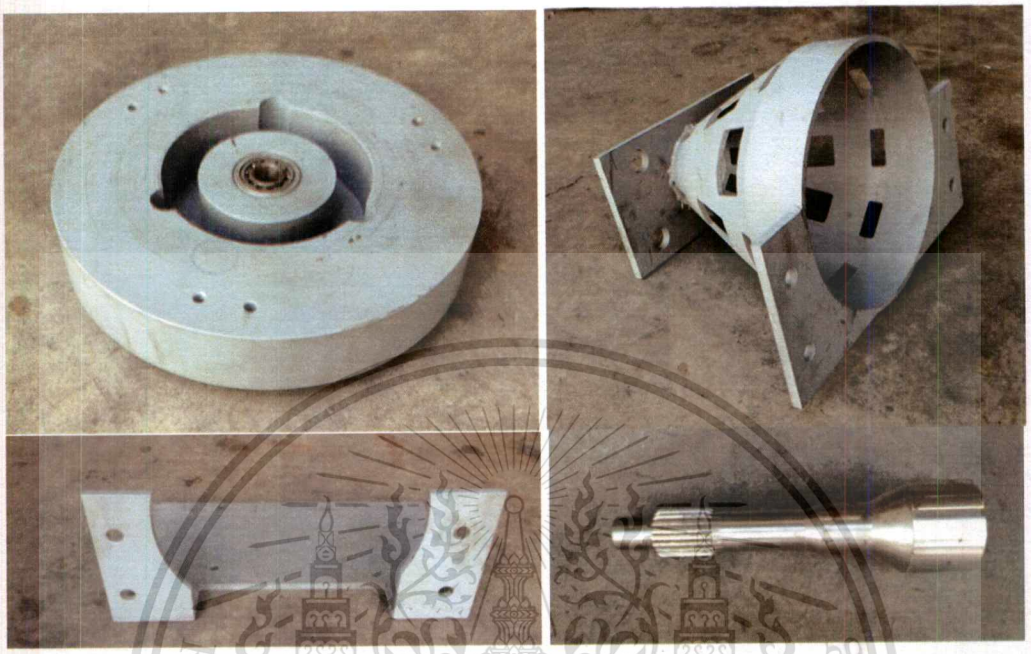

Figure 6.5 Constructed Prototype parts for the direct clutch system prototype

Figure 6.6 Selected commercial parts for the direct clutch prototype: (top) 3L toyota hilux clutch fork, (bottom) Toyota Hilux EXEDY Clutch set

Figure 6.7 Assembled Direct clutch system prototype for one-cylinder diesel engine

6.6 The Transmission performance test

This section was divided into three main parts, a belt transmission system, a direcct clutch system, and transmission systems performance comparison.

6.6.1 Belt transmission system

According to the belt transsmission test results from Chapter 5, the data were processed by averaging the results from three tests to determine a general characteristic of the transmission sytem.

First, the slip pecentage and Torque B were averaged and shown on Figure 6.8 and 6.9 In Figure 6.8, the graphs are divided by different belt tensions while each set of graphs compares a slip pencentage variation under different engine loads. For 1.7 Kg belt tension, the average slip percentage was increased from 0.4%-1.25% in the load L1 to 0.3%-2% of maximum slip that occurred during the load L4. For the load L2 and L3, the average slip percentage were about 0.7%-1.5%. For the next belt tension configuration of 2.3 Kg, a slip pencentage was 0.5% to 1% in load L1. When the load was added, the slip percentage was increased to 0.5%-1.3% in load L2 and 0.5%-1.75% in load L3 until the maximum values of 0%-2.5% in load L4. Furthermore, under 3 Kg of belt tension, the slip pencentage was about 0.8% in load L1 then increased to 0.5%-1.25% in load L2 and 0.6%-1.75, until 1%-2% in load L4. In conclusion, the slip in belt transmission system normally was about 1-1.5% and fluctuated about 1-2% in magnitude, callled a micro slip.

In Figure 6.9, Torque B was compared in same belt tension load case in order to display an increse in a transmitted torque when engine load was added. In 1.7 Kg belt tension case, average maximum torque B was started form 6 Nm and incresing to 19.5 Nm, 27.5 Nm,and 32.5 Nm under L1, L2, L3,and L4 respectively. Furthermore, in case of 2.3 Kg belt tension case, the average maximum Torque B was 6 Nm, 20 Nm, 28.5 Nm, and 34 Nm. Finally, under the 3 Kg belt tension, average maximum torque was founded to be 6 Nm, 20 Nm, 30 Nm, and 35 Nm.

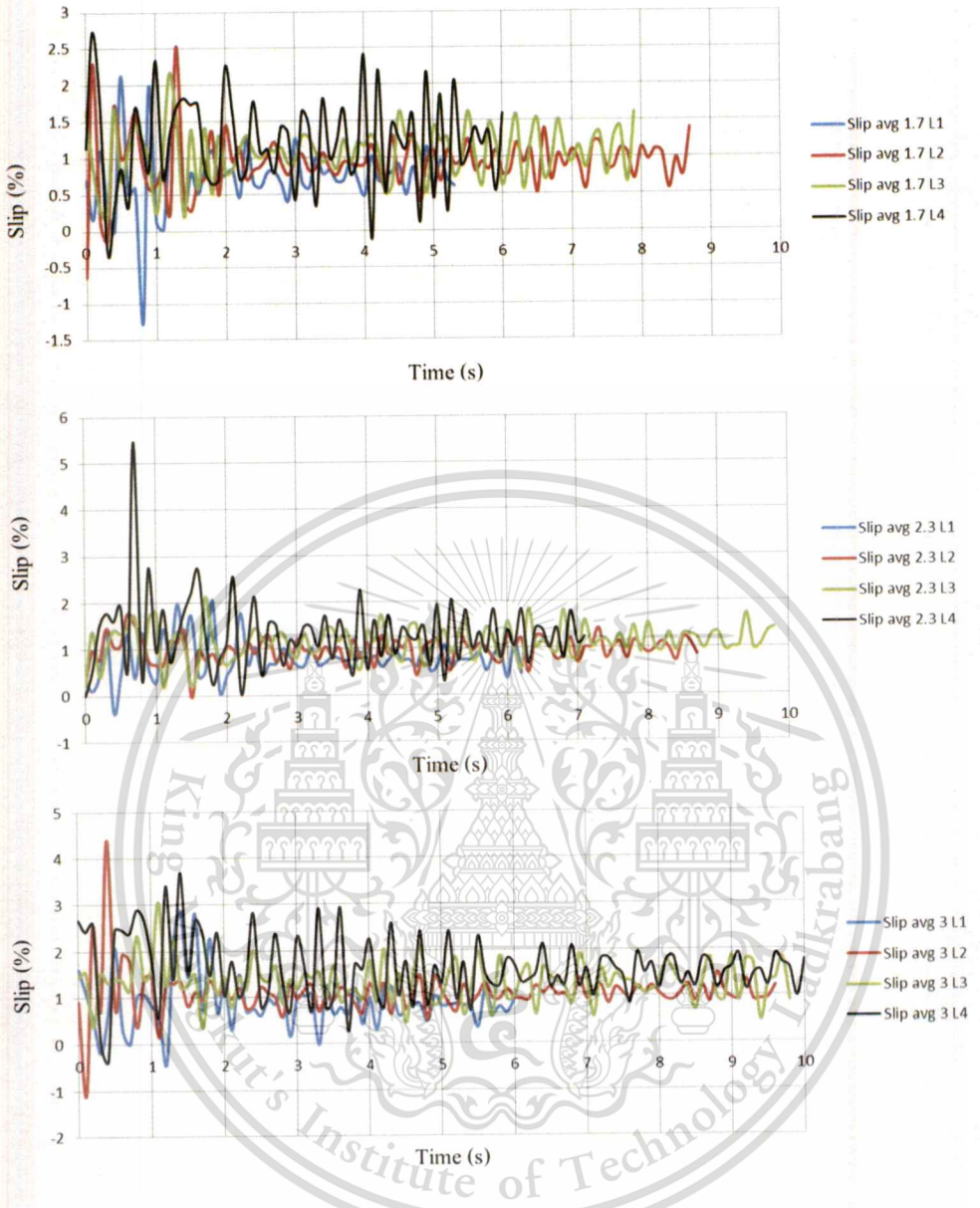

Figure 6.8 Belt transmission system averaged slip percentage comparison : (Top) 1.7Kg of belt tension case, (Middle) 2.3 Kg of belt tension case, (Bottom) 3Kg of belt tension case

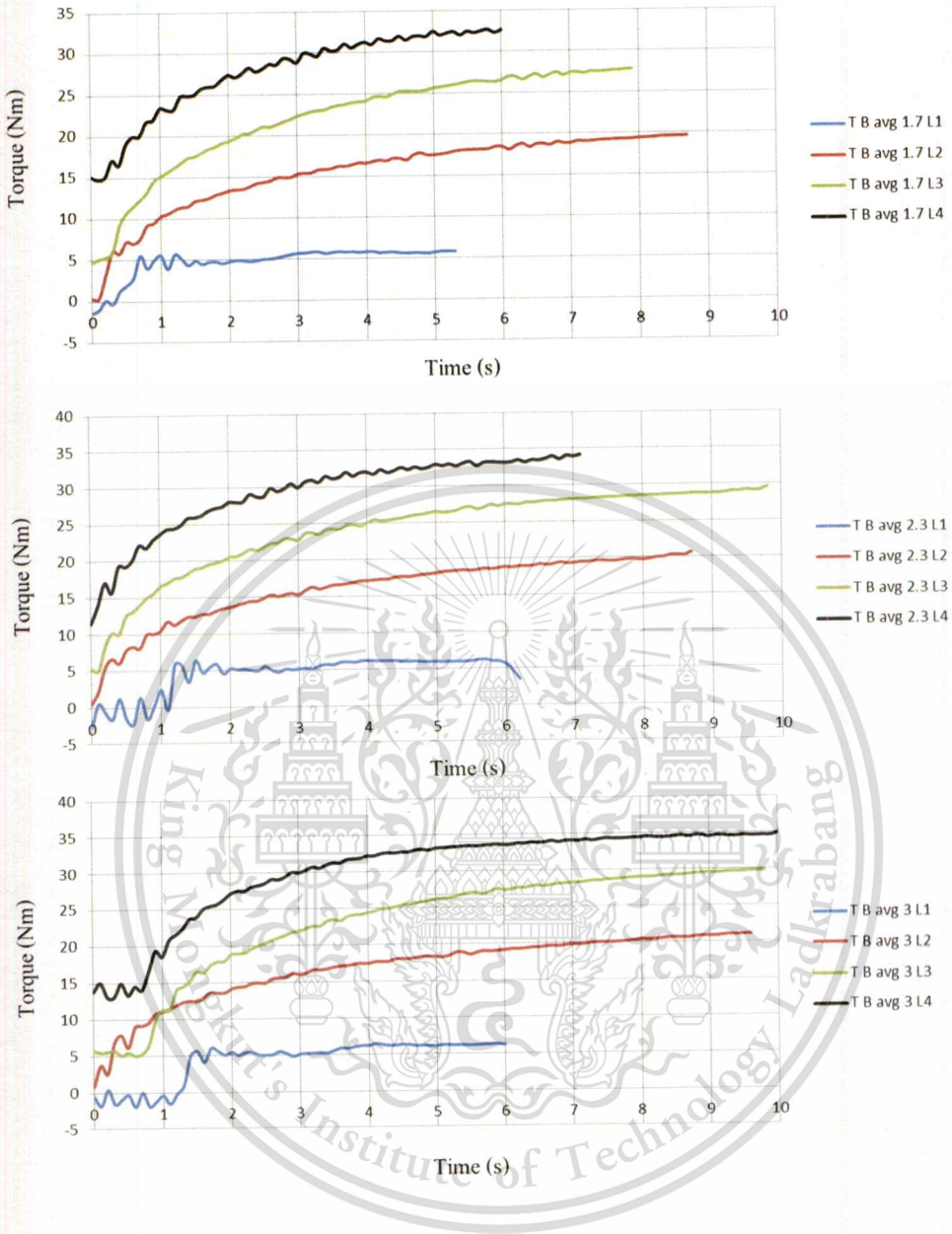

Figure 6.9 Belt transmission system averaged Torque B comparison : (Top) 1.7Kg of belt tension case (Middle) 2.3 Kg of belt tension case (Bottom) 3Kg of belt tension case

In addition, a chareacteristic of slip and torque variation during the tests was considered. The slip was got the highest rate and became most fluctuated with double of slip values during the initial stage of the engine acceleration at the beginning of the test. Then the slip was reduced to a normal minimum rate when the engine reached the steady state of the operation. By comparing the results in each configuration, it could be seen that the slip rate was reduced or the magnitude of fluctuation was

narrowed down when the belt tension became higher. For a torque, in the first section during acceleration the torque increased gradually with an exponential curve and reached the maximum when the system reached the maximum rpm with an increase in maximum torque of 1-2.5 Nm increasing rated of torque between for each engine load (L1-L4).

In order to illustare the efficiency of the belt transmission, the efficiency curves were calculated following equation 4.9 as mentioned in the methodology chapter. In figure 6.10, there are the efficiency curves seperated by 4 engine load cases. The results showed the efficiency gained from tightening the belt tension, with an increasing of 3%-5% in load L1case and 2%-3% in load L2 and load L3 cases. For load L4 case, the belt tension had a smaller effect by just 1%-2% of efficiency improvement. Overall, the maximum efficiency of this system was about 42%-50% under no load condition and was about 75%-80% with load. Additioanlly, the system displayed the maximum efficiency of 89% during load L4 case.

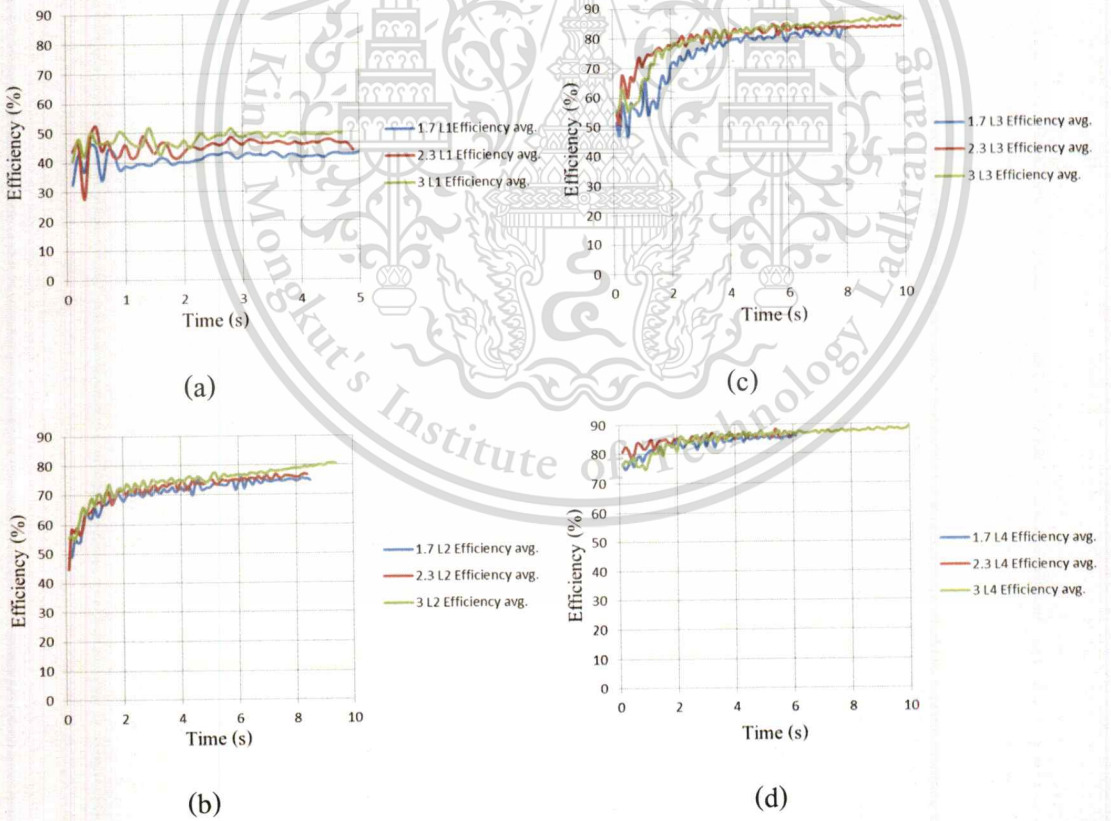

Figure 6.10 Belt transmission system efficiency comparison: (a) Efficiency in L1 case (b) Efficiency in L2 case (c)) Efficiency in L3 case (d) Efficiency in L4 case

6.6.2 Direct clutch transmission system

For the direct clutch system experimental results, the slip percentage and Torque B were averaged into a single data for each load case for comparitive study and disscusions. In Figure 6.11, the slip percentage was about ±0.35% in no load condition (L1). Then, the slip pecentage was raised up to ±0.4 in L2 and a slightly more in L3. For L4, slip occurred at about ±0.9%. For a characteristic of this system, the slip was also highly fluctuated with slightly higher in magnitude in first few seconds of the acceleration process. When the system got into a steady state, the slip was narrowed down and became less fluctuate.

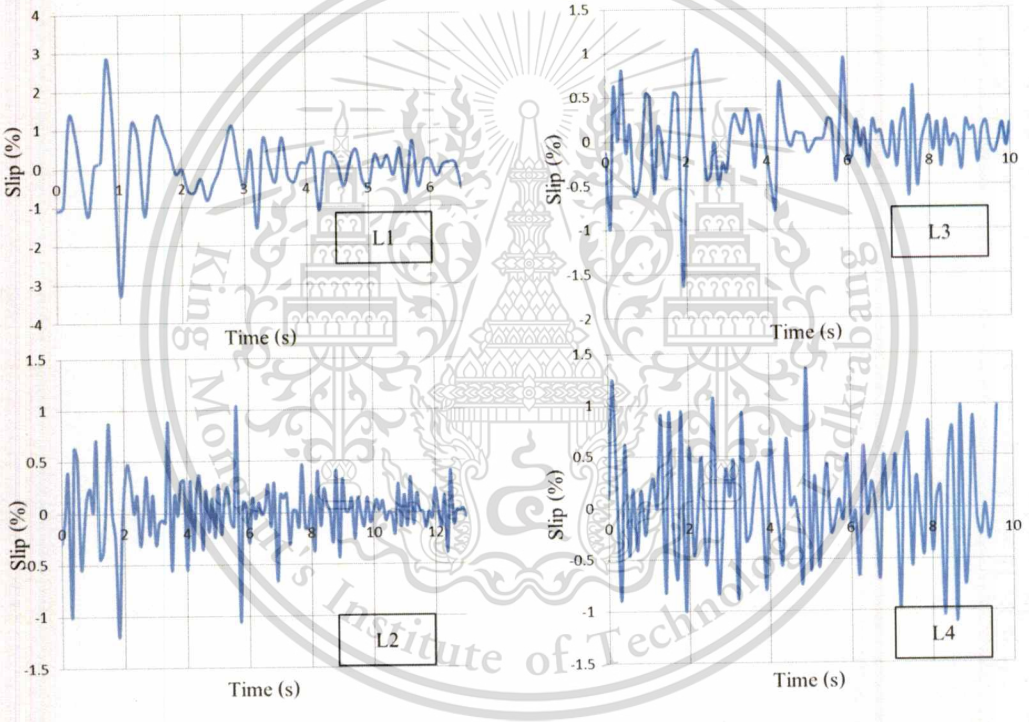

Figure 6.11 Direct clutch system: averaged slip percentage under each load conditions

For a torque, an averaged torque was plotted and shown in Figure 6.12. According to Figure 6.12, the averaged torque is shows in four load cases. The maximum torque was 5 Nm, 22.5 Nm, 32Nm, and 38 Nm. respective to L1, L2, L3, and L4.

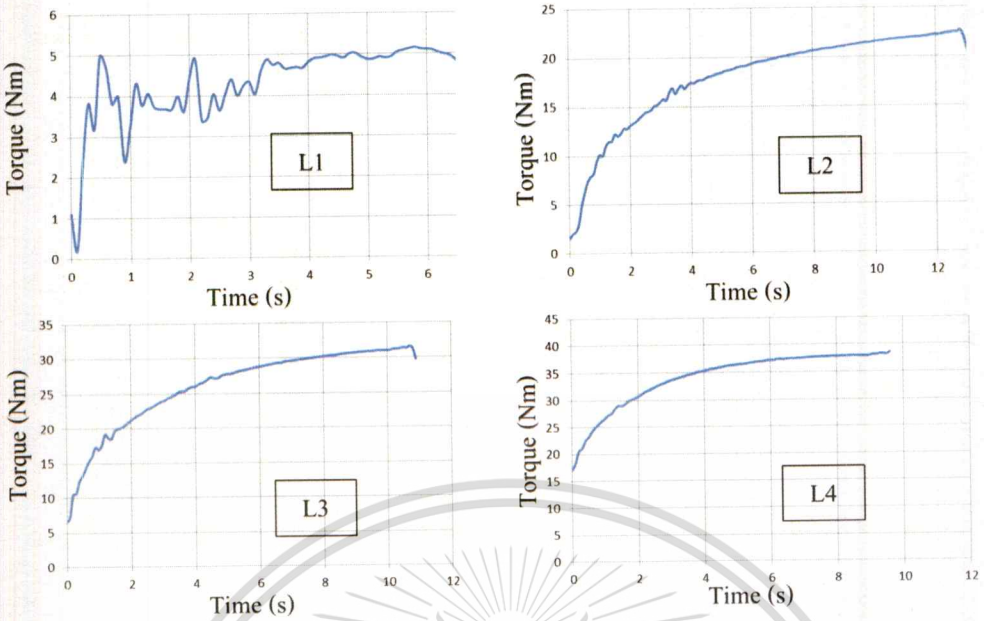

Figure 6.12 Direct clutch system: averaged torque in each load conditions

6.6.3 Direct clutch and Belt transmission system performance comparison

In order to compare a performance of two transmission systems, the experimental results were compared together using corresponding power, slip, and torque transmit characteristic observed in each configuration. According to the belt transmission results, only the data set of 2.3Kg and 3Kg were considered for data comparison. This was because 2.3Kg was an appropriate belt tension for common usage in practice and 3Kg gave the highest efficiency of the system. First, the slip percentage, and torque from both systems were compared as shown in Figure 6.13. In all load cases, the slip of direct clutch transmission system fluctuated at about 0% level while the range of variation became slightly wider when a load was increased. On the other hand, the slip percentage of belt transmission did not fluctuated at 0% level. There was an offset about 0.95% to 1.5% according to a load. For this reason, it could be concluded that the direct clutch system had a lower slip loss than that of the belt transmission.

The summary of slip percentage comparison is shown in Figure 6.14. The results were somewhat different from the belt tension theory such that a slip was increasing related to an increase of belt tension. This problem was believed to have occurred from averaging results for comparison. According to the raw experimental results shown in chapter 5, the slip was slightly increased with

increasing belt tension but the magnitude of fluctuation was deceased. So, this averaged value was calculated to be only used to compare the slip characteristics with the direct clutch system.

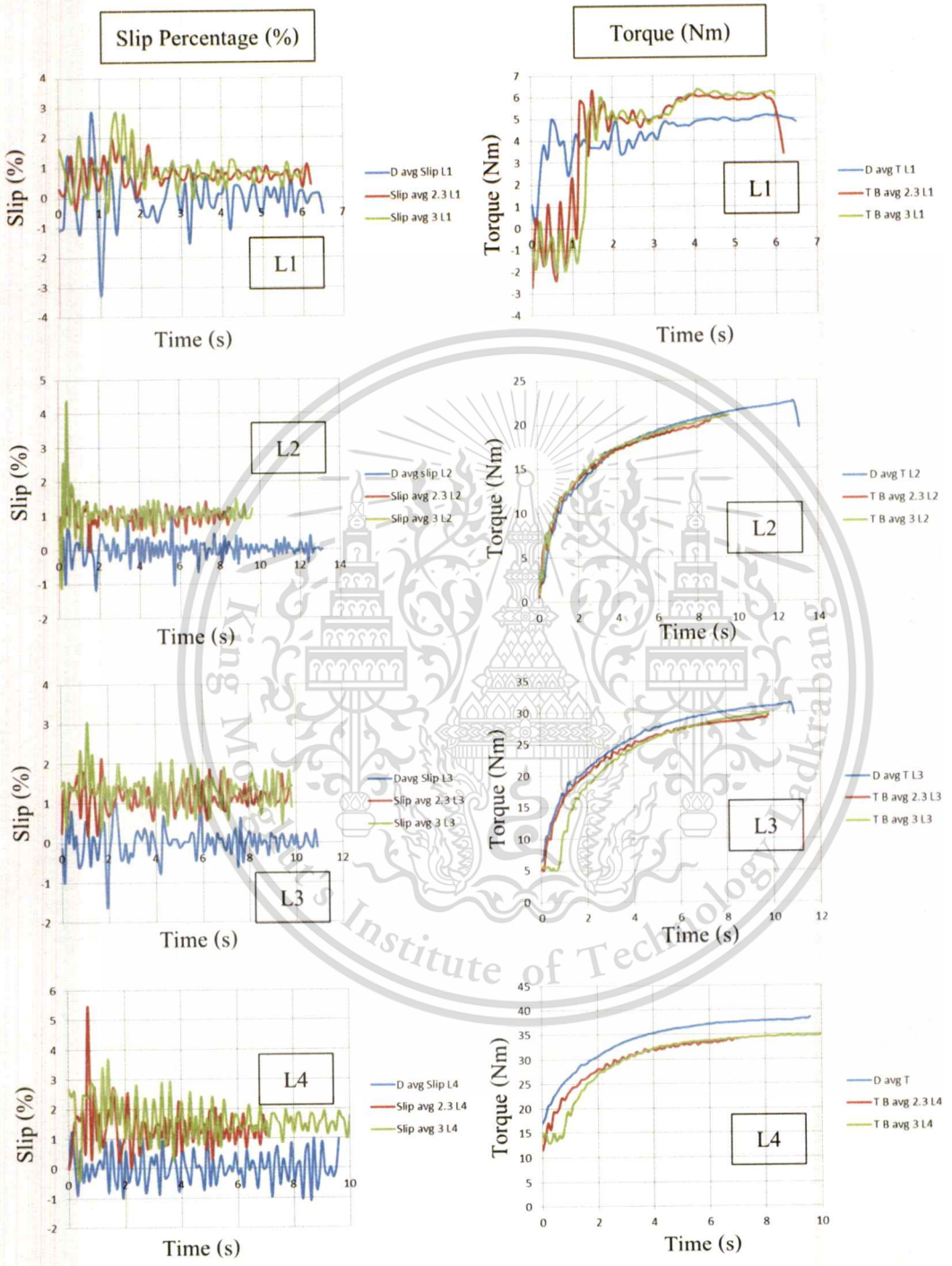

Figure 6.13 Direct clutch and belt transmission system comparison between a slip percentage (left) and a torque (right)

In detail of a transmitted torque in both systems, for L1 case, the belt transmission had a torque transmitted at about 1 Nm higher than that observed from the direct clutch system of just about 5 Nm. This was probably because under L1 load case, which was no load condition, the direct clutch system was free to operate compared to the belt system that had to overcome a bearing friction. For other load cases, the direct clutch system worked well in aspect of a torque transmission functioning with an improvement in transmitted torque of about 2-3.5 Nm higher than those in the belt transmission system as compared in Figure 6.15

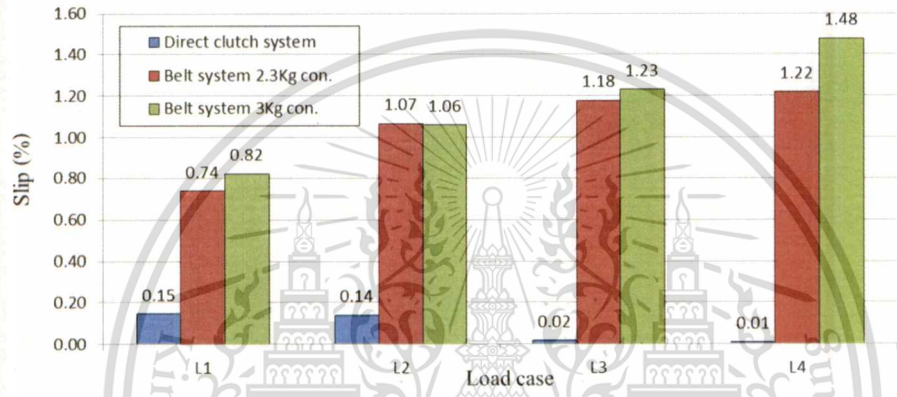

Figure 6.14 Slip percentage comparisons

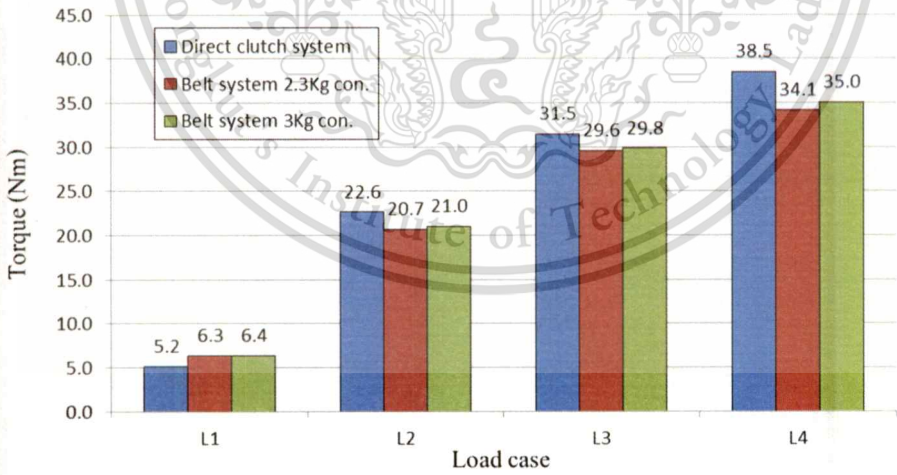

Figure 6.15 Torque output comparisons

In order to determine which system was better in the transmission performance, the power output in Kilowatt (KW) was calculated by using data of torque and revolution speed (rpm) to qualitatively explain a performance improvement as shown in Figure 6.16. According to Figure 6.16,

the direct clutch system had more power output than the belt transmission system in all L1, L2, L3, and L4 load case with a maximum gain of 0.5 KW in L4 when compared with an over tension case of 3Kg. Furthermore, the power output improved about 0.65KW while compared with a normal appropriate tension configuration of 2.3 Kg. These power output improvements while using the direct clutch system instead of the belt transmission system could be calculated into percentage for better understanding by the maximum efficiency improved about 14.28 % and 20% in L3 and L4 load case as shown in Table 6.2.

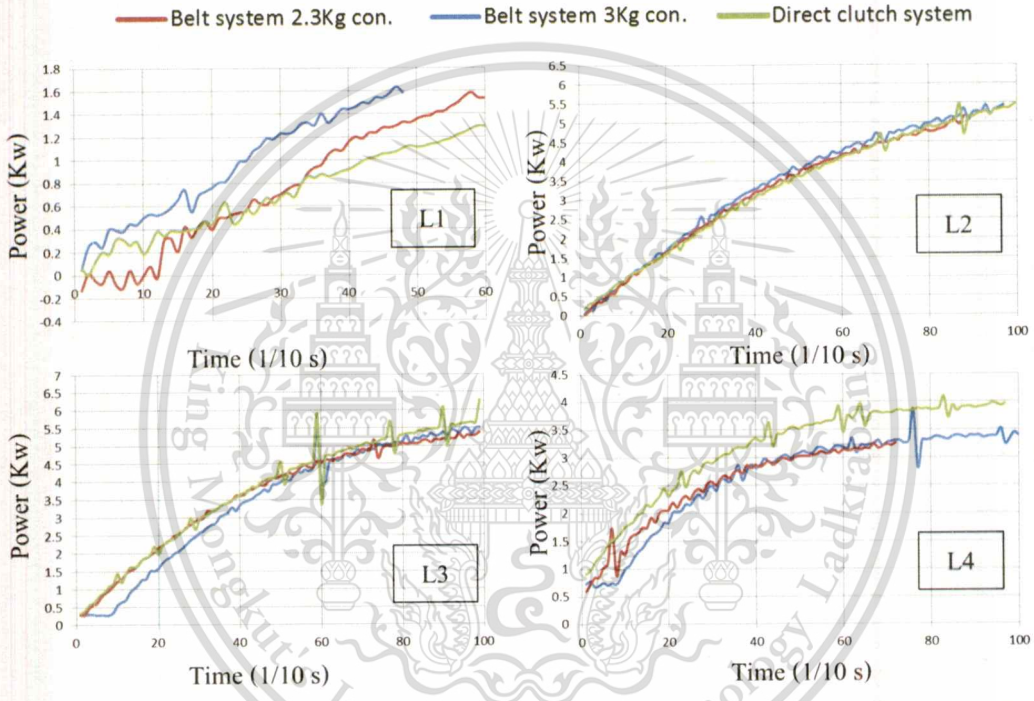

Figure 6.16 Power output comparisons between Belt transmission and direct clutch system

Table 6.2 Improvement of power output when using direct clutch instead of belt transmission

	Maximum power output (KW)	Power improvement			
		Belt transmission system			
		3 Kg of tension	2.3 Kg of tension	3 Kg of tension	2.3 Kg of tension
Direct Clutch system	3.9	0.45 KW	0.65 KW	13.04 %	**20 %**

6.7 Direct clutch and Belt transmission system general comparison

In this topic, the durability and advantage of direct clutch system are discussed. First, the direct clutch system had more advantage than a belt system in term of durability. The direct clutch system was expected to have a longer service life than a belt system. After being used in the first year, the belt tension and its physical properties would normally degrade and worn out due to a working environment and operating conditions. A belt tension adjustment would always be needed in the belt system as well as an eventual belt replacement. On the other hand, the direct clutch system would transmit the power by passing through a clutch disc. Generally, the clutch disc has a very low wear rate and less performance drop during a long-term usage. A clutch disc life is expected over 200,000 Kilometer with proper usage or 10 years with 50-Kilometer daily usage. In term of performance, the power output results proved that the direct clutch system could transmit a power from the engine to output driveline better than the belt transmission. This indicates that the direct clutch system offers more efficiency. From these reasons, the direct clutch system transmission type is the better choice for use in the multipurpose trucks with one cylinder diesel engine as a prime mover. However, a manufacturing cost of the direct clutch transmission prototype is definitely higher than that of the belt transmission type. Thus, the mass productions are required to decrease an involved manufacturing cost.

6.8 The Finite element model validation by actual strain measurement

In this section, measured stresses and calculated results were compared together and a resulting deviation percentage are shown graphically in Figure 6.17. According to a measured results, a large variation was found on every considered locations with a deviation of 108.39, 89.75, 154.34, 91.36, -262.05, and 45.95 %, respectively. Among these locations, location B was an outstanding location with the highest generated stress points at B1 where the resulting stress was higher than that at B2 by a ratio of 3.22. Similarly, from the FE simulation, B1 and B2 were also the highest stress generating points with B1 predicted to exhibit resulting stress greater than that of B2 by a ratio of about 3.93. However, from the validation perspective, the large difference between experimental and computational has occurred. Initially, the errors might have been due to an experimental setup conditions. As can been seen from Chapter 4 , loads from the engine vibration force were applied as

the boundary conditions of the clutch housing analysis on the base of a mouting plate and the clutch housing flange on a gearbox-side was assigned as a fix support. Realistically, this test was carried out such that an engine was mounted on the base of mounting plate while the other end of the clutch housing gearbox flange was left freely as could be seen in Figure 4.26. Moreover, these tests were carried out on the transmission test rig and both of a main frame base and a multi-transmission frame base were fasten together with bolts rigidly, that could also limit the engine vibration. From this reason, the clutch housing could move freely corresponding to an engine vibration and no stress was generated as it should have been. In order to solve this problem, the test rig frame bases have to be seperated from each other and the clutch housing gearbox box flange should be mounted to the multi-transmission frame base in rigidly conditions. From this solution, a free vibration of the engine and a clutch housing gear box flange fix condition will be allowed.

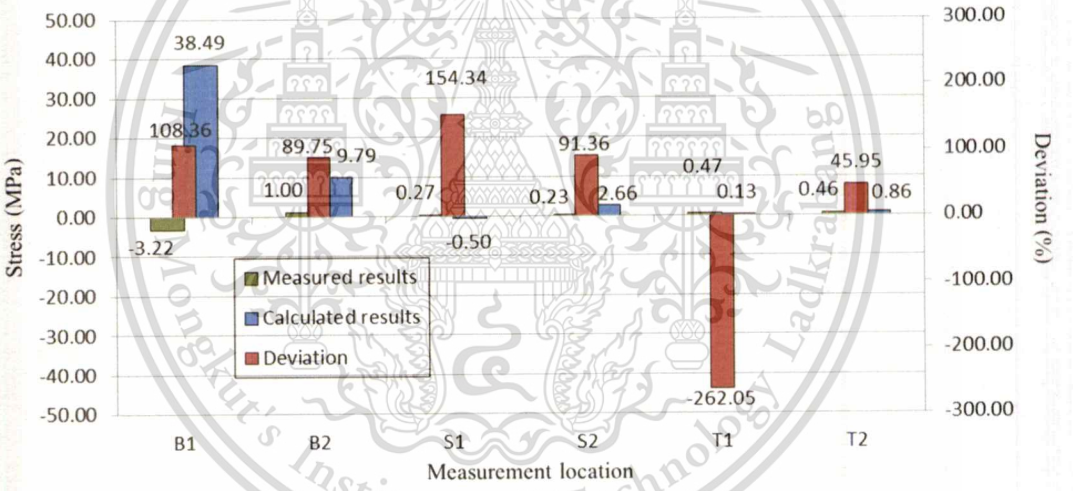

Figure 6.17 Comparison of measured results and calculated results with percentage deviation in each location

CHAPTER 7

CONCLUSIONS

7.1 Conclusions

A transmission improvement of agricultural truck or E-TAND was researched with an objective to replace a belt transmission that had conventionally been used. The direct clutch concept was introduced in this work. The designation and selection with specific concerned topics of the main parts for the direct clutch prototype, such as a clutch contact surface, a clutch housing, a shaft adapter, and a clutch set, were explained. The computer aided design (CAD) modeler was used to prepare computational models of components for part alignments and dimension checkings, as well as for relevant computational analyses. In case of the simulation work, each part was analyzed by using finite element analysis (FEA) according to various specific design issues such as stress analysis and fatigue analysis of an engine vibration load on the clutch housing, stress analysis of a clutch contact surface including attached bolts , and shaft adapter stress analysis when a transmission system lock up occurred. Furthermore, an optimization by response surface method (RSM) was performed on the clutch housing design in order to archive design goals of weight reduction and sufficient structural strength. After all designs were finalized, part prototypes were constructed and assembled for a performance test for a comparison with the conventional belt transmission system.

7.1.1 Parts analysis and optimization

For the clutch housing part, the main concern was how the housing would behave when subjected to an engine load. According to the response surface calculations, the sensitivity of each parameter that affect maximum von-Mises stress and weight of the clutch housing was investigated. In conclusion, the proposed best design model was the spokes-and-strips model with resulting 82.27

MPa of maximum von-Misses stress and 20.88% of weight reduction from the first design model. Moreover, fatigue failure was found at the same location as where the maximum von-Misses stress occurred when the safety of factor was lower than 3.

Additionally, in case of the clutch contact surface, the maximum von-Mises stress of 31.062 MPa was computed resulting in a corresponding safety factor of 8.45 which surpassed a minimum requirement of 4.4. In bolts attached analysis, a maximum von-Mises stress of 36.09 MPa was predicted under an extremely torsional loading condition. Consequently, the M10 class 8.8 bolts were selected to fasten a clutch contact surface to a flywheel. Moreover, the shaft adapter analysis displayed the relatively high stress distributions at the middle section and inner diameter of the shaft with a range of von-Misses stress between 16-30 MPa.

In addition, the results of analysis and optimization studies displayed several obvious advantages of the employed approaches such as;

- The sensitivity of each parameter could be shown and compared.
- Saving a computational time and shorten a design process.

The optimum point prediction gave very accurate result. The error approximated was not exceeding 1.7 % comparing to calculate result.

7.1.2 Transmission system test

The micro slip of the belt transmission system was measured to be about 0.74-1.48% of slip relative to a load. On the other hand, the system slip of about 0.01-0.15% was observed during the direct clutch system tests. An increasing of belt tension led to a reduction in a slip fluctuation magnitude. It has been determined that by employing the direct clutch system instead of the belt transmission with a normal belt tension configuration, an improvement in the power output of roughly 20% could be expected based on the calculation from measured operating parameterss by

torque transducer with an rotary encoder on the test rig specifically designed in this study. Lastly, the direct clutch system had less preload than the belt system about 18%.

7.1.3 Strain validation Experiment of the clutch housing

The raw data of strain was converted to stress by using Hooke's law. The large deviation of results was found on every measurement locations. This error might due to an experimental setup conditions.

7.2 Suggestions for further research

The suggestions for further research are listed as followed:

7.2.1 Clutch housing system prototype design, analysis and optimization

In this work, the direct clutch system was designed with an objective of adds-on parts. The contact surface had been designed for being attached onto the flywheel and caused the overall weight of flywheel to become much higher. Moreover, when the engine operated at low revolutions a torsional vibration was generated and might be cause damage to a gearbox internal mechanism. In order to improve the current design of the direct clutch system, the new design of flywheel with contact surface and mass damper is needed to reduce the overall flywheel mass and to add a damping effect to the existing level of vibration. In case of the flywheel materials, a special friction material with good heat dissipation property should be considered. Then, the clutch housing has to be re-designed according to a new flywheel. In case of computational analysis, the thermal analysis of a clutch contact surface is suggested for a study on the thermal failure of the clutch contact surface. In the end, the optimization should be carried out on a mounting plate and a clutch contact surface in order to find an optimum point under a design goal of weight reduction. For a clutch housing spoke model optimization, four parameters simultaneous optimization is suggested for further investigations.

7.2.2 Experimental test

The optimum direct clutch system prototype should be assembled onto one of platform structures of existing agricultural or E-TAND trucks for actual field tests and post-test investigation.

At the same time, the strain measurements in the clutch housing needs to be repeated with a new setup as mentioned in Chapter 6.

REFERENCES

[1] A. De Almeida , S. Greenberg. 1995. " Technology assessment: energy-efficient belt transmissions " **Energy and Buildings** Vol. 22: 245-253.

[2] S. Nadel, M. Shepard, S. Greenberg, G. Katz and A. De Almeida. 1991. " Energy-Efficient Motor Systems ", **American Council for an Energy-Efficient Economy,** Washington

[3] Maaike van der LAAN and Mark van DROGEN " Improving Push Belt CVT Efficiency by Clamping Force Control Strategies Based On Variator Slip Measurement " Van Doorne's **Transmissie b.v. Bosch Group**, The Netherlands.

[4] J. Sheperd and S. Piderit. 1983. " Improving the Energy Efficiency of V-belt Drives ", **Plant Eng.**

[5] T. F. Chen, D. W. Lee, and C. K. Sung. 1996. " An Experimental Study on Transmission Efficiency of a Rubber V-Belt CVT " **Mech. Mach. Theory** Vol. 33, No. 4, pp. 351-363.

[6] B. Bonsen, T.W.G.L. Klaassen, K.G.O. van de Meerakker, M. Steinbuch and P.A. Veenhuizen. 2003. " Analyzed the slip in a continuously variable transmission " **ASME International Mechanical Engineering Congress Washington.** November 15–21, 2003

[7] H. Yamaguchi, H.Tani, and K. Hayakawa " The Measurement and Estimation Technologies for Experimental Analysis of Metal V-Belt Type CVT " **R&D Review of Toyota** Vol.40 No.3.

[8] Lionel Manin, Guilhem Michon, Didier Remond, and Régis Dufour. 2009. " From Transmission Error Measurement to Pulley–Belt Slip Determination in Serpentine Belt drives: Influence of Tensioner and Belt characteristics " **Mechanism and Machine Theory** 44 (2009) 813–821

[9] William C. Orthwein. 2004. **Clutches and Brakes Design and Selection**. 2nd Edition. Published by Newyork : Marcel Dekker.

[10] **ANSYS 12.0**, User Manual.

[11] Richard G. Budynas, and J. Keith N. 2011. **Shigley's Mechanical Engineering Design**. 9th Edition, Published by McGraw-Hill.

REFERENCES (CONT.)

[12] Society of Automotive Engineers. 1968. **Fatigue Design Handbook,** Vol. 4, SAE.

[13] Bannantine Julie, Comer Jess, and Handrock James. 1990. **Fundamentals of Metal Fatigue Analysis**, Prentice Hall.

[14] Osgood, C. C. 1982. **Fatigue Design.** 2nd Edition, Pergamon Press.

[15] ASM International. 2008. **Elements of Metallurgy and Engineering Alloys**, Fatigue, Chapter 14, 243-264.

[16] Assoc.Prof. Dr. Pairote Wiriyacharee 2001, **Responsne Surface design**. 1st Edition Published by Faculty of Agro-Industry Chiang Mai University.

[17] Kwon-Hee Lee, Jeong-Wook Yi, Joon-Seong Park, Gyung-Jin Parkc. 2003. "An Optimization Algorithm Using Orthogonal Arrays in Discrete Design Space for Structures", **Finite Elements in Analysis and Design 40** 121–135

[18] Necmettin Kaya, Idris Karen, Ferruh Ozturk. 2010. " Re-Sesign of a Failed Clutch Fork using Topology and Shape Optimization by the Response Surface Method ", **Journal of Materials and Design 31,** 3008–3014

[19] H. Bayrakceken, S. Tasgetiren, I. Yavuz. 2007. "Two Cases of Failure in the Power Transmission System on Vehicles: A Universal Joint Yoke and a Drive Shaft", **Journal of Engineering Failure Analysis 14,** 716–724

[20] M. M. Rahman, K. Kadirgama, M. M. Noor, M. R. M. Rejab and S. A. Kesulai. 2009. "Fatigue Life Prediction of Lower Suspension Arm Using Strain-Life Approach", **European Journal of Scientific Research** ISSN 1450-216X Vol.30 No.3, 437-450

[21] M.M. Topa, H. Gunal , N.S. Kuralay. 2009. "Fatigue Failure Prediction of a Rear Axle Housing Prototype by Using Finite Element Analysis", **Journal of Engineering Failure Analysis 16,** 1474–1482

[22] Luk Clutch Course, **An Introduction to Clutch technology for Passenger Cars**

REFERENCES (CONT.)

[23] Thai Industrial Standards Institute, **Light duty diesel engine vehicles: safety requirements; emission from engine**, level 6, TIS 2155-2546

[24] **American National Standards Institute** -ANSI

[25] Good year. **Power Transmission Product Full Line Catalog**

[26] J. G. Hansen, J. M. Starbuck a, 2009 "Safety Assessment of PowerBeam Flywheel Technology" Materials Science and Technology division, ORNL/TM-2009/251

[27] L.S.T Group " RITZ Product Catalogue"

APPENDIX A

LABVIEW BLOCK DIAGRAM

- **BELT TRANSSMISSION PERFORMANCE TEST**
- **DIRECT CLUTCH SYSTEM PERFORMANCETEST WITH STRAIN MEASUREMENT**

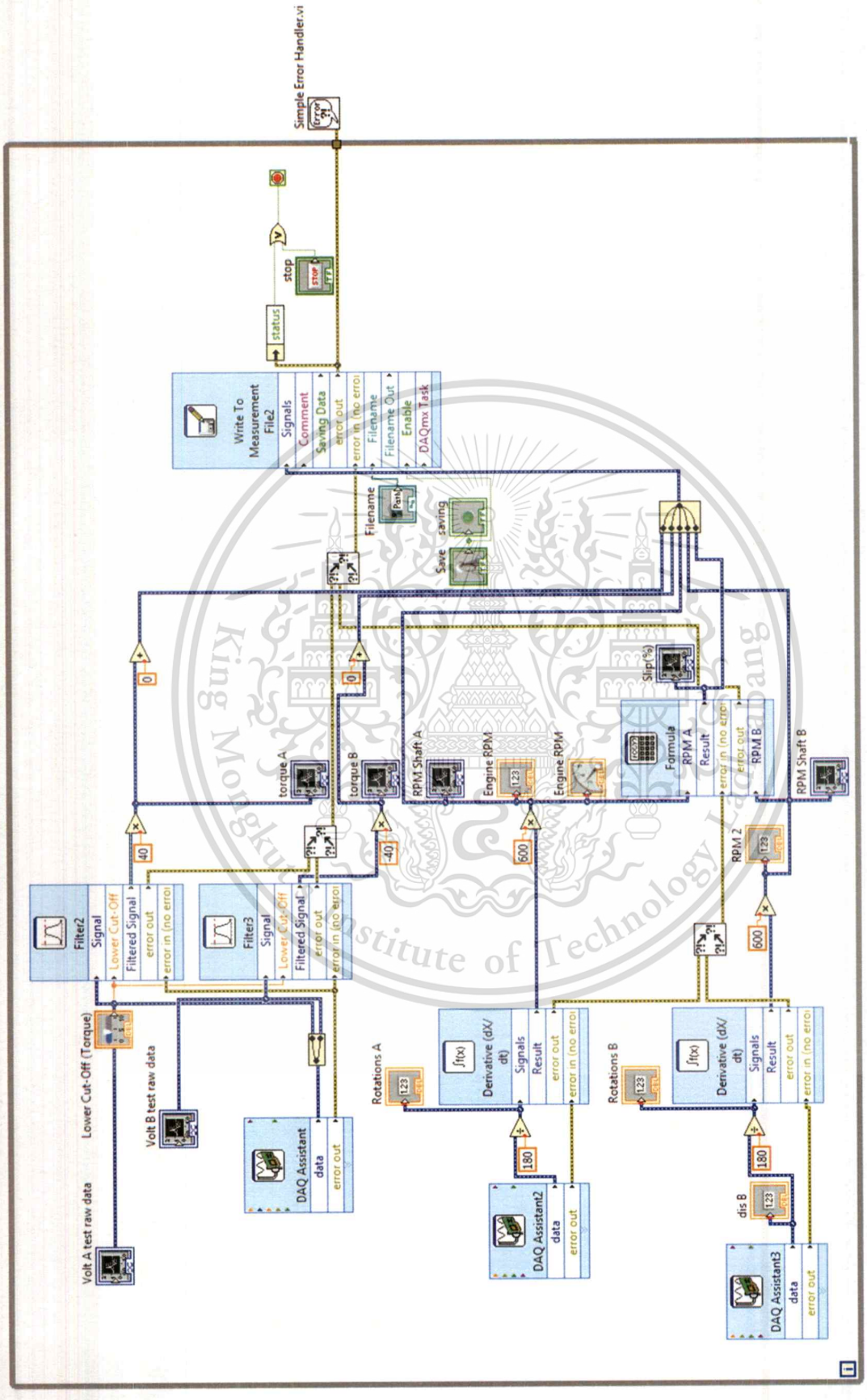

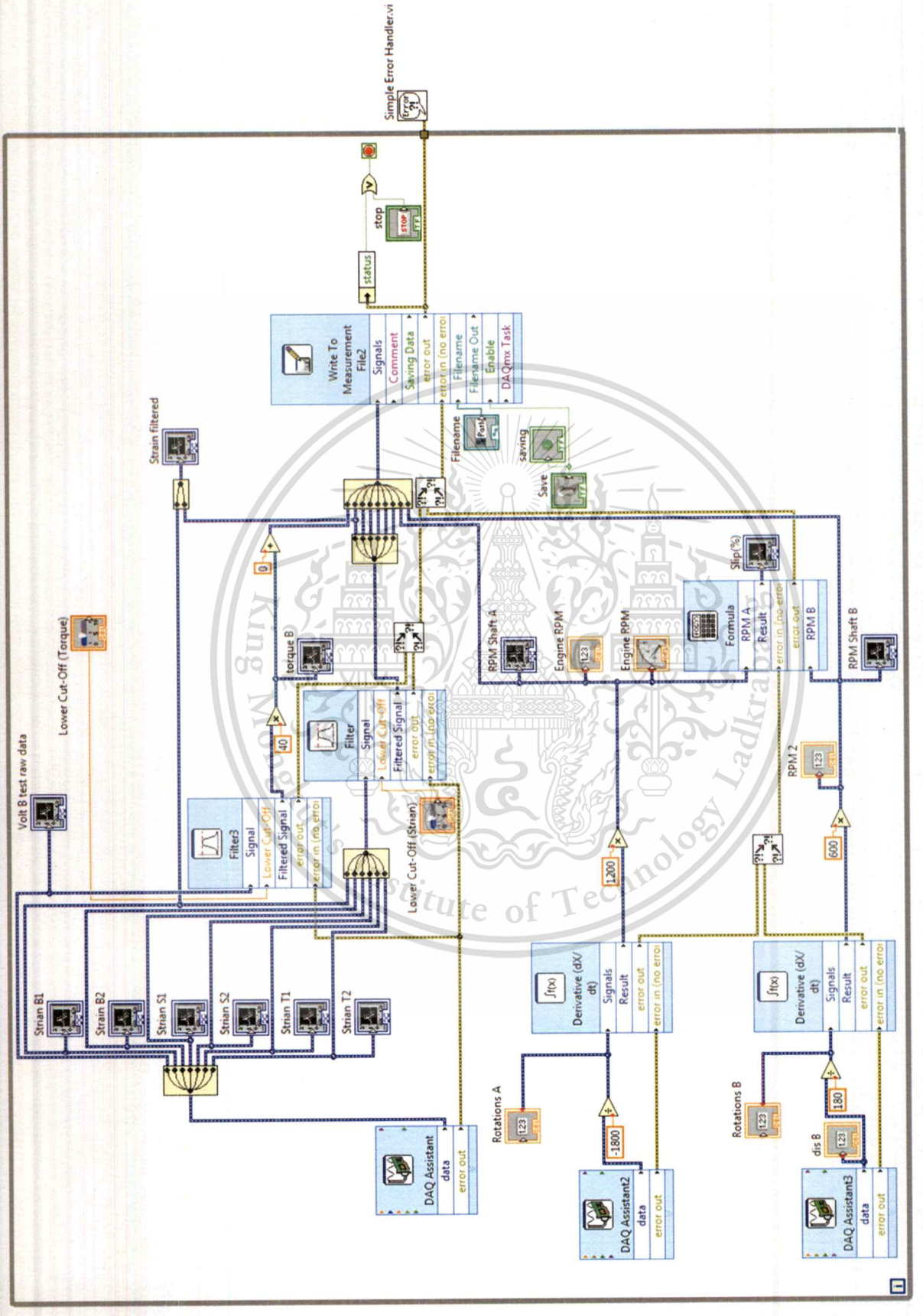

APPENDIX B

TRANSDUCER AND SENSOR SPECIFICATION

- **1 -AXIS ACCELEROMETER Brüel&Kjær MODEL TYPE 4507 B002**
- **TORQUE TRANSDUCER WITH AN ENCODER KISTLER MODEL 4502A200Ra**
- **AUTONIC ROTARY ENCODER MODEL E40S6-3600-6-L-5**
- **UNI AXIAL TML STRAIN GAGE UFLA-5-11-3LT**

Miniature DeltaTron Accelerometers Types 4507 and 4508

Brüel & Kjær

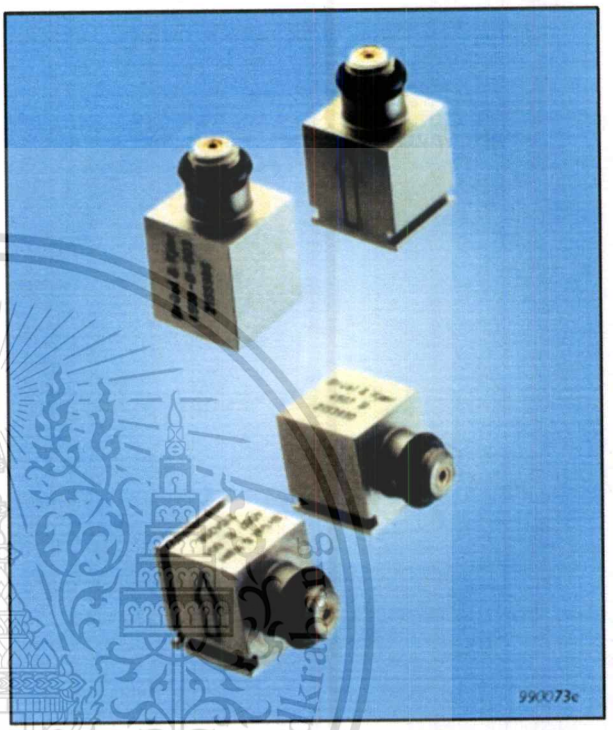

Common Specifications 4507 and 4508

Dynamic

Mounted Resonance Frequency:
4507: 18 kHz
4508: 25 kHz
Transverse Sensitivity: <5% of sensitivity

Max. Non-destructive Shock (±Peak): 50 kms^{-2}; 5000 g
Temp. Transient Sensitivity (3 Hz Lower Limiting Frequency):
4507: 0.2 ms^{-2}/°C
4508: 0.3 ms^{-2}/°C
Base Strain Sensitivity (Mounted on Adhesive Tape 0.09 mm Thick): 0.005 ms^{-2}/με
Magnetic Sensitivity: 3 ms^{-2}/T

Electrical

Constant Current Supply: 2 to 20 mA
Supply Voltage (Unloaded):
+24 to +30 V DC (for full specification range)
Min. +18 V DC (reduced measuring range)
Polarity: Positive (for an acceleration in the direction of the engraved arrows)

Environmental

Temperature Range: –54° to +121°C (–65° to +250°F)

Physical

Case Material: Titanium
Sensing Element: Piezoelectric
Design Configuration: ThetaShear
Connector: 10–32 UNF coaxial
Dimensions (H×W×L): 10×10×10 mm (0.4"), excl. connector
Weight: 4.8 gram (0.17 oz.)
Note: All values are typical at 25°C (77°F), unless measurement uncertainty is specified. All uncertainty values are specified at 2σ (i.e., expanded uncertainty using a coverage factor of 2)

KISTLER

measure. analyze. innovate.

4502A200Ra

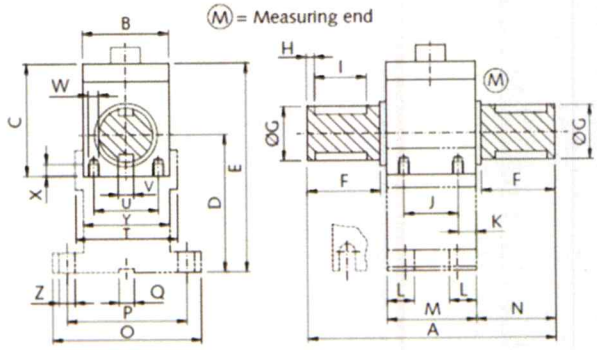

Table Version RA (with rotational angle measurement)

Type	Measuring range N·m	A	B	C	D	E	F	øG g6	H	I	J	K	L	M	N	O	P
4502A200RA	200	125	58	76	112	159	27	28	2	22	39	12,5	20	64	30,5	120	100

Technical Data

Mechanical Basic Data

Measuring range	N·m	±0,5 ... 1 000
Rated torque M_{nom}	N·m	0,5 ... 1 000
Overload capacity		
Service torque		1,5 x M_{nom}
Limiting torque		1,5 x M_{nom}
Rotational angle/- speed measurem. (Version QA, HA, RA, RAU)	pulses/ revolut.	2x360, 90° displaced, TTL
Nominal speed		
≤18 N·m	1/min	12 000
20 ... 160 N·m	1/min	9 000
250 ... 1 000 N·m	1/min	7 000
Version QA, HA, RA, RAU (rotational angle measurement)	1/min	7 000
Housing material		Anodized aluminum
Protection class		IP40

General Electrical Specifications

Cut-off frequency –3 dB	kHz	3
Accuracy class		0,2
Linearity error including hysteresis	% FSO	<±0,2
Output signal	VDC	±0 ... 5
at rated torque (rated value)	VDC	5
Load resistance	kΩ	>10
Temp. influence on the zero point	% FSO/°C	<±0,015
Temp. influence on the nominal value	% FSO/°C	<±0,015
Control signal	%	100 ±0,2
100 % control input	VDC	"On" 5 ... 30 "Off" 0 ... 2
Operating temperature range (Rated temperature range)	°C	10 ... 60
Service temperature range	°C	0 ... 70
Storage temperaure range	°C	–25 ... 80
Electrical connection		12 pin built-in connector
Supply voltage	VDC	11 ... 26
Power consuption	W	<1

E40S/E40H/E40HB/E80H SERIES

Autonics

E40S E40H E40HB E80H

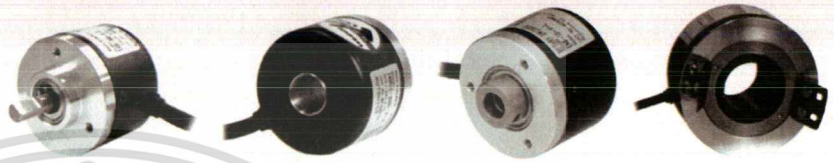

■ Specifications

Incremental Rotary encoder			ø 40mm Shaft type	ø40mm Hollow shaft type	ø40mm Hollow shaft Built- in type	ø80mm Hollow shaft type
Model		Totem Pole output	E40S□-□-□-T-□	E40H□-□-□-T-□	E40HB□-□-□-T-□	E80H□-□-□-T-□
		NPN open collector output	E40S□-□-□-N-□	E40H□-□-□-N-□	E40HB□-□-□-N-□	E80H□-□-□-N-□
		Voltage output	E40S□-□-□-V-□	E40H□-□-□-V-□	E40HB□-□-□-V-□	E80H□-□-□-V-□
		Line Driver output	E40S□-□-□-L-□	E40H□-□-□-L-□	E40HB□-□-□-L-□	E80H□-□-□-L-□
Resolution(P/R)			•1, •2, •5, 10, •12, 15, 20, 23, 25, 30, 35, 40, 45, 50, 60, 75, 100, 120, 125, 150, 192, 200, 240, 250, 256, 300, 360, 400, 500, 512, 600, 800, 1000, 1024, 1200, 1500, 1800, 2000, 2048, 2500, 3000, 3600, 5000 (Not indicated type is available to customize)			60, 100, 360, 500, 512, 1024, 3200
Output phase(※1)			(※1) A, B, Z phase(Line Driver output: A, $\overline{A}$, B, $\overline{B}$, Z, $\overline{Z}$ phase)			
Electrical specification	Phase difference between output		Output between A and B phase: $\frac{T}{4} \pm \frac{T}{8}$ (T= 1cycle of A phase)			
	Control output	Totem Pole output	•Low ☞ Load current: Max. 30mA, Residual voltage: Max. 0.4VDC •High ☞ Load current: Max. 10mA, Output voltage(Power voltage 5VDC): Min. (Power voltage-2.0)VDC, Output voltage(Power voltage 12-24VDC): Min. (Power voltage-3.0)VDC			
		NPN open collector output	Load current: Max. 30mA, Residual voltage: Max. 0.4VDC			
		Voltage output	Load current: Max. 10mA, Residual voltage: Max. 0.4VDC			
		Line Driver output	•Low ☞ Load current: Max. 20mA, Residual voltage: Max. 0.5VDC •High ☞ Load current: Max. -20mA, Output voltage(Power voltage 5VDC): Min. 2.5VDC, Output voltage(Power voltage 12-24VDC): Min. (Power voltage-3.0)VDC			
	Response time(Rise/Fall)	Totem Pole output	Max. 1㎲ (Cable length: 2m, I sink=20mA)			
		NPN open collector output				
		Voltage output				
		Line Driver output	Max. 0.5㎲ (Cable length: 2m, I sink=20mA)			
	Max. Response frequency		300㎑			200㎑
	Power supply		• 5VDC ±5%(Ripple P-P: Max. 5%)		• 12-24VDC ±5%(Ripple P-P: Max. 5%)	
	Current consumption		Max. 80mA (disconnection of the load), Line Driver output: Max. 50mA(disconnection of the load)			
	Insulation resistance		Min. 100㏁(at 500VDC megger between all terminals and case)			
	Dielectric strength		750VAC 50/60㎐ for 1 minute(Between all termials and case)			
	Connection		Cable outgoing type, 250mm Cable outgoing connector type			
Mechanical specification	Starting torque		Shaft Type: Max. 40gf·cm(0.004N·m), Hollow Type: Max. 50gf·cm(0.005N·m)			Max. 200gf·cm(0.02N·m)
	Moment of inertia		Max. 40g·cm²(4×10⁻⁶kg·m²)			Max. 800g·cm²(8×10⁻⁵kg·m²)
	Shaft loading		Radial: 2kgf, Thrust: 1kgf			Radial: 5kgf, Thrust: 2.5kgf
	Max. allowable revolution(※2)		5,000rpm			3,600rpm
Vibration			1.5㎜ amplitude at frequency of 10~55㎐ (for 1 min.) in each X, Y, Z direction for 2 hours			
Shock			Max. 50G			Max. 75G
Environment	Ambient temperature		-10 ~70℃, Storage: -25 ~ 85℃			
	Ambient humidity		35 ~ 85% RH, Storage: 35 ~ 90%RH			
Protection			IP50(IEC Standards)			
Cable			ø5mm, 5P, Length: 2m, Shield cable(Line Driver output: ø5mm, 8P) (AWG 24, Core wire diameter: 0.08mm, No. of core wire: 40, Insulator out diameter: ø1mm)			
Accessory			ø6mm coupling(Standard), ø8mm coupling(Option)	Bracket		
Approval			CE (Except for Line Driver output)			
Unit weight			Approx. 120g			Approx. 560g

TML STRAIN GAUGE TEST DATA

GAUGE TYPE	: UFLA-5-11-3LT	TESTED ON	: SS 400
LOT NO.	: A510611	COEFFICIENT OF THERMAL EXPANSION	: 11.8 ×10⁻⁶/℃
GAUGE FACTOR	: 2.12 ±1%	TEMPERATURE COEFFICIENT OF G.F.	: +0.08±0.05 %/10℃
ADHESIVE	: NP-50	DATA NO.	: U0049

THERMAL OUTPUT (ε app : APPARENT STRAIN)

$$\varepsilon app = -6.29\times10^{-1}+2.93\times10^{-1}\times T^{1}-1.28\times10^{-2}\times T^{2}-2.22\times10^{-6}\times T^{3}+5.14\times10^{-7}\times T^{4}\ (\mu m/m)$$

TOLERANCE : ±0.85 [(μm/m)/℃] , T : TEMPERATURE

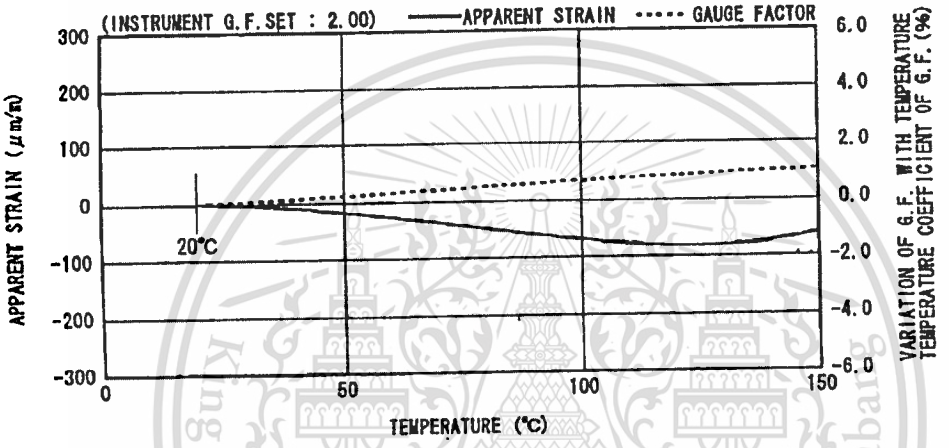

ひずみゲージ取扱いの注意事項

- ●上記の特性データは、リード線の取付けによる影響を含んでおりません。裏面記載のリード線の測定値への影響に従って補正してください。
- ●ゲージの使用温度は、接着剤の耐熱温度などにより変わります。
- ●絶縁抵抗などの点検は、印加電圧を５０Ｖ以下にしてください。
- ●ゲージリード線に無理な力を加えないでください。
- ●ゲージ裏面に接着剤を塗布して接着してください。
- ●ひずみゲージの裏面は脱脂洗浄してありますので、汚さないように取扱いしてください。
- ●ゲージの包装を開封後は、乾燥した場所で保管してください。
- ●ご使用に際してご不明な点などがございましたら、当社までお問い合わせください。

CAUTIONS ON HANDLING STRAIN GAUGES

- ● The above characteristic data do not include influence due to lead wires. Correct the data in accordance with the influence of lead wires on measured values described overleaf.
- ● The service temperature of strain gauge depends on the operating temperature of adhesive, etc.
- ● Check of insulation resistance, etc. should be made at a voltage of less than 50V.
- ● Do not apply an excessive force to the gauge leads.
- ● Apply an adhesive to the back of a strain gauge and stick the gauge to a specimen.
- ● As the back of strain gauge has been degreased and washed, do not contaminate it.
- ● After unpacking, store strain gauges in a dry place.
- ● If you have any questions on strain gauges or installation, contact TML or your local agent.

Made in Japan

TML 株式會社 東京測器研究所

〒 140-8560 東京都品川区南大井 6 - 8 - 2
TEL 03 - 3763 - 5611
FAX 03 - 3763 - 6128

Tokyo Sokki Kenkyujo Co., Ltd.

8 - 2, Minami - Ohi 6 - Chome
Shinagawa - ku, Tokyo 140-8560

APPENDIX C

DATA ACQUISITION SPECIFICATION

- **CHASSIS MODULE - cDAQ 9172**
- **ACCELEROMETER MODULE – NI 9234**
- **ANALOG INPUT MODULE- NI 9205**
- **DIGITAL INPUT/OUTPUT MODULE- NI 9401**
- **STRAIN GAGE MODULE - NI 9235**

NI cDAQ-9172

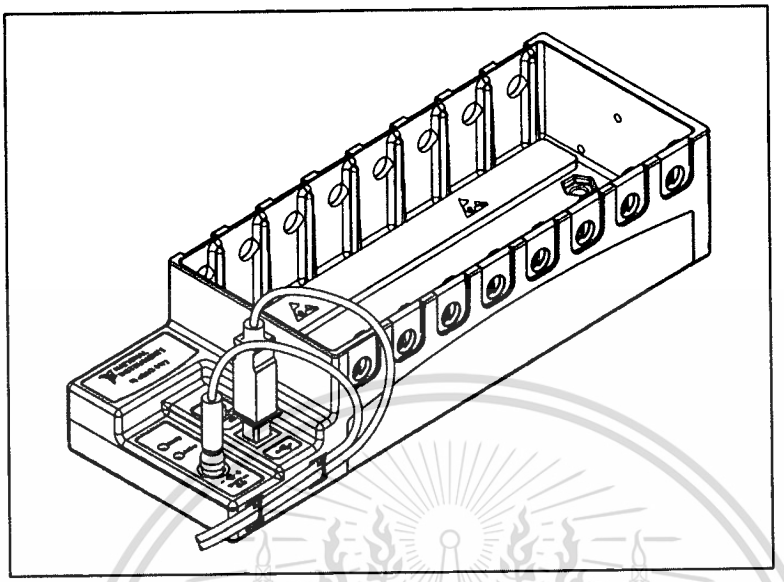

Analog Input

Input FIFO size	2,047 samples
Sample rate[1]	
Maximum	3.2 MS/s (multi-channel, aggregate)
Minimum	0 S/s
Timing accuracy[2]	50 ppm of sample rate
Timing resolution[2]	50 ns
Number of channels supported	Determined by the C Series I/O modules

Analog Output

Numbers of channels supported	
In hardware-timed task	16
In non-hardware-timed task	Determined by the C Series I/O modules
Maximum update rate	1.6 MS/s (multi-channel, aggregate)
Timing accuracy	50 ppm of sample rate
Timing resolution	50 ns
Output FIFO size	8,191 samples shared among channels used

Bus Interface

USB specification	USB 2.0 Hi-Speed
Power from USB	
4.10 to 5.25 V	500 µA maximum

NI 9234

4-Channel, ±5 V, 24-Bit Software-Selectable IEPE and AC/DC Analog Input Module

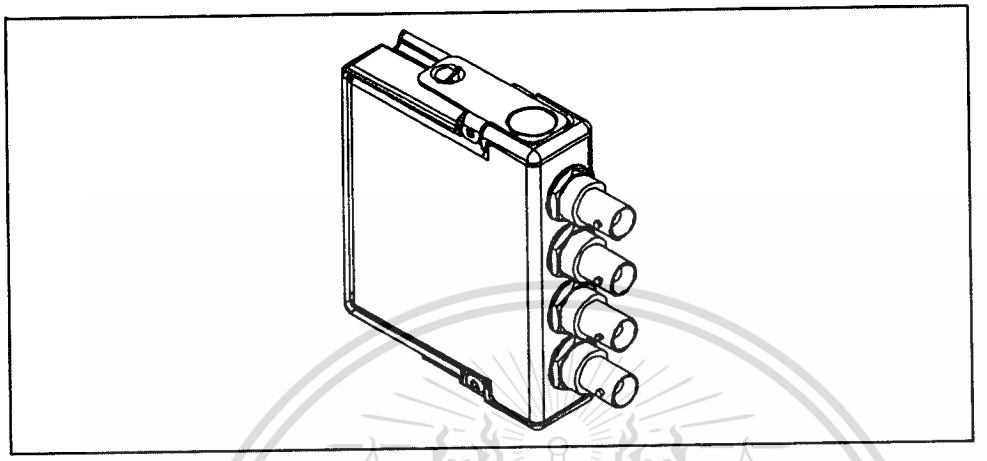

Input Characteristics

Number of channels ..... 4 analog input channels

ADC resolution ..... 24 bits

Type of ADC ..... Delta-Sigma (with analog prefiltering)

Sampling mode ..... Simultaneous

Type of TEDS supported ..... IEEE 1451.4 TEDS Class I

Internal master timebase (f_M)

- Frequency ..... 13.1072 MHz
- Accuracy ..... ±50 ppm max

Data rate range (f_s) using external master timebase

- Minimum ..... 0.391 kS/s
- Maximum ..... 52.734 kS/s

Data rates[1] (f_s) ..... $\frac{f_M \div 256}{n}$, $n = 1, 2, \ldots, 31$

Input coupling ..... AC/DC (software-selectable)

AC cutoff frequency

- –3 dB ..... 0.5 Hz
- –0.1 dB ..... 4.6 Hz max

NI 9205

32-Channel, ±200 mV to ±10 V, 16-Bit Analog Input Module

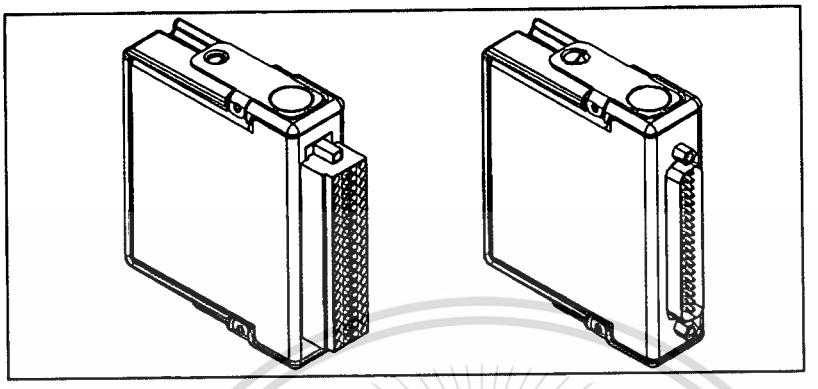

Analog Input Characteristics

Number of channels	32 single-ended or 16 differential analog input channels, 1 digital input channel, and 1 digital output channel
ADC resolution	16 bits
DNL	No missing codes guaranteed
INL	Refer to the *AI Absolute Accuracy Tables and Formulas*
MTBF	775,832 hours at 25 °C; Bellcore Issue 6, Method 1, Case 3, Limited Part Stress Method
Conversion time	
R Series Expansion chassis	4.50 µs (222 kS/s)
All other chassis	4.00 µs (250 kS/s)
Input coupling	DC
Nominal input ranges	±10 V, ±5 V, ±1 V, ±0.2 V
Minimum overrange (for 10 V range)	4%
Maximum working voltage for analog inputs (signal + common mode)	Each channel must remain within ±10.4 V of common

NI 9401

8-Channel, TTL Digital Input/Output Module

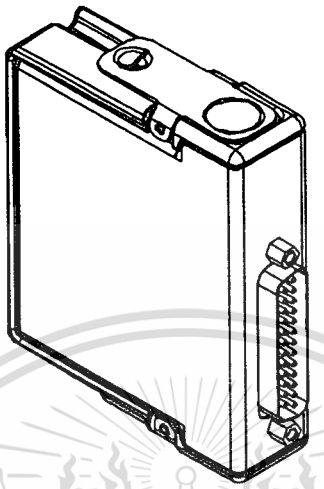

Input/Output Characteristics

Number of channels ..... 8 DIO channels

Default power-on line direction ..... Input

Input/output type ..... TTL, single-ended

Digital logic levels

- Input
  - Voltage ..... 5.25 V max
  - High, V_{IH} ..... 2 V min
  - Low, V_{IL} ..... 0.8 V max
- Output
  - High, V_{OH} ..... 5.25 V max
    - Sourcing 100 µA ..... 4.7 V min
    - Sourcing 2 mA ..... 4.3 V min
  - Low, V_{OL}
    - Sinking 100 µA ..... 0.1 V max
    - Sinking 2 mA ..... 0.4 V max

Maximum input signal switching frequency by number of input channels, per channel

- 8 input channels ..... 9 MHz
- 4 input channels ..... 16 MHz
- 2 input channels ..... 30 MHz

NI 9235/9236

8-Channel, 24-Bit Quarter-Bridge Analog Input Module

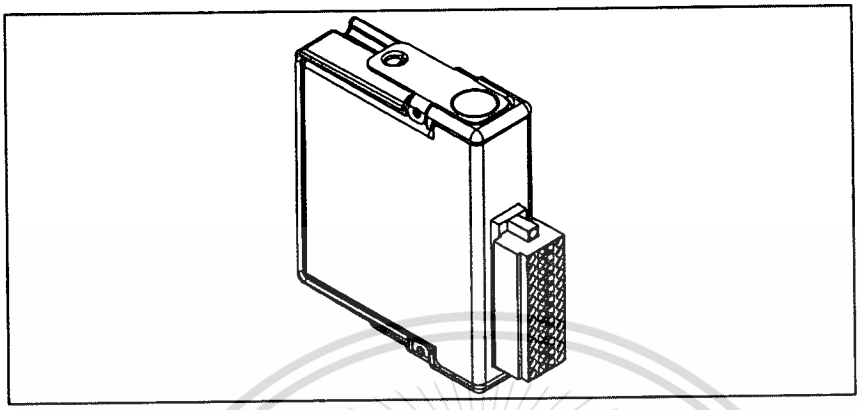

Input Characteristics

Number of channels ..... 8 analog input channels

Quarter-bridge completion

- NI 9235 ..... 120 Ω, 10 ppm/°C max
- NI 9236 ..... 350 Ω, 10 ppm/°C max

ADC resolution ..... 24 bits

Type of ADC ..... Delta-Sigma (with analog prefiltering)

Sampling mode ..... Simultaneous

Internal master timebase (f_M)

- Frequency ..... 12.8 MHz
- Accuracy ..... ±100 ppm max

Data rate range (f_s) using internal master timebase

- Minimum ..... 794 S/s
- Maximum ..... 10 kS/s

Data rate range (f_s) using external master timebase

- Minimum ..... 195.3125 S/s
- Maximum ..... 10.547 kS/s

Data rates[1] (f_s) ..... $\frac{f_M \div 256}{n}$, $n = \{2; 4, 5, ..., 63\}$

Full-scale range ..... ±29.4 mV/V (+62,500 με/–55,500 με)

Scaling coefficient ..... 3.5062 nV/V per LSB

Overvoltage protection between any two terminals ..... ±30 V

APPENDIX D

PROCEEDING

- **Appendix D-1 :** Design and analysis of a direct clutch system prototype for one cylinder diesel engine by using CAD/CAE.
- **Appendix D-**2 : Design and Analysis of Clutch Housing Prototype for One Cylinder Diesel Engine Direct Clutch System.
- **Appendix D-**3 : Model Improvement of Clutch Housing Prototype for Direct Clutch One Cylinder Diesel Engine.

Appendix D-1: Design and analysis of a direct clutch system prototype for one cylinder diesel engine by using CAD/CAE

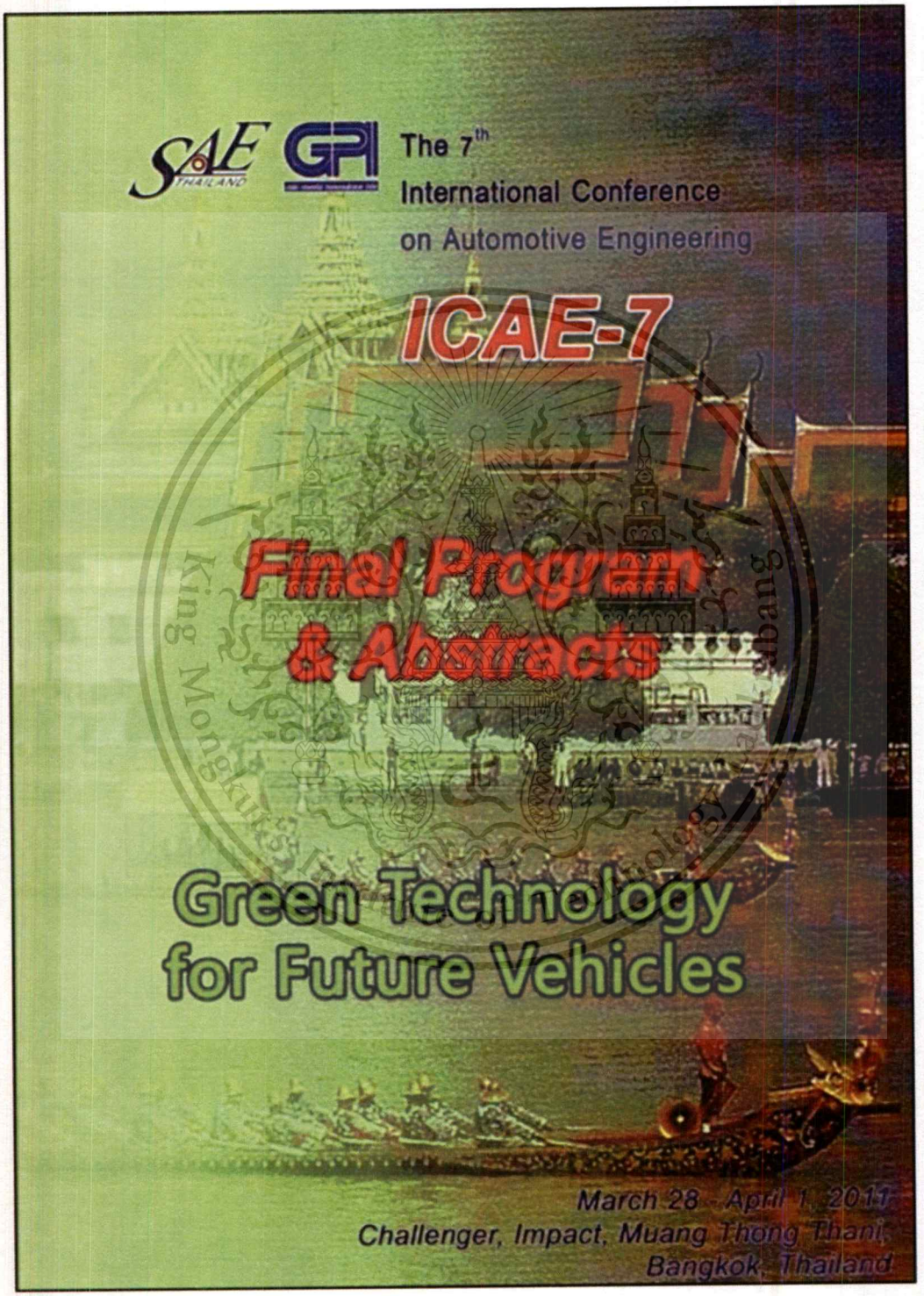

Design and analysis of a direct clutch system prototype for one cylinder diesel engine by using CAD/CAE

Suphakrit Koocharoenprasit
Automotive Engineering, International College, King Mongkut's Institute of Technology Ladkrabang, Thailand

Chi-na Benyajati, Jenwit Soparat
Automotive Laboratory, National Metal and Materails Technology Center (MTEC), Thailand

Jaruwat Charoensuk
Faculty of Engineering, King Mongkut's Institute of Technology Ladkrabang (KMITL), Thailand

Ichiro Hagiwara
Department of Mechanical Sciences and Engineering, Tokyo Institute of Technology, Japan

ABSTRACT

In order to develop an improved transmission system for an agricultural truck or E-TAND, a direct clutch system was designed for one-cylinder diesel engine to replace conventional belt transmission. Nevertheless, one-cylinder diesel engine was not originally designed for such clutch system. Thus, there were several parts that were needed to be designed in order to connect a clutch directly to a flywheel such as clutch contact surface, clutch housing, and clutch fork. All parts were designed by using CAD software. Moreover, CAD models were analyzed by using finite element method via ANSYS® software. The analyses were consisted of structural stress analysis, fatigue life analysis, and natural frequency depending on specific concerns and different loading types for each parts.

INTRODUCTION

An agricultural truck is used widely in rural parts of Thailand. The most basic and the most famous type is E-TAND because of its relatively low manufacturing and maintenance cost. E-TAND is also known as a multipurpose vehicle in some regions. A one-cylinder diesel engine is generally used as a prime mover from which the power will be transferred to gearbox via belts. V-belt type is generally selected; however this type of transmission is accompanied by considerable amount of loss. Furthermore, the problems associated with this kind of vehicle are low quality, no standard, low performance, and high loss. In order to develop an improved transmission system for an agricultural truck or E-TAND, a direct clutch system was designed for one-cylinder diesel engine to use instead of belt transmission. Nevertheless, one-cylinder diesel engine was not originally designed for such clutch system. Thus, the present work was focusing on re-designing of components that would connect a clutch directly to a flywheel i.e. clutch contact surface, clutch housing, and clutch fork.

BACKGROUND

BELT TRANSMISSION

Belt transmission has been used to transmit a power in many applications. The belt transmission can be used to transmitted

many kinds of load. However, this type of transmission is accompanied by many kind of loss such as hysteresis loss, fictional loss, creep loss and slip loss. In 1995, Anibal and Steve were conducting a survey on characteristics of different belt types, with a particular emphasis on their energy efficiency, cost-effectiveness and field of applications [1]. As a result, the highest efficiency of V- belt transmission type was when the system was operated near rated load capacity and also decreased when load deviated from 100% load capacity.

FINITE ELEMENT METHOD

Finite element method is used to approximate a problem of stress analysis, fluid flow, heat transfer, etc. In this work, all of analysis cases were related with the structural analysis. In recent years, there were many studies of the finite element method to predict failures or analysis resulting stress. In automotive industry, this method was used to analyze automotive parts such as analysis of failure in a universal joint yoke and a drive shaft by H. Bayrakceken et al.[2], fatigue life prediction of lower suspension arm by M. M. Rahman et al. [3]. Topaç et al. carried out a fatigue failure prediction of rear axle housing prototype by using finite element analysis [4]. These authors employed a similar kind of sequence or methodology to carry out the research. The common methodology were followed by modeling a CAD model, performing stress and fatigue life analysis (the boundary conditions and loads needed), and validating results by comparison with experimental results. In some cases, after the finite element was used to analyze a stress, the optimization was carried out to optimize a structure. N. Kaya et al. used the design of experiment (DOE) to optimize a clutch fork using topology and shape optimization by the response surface method [5].

SPECIFIC CONCERNS IN DESIGN

In order to obtain a final design of a direct clutch transmission system, there were several processes and specific concerns for each part. The overall layout of a direct clutch system prototype is shown in Figure 1

.

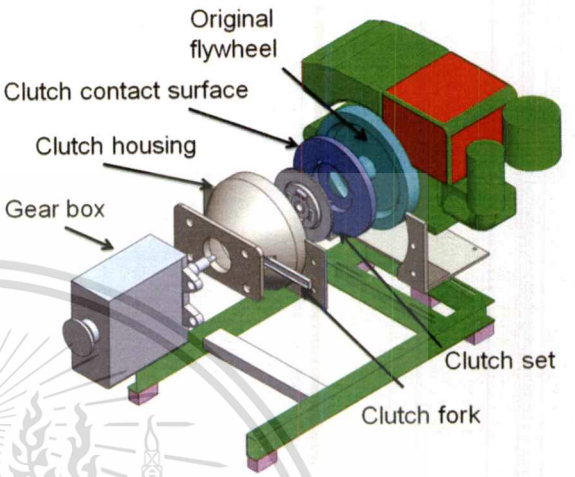

Figure 1. A layout of direct clutch system prototype

COMPONENTS DESIGN

In this section, specific concern for design in each part is presented.

Clutch contact surface

Clutch contact surface is the component transfers the power from the engine to the clutch system. Generally, a flywheel of a conventional car has a surface for a clutch disc contact. On the other hand, an one-cylinder diesel engine flywheel has no surface for contact of clutch disc. Therefore, clutch contact surface was needed to be designed. The design conditions of clutch contact surface are installation space, and minimum weight. The size of clutch contact surface is restricted by a dimension of clutch set, and mounting location on original flywheel. An initial of clutch contact surface prototype is shown in Figure 2.

Figure 2. Clutch contact surface prototype model (all dimensions in mm)

Clutch fork

Clutch fork is one of important parts of the mechanism for controlling the engagement between a clutch disc and a clutch contact surface on fly wheel. The concerning parameter was that the clutch fork must generate enough pressure on a spring diaphragm to release a clutch disc. The clutch fork model is shown in Figure 3 .

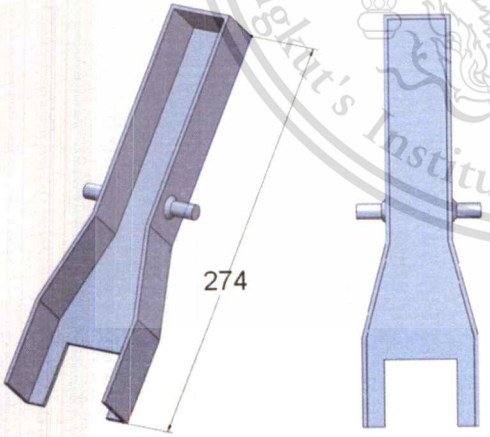

Figure 3. Clutch fork prototype model (all dimensions in mm)

Clutch housing

Clutch housing is a part located between engine and gearbox that covers all of the direct clutch system. The design was constrained by an access point of clutch fork, dimension of clutch system, and flange of gearbox. The clutch housing prototype model is shown in Figure 4.

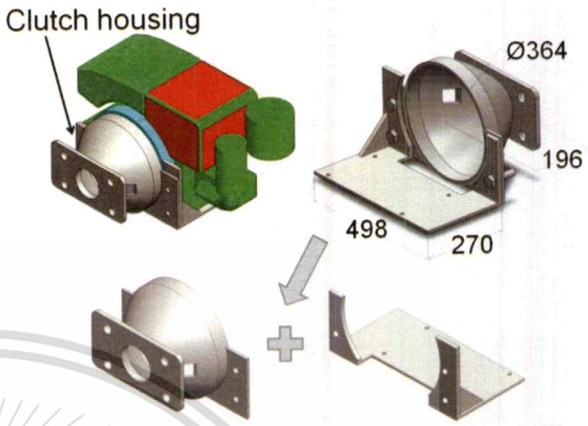

Figure 4. Clutch housing prototype model (all dimensions in mm)

COMPUTATIONAL DETAILS

MECHANICAL PROPERTIES

In an initial analysis, a structural steel was chosen as material of all parts. The mechanical properties were referred to Engineering data in ANSYS® software.

Young's Modulus MPa	= 2E+5
Density kg/m^3	= 7850
Yield Strength MPa	= 2.5E+2
Possion's Ratio	= 0.3

MODELS AND BOUNDARYCONDITIONS

Clutch housing

Normally, a clutch housing is attached directly with the engine. In addition, the vibration of an one-cylinder diesel engine can have a very high amplitude. Therefore, this analysis was setup to study the effect of engine vibration on the clutch housing. The boundary conditions of clutch housing are shown in Figure 5 . A fixed support condition would be applied on a gearbox side while a vibration load would be applied as a displacement load on the other side.

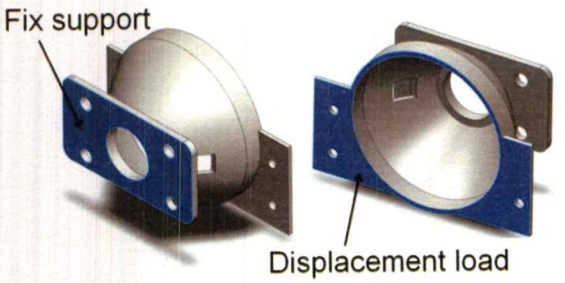

Figure 5. The clutch housing boundary conditions

Bolts on a clutch contact surface

This analysis was a simulation of a stress occurred on bolts when a torque was applied from an engine to a flywheel. An analysis was carried out under a critical condition where clutch contact surface did not move relative to a flywheel rotation. As a result, boundary conditions of this analysis were such that degrees of freedom (DOF) of the clutch contact surface and the flywheel was fixed apart from a rotation around y-axis. Then, a moment load was applied at the flywheel. The boundary conditions are shown graphically in Figure 6 .

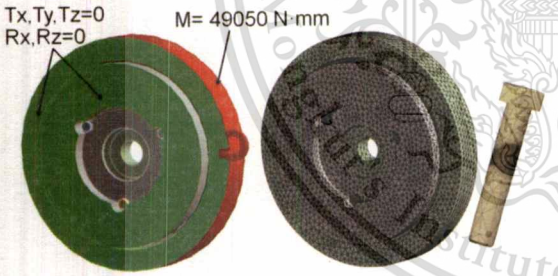

Figure 6. Boundary conditions and finite element model for bolt analysis

In this analysis, tetrahedron mesh element was used. As the analysis was concerned on stress generated in bolts on a flywheel, mesh elements was refined in the region of bolts. Mesh convergence was manually performed to obtain an appropriated size of 0.5 mm. The finite element model is shown in Figure 6.

Clutch fork

The boundary conditions of clutch fork was applied as followed [5].

- 600N Force was applied to the actuator point .
- At the fulcrums, five DOF were fixed, apart from a rotation around y-axis
- Translation along z-axis was fixed at the contact of release bearing.

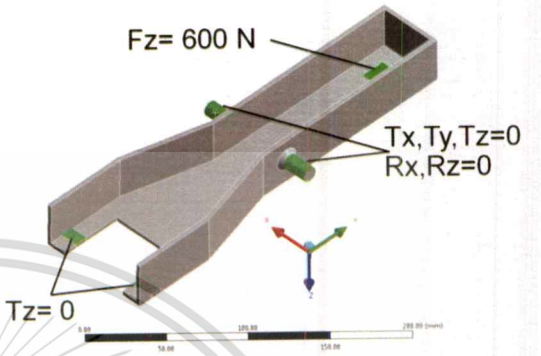

Figure 7. The clutch fork boundary conditions.

Additionally, in order to perform an optimization on clutch fork design, many cases had to be analyzed until the solution convergence could be achieved. For ANSYS® software, there are an option to automatically refine the mesh until the convergence is reached, called convergence tools [6]. However, using convergence tools in each analysis could be very time consuming. As a result, different mesh sizes were considered manually and compared with the results obtained using convergence tools function in order to determine an appropriate mesh size which could be employed in all analysis cases. Tetrahedron mesh element type size 2.5 mm was chosen for all design points. The mesh and equivalent Von-Mises stress comparisons are shown in Figure 8 and Table 1.

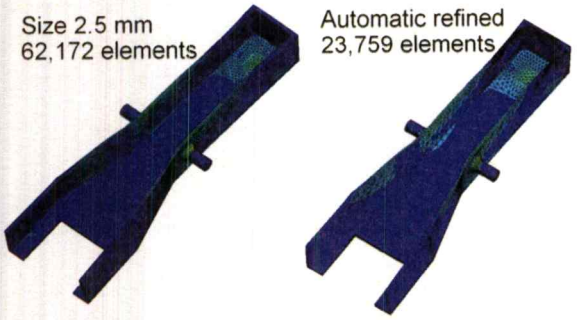

Figure 8. Mesh element comparison between manual and automatic refinement meshing

Table.1 Mesh element comparison

	Max. Equivalent Von-Mises stress	Mesh elements
2.5mm tetrahedron	110.42 MPa	62,172
Auto. refine mesh	106.52 MPa	23,759
	Diff. 3.66%	Diff.38,413 elements

RESULTS & DISCUSSIONS

BOLTS ON A CLUTCH CONTACT SURFACE

The analyzed result for Von-Mises stress, shear stress, and nominal stress was 29.352 MPa, 5.68 MPa, and 13.22 MPa respectively. The result is shown in Figure 9. These obtained values could be referred to as a guideline when selecting bolt types and materials for a use in a prototype later on.

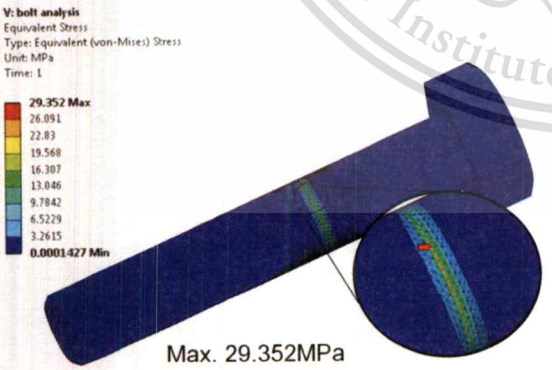

Figure 9. Von-Mises stress distribution in bolt.

CLUTCH FORK ANALYSIS & OPTIMISATION

Initially, the analysis was carried out with a 1.8 mm thickness. The simulation was done using static linear analysis with 2.5 mm mesh size. The resulting stress is shown in Figure 10. Maximum Von-Mises stress was 149.44 MPa which gave a safety factor of 1.67.

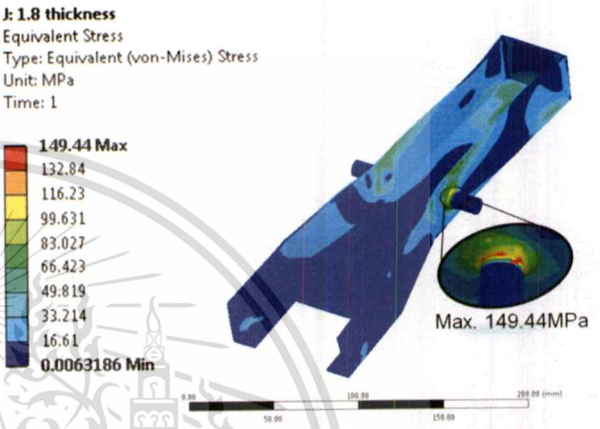

Figure 10. Von-Mises stress distribution in clutch fork, component thickness of 1.8 mm

Since the safety factor was lower than a target value of 3, the method of optimization was applied to find an appropriate thickness of this clutch fork to achieve such safety factor (Figure 11). A relationship between maximum equivalent Von-Mises stress and component thickness was studied during the optimization. The thickness was varied from 1.8 to 3.4 mm with an increment of 0.2 mm in each design point.

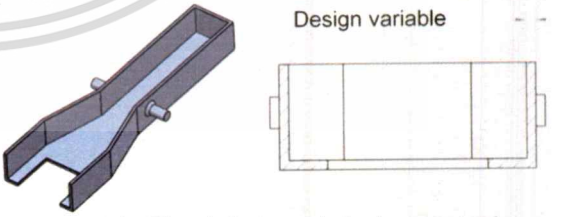

Figure 11. Clutch fork and design variable

Table.2 Design variable table

Thickness (mm)	Max. Equivalent Von-Mises stress (MPa)	Volume (mm^3)	Safety factor
1.8	149.44	213,107.36	1.67
2	144.15	220,928.98	1.73
2.2	138.12	230,584.99	1.81
2.4	125.76	253,234.57	1.99
2.6	115.04	276,839.57	2.17
2.8	115.04	276,839.57	2.17
3	110.42	288,406.39	2.26
3.2	100.14	318,024.10	2.50
3.4	95.42	333,743.78	2.62

The calculated results is shown in Table.2 while a graph showing a relation between maximum equivalent Von-Mises stress and thickness is shown in Figure 12. It can be seen from the results that resulting maximum stress reduced with an increase in thickness. Furthermore, second order polynomial curve fitting technique was used to approximate a correlation between stress and thickness. The obtained equation was:

$$y = 5x^2 - 60x + 240$$

where

y = Maximum Equivalent Von-Mises (MPa)
x = Thickness of a clutch fork (mm)

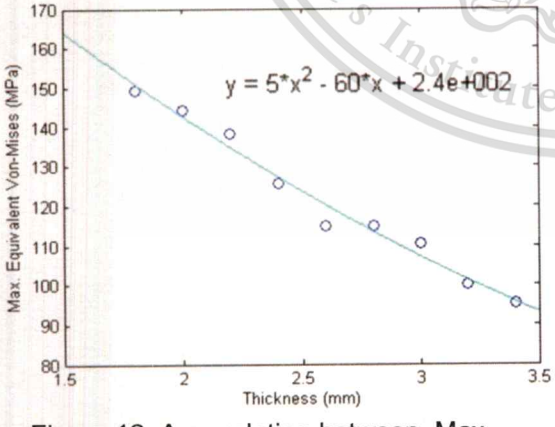

Figure 12. A correlation between Max. Equivalent Von-Mises stress and thickness of a clutch fork

In order to achieve a goal of design, a safety factor had to be higher than 3 or a maximum equivalent Von-Mises stress of 83.33 MPa. Therefore, an appropriate thickness were calculated from the equation shown in Figure 12. The result of appropriate thickness was 3.84 mm. This thickness was then used in a re-model analysis. The result is shown in Figure 13. The maximum equivalent Von-Mises stress was 87.149 MPa with a corresponding safety factor of 2.868. The percentage error of maximum equivalent Von-Mises stress and safety factor was 4.58% and 4.33% respectively which were in acceptable ranges.

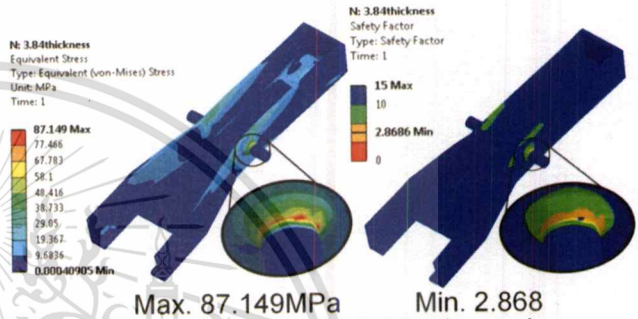

Max. 87.149MPa Min. 2.868

Figure 13. Analyzed stress distribution and safety factor of an optimized model, thickness 3.84 mm

CONCLUSION

The present work involved designing and analyzing a direct clutch system prototype for a one-cylinder diesel engine used in agricultural truck or E-TAND. The specific design concerns of each part were discussed and details of finite element analysis and optimization of a clutch fork were explained.

For finite element model preparation, a tetrahedron mesh type was chosen in this work. For bolts analysis, the results was analyzed to study a trend of generated stress. This results could be used as a selection criteria, i.e. types and materials of bolt, that will be used to bolt a clutch contact surface onto a flywheel in actual prototype.

In a clutch fork analysis, software-provided convergence tools feature was initially used to validate a result obtained from manual meshing to determine an appropriate mesh size for further use in every optimization

cases. The advantage of using the selected manual meshing size was a reduced computational time.

The optimization of a clutch fork showed that the overall strength of the component increased with increasing thickness. The correlation between maximum Von-Mises stress and thickness could be approximated into a 2nd order polynomials equation. Such equation could be used to predict an appropriate thickness according to a desired safety factor. However, results of prediction displayed some errors that could occur from the curve fitting process. Nonetheless, the error was not exceeding 5%. Therefore this approach could be used to predict a thickness or other design variables provided that the deviation of data was not too fluctuated.

For future work, a clutch fork will be investigated by measuring stress distribution from experiment to validate the optimized analytical results. Furthermore, for clutch housing analysis, the vibration of the engine and torque characteristic will be investigated to obtain boundary conditions in fatigue analysis of clutch housing. The experiment has been set up as shown on Figure 14. Vibration and torque are measure by accelerometers and a torque transducer respectively.

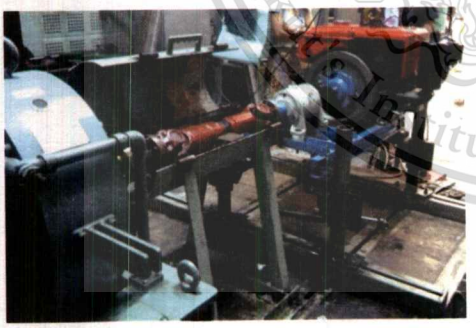

Figure 14. An experimental setup for studying engine vibration load and torque characteristic

ACKNOWLEDGMENTS

The authors would like to thank the National Metal and Materials Technology Center (MTEC) for the support of this work.

REFERENCES

[1] **Anibal De Almeida, Steve Greenberg**, "Technology assessment: energy-efficient belt transmissions", Journal of Energy and Buildings 22 (1995) 245-253

[2] **H. Bayrakceken, S. Tasgetiren, I. Yavuz**, "Two cases of failure in the power transmission system on vehicles: A universal joint yoke and a drive shaft", Journal of Engineering Failure Analysis 14 (2007) 716–724

[3] **M. M. Rahman, K. Kadirgama, M. M. Noor, M. R. M. Rejab and S. A. Kesulai,** "Fatigue Life Prediction of Lower Suspension Arm Using Strain-Life Approach", European Journal of Scientific Research ISSN 1450-216X Vol.30 No.3 (2009), pp.437-450

[4] **M.M. Topa, H. Gunal , N.S. Kuralay**, "Fatigue failure prediction of a rear axle housing prototype by using finite element analysis", Journal of Engineering Failure Analysis 16 (2009) 1474–1482

[5] **Necmettin Kaya, Idris Karen, Ferruh Ozturk,** "Re-design of a failed clutch fork using topology and shape optimization by the response surface method", Journal of Materials and Design 31 (2010) 3008–3014

[6] ANSYS Workbench User's Guide

Appendix D-2 : Design and Analysis of Clutch Housing Prototype for One Cylinder Diesel Engine Direct Clutch

CTS 17
The Second TSME International Conference on Mechanical Engineering
19-21 October, 2011, Krabi, Thailand

Design and Analysis of Clutch Housing Prototype for One Cylinder Diesel Engine Direct Clutch System

Suphakrit Koocharoenprasit[1*], Chi-na Benyajati[2], Jenwit Soparat[2], Sittikorn Lapapong[2], Jaruwat Charoensuk[3] and Ichiro Hagiwara[4]

[1] Automotive Engineering, International College, King Mongkut's Institute of Technology Ladkrabang, Thailand

[2] Automotive Laboratory, National Metal and Materials Technology Center (MTEC), Thailand

[3] Faculty of Engineering, King Mongkut's Institute of Technology Ladkrabang (KMITL), Thailand

[4] Department of Mechanical Sciences and Engineering, Tokyo Institute of Technology, Japan

*Corresponding Author: K_suphakrit@hotmail.com, Telephone Number (+66)81-832-2544

Abstract

In this work, a design of clutch housing for one cylinder diesel engine in an agricultural truck or E-TAND using CAD and CAE was carried out. A CAD model was analyzed by using finite element method ANSYS® software. The analyses were consisted of structural stress and fatigue life analysis by converting vibration profile into corresponding forces which were used as a load parameter. In order to collect relevant load profiles, an experiment was set up to measure vibration amplitude by the engine using accelerometers. Moreover, an optimization technique was used to find an optimum design of a clutch housing suitable for one cylinder diesel engine application. Overall design frame work, concerning design problem, load collecting experiment, and computational analysis results were reported and discussed. After achieving the goal of design, all parts will be ready for prototype manufacturing and assembly for a direct clutch system in an agricultural truck.

Key words: Finite element analysis, Stress analysis, Design optimization

1. Introduction

An agricultural truck is used widely in rural parts of Thailand. The most basic and the most famous type is E-TAND because of its relatively low manufacturing and maintenance cost. E-TAND is also known as a multipurpose vehicle in some regions. A one cylinder diesel engine is generally used as a prime mover from which the power will be transferred to gearbox via belts. V-belt type is generally selected. However this type of transmission is accompanied by considerable amount of loss. In order to develop an improved transmission system for E-TAND, a direct clutch system was designed for one cylinder diesel engine. Nevertheless, one cylinder diesel engine was not originally designed for such clutch system. Thus, there were several parts that were needed to be designed in order to connect a clutch directly to a flywheel such as clutch contact surface, clutch housing, and clutch fork. In this work, a design of clutch housing was focused

using finite element analysis and optimization tool. All design processes involved in this work are summarized in Fig.1

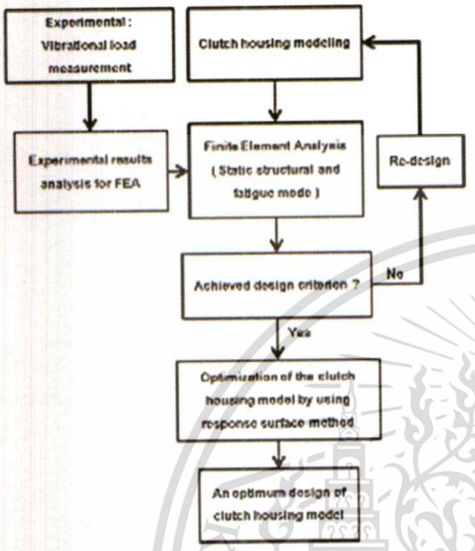

Fig. 1 Clutch housing design flowchart

The finite element method is used to approximate a problem of stress analysis, fluid flow, heat transfer, etc. In recent years, there were many studies using the finite element method to predict failures or analyze resulting stresses. In automotive industry, this method was used to analyze failure or fatigue life of various automotive parts such as universal joint yoke and a drive shaft [1], fatigue life prediction of lower suspension arm [2], rear axle housing [3]. These authors employed a similar kind of sequence or research methodology which involved modeling a CAD model, performing stress and fatigue life analysis in which the boundary conditions and loads were needed, and validating results by comparison with experimental results. In some cases, after the finite element method was used to analyze a stress, an optimization process was carried out to determine a suitable redesign for structure. Various algorithms has been investigated in literature. For example, N. Kaya et al. used the design of experiment (DOE) to optimize a clutch fork using topology and shape optimization by the response surface method [4]. In addition, an optimization algorithm using orthogonal arrays in discrete design space for structures was carried out by Kwon-Hee Lee et al.[5].

2. Clutch Housing Design

2.1 Specific concerns in clutch housing design for one cylinder diesel engine

As shown in Fig.2 clutch housing is a part located between engine and gearbox that covers all of the clutch system. The design was constrained by an access point of clutch fork, dimension of clutch system, and flange of gearbox. The special concerning was a potential failure caused by the vibration of engine. In addition, an alignment problem between gearbox and engine was considered.

2.2 Clutch housing modeling

Clutch housing was designed according to the dimension of clutch set and a mounting location. According to its characteristic, one cylinder diesel engine is a high vibration engine. Therefore, a mounting plate was designed to avoid a misalignment between gearbox and engine when acceleration was required. Components of clutch housing prototype model are shown in Fig.3.

CTS 17
The Second TSME International Conference on Mechanical Engineering
19-21 October, 2011, Krabi, Thailand

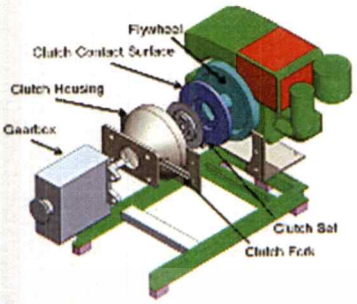

Fig. 2 A layout of direct clutch system prototype

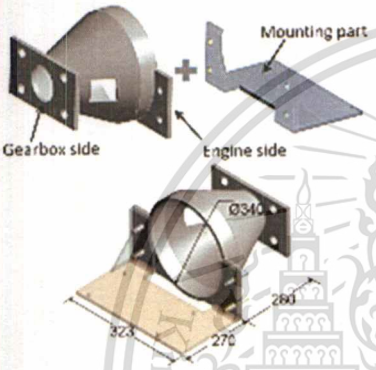

Fig. 3 A clutch housing prototype model (in mm.)

3. Experimental - Engine Vibration Profile Measurement

In present work, vibrational load profiles measurement at various engine load conditions was carried out on a dynamometer test configuration.

3.1 Experimental apparatus

The apparatus of this experiment(Fig. 4) were consisted of

- 14HP,Direct injection engine (KUBOTA RT140)
- Data acquisition tools :NIcDAQ-9172 and NI 9234
- Accelerometers; Brüel&Kjær Type 4507 B002
- Dynamometer with Dynamo controller
- NI Sound and Vibration Assistant software

3.2 Experimental setup

In this experiment, the engine was operated at 3 different load cases which were idle load(1120 rpm), partial load (60% of throttle, 1800 rpm), and full load (100% of throttle, 2200 rpm). The accelerometers were connected with NI DAQ set and were attached at front and rear end of engine wood base plate as shown in Fig. 5. The results were recorded by using NI Sound and Vibration Assistant software with a sampling rate of 1000Hz. The experiments were repeated for 3 times at each location for all load cases to confirm a repeatability of the results.

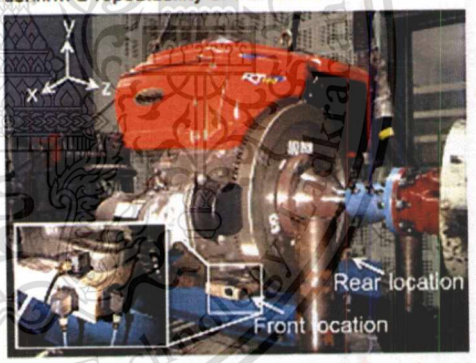

Fig. 5 Accelerometers attachment configuration near engine base

Fig. 4 An experimental set up for vibration load measurement: (from left) DAQ equipments and accelerometer, dynamometer load controller, and dynamometer chassis with test engine.

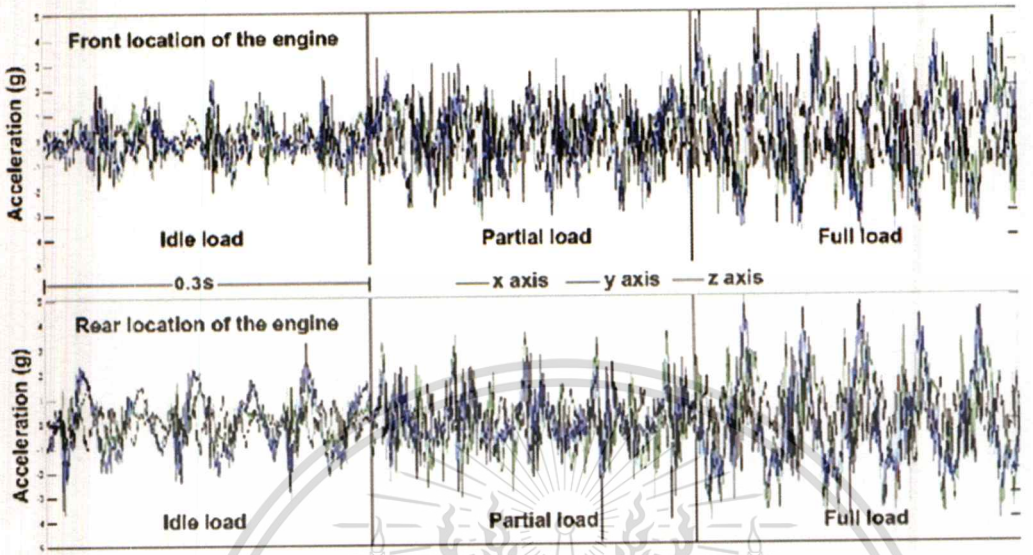

Fig. 6 The engine vibration profiles measured at various loads.

3.3 Experimental results

The results were separated into three main cases with two measurement sensor locations for each case. The results are shown in Fig. 6. Generally, all measured responses displayed a sinusoidal pattern for all load cases. Highest vibration amplitudes were observed during full load conditions in x and y axis directions.

In order to use the experimental data effectively in simulation, the data were passed through a low pass filter to collect corresponding data in frequency range under 60Hz. A graphical comparison between raw data and filtered data is shown in Fig. 7.

Additionally, in order to carry out a structural and optimization analysis, an input parameter should be applied as a force. Therefore, the measured acceleration was converted into corresponding force by multiplying with an engine effective mass. Assuming that C.G. of engine was located at center of a flywheel, effective mass of engine at front and rear support locations were calculated to be 73.66 kg and 38.44kg.

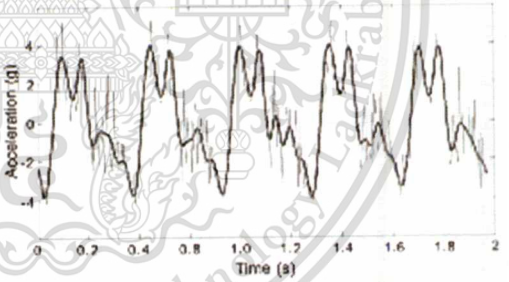

Fig. 7 Comparison between filtered and non-filtered vibration data

The calculated maximum forces in each load case which were used in simulation can be summarized in Table. 1. It can be seen that the maximum force under full load condition was higher than those under partial and no load conditions by approximately a factor of 1.89 and 2.84 respectively.

Table. 1 Maximum force in each load case

Cases	Maximum Force (N)		
	X	Y	Z
Front no load	1232	1564	702
Front partial load	1590	1640	1345
Front full load	2672	3046	2620
Rear no load	852	634	360
Rear partial load	1224	916	717
Rear full load	2346	1686	1446

Furthermore, for fatigue failure mode simulation, a load history was required. As a results, vibration profiles from each experiment cases were combined together with reference to TIS (Thai Industrial Standard) 2155-2546 driving cycle which is an equivalent of EUDC (European Driving Cycle Test) shown in Fig. 8. The assumption of a relationship between a driving cycle and an engine load were defined such that while the vehicle was accelerate, the engine ran with full load. On the other hand, the engine ran at partial load and no load, when vehicle ran on cruise speed and decelerated respectively. The loading history which was used in this study can be seen in Fig. 9.

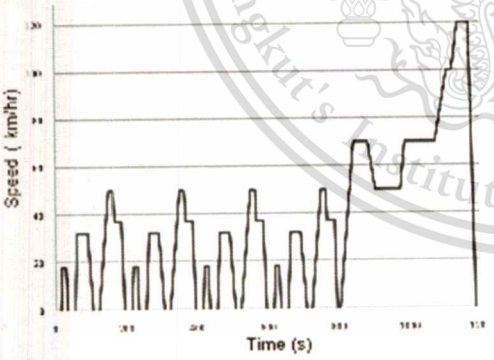

Fig. 8 EUDC standard: Driving cycle for 1 day.[6]

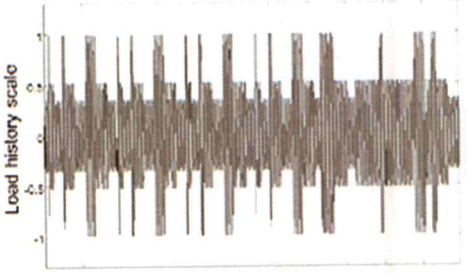

Fig. 9 Combined loading history for fatigue analysis

4. Finite Element Analysis

In order to determine the stress generated and analyze a fatigue failure of the clutch housing, the finite element analysis was applied on to the CAD model.

4.1 Finite element modeling

Mesh model of assembled clutch housing was prepared using ANSYS® software. Two types of mesh element were used, i.e. hexahedron for bolts and mounting part, and tetrahedron for clutch housing with a global element size of 6mm, 4mm, and 5mm respectively. In addition, each part was contained with elements which had skewness value lower than 0.75. The clutch housing FE model is illustrated in Fig. 10.

Fig. 10 Finite element model of clutch housing

4.2 Computational setup

For all computational analysis, a structural steel was chosen as material for all parts. Corresponding mechanical properties were taken from engineering data in ANSYS® software, including S-N curve for fatigue analysis. For an initial simulation, all components were assigned a thickness of 13mm with Clutch housing slope angle of 65 degree.

Boundary conditions applied in this study are shown in Fig. 11. The clutch housing was considered under a stress when loaded by engine vibration. The loads collected from the experiment were applied as a force loading. An amplitude of force loading was referred to maximum force in full load vibration (Table. 1). In addition, the input force loading was applied on both front and rear holes at the engine base plate of mounting part. A amplitude force was used in a static structural analysis while combined force amplitudes (Fig. 9) were applied as a load history for fatigue analysis. On the other hand, a fixed support was applied on the inner holes surface flange of clutch housing at the gearbox side. Moreover, the mean stress Goodman criterion was used in this work.

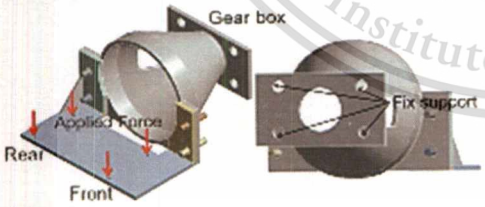

Fig. 11 Boundary conditions for clutch housing analysis

5. Size Optimization by Response Surface Method

ANSYS® Design Exploration Response Surface with the full 2nd order polynomial algorithm was used in this study to optimize the clutch housing prototype model. The thickness of clutch housing (DV1) and slope angle of clutch housing (DV2) shown in Fig. 12 were set as variable parameters. A relationship between maximum von-Mises stress and component geometries was studied during the optimization process by varying the clutch housing thickness was varied from 7mm to 13mm and the slope angle of clutch housing from 64 degree to 67 degree. The goals of this optimization were to reach a safety factor target of 3, to minimize volume of clutch housing, and to have no failure in fatigue mode. The design of experiment (DOE) used 3 factor levels and 2 parameters (3^n factorial design) i.e. $3^2 = 9$ design points. Each parameter was divided into 3 ranges of value, maximum, middle, and minimum for each factor design point. After 9 design points were completed, a response surface model was plotted using the full 2nd order polynomial.

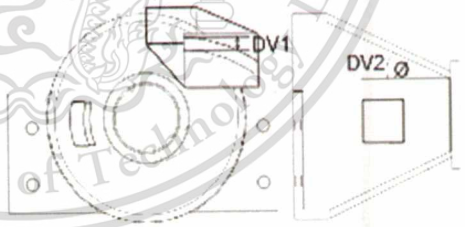

Fig. 12 Design variable of clutch housing optimization, thickness (DV1), slope angle (DV2)

6. Results & Discussions

Initially, the analysis was carried out with a 13 mm thickness and 65 degree of slope angle. The resulting stress is shown in Fig. 13.

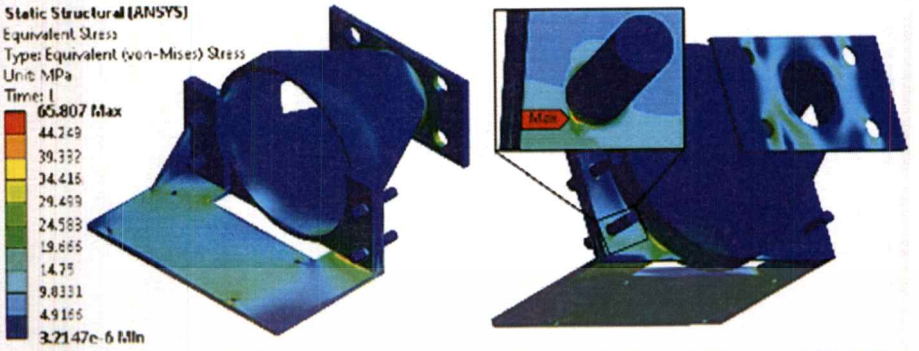

Fig. 13 von-Mises stress distribution in clutch housing, component thickness of 13 mm and 65 degree of slope angle.

Maximum von-Mises stress was 65.807 MPa which gave a safety factor of 3.799 with non-failure of fatigue mode. Since the safety factor was higher than a target value of 3, indicating overdesign, the method of optimization was applied to find an appropriate thickness and slope angle of clutch housing to achieve the design goals. During optimization, the DOE was carried out as explian in previous section and the calculated results are shown in Table. 2.

Table. 2 DOE- 3^2 design table results

Run #	DV1 (mm)	DV2 (degree)	Maximum von-Mises Stress (MPa)	Volume ($\times 10^3$ mm^3)	Minimum Life (Days)
1	7	65.5	116.45	5033.19	188.22
2	7	67	112.02	5033.74	260.06
3	7	64	123.49	5025.80	121.64
4	10	65.5	81.05	5794.78	27563
5	10	67	83.81	5838.62	27563
6	10	64	87.05	5731.12	27563
7	13	65.5	63.93	6573.23	27563
8	13	67	58.54	6593.86	27563
9	13	64	69.82	6453.66	27563

Based on the DOE results in Table. 2, the relationship between DV1, DV2, and maximum von-Mises stress as well as volume was constructed to form a response surface by using 2nd order polynomial algorithm. The equations of relationship are shown in Eqs. (1) and (2) where x is DV1 and y is DV2.

$$\text{Max. von-Mises stress (MPa)} = -2660.323 - 40.6072x + 96.0588y + 1.5688x^2 - 0.7712y^2 + 0.0056xy \quad \text{Eq.1}$$

$$\text{Volume } (\times 10^3 \text{ mm}^3) = 1431.32 - 7.3375x + 61.6688y + 0.9426x^2 - 0.47134y^2 + 3.541xy \quad \text{Eq.2}$$

The corresponding response surface of clutch housing design parameters for maximum von-Mises stress is displayed graphically in Fig.14.

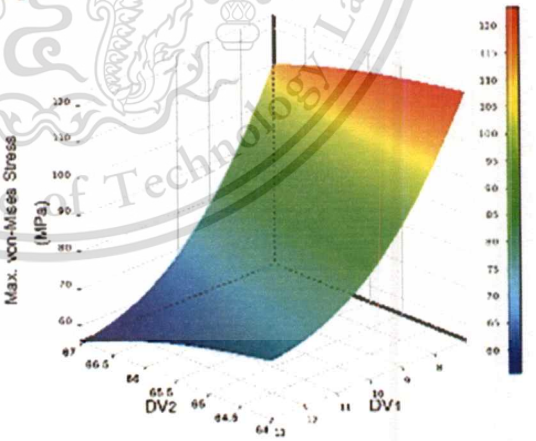

Fig. 14 Maximum von-Mises stress response surface for clutch housing design parameters (DV1,DV2).

According to the response surface, a sensitivity of the clutch housing slope angle was relatively low since incresing of slope angle resulting in a slight decrease in a maximum von-Mises stress. In contrast the variation of clutch housing thickness showed very high sensitivity such that maximum von-Mises stress significantly increased while the thickness was decreased. In addition, increasing of both parameters would result in an increase of the total volume of the model.

In this optimization, one of the goals was to minimise volume while a safety factor had to be higher than 3 or a maximum von-Mises stress of 83.33 MPa. Hence, 83.33 MPa was used as max. von-Mises stress in Eq. (1), to calculate possible x and y. Moreover, every possible combinations of x and y results were substituted into Eq. (2) to determine the minimum volume. From this calculation, the optimum point result was 8.7 mm of thickness and 67degree of clutch housing slope angle.

In addition, this optimum point was used in analysis to validate the results. Maximum von-Mises stress was 84.74MPa with a corresponding safety factor of 2.95 and structural volume of 5515.43 $x10^3 mm.^3$, while fatigue life was also achieved. The percentage error of maximum von-Mises stress, safety factor, and volume was 1.67%, 1.69%, and 0.06% respectively which were in acceptable ranges. Therefore, 8.7 mm. of thickness and 67degree of slope angle were optimum point of this clutch housing

Table. 3 Results comparison of optimum design point from response surface method

	Calculation	Simulation	Error(%)
Max. von-Mises stress (Mpa)	83.33	84.74	1.67
Safety factor	3	2.95	1.69
Volume ($x10^3 mm^3$)	5518.84	5515.43	0.06
Fatigue life		Pass	

7. Conclusion

The present work involved designing and analyzing a clutch housing for a direct clutch system prototype for a one-cylinder diesel engine used in agricultural truck or E-TAND. The specific design concerns were discussed and details of vibration loading measurement, finite element analysis, and optimization of a clutch housing were explained.

In vibration loading measurement, an engine vibration loading was measured and was later applied as input parameters (load) in a finite element analysis. The experiment showed that vibration loading amplitude of one cylinder diesel engine could increase from 0.002g to 4.22g with increasing engine load. The dominant vibration amplitude occurred on a plane corresponding to piston cylinder movement. Also, in order to use measured data effectively, a low pass filtering was needed.

For finite element method and optimization method, these methods were used to show the result of clutch housing behavior when under load. According to the response surface calculation, the sensitivity of both parameters that affect maximum von-Mises stress and volume of the clutch housing were

presented. An increase of thickness significantly decreased a maximum von-Mises stress while increased a volume. In contrast, a variation of slope angle was accompanied by only slight effect. Therefore, the main concerned parameter was a thickness of clutch housing. Furthermore, the optimum points were founded at thickness of 8.7 mm. and 67 degree of slope angle with a coressponding maximum von-Mises stress and volume of 84.74 MPa and 5515.43 $x10^{3}mm.^{3}$, respectively. In addition, results of current study display obvious advantages of the employed approaches such that;

- The sensitivity of each parameter can be shown and compared.
- Saving a computational time and shorten a design process.
- The optimum point prediction gave very accurate result. The error was not exceeding 1.7 %.

For future work, this optimum clutch prototype model will be manufactured and assembly into direct clutch system in agricultural or E-TAND for flied test and failure investigated.

8. Acknowledgement

The authors would like to thank the National Metal and Materials Technology Center (MTEC) for support of this work.

9. References

[1] H. Bayrakceken, S. Tasgetiren, I. Yavuz, "Two cases of failure in the power transmission system on vehicles: A universal joint yoke and a drive shaft", Journal of Engineering Failure Analysis 14 (2007) 716–724

[2] M. M. Rahman, K. Kadirgama, M. M. Noor, M. R. M. Rejab and S. A. Kesulai, "Fatigue Life Prediction of Lower Suspension Arm Using Strain-Life Approach", European Journal of Scientific Research ISSN 1450-216X Vol.30 No.3 (2009), pp.437-450

[3] M.M. Topa, H. Gunal , N.S. Kuralay, "Fatigue failure prediction of a rear axle housing prototype by using finite element analysis", Journal of Engineering Failure Analysis 16 (2009) 1474–1482

[4] Necmettin Kaya, Idris Karen, Ferruh Ozturk, "Re-design of a failed clutch fork using topology and shape optimization by the response surface method", Journal of Materials and Design 31 (2010) 3008–3014

[5] Kwon-Hee Lee, Jeong-Wook Yi, Joon-Seong Park, Gyung-Jin Parkc, "An optimization algorithm using orthogonal arrays in discrete design space for structures", Finite Elements in Analysis and Design 40 (2003) 121–135

[6] Thai Industrial Standards Institute, Light duty diesel engine vehicles: safety requirements; emission from engine, level 6, TIS 2155-2546

[7] ANSYS Workbench User's Guide

Appendix D-1: Model Improvement of Clutch Housing Prototype for Direct Clutch One Cylinder Diesel Engine.

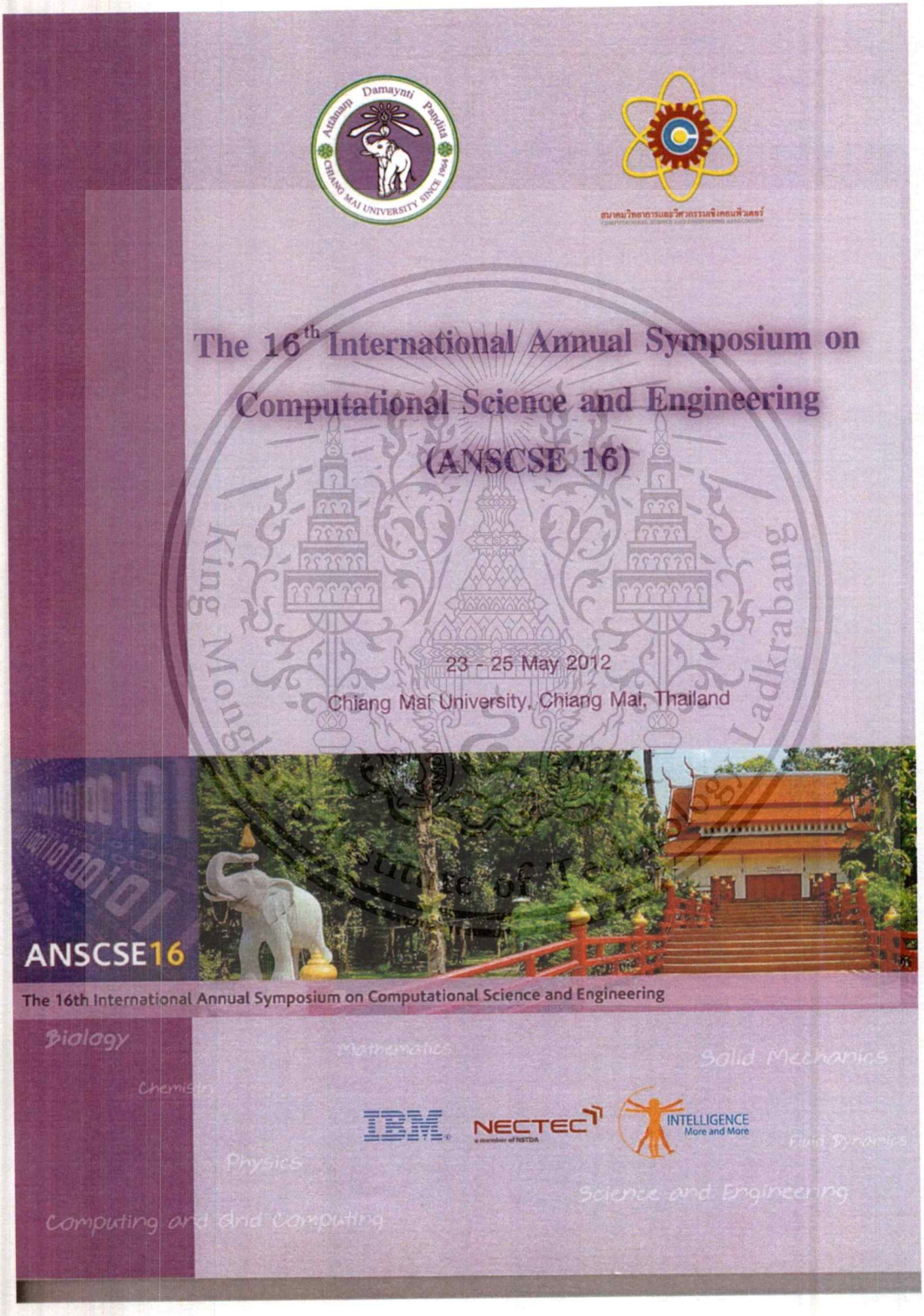

Model Improvement of Clutch Housing Prototype for Direct Clutch One Cylinder Diesel Engine

S. Koocharoenprasit[1c], C. Benyajati[2], J. Soparat[2], J. Charoensuk[3], I. Hagiwara[4]
[1]*Automotive Engineering, International College, King Mongkut's Institute of Technology Ladkrabang, Thailand*
[2]*Automotive Laboratory, National Metal and Materials Technology Center (MTEC), Thailand*
[3]*Faculty of Engineering, King Mongkut's Institute of Technology Ladkrabang (KMITL), Thailand*
[4]*Department of Mechanical Sciences and Engineering, Tokyo Institute of Technology, Japan*
E-mail: k_suphakrit@hotmail.com; **Tel.** 086-393-0447

ABSTRACT

In this work, a previously optimized clutch housing prototype was improved further with an objective of weight reduction. According to earlier design and analysis, the clutch housing was optimized by variation of clutch housing thickness and slope angle to find the optimum model for the first design. After the first optimization was done, it was observed that a middle section of the housing was subjected to a relatively low level of stress distribution. As a result, the middle section was modified by using the spokes pattern and strips cross structure to reduce the overall weight while maintaining the strength similar to that of the first optimum model. In addition, this new optimum model was constructed with a view of mass production for an agricultural truck (E-TAND). However, for prototyping purpose, a simple type clutch housing model was designed and presented for simplicity and cost. Finally, all 3 clutch housing models were compared and their respective advantages and differences were discussed.

Keywords: Stress analysis, Design optimization, and Response surface method.

1. INTRODUCTION

An agricultural truck is used widely in rural parts of Thailand. The most basic and the most famous type is E-TAND because of its relatively low manufacturing and maintenance cost. E-TAND is also known as a multipurpose vehicle in some regions. A one cylinder diesel engine is generally used as a prime mover from which the power will be transferred to gearbox via belts. V-belt type is generally selected. However this type of transmission is accompanied by considerable amount of loss. In order to develop an improved transmission system for E-TAND, a direct clutch system was designed for one cylinder diesel engine. Nevertheless, one cylinder diesel engine was not originally designed for such clutch

system. Thus, there were several parts that were needed to be designed in order to connect a clutch directly to a flywheel such as clutch contact surface, clutch housing, and clutch fork.

2. FINITE ELEMENT MOTHOD AND DESIGN OPTIMIZATION BACKGROUND

The finite element method is used to approximate a problem of stress analysis, fluid flow, heat transfer, etc. In recent years, there were many studies using the finite element method to predict failures or analyze resulting stresses. In automotive industry, this method was used to analyze failure or fatigue life of various automotive parts such as universal joint yoke and a drive shaft [1], fatigue life prediction of lower suspension arm [2], rear axle housing [3]. These authors employed a similar kind of sequence or research methodology which involved modeling a CAD model, performing stress and fatigue life analysis in which the boundary conditions and loads were needed, and validating results by comparison with experimental results. In some cases, after the finite element method was used to analyze a stress, an optimization process was carried out to determine a suitable redesign for structure. Various algorithms has been investigated in literature. For example, N. Kaya et al. used the design of experiment (DOE) to optimize a clutch fork using topology and shape optimization by the response surface method [4]. In addition, an optimization algorithm using orthogonal arrays in discrete design space for structures was carried out by Kwon-Hee Lee et al.[5].

3. CLUCTH HOUSING PROTOTYPE AND ANALYSIS

3.1 CLUTCH HOUSING PROTOTYPE

Clutch housing was designed according to the dimension of clutch set and a mounting location. According to its characteristic, one cylinder diesel engine is a high vibration engine. Therefore, a mounting plate was designed to avoid a misalignment between gearbox and engine when acceleration was required. Components of clutch housing prototype model are shown in Fig. 1.

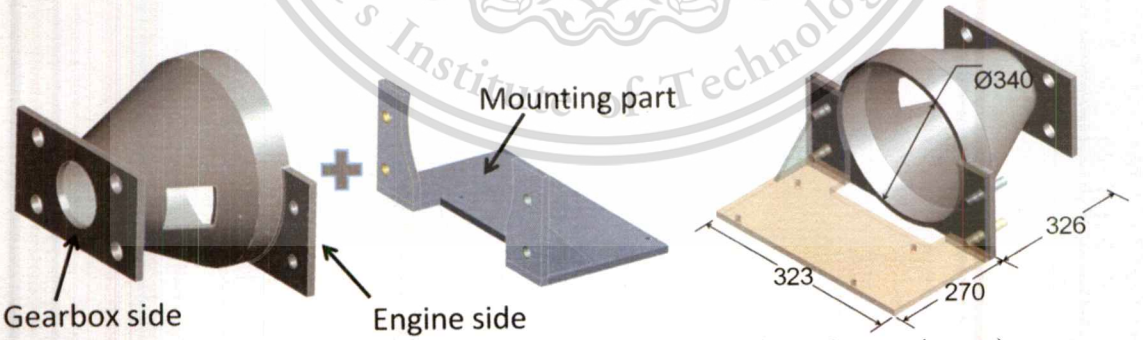

Figure 1. A clutch housing prototype model (all dimensions are in mm.)

3.2 FINITE ELEMENT ANALYSIS AND OPTIMIZATION

In order to determine the stress generated and analyze a fatigue failure of the clutch housing, the finite element analysis was applied on to the CAD model.

3.2.1 Finite element modeling

Mesh model of assembled clutch housing was prepared using ANSYS® software. Two types of mesh element were used, i.e. hexahedron for bolts and mounting part, and tetrahedron for clutch housing. The clutch housing FE model is illustrated in Fig. 2.

Figure 2. Finite element model of clutch housing

3.2.2 Computational set up

For all computational analysis, a structural steel was chosen as material for all parts. Corresponding mechanical properties were taken from engineering data in ANSYS® software, including S-N curve for fatigue analysis. For an initial simulation, all components were assigned a thickness of 13mm with Clutch housing slope angle of 65 degree.

Boundary conditions applied in this study are shown in Fig. 3. The clutch housing was considered under a stress when loaded by engine vibration. The loads collected from the experiment were applied as a force loading. Amplitude of force loading was referred to maximum force in full load vibration (Table. 1). In addition, the input force loading was applied on both front and rear holes at the engine base plate of mounting part. The measured forces in each direction were used in a static structural analysis while combination of forces from different engine conditions according to EUDC (Extra Urban Driving Cycle) were applied as a load history for fatigue analysis as shown in Fig. 4. On the other hand, a fixed support was applied on the inner holes surface flange of clutch housing at the gearbox side. Moreover, the mean stress Goodman criterion was used in this work.

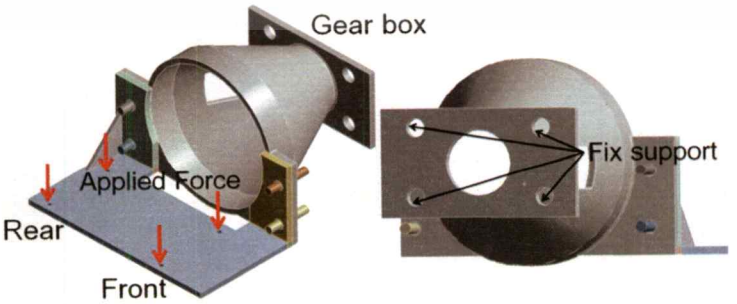

Figure 3. Boundary conditions for clutch housing analysis

Table 1. Maximum engine vibration forces

Cases	Maximum Force (N)		
	X	Y	Z
Front full load	2872	3048	2620
Rear full load	2346	1686	1446

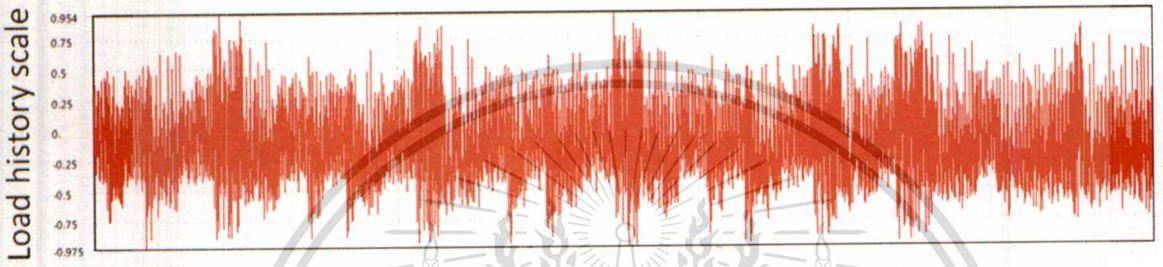

Figure 4. Combined loading history for fatigue analysis

3.2.3 Size optimization by response surface method

ANSYS® Design Exploration Response Surface with the full 2nd order polynomial algorithm was used in this study to optimize the clutch housing prototype model. The thickness of clutch housing (DV1) and slope angle of clutch housing (DV2) shown in Fig. 5 were set as variable parameters.

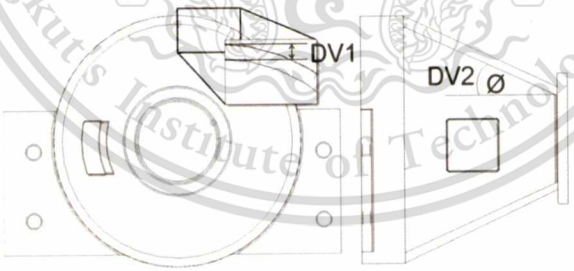

Figure 5. Design variables of clutch housing optimization, thickness (DV1), slope angle (DV2)

The goals of this optimization were to reach a safety factor target of 3, to minimize volume of clutch housing, and to have no failure in fatigue mode.

3.2.4 Result of post model analysis and optimization

Initially, the analysis was carried out with a 13 mm thickness and 65 degree of slope angle. The resulting stress is shown in Fig. 6. maximum von-Mises stress was 65.807 MPa which gave a safety factor of 3.799 with no fatigue failure. Since the safety factor was higher than a target value of 3, indicating overdesign, the method of optimization was applied to find an appropriate thickness and slope angle of clutch housing to achieve the design goals.

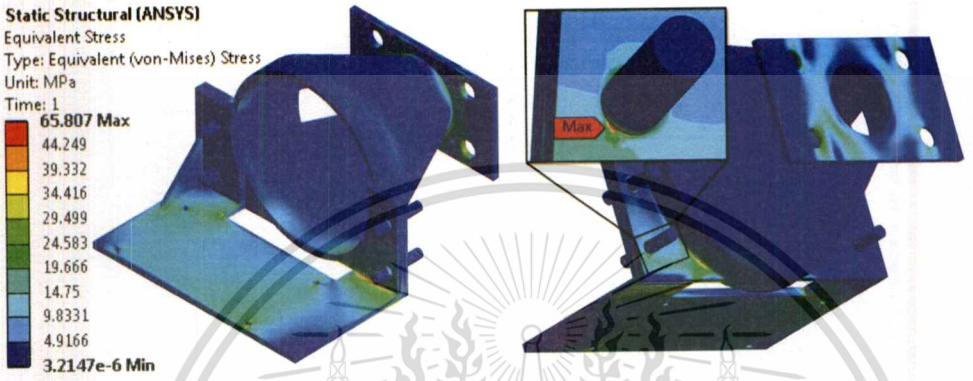

Figure 6. Von-Mises stress distribution in clutch housing, component thickness of 13 mm and 65 degree of slope angle.

To achieve the goals of Safety factor of 3, or a maximum von-Mises stress of 83.33 MPa, and no fatigue failure, the response surface was constructed to analyze the optimum point. The optimum point was found on the response surface at 8.7 mm. of thickness and 67degree of slope angle as shown on Fig. 7 with a coressponding maximum von-Mises stress and volume of 84.74 MPa and 5515.43×10^3 mm^3

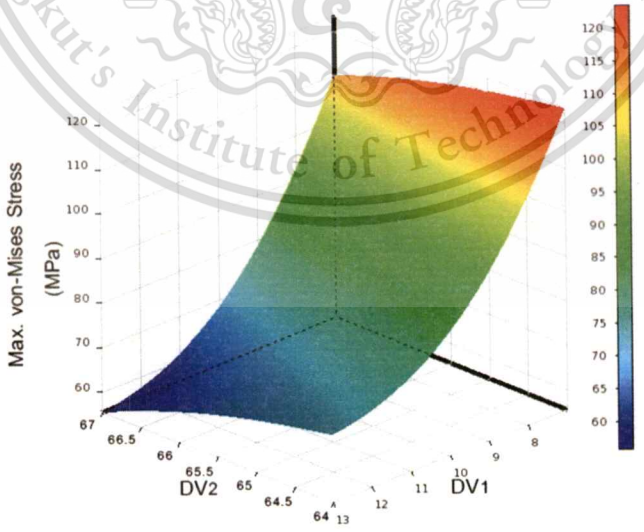

Figure 7. Maximum von-Mises stress response surface for clutch housing design parameters (DV1and DV2)

According to the stress distribution results, the middle portion of optimum clutch housing was subjected to very low stress as shown in Fig. 8. Therefore, this area can be redesign to manage the better stress distribution with under the goal of weight reduction.

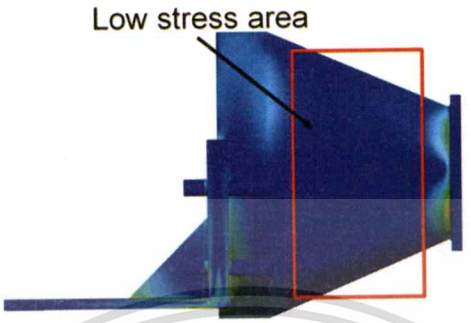

Figure 8. A side view of the initially optimized clutch housing prototype design with resulting stress distribution.

4. POST ANALYSIS AND DESIGN OF MIDDLE SECTION CLUTCH HOUSING

4.1 OPTIMUM AMOUNT OF SPOKES

From a result of the initial optimization on clutch housing, the middle section clutch housing was found to be under a relatively smaller amount of stress. Thus, this particular section of clutch housing was redesigned into a spoke configuration, as shown in Fig. 9. The purpose was to investigate the effect of amount of spokes on maximum von-Mises stress by varying the amount of spokes from 4 -11.

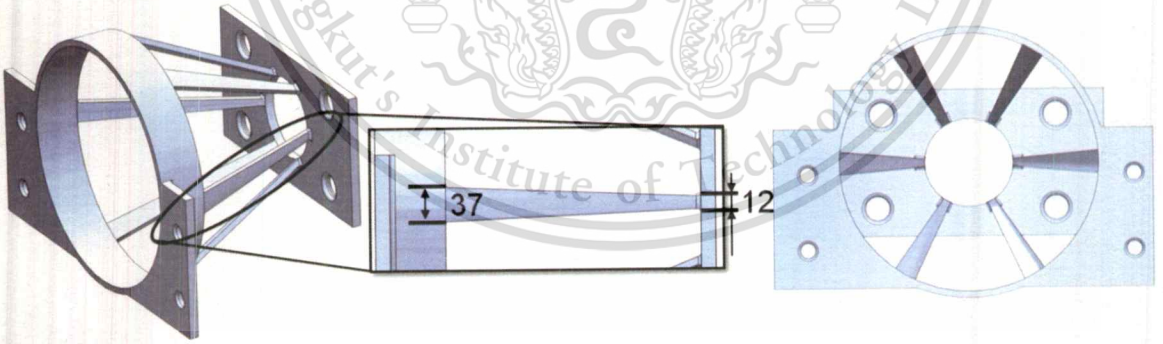

Figure 9. Clutch housing model with 6 spokes configuration (all dimensions are in mm.)

Each varied spokes model was analyzed by using the similar conditions as in the previous model prototype. Then, the results were used to construct the relationship between amount of spokes and maximum von-Mises stress slope as displayed in Fig. 10.

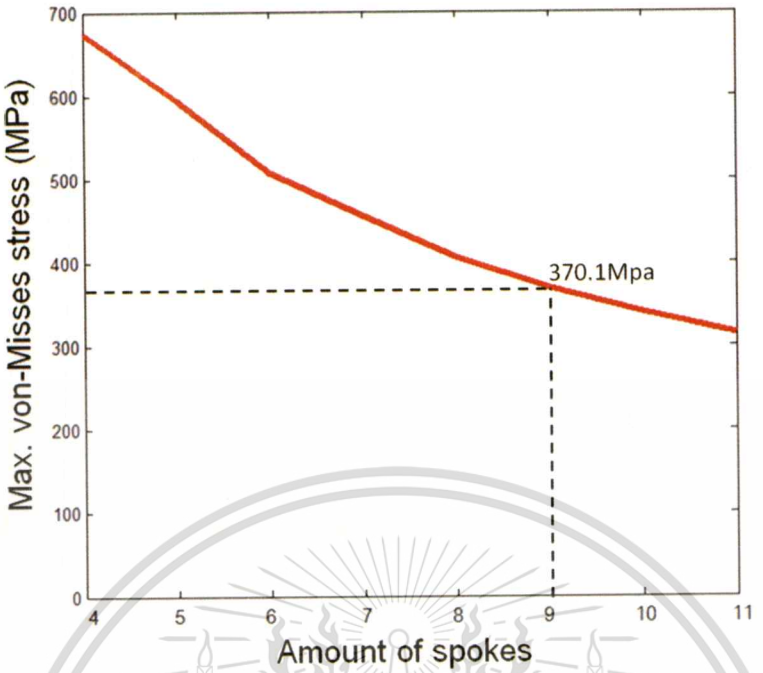

Figure 10. A relationship between amount of spokes and maximum von-Mises stress

From results of number of spokes and maximum von-Mises stress, the resulting stress decreased when increasing amount of spokes. However, overall maximum von-Mises stresses in all cases were currently high. Therefore, the 9 spokes clutch housing model was selected for further improvement by assigning spoke width to be double.

In this step, the 9 spokes clutch housing was selected to as an optimum amount of spoke figurations. But, this clutch housing model still contains a maximum von-Mises stress of 139.35 MPa which was still higher than the required 83.33 MPa (Fig. 11). Therefore, a cross structure con was added to increase the overall stiffness of a model.

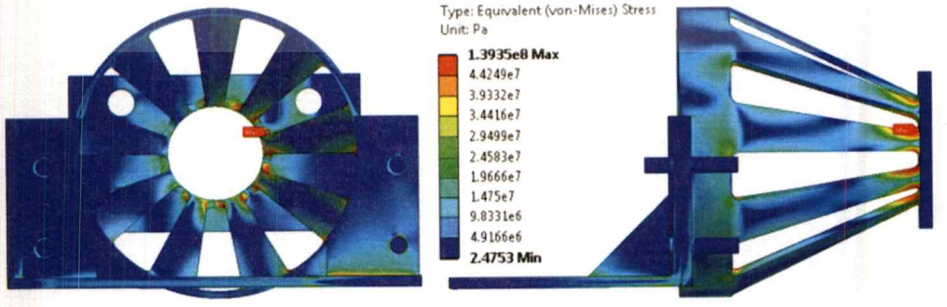

Figure 11. Von-Mises stress distribution in 9 spokes clutch housing with double-sized spoke.

4.2 CROSS STRUCTURE ADDITION

For an addition of cross structure configuration, strips structures were added into the middle section of a 9 spokes (double-sized) clutch housing model as shown in Fig. 12. Furthermore, the size and gap between each adjacent strip were varied. Each parameter sensitivity was investigated by varying the distant between each strip and the width of a strip from 50-100mm and 20-50mm respectively.

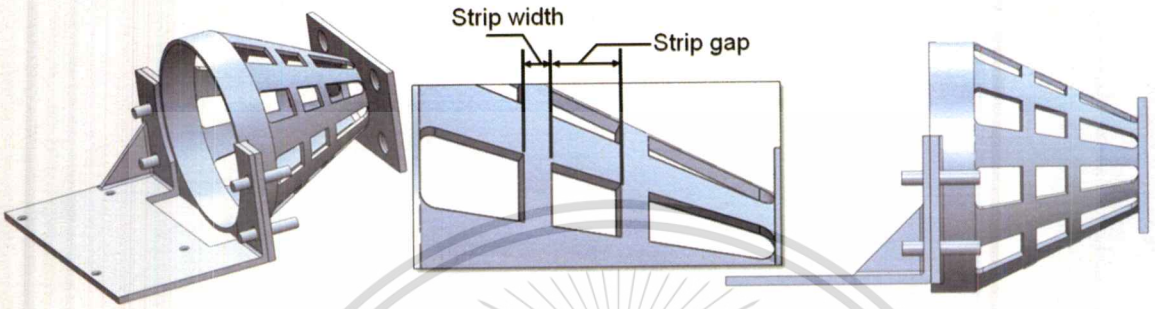

Figure 12. Clutch housing model with strip structure and relevant design parameters

(Strip width, Strip gap)

After all design points were analyzed, the results were used to construct the equation of relation between parameter and maximum von-Mises stress and the response surface (Fig. 13) to predict the optimum point. The results of each design point are show in Table. 2.

Table 2. Parameter variation analysis results

Design points	Strip width (mm)	Strip gap (mm)	Max. von-Mises stress (MPa)
1	20	50	106
2	35	50	100.04
3	50	50	93.86
4	20	75	103.52
5	35	75	95.19
6	50	75	88.164
7	20	100	98.44
8	35	100	89.32
9	50	100	80.28

The following equation of relation could then derived

Max. von-Mises stress (MPa) $= 110.98 - 0.2666x_1 + 0.3208x_2 + 0.0009x_1^2 - 0.0062x_2^2 - 0.008x_1x_2$

Where x_1 = Strip width (mm)

x_2 = Strip gap (mm)

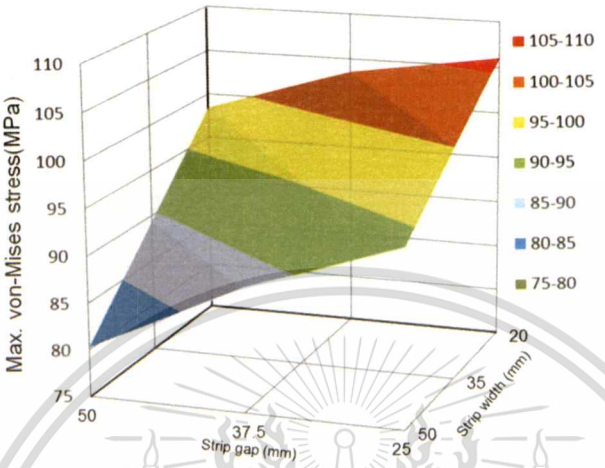

Figure 13. Maximum von-Mises stress response surface for clutch housing design parameters of strip gap and strip width

From the obtained response surface in Fig. 13, the optimum point was found at 47.2 mm strip width and 96.2 mm strip gap with resulting maximum von-Mises stress of 83.27 MPa and fatigue life condition satisfied. The corresponding stress distribution result is shown in Fig.14.

Figure 14. Von-Mises stress distribution in optimum spokes-and-strips clutch housing

5. PROTOTYPE MODEL FOR PROTOTYPING

For a prototype manufacturing, casting process is possibly the best way for a production of optimized clutch housing model with spokes and strip configuration. However, for low quantity production or prototyping, the cost involved with the casting process could be very high. Therefore, a simple model of clutch housing was designed for prototyping such that it could be used in an assembly for a direct clutch system test later on.

The simple model was designed using similar concerns as in previous model but with more specific concern in prototype manufacturing process. The proposed simple clutch housing prototype model is shown in Fig. 15. This clutch housing was analyzed to examine the structural strength of a model. The maximum von-Mises stress of 82.46 MPa was observed as shown in Fig. 16.

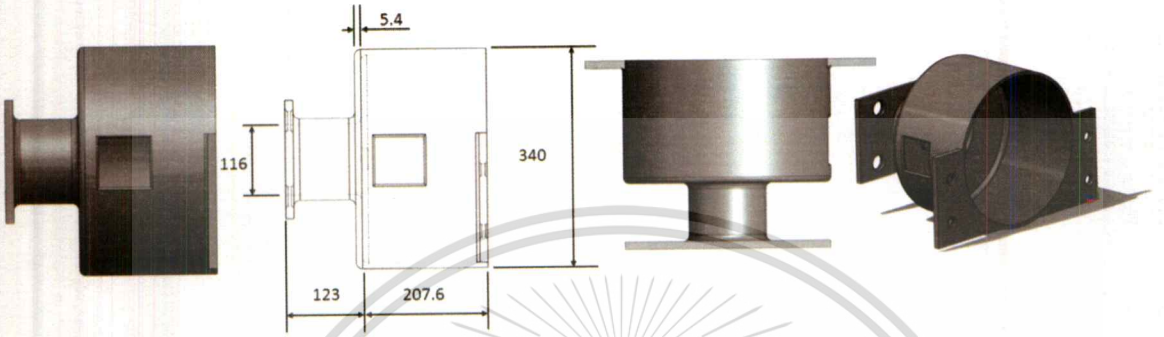

Figure 15. A simple clutch housing prototype model (all dimensions are in mm.)

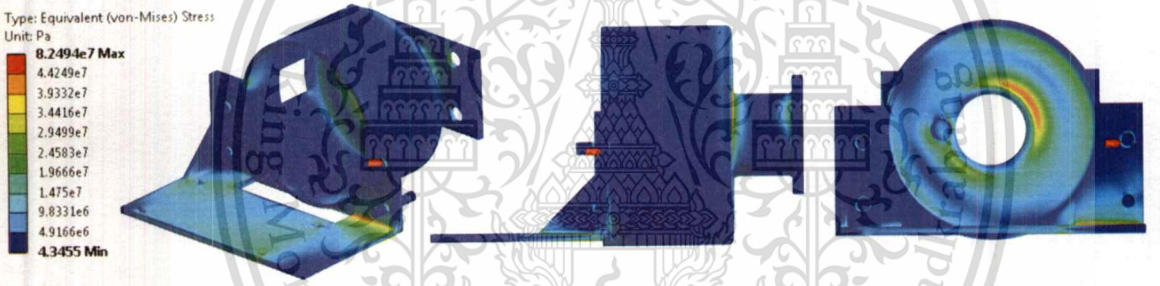

Figure 16. Calculated von-Mises stress distribution in a simple clutch housing

6. 3 MODELS COMPARISON

In this section, 3 proposed clutch housing models i.e. simple model, first optimum model, and spokes with strips optimum model, were compared to each other to show the improvement regarding weight effectiveness which is a result of model developing using optimization technics. The resulting weight and comparative percentage reduction are shown in Table. 3.

Table 3. Model comparison table

Model types	Weight (Kg)	Weight reduction (%)	
		Simple model	First optimum model
Simple model	44.01	-	-
First optimum model	40.37	8.27	-
Spokes with strips optimum model	35.86	18.52	11.17

7. DISCUSSION

Three different models were designed and considered in this study. In the first design, the clutch housing was designed to be a sloped housing model. According to the first response surface (Fig. 7), a sensitivity of the clutch housing slope angle was relatively low since incresing of slope angle resulting in a slight decrease in a maximum von-Mises stress. In contrast, the variation of clutch housing thickness showed very high sensitivity such that maximum von-Mises stress significantly increased while the thickness was decreased. In addition, increasing of both parameters would result in an increase of the total volume of the model. Finally, the weight of this optimum model was 40.37 Kg.

After the first analysis, it was observed that the middle section of clutch housing slope model was containing a low stress distribution. Therefore, the middle section was design to be a spoke model. For an analysis of spokes variation the sensitivity of maximum von-Mises stress was highly decreased with an increasing number of spokes. However, the maximum von-Mises stress was still over the required value of 83.33 MPa. The double-sized spokes was assigned to decrease the maximum von-Mises stress. The optimum number of double-sized spokes number was 9 which generated 139.35 MPa of maximum von-Mises stress, 265.55% decrease from 370.01 MPa with smaller spokes. The reason for choosing 9-spokes model was that it was the highest number of spoke which could be fitted in the available space after doubling a spoke width.

For strips-added model, the response surface optimization technics was used to find the optimum location and size of strips. As a result, the maximum von-Mises stress was decreased with and increasing strip gap and strip width by strip gap was a much more sensitive parameter. Lastly, the optimum spokes strips model was found on the response surface at 47.2 mm strip width and 96.2 mm strip gap under the maximum von-Mises stress of 83.27 MPa, with satisfactory fatigue performance and 35.86Kg.

For simple clutch housing model, the maximum von-Mises stress was 82.49 MPa, but the weight of model was 44.01Kg.

In addition, all models were compared to present the difference of each model. For the weight effective, the spokes-and-strips clutch housing model was the best in weight effective such that the weight was reduced from 44.01 Kg of simple model to 35.86 Kg. In other words, the weight decreased by 18.52%. While the first optimum model weight was reduced from simple model by just 8.27%. Moreover, when comparing in a dimension, the spokes-and-strips model was smaller than the simple model as shown on Fig. 17.

Figure 17. Geometric comparison between simple model and spokes-and-strips model.

8. CONCLUSION

The present work involved designing and analyzing a clutch housing model of a direct clutch system prototype for a one-cylinder diesel engine used in agricultural truck or E-TAND. The specific design concerns and details of finite element analysis were discussed, and the optimizations of clutch housing models were explained. For finite element method and optimization method, these methods were used to show the result of clutch housing behavior when subjected to an engine load. According to the response surface calculation, the sensitivity of each parameter that affect maximum von-Mises stress and weight of the clutch housing were presented.

In conclusion, the best design model was the spokes-and-strips model. The spokes-and-strips model had lowest weight and smallest shape, but this might be appropriate for mass production manufacturing only because it needed to be constructed by casting process. Therefore, for prototyping purpose, the simple clutch housing model was still the appropriate model under the reason of manufacturing method and cost.

In addition, results of current study displayed obvious advantages of the employed approaches such that;

- The sensitivity of each parameter can be shown and compared.
- Saving a computational time and shorten a design process.
- The optimum point prediction gave very accurate result. The error approximated was not exceeding 1.7 %.

For future work, this optimum clutch prototype model will be manufactured and assembled into a direct clutch system in agricultural or E-TAND for field test and failure investigation.

REFERENCES

1. H. Bayrakceken, S. Tasgetiren, I. Yavuz, "*Two cases of failure in the power transmission system on vehicles: A universal joint yoke and a drive shaft*", Journal of Engineering Failure Analysis 14 (2007) 716–724
2. M. M. Rahman, K. Kadirgama, M. M. Noor, M. R. M. Rejab and S. A. Kesulai, "*Fatigue Life Prediction of Lower Suspension Arm Using Strain-Life Approach*", European Journal of Scientific Research ISSN 1450-216X Vol.30 No.3 (2009), pp.437-450
3. M.M. Topa, H. Gunal , N.S. Kuralay, "*Fatigue failure prediction of a rear axle housing prototype by using finite element analysis*", Journal of Engineering Failure Analysis 16 (2009) 1474–1482
4. Necmettin Kaya, Idris Karen, Ferruh Ozturk, "*Re-design of a failed clutch fork using topology and shape optimization by the response surface method*", Journal of Materials and Design 31 (2010) 3008–3014
5. Kwon-Hee Lee, Jeong-Wook Yi, Joon-Seong Park, Gyung-Jin Parkc, "*An optimization algorithm using orthogonal arrays in discrete design space for structures*", Finite Elements in Analysis and Design 40 (2003) 121–135
6. ANSYS Workbench User's Guide

ACKNOWLEDGMENTS

The authors would like to thank automotive laboratory the National Metal and Materials Technology Center (MTEC), for the support of this work.

BIOGRAPHY

Name: Mr. Suphakrit Koocharoenprasit

Date of Birth: December 4, 1986

Place of Birth: Bangkok, Thailand

Education:

2005-2008 B. Eng. in Mechanical Engineering, Sirindhorn International Institute of Technology (SIIT)

2009-2014 M. Eng. in Automotive Engineering (International program), International College, King Mongkut's Institute of Technology Ladkrabang (KMITL)

Honour and Scholarship:

2009-2011 TAIST-Tokyo Tech scholarship, the Master's Degree in Automotive Engineering funded by National Science and Technology Development Agency (NSTDA), Thailand

Proceedings:

1. **Koochareonprasit K.,** Benyajati C., Soparat J., Charoensuk., and Hagiwara I., 2011 *"Design and analysis of a direct clutch system prototype for one cylinder diesel engine by using CAD/CAE"* The 7th International Conference on Automotive Engineering, Bangkok, Thailand.
2. **Koochareonprasit K.,** Benyajati C., Soparat J., Lapapong S., Charoensuk., and Hagiwara I. *"Design and Analysis of Clutch Housing Prototype for One Cylinder Diesel Engine Direct Clutch System"* The 2nd TSME International Conference on Mechanical Engineering, Krabi, Thailand.
3. **Koochareonprasit K.,** Benyajati C., Soparat J., Lapapong S., Charoensuk., and Hagiwara I. *"Model Improvement of Clutch Housing Prototype for Direct Clutch One Cylinder Diesel Engine"* The 16th International Annual Symposium on Computational Science and Engineering, Chiang Mai, Thailand.